Regulation of postharvest inflorescence senescence in *Arabidopsis thaliana*

A thesis presented in partial fulfilment of the requirements for the degree of

Doctor of Philosophy

in

Plant Science

at Massey University, Palmerston North, New Zealand.

Xi Xu

2020

Abstract

Senescence is critical for plant survival and fitness as it ensures the most efficient use of nutrients for development and production of offspring. Senescence is a genetically controlled and hormone-mediated programme. Besides being induced in an age-dependent manner, senescence can also be initiated precociously from harvest-induced stress such as light- and sugar-deprivation. Understanding the biological mechanisms behind dark-mediated senescence is important as it helps to provide a new strategy for extending shelf life of crop plants.

This project aims to understand the regulation of dark-induced inflorescence senescence in model plant *Arabidopsis thaliana* by using a forward genetic approach. Arabidopsis mutants showing *accelerated* and *delayed inflorescence senescence* (named *ais* and *dis*) were identified previously. Here, I rescreened 23 mutants and confirmed the altered time to senescence phenotype of nine mutants, including two *ais* and seven *dis* mutants. Of those, the *dis2*, *dis9*, *dis15* and *dis51* mutants were used for further analysis. The delayed degreening phenotype was also observed in detached dark-held leaves of *dis2* and *dis51* mutants, indicating that the causal mutations affected genes that regulate both leaf and inflorescence senescence. Segregation analysis was used to determine the genetic nature of *dis* traits in the *dis2* and *dis51* mutants. The *dis2* trait was found to be monogenic recessive while the *dis51* trait is dual-genic recessive. The *dis2* mutant showed an extended “stay-green” phenotype and retained higher chlorophyll (Chl) *b* than Chl *a*. These findings were consistent with a lesion in the *NON-YELLOW COLORING1* (*NYC1*) gene. Sequencing revealed a C/T transition in exon 8 of *NYC1*, which caused a highly conserved proline to be substituted by serine at amino acid position 360 of the NYC1 protein. By contrast, *dis51* retained a similar amount of Chl *a* and Chl *b*. One of the genetic lesions in this mutant was mapped to a ~665 kb region at the top arm of chromosome 5 by using High Resolution Melt (HRM)-based mapping technology. The *ETHYLENE INSENSITIVE2* (*EIN2*) gene was considered as a promising candidate because similar phenotypes were observed in *ein2* mutants and *dis51* seedlings did not show triple response

when treated with the ethylene precursor ACC in the dark. PCR-based sequencing showed a G to A mutation in exon 6 of *EIN2*, resulting in a premature stop codon, which thereby resulted in a truncated EIN2 protein missing part of the C-terminal region that is required for ethylene signal transduction. In addition, the *dis51* mutant emitted a pleasant aroma, which is abnormal in Arabidopsis. Four compounds (benzaldehyde, benzyl alcohol, phenylacetaldehyde and phenylethanol) were detected by using GC-MS analysis. However, it is not clear if the mutation causing the aroma phenotype also contributed to the *dis51* phenotype.

The mutations in the *dis9* and *dis15* mutants were previously mapped to chromosome 3 and chromosome 2, respectively. Here, further HRM and whole genome sequencing (WGS) data analyses were used to identify the causal mutation in the *dis9* mutant. The mutation changed a highly conserved Ser-97 to Phe in the active site of strigolactone (SL) receptor gene *DWARF14* (*D14*), likely causing loss-of-activity. Since *dis15* showed similar phenotypes to *dis9*, I hypothesised that the genetic lesion in *dis15* may also have occurred in an SL pathway gene. The *MORE AXIALLY GROWTH1* (*MAX1*) SL biosynthesis gene was present within the previously mapped region of this mutant. By using WGS data, I found a G/A mutation in the coding region of *MAX1*. The mutation in *MAX1* substituted a highly conserved Gly-469 (G469) with Arg (R) in the haem-iron ligand signature of the Cytochrome P450 proteins. Using a *N. benthamiana* transient expression system, I found that the G469R substitution caused loss-of-activity of MAX1. In addition, the delayed sepal degreening of *dis9* and *dis15* was also observed *in planta*, suggesting a role of SL in regulation of both developmental and dark-induced sepal/inflorescence senescence. nCounter transcript counting technology was used to investigate the relationship between SL biosynthesis and signalling, sugar signalling and dark-induced senescence. There was no evidence of SL biosynthesis during the normal night in the inflorescences. During the extended night, the expression patterns of the SL biosynthetic gene *MAX3* and signalling gene *SUPPRESSOR OF MAX2-LIKE7* (*SMXL7*) best correlated with the sugar-responsive senescence regulatory genes [*ARABIDOPSIS NAC DOMAIN CONTAINING PROTEIN92* (*ANAC092*) and *NAC-LIKE, ACTIVATED BY AP3/PI* (*NAP*)] and senescence marker gene

(*SENESCENCE-ASSOCIATED GENE12*; *SAG12*), suggesting an interaction between SL and sugar signalling in controlling dark-induced inflorescence senescence. *ANAC092* and *NAP* were further induced in the *max1* mutant by the SL analogue, GR24, suggesting they are SL-inducible genes.

The overall findings in this project reflect a complex regulatory network, which involves multiple phytohormones and degradation pathways, during dark-induced inflorescence senescence in Arabidopsis. Here, I proposed a model in which prolonged darkness first causes sugar-starvation in the excised inflorescence; the plant hormones ethylene and SL subsequently work together to regulate inflorescence senescence, including NYC1-regulated Chl degradation.

Acknowledgements

I would like to give my sincere thanks to my supervisors Associate Professor Paul Dijkwel, Dr. Donald Hunter and Associate Professor Andrew Sutherland-Smith for their useful advice and kind help in their own research areas during my PhD study. I thank Paul and Don for tolerating my arguments during academic discussions. Special thanks to Paul for his understanding, moral support and insightful advice during my PhD study, especially during thesis and manuscript writing. I am also very impressed by his intelligence on genetics, in which area I have learnt a lot from him. Special thanks to Don for offering Arabidopsis mutants, for every support when I did my work in Plant & Food Research (PFR) and for his brilliant advice on presentation of nCounter data. Also, I thank Don and his family for taking care of me when I was sick and for comforting me when my grandma passed away. I am grateful for Andrew's guide and help for the protein structure analysis and his encouragement when I was stuck at my research.

For the collaborative research, I acknowledge Prof. Harro Bouwmeester at the University of Amsterdam and everyone in his group, especially Yanting Wang, Kristyna Flokova, Lemeng Dong and Olka for hosting me and assisting me with the transient expression assay when I was in their lab. For technical support, I want to give my sincere thanks to Dr. Axel Heiser at AgReserch for all the support and kind help when I did nCounter experiment in his lab. I also appreciate Prof. Pilar Cubas at Centro Nacional de Biotecnología/Consejo Superior de Investigaciones Científicas for providing the D14 construct for genetic complementation.

I also want to thank the following people for their help or advice: Dave Wheeler for help with WGS data analysis; Andrew McLachlan for the linear mixed model analysis; Martin Hunt for the GC-MS analysis; David Chagné for his advice and support on HRM analysis; Ian king for his kind help in the plant house; Huaibi Zhang and Nick Albert for their useful advice on some lab work; Kimberley Snowden and Bart Janssen for their useful feedback towards the manuscript.

I thank Dave Brummell, Marian McKenzie, and Erin O'Donoghue, David Lewis for always being nice and friendly to me when I was in PFR. I thank Sheryl and Steve for their assistance in the lab. Also, I thank my colleagues and friends in PFR (Sarah, Lei, Chethi, Chris, Marzi, Evie, Zoe, Ronan) and in Massey (Tina, Nikolai, Meriem, Elva and Rama) for their friendship, company and moral support. Especially, I want to thank Sarah for her understanding and comfort during the hard time of my research and life, and to Nikolai for sharing experience with me for some bioinformatic analysis. I thank Flavia and Maria for their kind help in Torino when I attended the conference there. I thank Bea for her friendship, help and company when I was in Amsterdam.

Special thanks to Ann Truter and Kathryn Stowell for all their support during my PhD study. I thank the Massey foundation, IFS department and NZSPB for their financial support to attend the international conference and to go to the Netherlands for conducting some work. I acknowledge Massey University Joint Graduate School of Horticulture and Food Enterprise for a doctoral scholarship and PFR SSIF funding: 1972 – "Breeding Technology Development" for financial assistance to conduct my research in PFR.

Finally, but the most important, I want to thank my dearest parents for everything they did for me in my life. No word in this world can express my appreciation and love to them. Thank you so much for everything!!! All in all, thanks to everyone who helped and supported me in this project as well as life.

Contents

Abstract I
Acknowledgements IV
Contents VI
List of tables XI
List of figures XII
Abbreviations XV
1. General introduction 1
1.1. Overview of plant Senescence 1
1.2. Leaf senescence 3
1.2.1. Regulation of developmental-dependent leaf senescence 3
1.2.1.1. Senescence associated genes and transcription factors 3
1.2.1.2. Phytohormone-modulated leaf senescence 8
1.2.1.3. Degradation pathways 15
1.2.2. Regulation of postharvest stress-induced leaf senescence 20
1.2.2.1. Genes and transcription factors 20
1.2.2.2. Phytohormones 21
1.2.2.3. Senescence-induced nutrient catabolism 22
1.3. Flower senescence 24
1.3.1. General introduction of flower senescence 24
1.3.2. Regulation of petal senescence 25
1.3.3. Regulation of postharvest stress-induced inflorescence senescence 29
1.4. Research background 33
1.5. Project aims 35
2. Materials and Methods 36
2.1. Plant materials 36
2.2. Chemicals and reagents 36
2.3. Phenotypic analysis 37
2.3.1. General plant growth conditions 37
2.3.2. Arabidopsis inflorescence degreening assay 38
2.3.3. Calculation of bolting and flowering percentages 38
2.3.4. Synchronisation of flowering time 38

2.3.5. Degreening assay of detached and dark-held leaves 39
2.4. Physiological analysis 39
2.4.1. Chlorophyll analysis 39
2.4.2. Phytohormone treatment 40
2.4.2.1. Ethylene treatment 40
2.4.2.2. Strigolactone treatment 41
2.5. Genetic and high-resolution melt (HRM)-analysis 41
2.5.1. Determination of genetic nature of selected *ais* or *dis* mutants 41
2.5.2. Primer design 41
2.5.3. HRM-based polymerase chain reaction (PCR) 42
2.5.4. Linkage analysis 43
2.6. Molecular cloning 43
2.6.1. Plasmid constructions 43
2.6.2. Plant genomic DNA isolation 44
2.6.3. Standard polymerase chain reaction (PCR) 44
2.6.4. Site-directed mutagenesis 45
2.6.5. Agarose gel electrophoresis 46
2.6.6. PCR product purification 47
2.6.7. Restriction enzyme digestions 47
2.6.8. Ligation 47
2.6.9. Bacterial transformation 47
2.6.9.1. Preparation of Luria-Bertani (LB) medium 47
2.6.9.2. Bacterial strains and general growth conditions 48
2.6.9.3. Preparation of competent cells 48
2.6.9.4. Bacterial transformation methods 49
2.6.9.5. Antibiotics selection 50
2.6.10. Colony PCR 50
2.6.11. Plasmid DNA isolation 50
2.6.12. Standard DNA sequencing 51
2.6.13. Gateway cloning 51
2.7. Transcriptional analysis 52
2.7.1. RNA isolation 52
2.7.2. cDNA synthesis 52

2.7.3. Quantitative Real-Time PCR (qRT-PCR) 53
2.7.4. nCounter analysis 53
2.8. Whole genome sequencing (WGS) 54
2.9. Plant transformation 54
2.9.1. Arabidopsis transformation 54
2.9.1.1. Floral dip methods 54
2.9.1.2. Transgenic plants selection 55
2.9.2. Transient expression in leaves of *N. benthamiana* 56
2.10. Biochemical analysis 57
2.10.1. Analysis of carlactone and carlactonoic acid in *N. benthamiana* 57
2.10.2. Volatile analysis by Gas Chromatography–Mass Spectrometry (GC-MS) 58
2.11. Bioinformatic analysis 58
2.11.1. *In silico* analysis 58
2.11.2. WGS data analysis 59
2.11.3. Standard sequence alignments 59
2.11.4. Accession numbers 59
2.12. Statistical analysis 60
3. Mutant defective in NYC1 exhibits a “stay-green” phenotype of excised Arabidopsis inflorescence upon dark treatment 61
3.1. Introduction 61
3.2. Results 64
3.2.1. Phenotypic analysis of Arabidopsis EMS mutants 64
3.2.2. *dis2*, *dis3*, *dis7* and *dis51* exhibit stable delayed degreening phenotypes in subsequent generation 69
3.2.3. Chlorophyll analysis of *dis2*, *dis3*, *dis7* and *dis51* during dark incubation 69
3.2.4. *dis2* exhibits delayed time to bolting and flowering 70
3.2.5. The delayed inflorescence degreening of *dis2* is not caused by delayed time to flowering 71
3.2.6. Detached cauline leaves of *dis2* exhibit delayed yellowing during dark incubation 72
3.2.7. The *dis2* phenotype is caused by a monogenic recessive trait 72
3.2.8. *dis2* has a missense mutation in the coding sequence of *NYC1* 73
3.3. Discussion 76

3.3.1. Altered degreening phenotypes are confirmed in some EMS mutants 76
3.3.2. *dis2* has a defect in Chl catabolism and the mutation causes a P360S substitution in the NADPH binding pocket of the NYC1 protein ... 78
4. Mutation in EIN2 contributes to the delayed degreening phenotypes of the *dis51* mutant 81
4.1. Introduction 81
4.2. Results 83
4.2.1. *dis51* exhibits delayed time to bolting and flowering 83
4.2.2. The *dis* phenotype of *dis51* is not due to delayed time to flowering 83
4.2.3. *dis51* shows delayed yellowing of detached dark-held cauline leaves 84
4.2.4. The *dis* phenotype of *dis51* is caused by a dual-genic recessive trait 85
4.2.5. HRM-based mapping of *dis* locus in *dis51* 86
4.2.6. Senescence-related genes in the mapped region for *dis* locus of *dis51* 88
4.2.7. *dis51* does not display triple response phenotype upon ACC treatment in the dark 89
4.2.8. *dis51* has a nonsense mutation in the coding region of *EIN2* 90
4.2.9. *dis51* aroma phenotype is due to the volatile compounds phenylacetaldehyde and phenylethanol 93
4.3. Discussion 96
4.3.1. A nonsense mutation in the C-terminal region of EIN2 contributes to multiple *dis51* phenotypes 96
4.3.2. Floral fragrance compounds phenylacetaldehyde and phenylethanol are likely the cause for the aroma phenotype of *dis51* 98
5. Strigolactone defective mutants of Arabidopsis exhibit delayed sepal senescence 103
5.1. Introduction 103
5.2. Results 106
5.2.1. Phenotypic analysis of *dis9* and *dis15* mutants 106
5.2.2. Chlorophyll quantification of *dis9* and *dis15* 107
5.2.3. Transcript abundance of senescence marker genes are suppressed in *dis9* and *dis15* upon dark incubation 108

5.2.4. Segregation analysis of *dis9* and *dis15* mutants 109
5.2.5. HRM-based mapping of *dis9* locus 110
5.2.6. WGS analysis of *dis9* 113
5.2.7. Genetic complementation of *dis9* 113
5.2.8. Identification of genetic lesion in *dis15* 114
5.2.9. Genetic complementation of *dis15* 117
5.2.10. Highly conserved amino acid is substituted in *d14-6*/*dis9* (S97F) 119
5.2.11. Highly conserved amino acid is substituted in *max1-5*/*dis15* (G469R) 120
5.2.12. G469R substitution in *max1-5*/*dis15* disrupts enzyme activity of MAX1 121
5.2.13. MAX1 remains functional when Gly-469 is replaced by Ala 123
5.2.14. Treatment with rac-GR24 rescues delayed sepal degreening of *max1-5*/*dis15* but not *d14-6*/*dis9* 124
5.2.15. Strigolactone biosynthetic and response genes are up-regulated by 24 h of dark incubation in inflorescences 125
5.2.16. Strigolactone signalling but not biosynthetic genes respond rapidly to the light-dark transition 127
5.2.17. GR24 supresses the transcript abundance of *SnRK1*-related genes in *max1-5*/*dis15* during an extended night 130
5.3. Discussion 133
5.3.1. Strigolactones regulate sepal senescence in Arabidopsis 133
5.3.2. Gly-469 of MAX1 is essential for catalysing the conversion of CL into CLA 133
5.3.3. Substitution of catalytic Ser-97 affects activity of D14 134
5.3.4. Strigolactones regulate dark-induced inflorescence senescence in association with a change of carbon status during the extended night 135
6. Conclusion and potential future work 140
6.1. Summary and conclusion 140
6.2. Potential future work 143
References 145
Appendices 174

List of tables

Table 2.1. Details of 22 previously identified EMS mutants 37
Table 2.2. HRM-PCR reaction components 42
Table 2.3. HRM-PCR conditions 42
Table 2.4. PCR reaction components 45
Table 2.5. PCR conditions 45
Table 2.6. Antibiotics preparation and selection 50
Table 2.7. Combinations of different gene constructs for infiltration 57
Table 3.1. Pearson's chi-squared test for F2 population of *ais*/*dis* x L*er*-0 67
Table 3.2. Summarised phenotypes of 21 EMS mutants 67
Table 4.1. Pearson's chi-squared test for F2 progenies of *dis51* x L*er*-0/Col-0 86
Table 4.2. Senescence-related genes in the mapped region for the *dis* locus/loci in *dis51* 89
Table 4.3. Potential volatile compounds that are responsible for the aroma phenotype in *dis51* mutant 94
Table 5.1. Pearson's chi-squared test for F2 progenies of *dis9* x L*er*-0/Col-0 and *dis15* x L*er*-0/Col-0 110
Table 5.2. Name and AGI number of strigolactone-pathway genes 115

List of figures

Figure 1.1. The biosynthesis and signalling of ethylene in *Arabidopsis thaliana* 10

Figure 1.2. The PAO pathway of Chl catabolism 16

Figure 1.3. Screening of detached-dark-held inflorescences of EMS mutants via AIDA 34

Figure 3.1. Degreening of detached and dark treated inflorescences 66

Figure 3.2. *In planta* phenotypes of *ais3*, *ais20*, *ais61*, *dis7* and *dis51* 68

Figure 3.3. The stability of *dis* phenotype in *dis2*, *dis3*, *dis7* and *dis51* 69

Figure 3.4. Chl retention of *dis* mutants during dark incubation 70

Figure 3.5. Time to bolting and flowering of *dis2* 71

Figure 3.6. Degreening of inflorescences of *dis2* at synchronised flowering time 72

Figure 3.7. Degreening of detached dark-held leaves of *dis2* 72

Figure 3.8. Example for segregation of F2 population of *dis2* x L*er*-0 73

Figure 3.9. Amplification of *NYC1* in genomic DNA of *dis2* 74

Figure 3.10. Sequencing of *NYC1* region in *dis2* 75

Figure 4.1. Time to bolting and flowering of *dis51* 83

Figure 4.2. Degreening of inflorescences of *dis51* at synchronised flowering time 84

Figure 4.3. Degreening of detached dark-held leaves of *dis51* 84

Figure 4.4. Example for segregation of F2 population of *dis51* x L*er*-0/Col-0 86

Figure 4.5. HRM-based mapping of *dis* locus in *dis51* mutant 88

Figure 4.6. The triple response assay for L*er*-0 and *dis51* mutant 90

Figure 4.7. Amplification of *EIN2* in genomic DNA of *dis51* 91

Figure 4.8. Sequencing of *EIN2* region in *dis51* 92

Figure 4.9. GC-MS profiles of volatile compounds in L*er*-0 and *dis51* from preliminary scanning 94

Figure 4.10. GC-MS profiles of volatile compounds in L*er*-0 and *dis51* with one flower for each genotype 95

Figure 4.11. Schematic representation of the biosynthetic pathways for phenylacetaldehyde, phenylethanol, benzaldehyde and benzyl alcohol 100

Figure 5.1. The strigolactone biosynthetic and signalling pathways in *Arabidopsis thaliana* 104

Figure 5.2. Delayed inflorescence degreening and bushy phenotypes of *dis9* and *dis15* 106

Figure 5.3. Delayed sepal degreening of *dis9* and *dis15 in planta* and in detached inflorescences held in long day conditions 107

Figure 5.4. Chlorophyll quantification of detached dark-held inflorescences in *dis9* and *dis15* mutants 108

Figure 5.5. Transcript abundance based on qPCR analysis of *ANAC092* and *SAG12* in L*er*-0 and *dis* mutants at 0 h and 72 h 109

Figure 5.6. An example for screening of *dis9* x Col-0 F2 population 110

Figure 5.7. HRM and WGS analysis of *dis9* 112

Figure 5.8. Genetic complementation of *dis9* 114

Figure 5.9 Positions of strigolactone-pathway genes and markers indicating mapped region for *dis15* locus in Arabidopsis chromosomes 115

Figure 5.10 Identification of G to A mutation in WGS data of *dis15* 116

Figure 5.11. Genetic complementation of *dis15* 118

Figure 5.12. The serine to phenylalanine substitution in the D14 protein 120

Figure 5.13. The glycine to arginine substitution in the MAX1 protein 121

Figure 5.14. Analysis of CL and CLA in *N. benthamiana* leaves infiltrated with strigolactone biosynthetic gene constructs 123

Figure 5.15. Sepal degreening of excised inflorescences treated with rac-GR24 124

Figure 5.16 Transcript abundance changes of strigolactone pathway and senescence-related genes during a period of 72-h of dark treatment 126

Figure 5.17 Confirmation of transcriptional changes of strigolactone-pathway and senescence-related genes by qRT-PCR analysis 127

Figure 5.18 Transcriptional changes of sugar- and senescence-related genes during the regular night 129

Figure 5.19 Transcriptional changes of strigolactone pathway genes during the regular night 130

Figure 5.20 Transcriptional changes of sugar, senescence and strigolactone pathway genes during the extended night 132

Figure 5.21 Transcriptional change of *NAP* gene during a period of 72 h of dark treatment 139

Figure 6.1 A model for dark and starvation-induced, ethylene and strigolactone mediated inflorescence senescence including NYC1-regulated chlorophyll degradation 142

Abbreviations

AADC	group II pyridoxal 5'-phosphate-dependent amino acid decarboxylase
AAS	aromatic aldehyde synthase
ABA	abscisic acid
ACC	1-aminocyclopropane-1-carboxylic acid
ACO	1-AMINOCYCLOPROPANE-1-CARBOXYLATE OXIDASE
ACS	1-AMINO-CYCLOPROPANE-1-CARBOXYLATE SYNTHASE
AGI	Arabidopsis Genome Initiative
AGL	AGAMOUS like
AHK	*ARABIDOPSIS* HISTIDINE KINASE
AIDA	Arabidopsis inflorescence degreening assay
ais	*accelerated inflorescence senescence*
ANAC	ARABIDOPSIS NAC DOMAIN CONTAINING PROTEIN
AOC	ALLENE OXIDE CYCLASE
AP2/EREBP	APETALA2/ETHYLENE RESPONSIVE ELEMENT BINDING PROTEIN
ARF	AUXIN RESPONSE FACTOR
ARR	ARABIDOPSIS RESPONSE REGULATOR
ASN	asparagine
ATS	attached shaded leaves
AZF2	Cys2/His2 type zinc finger protein
BR	brassinosteroid
bZIP	Basic-leucine zipper
Cas9	CRISPR associated protein 9
CDS	coding sequence
CEND	carboxyl-terminal end
ChIP	Chromatin Immunoprecipitation
Chl	chlorophyll
CK	cytokinin
CL	carlactone
CLA	carlactonoic acid

CLIM	covalently linked intermediate molecule
coi	*coronatine-insensitive*
Col	Columbia
CRF	CYTOKININ RESPONSE FACTOR
CRISPR	Clustered regularly-interspaced short palindromic repeats
CTR/*ctr*	CONSTITUTIVE TRIPLE RESPONSE/*constitutive triple response*
D14	DWARF14
dis	*delayed inflorescence senescence*
DMSO	Dimethyl sulphoxide
DOX	DIOXYGENASE
dsDNA	double-stranded DNA
DVB	divinylbenzene
EBF	EIN3-BINDING PROTEIN
EDF	Ethylene Response DNA-binding Factors
EDTA	ethylenediaminetetraacetic acid
EIL	EIN3-LIKE
EIN/*ein*	ETHYLENE INSENSITIVE/*ethylene insensitive*
EMS	ethyl methanesulfonate
EPH	EPHEMERAL
ERF	ETHYLENE RESPONSE FACTOR
ERS	ETHYLENE RESPONSE SENSOR
ET	Ethylene
ETP	TARGETING PROTEIN
ETR/*etr*	ETHYLENE RESPONSE/*ethylene receptor*
FYF	FOREVER YOUNG FLOWER
GA	gibberellic acid
GABA	4-aminobutyrate
GC-MS	Gas Chromatography–Mass Spectrometry
GLN	glutamine
GR24	(3E,3aR,8bS)-3-[[(2S)-4-methyl-5-oxo-2H-furan-2-yl]oxymethylidene]-4,8b-dihydro-3aH-indeno[1,2-b]furan-2-one

HCAR	7-HYDROXYMETHYL Chl *a* REDUCTASE
HRM	High-resolution melt
IPT	ISOPENTENYL TRANSFERASE
JA	Jasmonic acid
JAZ	JASMONATE-ZIM-DOMAIN PROTEIN
KAI	KARRIKIN INSENSITIVE
KAR	karrikin
LB	Luria-Bertani
LBO	LATERAL BRANCHING OXIDOREDUCTASE
L*er*	Landsberg *erecta*
LHC	light-harvesting complex
LOX	LIPOXYGENASE
L-Phe	L-phenylalanine
MAX	MORE AXILLARY GROWTH
MCS	metal chelating substance
MeCLA	methyl carlactonoate
MeJA	methyl jasmonate
mg	milligram
mL	milliliter
mM	millimolar
MS	Murashige and Skoog or Mass Spectrometry
MYB	MYELOBLASTOSIS
NAC	NAM (NO APICAL MERISTEM), ATAF1,2 (*Arabidopsis thaliana* NAC transcription factor1,2) and CUC2 (CUP SHAPED COTYLEDON 2)
NADH	reduced form of nicotinamide adenine dinucleotide
NADPH	reduced form of nicotinamide adenine dinucleotide phosphate
NahG	SALICYLIC HYDROXYLASE
NAP	NAC-LIKE ACTIVATED BY AP3/PI
NCC	non-fluorescent Chl catabolite
NLS	nuclear localization signal
NOL	NYC1-LIKE

NYC	NONYELLOW COLORING
OD	Optical density
old	*onset of leaf death*
ORE/*ore*	*ORESARA*/*oresara*
ORS	ORE1 SISTER
PAAS	phenylacetaldehyde synthase
PAO	pheophorbide *a* oxygenase
PAR	phenylacetaldehyde reductase
PCD	programmed cell death
PCR	Polymerase Chain Reaction
PE	phenylethanol
pFCC	primary fluorescent Chl catabolite
PFR	New Zealand Institute for plant & food research
PHA or PAld	phenylacetaldehyde
pheide *a*	pheophorbide *a*
PPH	pheophytinase
r.p.m	Revolutions per minute of rotor
rac-GR24	a racemic mixture of GR24
RAV1	RELATED TO ABI3/VP1
RCC	red chlorophyll catabolite
RCCR	red chlorophyll catabolite reductase
RCF	Relative Centrifugal Force or G-force
RNAi	RNA interference
ROS	reactive oxygen species
Rubisco	ribulose-1,5-bisphosphate carboxylase/oxygenase
SA	salicylic acid
SAG	senescence-associated gene
SAM	S-Adenosylmethionine
SDR	short-chain dehydrogenase/reductase
SDS	sodium dodecyl sulfate
SGR	STAY-GREEN
SIRK	senescence-induced receptor like kinase
SL	strigolactone

SMXL	SUPPRESSOR OF MAX2-LIKE
SNP	single nucleotide polymorphism
SnRK1s	Snf1-related protein kinases
SPME	solid-phase microextraction
T-6-P	trehalose-6-phosphate
TE	Tris-EDTA buffer
TF	transcription factor
UTR	untranslated regions
WT	wild type
ygl	*yellow-green leaf*
µL	microlitre
µM	micromolar

1. General introduction

1.1. Overview of plant Senescence

Senescence is the final phase of plant or organ development and eventually leads to the death of the organ or whole plant. Senescence typically occurs in mature cells of tissues, after their growth phase has ceased, to enable efficient recycling of nutrients to new growing sinks or seeds (Thomas, 2013). At the whole plant level, senescence is considered critical for plant fitness, enabling plants to survive optimally in their given environments.

The ability to senesce was proposed to require a change in competency of the tissue that occurs during aging. When such competency is acquired, age- or developmentally-induced senescence can be induced (Jing *et al.*, 2005; Fracheboud *et al.*, 2009). Age-induced senescence is an active process and is regulated by interaction between developmental (e.g. age and hormones) and environmental (e.g. day/night length) signals and it requires involvement of numerous senescence-associated genes (*SAGs*) (Lim *et al.*, 2003). Nevertheless, imposition of stresses (e.g. wounding and prolonged darkness) can make tissues senesce early, possibly as an adaptive response to allow survival of the plant as a whole (Kanojia and Dijkwel, 2018).

Molecular genetic studies showed senescence is a genetically controlled programme as altered leaf longevity has been observed in some senescence associated mutants such as the *onset of leaf death* (*old*) and stay-green mutants (Jing *et al.*, 2002; Hörtensteiner, 2009). The *old* mutants were isolated by an ethylene (ET)-induced senescence screen and they showed altered timing of onset of leaf senescence. The studies of *old* mutants suggest that ET promoted leaf senescence is restricted by the age of the leaf (Jing *et al.*, 2002; Jing *et al.*, 2005). Stay-green mutants exhibit a delay in leaf degreening compared with wild type (WT) and can be classified into functional and non-functional (cosmetic) mutants. Functional stay-green mutants exhibit a coupled retention of chlorophyll (Chl) and photosynthetic activity; whereas cosmetic stay-green mutants only show a defect in Chl catabolism coupled with

disruption of photosynthetic activity, while other senescence processes still take place (Hörtensteiner, 2009).

In addition to genetic mutant screens, transcriptome analysis was also extensively used to identify key genes that control both developmental- and stress-induced leaf senescence (Buchanan-Wollaston *et al.*, 2005; van der Graaff *et al.*, 2006; Breeze *et al.*, 2011; Guo and Gan, 2012). Numerous *SAG*s which are differentially expressed during leaf senescence were identified in model plant Arabidopsis. For example, senescence marker gene *SAG12*, genes encoding NAC and WRKY transcription factor (TF) families and genes involved in hormone biosynthesis and signalling (Buchanan-Wollaston *et al.*, 2005; van der Graaff *et al.*, 2006).

Phytohormones have long been known to play key roles in the regulation of senescence. Ethylene (ET), salicylic acid (SA), abscisic acid (ABA), jasmonic acid (JA) and brassinosteroid (BR) promote the onset or progression of senescence; whereas cytokinin (CK), gibberellic acid (GA) and auxin delay senescence (Gan and Amasino, 1997; Lim *et al*., 2007). More recently, strigolactones (SLs), which are well-known for their function in regulating seed germination in parasitic plants (Toh *et al.*, 2012; Wang and Bouwmeester, 2018) and plant shoot branching (Gomez-Roldan *et al*., 2008; Umehara *et al*., 2008), were reported to regulate natural- and dark-induced leaf senescence (Woo *et al.*, 2001; Snowden *et al.*, 2005; Yan *et al*., 2007; Hamiaux *et al.*, 2012; Yamada *et al.*, 2014; Ueda and Kusaba, 2015). The plant hormones do not work alone, but rather in concert with, or against, each other to control senescence progression (Jibran *et al.*, 2013; Ma *et al.*, 2018). For example, ET, ABA and jasmonates have been found to crosstalk with each other to control leaf senescence in Arabidopsis (Kim *et al*., 2011).

Leaf senescence involves cell transitioning from anabolic to catabolic metabolism (Bate *et al.*, 1991; Bleecker and Patterson, 1997). It is accompanied by a series of physiological and biochemical events, which proceed orderly in senescing cells (Lim *et al.*, 2007). Degradation of Chl, proteins, and membrane lipid are three hallmarks of leaf senescence (Trivellini

et al., 2012). Chloroplast degradation is the earliest event during leaf senescence which results in visible yellowing of leaves (Matile *et al.*, 1996; Gan and Amasino, 1997). This process is required to prevent phototoxicity in the cells and therefore essential for survival of senescing cells to facilitate nitrogen remobilization and progression of senescence (Hörtensteiner, 2004, 2006). Metabolism of membrane lipids also occurs early during leaf senescence, which causes an increased membrane permeability and loss of ionic gradients (Thompson *et al.*, 1998; Rolny *et al.*, 2011). Other macromolecules such as sugars, specifically sucrose, are catabolized and exported as hexoses from the senescing 'source' leaves (leaves that produce sugars are called 'source' leaves) to 'sinks' organs (e.g. young leaves and seeds, which require sugars for growth) (Rolland *et al.*, 2006).

Beside relatively well-characterised leaf senescence, senescence of floral organs, especially petals, has also been widely investigated (Tripathi and Tuteja, 2007; Rogers, 2013; Ahmad and Tahir, 2016; Ma *et al.*, 2018). Both similarities and differences were found between flower and leaf senescence. For instance, at the molecular level, large numbers of genes are involved in both leaf and flower senescence (Price *et al.*, 2008; Trivellini *et al.*, 2012), indicating a similarity. As for hormone regulation, however, ET-insensitive flower systems exist during flower but not leaf senescence (Woltering and Vandoorn, 1988).

In this introduction, senescence-related physiological changes, regulatory genes and plant hormones during age- and postharvest stress-induced leaf and flower senescence are reviewed.

1.2. Leaf senescence

1.2.1. Regulation of developmental-dependent leaf senescence

1.2.1.1. Senescence associated genes and transcription factors

In order to elucidate the molecular mechanisms underlying leaf senescence, genome-wide transcriptome analysis was used extensively over the past decades to identify key regulators that control both age- and artificially induced

leaf senescence in different plant species (Lin and Wu, 2004; Buchanan-Wollaston *et al.*, 2005; van der Graaff *et al.*, 2006; Breeze *et al.*, 2011; Guo and Gan, 2012; Zhang *et al.*, 2014a).

In Arabidopsis, a large number of genes have been found to be differentially expressed during developmental leaf senescence. Of them, downregulated genes are overrepresented for genes involved in anabolic processes including photosynthesis activity, carbon fixation and amino acid metabolism. By contrast, upregulated genes are enriched for genes participated in degradation of proteins, lipids and nucleotides (Buchanan-Wollaston *et al.*, 2005; van der Graaff *et al.*, 2006; Breeze *et al.*, 2011). Such extensive transcriptional changes of *SAGs* revealed a dramatic alteration in cell metabolism at the transition phase from anabolism to catabolism. In addition, genes involved in plant hormone biosynthesis and signalling are also differentially expressed (Buchanan-Wollaston *et al.*, 2005; van der Graaff *et al.*, 2006). For instance, genes encoding regulators involved in CK signalling (e.g. type A response regulators ARR4, ARR6, ARR7 and ARR9) were down regulated during developmental leaf senescence; whereas those encoding ET biosynthetic enzymes (e.g. ACC synthases *At*ACS2, *At*ACS5, and *At*ACS6) were up-regulated significantly (Buchanan-Wollaston *et al.*, 2005; van der Graaff *et al.*, 2006).

Senescence marker gene *SAG12*

Of up-regulated *SAGs*, *SAG12* perhaps is the most famous one because it is used frequently as a marker gene for indicating the timing of developmental senescence and it reaches the highest expression level at late stages of senescence (Noh and Amasino, 1999a; Olsen *et al.*, 2005a). *SAG12* encodes a cysteine protease, whose promoter has a highly conserved region that specifically responds to age-related senescence cues (Lohman *et al.*, 1994; Noh and Amasino, 1999a). However, the up-regulation of *SAG12* has also been reported in dark-induced senescence in both attached and detached leaves (van der Graaff *et al.*, 2006). Its whole promoter has been used to drive expression of the *isopentenyl transferase* (*IPT*) gene (a bacterial CK biosynthesis gene) to delay leaf senescence by increasing endogenous CK

production in transgenic tobacco plants (Gan and Amasino, 1995). Remarkably, this auto-regulated pro*SAG12*:*IPT* system has been successfully applied in many crop species, including lettuce, rice, tomato, cauliflower, wheat and broccoli, to delay senescence (Zwack and Rashotte, 2013). This suggests that the regulation of developmental-senescence-specific SAG12 is highly conserved in both monocots and dicots. Interestingly, although *SAG12* is specifically-induced upon senescence, when this gene was knocked out in Arabidopsis mutants, the plants did not show an altered senescence phenotype (Otegui *et al.*, 2005). It could be that SAG12 function is compensated by the activity of other proteases when *SAG12* is mutated (Pružinská *et al.*, 2017). SAG12 is expressed predominantly in senescence-associated vacuoles (Otegui *et al.*, 2005; Carrión *et al.*, 2013), and it has been suggested to be involved in degradation of ribulose-1,5-bisphosphate carboxylase/oxygenase (Rubisco) in tobacco leaves (Martínez *et al.*, 2008; Carrión *et al.*, 2013), whereas another study suggested that lacking *SAG12* is not detrimental for Rubisco breakdown in Arabidopsis and soybean (Otegui *et al.*, 2005). Recently, James *et al.* (2018) found that the *sag12* mutant did affect yield of Arabidopsis under the low nitrogen condition. Thus, the authors suggested a role of SAG12 in nitrogen remobilisation during the leaf senescence for seed filling (James *et al.*, 2018).

Senescence-related transcription factors

The regulation of leaf senescence requires TFs that bind to specific motifs in the regulatory regions of their target genes. Transcription profile analysis of differentially expressed TFs during different developmental stages or under various environmental stresses provides a global picture of the gene regulatory network of leaf senescence in Arabidopsis (Chen *et al.*, 2002; Buchanan-Wollaston *et al.*, 2005; Breeze *et al.*, 2011). Buchanan-Wollaston *et al.* (2005) reported that 96 putative TF genes (within 827 up-regulated genes) increased their transcript abundances during developmental leaf senescence. These include WRKY, NAC, MYB, bZIP and AP2/EREBP (AP2/ERF) TF families. More recently, Breeze *et al.* (2011) used a time-course microarray analysis to investigate the regulation of leaf senescence at various developmental stages in Arabidopsis. By analysing transcriptional profiles of 6323 differentially

expressed genes, they found that the NAC and WRKY TF families showed particular over-representation in the SAG pool, suggesting members of these families play important roles in the leaf senescence programme (Breeze *et al.*, 2011). These are consistent with the findings in molecular genetic studies that many members of these two families are critical for cascades of a diverse range of biological processes during leaf senescence (Robatzek and Somssich, 2001; Miao *et al.*, 2004; Olsen *et al.*, 2005b; Rushton *et al.*, 2010; Podzimska-Sroka *et al.*, 2015).

NACs (for NAM-ATAF1/2-CUC2) constitute one of the largest plant-specific TF families (Olsen *et al.*, 2005b). In Arabidopsis, more than 100 genes encoding NAC proteins have been identified (Nakashima *et al.*, 2012). Transcriptome analyses revealed that many NAC genes are senescence associated (Guo *et al.*, 2004; Buchanan-Wollaston *et al.*, 2005; Balazadeh *et al.*, 2008; Breeze *et al.*, 2011). Of them, *NAP* (also known as *ANAC029*), *ANAC092* (also known as *NAC2* and *ORE1*) and its paralog *ORS1* (also known as *ANAC059*) are known to have significant roles during leaf senescence, and they are up-regulated during both age- and stress-induced (e.g. darkness, salt or ROS treatment) senescence (Guo and Gan, 2006; Kim *et al.*, 2009; Balazadeh *et al.*, 2010; Balazadeh *et al.*, 2011; Yang *et al.*, 2014). Mutants defective in these genes exhibited delayed senescence; while their overexpression lines showed precocious senescence in Arabidopsis (Guo and Gan, 2006; Kim *et al.*, 2009; Balazadeh *et al.*, 2010; Balazadeh *et al.*, 2011). These results suggested that they positively regulate senescence in a non-redundant manner. *NAP* promotes rosette leaf senescence in Arabidopsis and appears primarily up-regulated by age (Guo and Gan, 2006). However, a recent study found that *NAP* transcripts were significantly increased upon dark treatment and it promoted Chl degradation by enhancing transcription of the ABA biosynthetic gene AAO_3 (Yang *et al.*, 2014). ANAC092 is considered as the central regulator of senescence because it targets huge numbers of *SAGs* during both developmental and stress-induced senescence (Balazadeh *et al.*, 2010; Breeze *et al.*, 2011). Both *ANAC092* and *NAP* are directly up-regulated by EIN3, a key TF downstream of EIN2-dependent ET signalling pathway (Kim *et al.*, 2014). Transcriptional analysis found that they regulated both common (e.g. *ANAC041*,

ANAC079, and *VNI2*) and distinct targets (e.g. *ANAC087* and *ANAC102* are only regulated by *ANAC092*) during senescence, suggesting that both overlapping and distinct gene regulatory networks for ANAC092 and NAP exist (Kim *et al.*, 2014). Consistently, the *anac092/nap* double mutant showed partially additive delayed senescence phenotypes as compared to their single mutants, which indicated independent regulatory pathways for these two genes (Kim *et al.*, 2014). Although *ORS1* also controls developmental leaf senescence, this gene itself was strongly induced by H_2O_2 and transcriptome analysis found high percentages of its target genes were induced by salt-stress and H_2O_2 treatment, suggesting it also involved in stress-induced senescence (Balazadeh *et al.*, 2011).

The second largest plant-specific TF family for regulating leaf senescence is the WRKY superfamily (Guo *et al.*, 2004). In Arabidopsis, it consists of up to 100 members (Eulgem *et al.*, 2000). TFs in this family, in addition to having important roles in the regulation of leaf senescence and hormone pathways, also participate in plant defence responses in response to various biotic and abiotic stresses (Rushton *et al.*, 2010; Chen *et al.*, 2012). WRKYs regulate leaf senescence by binding to the W-box element (C/T)TGAC(C/T) in the promoters of targets (Eulgem *et al.*, 2000). WRKYs regulate the expression of *SAGs* either alone or by interacting with other TFs. For example, *WRKY6* is strongly and specifically expressed in senescent leaves of Arabidopsis where it regulates leaf senescence by targeting and activating the transcription of *SAGs* such as the senescence-induced receptor like kinase *SIRK* (Robatzek and Somssich, 2001, 2002). The regulation of senescence by WRKY30 is more complex and can be positive or negative depending on what other WRKY TFs it interacts with. WRKY30 positively regulates leaf senescence when it interacts with WRKY53 and negatively regulates leaf senescence when it interacts with both WRKY54 and WRKY70, which show some degree of functional redundancy with each other and with WRKY30 in their senescence regulation (Besseau *et al.*, 2012). These findings suggest that several WRKY TFs are important regulatory components of the senescence programme and that they provide the tissue with a mechanism to finely control the promotion or inhibition of the programme.

1.2.1.2. Phytohormone-modulated leaf senescence

Phytohormones have profound effects on almost every biological event during plant development and defence, including seed germination, floral organ maturation and abscission, leaf/flower senescence and in response to various biotic (e.g. pathogen infection) and abiotic (e.g. drought and darkness) stresses (Gray, 2004; Smith *et al.*, 2017). The wide involvement and diverse functions of plant hormones reveal complex and overlapped regulatory networks. This makes it difficult to determine the function of a single hormone during a specific biological process. Nevertheless, the roles of phytohormones in modulating leaf senescence have been extensively documented (Schippers *et al.*, 2007; Jibran *et al.*, 2013; Khan *et al.*, 2014; Akhtar *et al.*, 2019). Based on their senescence-associated functions, phytohormones can be classified into two groups that are stimulators and inhibitors. The stimulators, including ET, SA, ABA, JA, BR, and SL, promote the onset or progression of senescence; whereas, the inhibitors, including CK, and GA, delay senescence (Schippers *et al.*, 2007; Jibran *et al.*, 2013; Yamada and Umehara, 2015). However, the senescence regulatory role of auxins is debatable. Evidences for the involvement of this hormone in promoting or inhibiting leaf senescence were reviewed in Mueller-Roeber and Balazadeh (2014) and Wojciechowska *et al.* (2018). Of the senescence-stimulating hormones, some, e.g. ET, JA, SA and SLs, are also involved in plant defence response (Breeze *et al.*, 2011; von Saint Paul *et al.*, 2011; Guo and Gan, 2012; Torres-Vera *et al.*, 2014; Marzec, 2016). The phytohormones do not work alone, but rather in concert with each other to control senescence progression. For example, ET, ABA and JA have been found to crosstalk with each other to control leaf senescence in Arabidopsis (Kim *et al.*, 2011). Other regulators including TFs (e.g. EIN3, AP2/ERF and ARFs) and proteins (e.g. F-box proteins and suppressors) are also involved in phytohormone-mediated senescence and plant hormone signalling (Woo *et al.*, 2001; Potuschak *et al.*, 2003; Lim *et al.*, 2010). In this chapter, ET, SL and CK, whose biological functions are well-established and are relevant to this project, are highlighted.

Ethylene

Ethylene (ET), a gaseous phytohormone, has crucial roles in a range of biological processes during plant development (Schaller, 2012; Dubois *et al.*,

2018). For instance, it affects the morphology of etiolated seedlings (seedlings grown in the dark) (Goeschl *et al.*, 1966). Exposure of dark-grown seedlings to a saturating concentration of ET results in a characteristic phenotype known as the triple response (Guzman and Ecker, 1990). In Arabidopsis, the triple response consists of three distinct alterations: shorter and thicker hypocotyls and roots and an exaggerated curvature of the apical hook of the WT seedlings grown in the dark (Guzman and Ecker, 1990; Merchante and Stepanova, 2017). Since these phenotypes are robust and easy to screen, the triple response assay was used frequently to identify ET-related mutants and numerous ET-insensitive mutants have been isolated [summarised in Merchante and Stepanova (2017)].

ET is also well-known as a positive regulator of plant organ senescence (Abeles *et al.*, 1988; Lim *et al.*, 2007). Endogenous ET increases during both organ senescence and stress response in many plants (Lim *et al.*, 2007). Consistently, genes encoding enzymes involved in ET biosynthesis, including *1-AMINOCYCLOPROPANE-1-CARBOXYLIC ACID* (*ACC*) *SYNTHASE*s (*ACS*s; e.g. *ACS2* and *ACS5*) and *ACC OXIDASE*s (*ACO*s; e.g. *EAT1*), were up-regulated during senescence (van der Graaff *et al.*, 2006). In Arabidopsis, exogenous ET treatment induces premature leaf senescence (Jing *et al.*, 2005). However, the presence of this hormone seems not absolutely required to promote the onset or progression of the senescence in many cases because ET defective mutants eventually senesce (Grbić and Bleecker, 1995; Jing *et al.*, 2002). In addition, the studies of *old* mutants also suggested that the effect of ET on senescence induction relies on age-related signals or factors (Jing *et al.*, 2005).

The molecular basis of ET-modulated senescence has been characterised by identification of ET-defective mutants. Mutants with defects in ET biosynthesis or signalling exhibited altered timing of senescence (Graham *et al.*, 2012; Bennett *et al.*, 2014; Schippers *et al.*, 2015). For example, transgenic plants which accumulated high-level of ACS7 protein exhibited precocious senescence of Arabidopsis leaves (Sun *et al.*, 2017). In addition, two ET insensitive mutants *ethylene receptor1-1* (*etr1-1*) and *ethylene insensitive2*

(*ein2*) showed delayed leaf senescence (Grbić and Bleecker, 1995; Alonso *et al.*, 1999); whereas overexpressing *EIN3*, a key gene involved in ET signalling, resulted in accelerated leaf senescence (Li *et al.*, 2013).

With the help of genetic and biochemical analyses (Guo and Ecker, 2004), the ET biosynthetic and signalling pathways have been established in Arabidopsis (Figure 1.1). ET is synthesised from precursor S-Adenosylmethionine (SAM) which is derived from methionine and is the activated form of this amino acid (Yang and Hoffman, 1984; Wang *et al.*, 2002). The following reactions require activity of ACS and ACO to sequentially catalyse SAM to ACC and then to ET (Yang and Hoffman, 1984; Wang *et al.*, 2002).

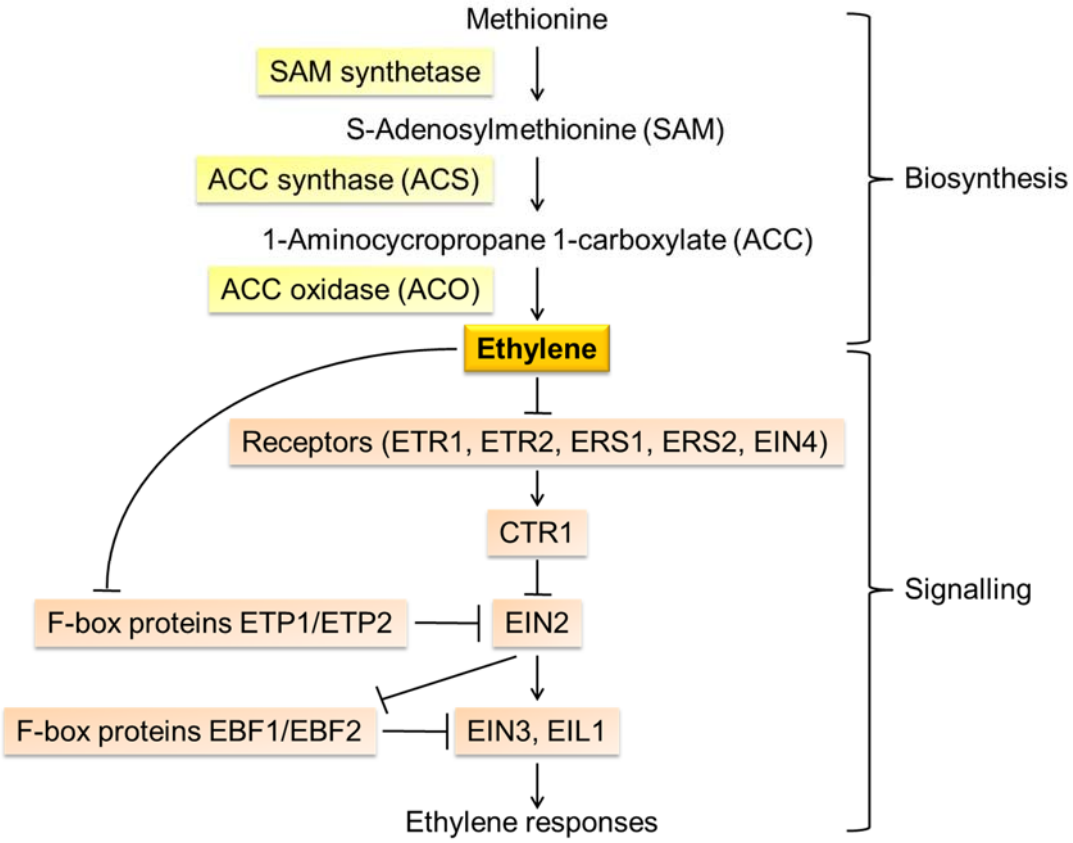

Figure 1.1. The biosynthesis and signalling of ethylene in *Arabidopsis thaliana*
Simplified pathways are shown in the figure. Enzymes involved in biosynthesis are highlighted with light yellow background; receptors, proteins, protein kinase and TFs of ethylene signalling are highlighted with light orange background. Intermediate products are indicated, and ethylene is highlighted with an orange-yellow background.

ET is perceived by five endoplasmic reticulum-localised receptors, including ETHYLENE RESPONSE1 (ETR1), ETR2, ETHYLENE RESPONSE SENSOR1

(ERS1), ERS2, and ETHYLENEINSENSITIVE4 (EIN4) (Chang *et al.*, 1993; Hua *et al.*, 1995; Hua and Meyerowitz, 1998; Sakai *et al.*, 1998). These receptors have distinct but also overlapping functions in regulating ET signalling (Hao *et al.*, 2017), and they negatively regulate ET response via downstream CONSTITUTIVE TRIPLE RESPONSE1 (CTR1), a Raf-like protein kinase (Kieber *et al.*, 1993; Hua and Meyerowitz, 1998; Huang *et al.*, 2003). The ET signalling relies on the function of EIN2, an integral membrane protein that locates at the endoplasmic reticulum and acts downstream of CTR1 as a positive and central regulator of the ET response (Bisson *et al.*, 2009; Bisson and Groth, 2011). The stability of EIN2 is regulated by two F-box proteins, EIN2 TARGETING PROTEIN 1 (ETP1) and ETP2, which target the carboxyl-terminal end (CEND) of EIN2 and mediate EIN2 degradation through the ubiquitin–proteasome system (Qiao *et al.*, 2009). When ET is absent, both ET receptors and CTR1 are active, and CTR1 inhibits EIN2 activity by phosphorylation of the EIN2-CEND (Ju *et al.*, 2012). This results in an EIN3-BINDING PROTEIN 1 (EBF1)/EBF2-mediated proteasomal degradation of downstream TFs EIN3/EIN3-LIKE1(EIL1) (Guo and Ecker, 2003; Potuschak *et al.*, 2003; An *et al.*, 2010), key positive regulators for transcriptional activation of all ET response genes (Chao *et al.*, 1997; Chang *et al.*, 2013), and therefore the ET response is not activated. In the presence of ET, the EIN2-CEND is dephosphorylated, which is critical for its cleavage and translocation into the cytoplasm-localised P-bodies (Li *et al.*, 2015; Merchante *et al.*, 2015) or into the nucleus (Qiao *et al.*, 2012). In the P-body, EIN2-CEND represses the translation of EBF1/EBF2 (Li *et al.*, 2015; Merchante *et al.*, 2015). In the nucleus, EIN2-CEND stabilises EIN3/EIL1 proteins and thereby activating EIN3-based ET response (An *et al.*, 2010; Chang *et al.*, 2013).

Since ET promotes the senescence in different plant species, Schippers *et al.* (2015) have investigated and compared the EIN3-based transcriptional network between Arabidopsis and rice. They examined the promoters of the rice orthologs of 159 Arabidopsis *SAGs* to which EIN3 can bind (Guo *et al.*, 2004; Buchanan-Wollaston *et al.*, 2005), and over 90% of them showed at least one EIN3 core binding site. This conservation in apparent EIN3 binding sites

suggests that ET signalling pathways during leaf senescence might be similar between monocots and dicots (Schippers *et al.*, 2015).

Strigolactones

Strigolactones (SLs) are plant hormones that have important roles in plant development including seed germination (Toh *et al.*, 2012), shoot branching (Gomez-Roldan *et al.*, 2008; Umehara *et al.*, 2008), root architecture (Kapulnik *et al.*, 2011; Ruyter-Spira *et al.*, 2011; Rasmussen *et al.*, 2012) and in responses to environmental stresses such as drought and salt stress (Bu *et al.*, 2014; Ha *et al.*, 2014). SL has also been suggested to regulate natural- and dark-induced leaf senescence based on SL-deficient and -insensitive mutants showing a delayed senescence phenotype in Arabidopsis, petunia and rice (Woo *et al.*, 2001; Snowden *et al.*, 2005; Yan *et al.*, 2007; Hamiaux *et al.*, 2012; Yamada *et al.*, 2014; Ueda and Kusaba, 2015).

In Arabidopsis, the *oresara9* (*ore9*) mutant (the first identified SL-related mutant), which later was found to have a defect in SL signalling gene *MORE AXILLARY GROWTH2* (*MAX2*), exhibited delayed age-dependent leaf senescence and increased shoot branching (Woo *et al.*, 2001; Stirnberg *et al.*, 2002). *MAX2* is a F-box protein that regulates both SL and karrikin (KAR; a class of butanolide compounds discovered in smoke and are known to promote seed germination) signalling (Nelson *et al.*, 2011; Waters *et al.*, 2012). However, only the mutants that have defects in SL biosynthetic genes (*MAX1*, *MAX3* and *MAX4*) and receptor gene *DWARF14* (*AtD14*) but not the KAR signalling gene (*KARRIKIN INSENSITIVE2*; *KAI2*) showed a delay in dark-induced leaf senescence. This suggests that only SL and not KAR is involved in the regulation of leaf senescence (Ueda and Kusaba, 2015). The developmental senescence of the SL signalling and biosynthesis mutants, *max2-4* and *max4-11*, have also been examined, and the delayed yellowing has been observed supporting the involvement of SLs during age-dependent senescence (Ueda and Kusaba, 2015). Exogenously treated SL analogue *rac*-GR24 (a racemic mixture of GR24) restored normal senescence phenotype in the mutants defective in SL biosynthesis but not signalling upon dark incubation (Ueda and Kusaba, 2015).

The SL biosynthetic genes *MAX1*, *MAX3* and *MAX4* increase their transcript abundances during dark-induced leaf senescence, suggesting their involvement in this process (Ueda and Kusaba, 2015). However, it is difficult to determine whether SLs are synthesised in the leaf or transported from roots to promote senescence due to the technique limitation for measuring endogenous SL content (Seto *et al.*, 2014; Lv *et al.*, 2018). Ueda and Kusaba (2015) performed a grafting experiment and used Col-0 WT as the scion and *max4-11* mutant as the stock. They found that leaves from *max4-11* showed delayed senescence compared to that of WT suggesting SLs are likely produced in WT leaves in the dark to promote senescence because they cannot be produced by the SL-deficient mutant *max4-11* (Ueda and Kusaba, 2015).

Although the mechanism behind SL-mediated natural- or dark-induced senescence is still not clear, SL has been recently proposed to accelerate leaf senescence by enhancing the action of ET in *Arabidopsis* (Ueda and Kusaba, 2015).

Cytokinin

Cytokinins (CKs) have been considered to have the strongest influence on delaying leaf senescence compared with other hormones (Schippers *et al.*, 2007). It has been reported that CK delays senescence by preventing chloroplast degradation (Eugenia Gómez-Lobato *et al.*, 2012).

Endogenous CK levels decline before senescence starts and this is thought to be one of the key events that initiates senescence (Gan and Amasino, 1995). Consistently, transcriptome analysis found that transcript abundances of many CK-associated genes, which are involved in CK biosynthesis, such as genes encoding CK synthase and isopentenyl phosphotransferase, and in CK signalling including the type A response regulators (ARR4, ARR5, ARR6, ARR7 and ARR9), are decreased during leaf senescence; while a CK oxidase gene that functions in CK degradation is up-regulated during senescence (Buchanan-Wollaston *et al.*, 2005). This supported the hypothesis that CK has an antagonistic function in leaf senescence.

Since a reduced level of endogenous CK appears essential for the initiation of senescence (Breeze *et al.*, 2011), it was expected that over-production of CK could increase the longevity of leaves. This has been confirmed by the observation that transgenic plants with the pro*SAG12*:*IPT* transgene show delayed age-induced senescence (Gan and Amasino, 1995; Zwack and Rashotte, 2013). A similar system was also used for delaying stress-induced senescence by using a stress-induced promoter to drive *IPT* expression (Rivero *et al.*, 2007). Therefore, increasing exogenous CK production can delay both age-related and stress-induced senescence.

In *Arabidopsis*, the CK signal is perceived by three histidine kinase receptors, AHK2 (Arabidopsis histidine kinase), AHK3 and AHK4 (Ueguchi *et al.*, 2001). Of these three receptors, AHK3 plays a major role in regulating CK-dependent leaf senescence by specific phosphorylation of type B response regulator ARR2 and transcriptional induction of CK response factor CRF6 (Kim *et al.*, 2006a; Zwack *et al.*, 2013). However, whether ARR2 interacts with CRF6 in regulating leaf senescence remains to be examined. CRF6 acts as a negative regulator of dark-induced leaf senescence and its transcription is induced by CK and multiple abiotic stresses (Zwack *et al.*, 2013). For example, CRF6 has been reported to be transcriptionally induced by oxidative stress and it repressed CK-related genes in response to stress (Zwack *et al.*, 2016).

Although several key receptor genes and TFs involved in upstream CK signalling have been identified, the mechanism of downstream signalling in delaying leaf senescence is not well-understood. One probability is that CK delays senescence by increasing the activity of extracellular invertase (Lara *et al.*, 2004). The function of invertase is to catalyse hydrolytic cleavage of sucrose into hexoses, which are then uploaded to the sink organs to be metabolised and eventually transported into adjacent cells (Roitsch and Gonzalez, 2004). The rate of this metabolism is a key determinant of the sink strength of plant tissues (Roitsch and Tanner, 1996). By elevating the extracellular invertase activity, CK increases the sink feature of plant tissues. Once the enzyme activity is inhibited, CK fails to prevent leaf senescence in transgenic tobacco plants (Lara *et al.*, 2004). Although CK seems to modulate senescence by regulating

the activity of extracellular invertase, the link between upstream regulators such as ARR2 and CRF6 and downstream enzyme activity is still not clear and further investigation is required.

1.2.1.3. Degradation pathways

Chloroplast degradation

Visible yellowing is the most conspicuous phenotype of senescence, which is caused by the ordered dismantling of chloroplasts and breakdown of Chl in mesophyll cells during early stages of senescence (Hörtensteiner and Feller, 2002). The significance of Chl breakdown during senescence is to detoxify the phototoxic pigments (coloured Chl intermediates) to sustain viability of the senescing cell for degradation of chloroplast proteins and thereby facilitating the efficient remobilization of nitrogen (Hörtensteiner, 2004, 2006). Chloroplast degradation involves both Chl breakdown and proteolysis, and their catabolic pathways are normally correlated during senescence (Hörtensteiner and Feller, 2002).

Chlorophyll catabolism (PAO pathway)

In the absence of a functional light-harvesting complex (LHC) and photosynthetic apparatus, Chl is highly phototoxic. Chl catabolism is therefore essential for the survival of senescing cells and recycling of nitrogen because it is a prerequisite for degradation of chlorophyll-binding proteins such as LHC II which account for approximately 20% of cellular nitrogen (Hörtensteiner and Feller, 2002; Hörtensteiner and Kräutler, 2011).

So far, the best characterised mechanism of Chl breakdown is the 'PAO pathway' (Figure 1.2), which is named after a key enzyme pheophorbide *a* oxygenase (PAO) in this pathway (Hörtensteiner, 2013). PAO accounts for the oxygenolytic opening of chlorine macrocycle of pheophorbide *a* (pheide *a*), which provides the typical structural basis identified in all downstream catabolic products (Hörtensteiner, 2013). The PAO pathway can be separated into two parts. In the first part (also known as detoxification of coloured Chl intermediates), the reactions are localised in the plastid and start with removal of the Mg atom in the centre of chlorin ring and end with formation of a non-

phototoxic primary fluorescent Chl catabolite (pFCC). The second part includes subsequent modification of pFCC and isomerisation of modified FCCs to non-fluorescent Chl catabolites (NCCs) and these reactions occur in the cytosol and vacuole respectively (Hörtensteiner, 2013). At least five enzymes have important roles in the Chl catabolic pathway (Sakuraba *et al.*, 2012), which are NONYELLOW COLORING1 (NYC1), NYC1-LIKE (NOL), pheophytinase (PPH), PAO and red Chl catabolite reductase (RCCR).

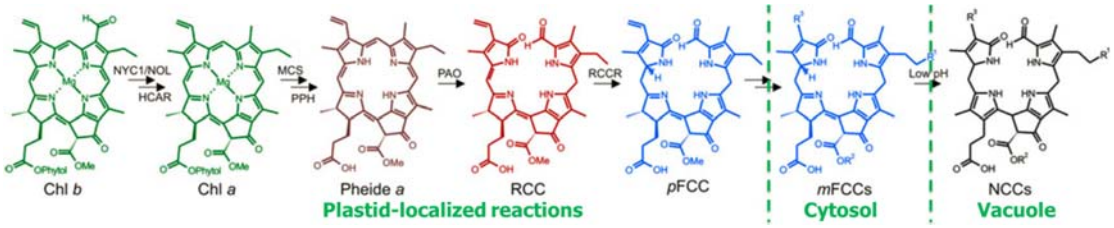

Figure 1.2. The PAO pathway of Chl catabolism
The chemical structures of chl and chl catabolites and relevant catabolic enzymes are displayed. R1–R3 in mFCCs and NCCs represent the species-specific modifications. Green dash lines separate the reactions that occur in plastid, cytosol and vacuole. Abbreviations: Chl, chlorophyll; FCC, fluorescent Chl catabolite; HCAR, hydroxy-Chl *a* reductase; MCS, metal-chelating substance; mFCC, modified FCC; NCC, non-fluorescent Chl catabolite; NYC1/NOL, NON YELLOW COLORING1/NYC-ONE LIKE; PAO, pheide a oxygenase; pFCC, primary FCC; Pheide, pheophorbide; PPH, pheophytinase; RCC, red Chl catabolite; RCCR, RCC reductase. Figure was edited from Hörtensteiner (2013).

Conversion of Chl *b* to Chl *a* has been considered to be the initial step of Chl breakdown as all NCCs are derived from Chl *a* in higher plants (Hörtensteiner *et al.*, 1995). This two-step reaction is catalysed by Chl *b* reductase (encoded by two genes *NYC1* and *NOL* in *Arabidopsis* and rice) and 7-HYDROXYMETHYL Chl *a* REDUCTASE (HCAR), respectively (Kusaba *et al.*, 2007; Horie *et al.*, 2009; Meguro *et al.*, 2011). In the following step, the central Mg atom of Chl *a* is removed by metal chelating substance (MCS) which converts Chl *a* to phein *a*, and then PPH dephytylates phein *a* to pheide *a* (Schelbert *et al.*, 2009). The next reaction is catalysed by PAO, which oxygenolytically opens the chlorine macrocycle of pheide *a* and yields red Chl catabolite (RCC) (Hörtensteiner, 2009). By the end of the first part, RCCR catalyses the site-specific reduction of RCC to colourless pFCC (Hörtensteiner, 2013). This product is then transported to cytosol for species-specific

modification, and finally to be isomerised and stored in vacuole as NCCs (Christ and Hörtensteiner, 2013).

Stay-green mutants

Stay-green mutants refer to the mutants that exhibit a delayed tissue degreening. They can be classified into two major categories, functional and non-functional (cosmetic) mutants (Thomas and Howarth, 2000; Hörtensteiner, 2009). Functional stay-green mutants exhibit a defect in initiation (type A) or progression (type B) of senescence and their delayed Chl degradation (compared with WT) is correlated with retention of photosynthetic activity; whereas non-functional stay-green mutants (type C) only affect the Chl breakdown but not progression of senescence (Thomas and Howarth, 2000; Hörtensteiner, 2009). Consistently, in type C stay-green mutants, Chl degradation is compromised, while stromal proteins, specifically Rubisco, still degrade as in the WT (Thomas *et al.*, 2002; Park *et al.*, 2007).

Functional stay-green mutants have both agronomic and economic importance as they seem to have a positive influence on crop yield by delaying leaf senescence and maintaining photosynthetic capacity (You *et al.*, 2007; Hörtensteiner, 2009). For instance, a field experiment found that the highest yield of maize was obtained from the variety FS854 that has a stay-green trait (Thomas and Howarth, 2000). Similarly, a type B functional stay-green variant of *japonica* rice (named SNU-SG1) showed positive correlation with grain yield (You *et al.*, 2007). These findings support the hypothesis that functional stay-green mutants delay the onset or progression of senescence rather than only disrupt by Chl breakdown.

Non-functional stay-green phenotype is commonly caused by a defect of the genes that encoding Chl catabolic enzymes. For example, Mutants defective in *NYC1*, *NOL* and *PPH* show a stay-green phenotype with delayed degradation of LHC II subunits but not of Rubisco, which is one of the distinctive features of cosmetic stay-green mutants (Kusaba *et al.*, 2007; Horie *et al.*, 2009; Schelbert *et al.*, 2009). Interestingly, mutating *NYC1* in either *Arabidopsis* or rice but only *NOL* in rice exhibit a stay-green phenotype, which indicates NOL may function

differently in these two species. In addition, these mutants exhibit high retention of Chl *b* and LHC II, suggesting Chl *b* reductase might play an important role in LHC II degradation though the mechanism is unclear so far (Kusaba *et al.*, 2007; Horie *et al.*, 2009). Likewise, mutants defective in PAO and RCCR retain more Chl than WT, while they also induce lesion mimic phenotypes (mutants show necrotic lesions without presence of pathogens) which is due to the accumulation of phototoxic Chl catabolic intermediates (Lim *et al.*, 2007). This reveals the importance of detoxification of coloured Chl catabolites during senescence. Furthermore, stay-green phenotypes in many plant species are also caused by mutations in another gene termed *STAY-GREEN* (*SGR*). SGR proteins are not directly involved in Chl catabolism, but they are required for destabilization of Chl binding protein complexes and therefore facilitate the Chl catabolic enzymes to interact with their substrate (Hörtensteiner, 2009; Hörtensteiner, 2013).

Degradation of chloroplast proteins

Chloroplasts contribute up to 75% of the nitrogen in mesophyll cells, and the majority of the nitrogen (55%) is contributed by stromal proteins (mostly in the form of Rubisco) while the remaining fraction (20%) is from thylakoid proteins (especially LHC II) (Hörtensteiner and Feller, 2002; Lee *et al.*, 2013). Degradation of proteins and subsequent export of resulting catabolites from aging leaves provide the majority of the nitrogen for the sink organs during senescence (Hörtensteiner and Feller, 2002).

The chloroplast stroma contains many enzymes involved in photosynthesis and nitrogen assimilation such as glutamine synthetase and Rubisco (Hörtensteiner and Feller, 2002). During early stages of senescence, these proteins degrade rapidly in intact chloroplasts and their degradation leads to the decline of photosynthetic capacity. Rubisco, a dominant stromal enzyme in plants, is a major contributor of nitrogen in chloroplast. It has been proposed that the initiation of Rubisco degradation is induced by reactive oxygen species (ROS), because the large subunit of Rubisco could be directly cleaved by active oxygen (Ishida *et al.*, 1997; Hörtensteiner and Feller, 2002). The degradation of Rubisco has long been considered to occur in the chloroplast. However, as yet

no chloroplast protease has been identified that specifically breaks down Rubisco (Lee *et al.*, 2013; Carrion *et al.*, 2014). On the other hand, an extra-plastidial degradation pathway has been proposed, which suggests that Rubisco might be transported to the senescence-associated vacuoles and degraded by the cysteine proteases inside (Carrion *et al.*, 2014). However, this hypothesis needs to be further confirmed.

Although degradation of thylakoid proteins is not well understood, LHC II and Rubisco subunits degrade at similar rates during senescence in WT plants. In contrast, Chl catabolic mutants retain more Chl and LHC II, but not Rubisco subunits (Hörtensteiner and Feller, 2002). This suggests that Chl breakdown is the prerequisite for degradation of LHC II. However, enzymes that participated in digestion of LHC II have not been identified so far.

Other catabolic processes

Macromolecules, such as regulatory proteins, lipids and sugars, are also degraded and recycled during leaf senescence. Protein turnover and nutrient reallocation appear to be controlled by the ubiquitin-26S proteasome pathway, which is different from degradation of chloroplast proteins (Yoshida, 2003; Lin and Wu, 2004). Metabolism of lipids, particularly membrane lipids, occurs in early stages of leaf senescence and leads to increased membrane permeability and electrolyte leakage (Thompson *et al.*, 1998; Rolny *et al.*, 2011). Membrane lipids are catabolized by four lipolytic enzymes (phospholipase D, phosphatidic acid phosphatase, lipolytic acyl hydrolase and lipoxygenase) and this process is important for remobilization of lipid phosphate and fatty acids (Thompson *et al.*, 1998). Sugars derived from photosynthesis in mature ‘source’ leaves, especially sucrose, is catabolized and exported in the form of hexoses to growing sinks such as young leaves and seeds (Rolland *et al.*, 2006). By contrast, the nucleus and mitochondria remain intact until the final stages of senescence, probably because they provide instructions and energy respectively for the completion of senescence (Lim *et al.*, 2007).

1.2.2. Regulation of postharvest stress-induced leaf senescence

Senescence of plant organs can be prematurely induced by a range of postharvest stresses including wounding (e.g. detachment), energy deprivation (e.g. darkness and sugar starvation) and water deficiency (Hunter *et al.*, 2011; Trivellini *et al.*, 2012; Liebsch and Keech, 2016). Understanding the genetic and molecular mechanisms behind such organ deterioration may provide a new strategy for extending storage and shelf life of agriculturally important plants and plant products by manipulating key genes that control postharvest senescence.

1.2.2.1. Genes and transcription factors

Comparison of transcriptome data between detached-dark-induced and age-dependent senescence

It has long been thought that the genetic programmes of senescence in attached leaves and detached dark-held leaves are very different (Becker and Apel, 1993; Weaver *et al.*, 1998). This was also supported by microarray meta-analysis done by Buchanan-Wollaston *et al.* (2005) who compared transcriptome changes occurring in leaves of dark-held plants, sucrose-starvation induced cell cultures and natural senescence. However, another transcriptome study has revealed that in addition to these differences there are also remarkable similarities (van der Graaff *et al.*, 2006). For instance, approximately 77% of the genes up-regulated during senescence of detached dark-held leaves are also upregulated during natural senescence. However, the total number of genes specific to natural senescence is nearly two times higher than that of genes specific to senescence of detached dark-held leaves or attached shaded leaves (van der Graaff *et al.*, 2006). This might imply that more metabolic processes are activated during natural senescence compared with senescence of detached dark-held leaves and attached shaded leaves. Interestingly, the gene expression patterns of senescence induced by various treatments are similar to those of natural senescence at the execution stage of senescence (after the senescence is initiated) but are significantly different at the initiation stage (Guo and Gan, 2012). This suggests that the progression of natural senescence and artificially-induced senescence share many catabolic processes.

Transcription factors

Although some WRKY TFs such as WRKY6 and WRKY53 play important roles in developmental-dependent senescence, other members in this family are also found to be key regulators in stress-induced senescence. For example, over-expression of *AtWRKY22* and *OsWRKY23* accelerate detached dark-held leaf senescence in *Arabidopsis* and rice respectively (Jing *et al.*, 2009; Zhou *et al.*, 2011). *AtWRKY22* expression is strongly induced by darkness and H_2O_2 but suppressed by light, suggesting its role in response to abiotic stress. It has been suggested that AtWRKY22 regulates dark-induced senescence by mutual interaction with other WRKY TFs including WRKY53, WRKY6 and WRKY70 (which are key regulators in age-related senescence) and thereby indirectly influence the expression of several *SAG*s such as *SAG12* and *SAG20* (Zhou *et al.*, 2011). This implies that WRKY TFs control both age- and stress-induced senescence in a rather complex manner and further studies are required for uncovering their regulatory network.

Unlike dark-induced *AtWRKY22* and *OsWRKY23*, several TFs are involved in regulating both developmentally- and detachment-dark-induced leaf senescence processes. Some representative examples of these TFs are ANAC092/AtNAC2/ORE1 (NAC TF) (kim, 2009; Balazadeh *et al.*, 2010), RAV1 (RAV TF) (Woo *et al.*, 2010), EIN3 (Chao *et al.*, 1997) and AZF2 (Cys2/His2 type zinc finger protein) (Li *et al.*, 2012). All of them are the positive regulators of developmentally- and detachment-dark-induced leaf senescence. Taken together, these findings reveal that TFs regulate age- and stress-induced senescence; however, how distinct TFs interact to contribute to senescence is not clearly understood.

1.2.2.2. Phytohormones

Plant hormones have important roles in both age-dependent and stress-induced senescence and their signalling pathways show both similarities and differences. For example, ET, JA and SA pathways control gene expression during natural senescence and ET and JA (but not SA) pathways regulate gene expression during leaf senescence of dark-held plants and sucrose-starvation induced cell cultures (Buchanan-Wollaston *et al.*, 2005).

A detailed characterization of JA-related genes found that 11 of 19 JA-biosynthesis and 6 of 11 JA-response or signalling genes are differentially expressed but some of them show remarkably different expression patterns in natural senescence, senescence of detached dark-held leaves and attached shaded leaves (van der Graaff *et al.*, 2006). For instance, eight of 11 differentially expressed JA-biosynthesis genes are specifically and transiently activated in natural senescence but not in senescence of detached dark-held leaves or attached shaded leaves. However, two JA-biosynthesis genes encoding AtLOX1 and AtαDOX1 are only activated in senescence of detached dark-held leaves but not in natural senescence or attached shaded leaves, indicating these two genes are induced by wounding.

The SA-regulated signalling pathway is essential for plant stress response and it seems to be specifically involved in developmental- but not dark-induced senescence, because most of senescence-associated SA-responsive genes are up-regulated in response to age-related senescence but are either not or weakly expressed in detached dark-held leaves or attached shaded leaves (van der Graaff *et al.*, 2006). In Arabidopsis, transgenic plants with reduced SA levels, caused by overexpression of bacterial gene *SALICYLIC HYDROXYLASE* (*NahG*), exhibit delayed leaf degreening during age-related but not dark-induced senescence (Morris *et al.*, 2000; Buchanan-Wollaston *et al.*, 2005).

1.2.2.3. Senescence-induced nutrient catabolism

Nitrogen remobilisation

Nitrogen remobilization, a crucial catabolic process during senescence, shows alternative pathways in natural senescence and senescence of detached dark-held leaves (Lin and Wu, 2004; Buchanan-Wollaston *et al.*, 2005; van der Graaff *et al.*, 2006). Nitrogen is transported as glutamine (GLN) during natural senescence but as asparagine (ASN) during senescence of detached dark-held leaves. This makes biological sense as ASN contains less carbon than GLN and therefore serves as a major nitrogen carrier during carbon deprivation-induced senescence that is caused by darkness (Lam *et al.*, 1994; Lin and Wu, 2004; Buchanan-Wollaston *et al.*, 2005). Consistently, the transcript abundance

of genes encoding the ASN-biosynthetic enzymes such as *ASPARAGINE SYNTHASE* and *GLUTAMATE DEHYDROGENASE* is substantially increased during dark-induced senescence but not during natural senescence. In contrast, genes involved in ammonia assimilation (e.g. *GLUTAMINE SYNTHETASE*) and genes encoding glutamate decarboxylases are up-regulated in natural senescence but not in senescence of detached dark-held leaves (Buchanan-Wollaston *et al.*, 2005; van der Graaff *et al.*, 2006). Glutamate decarboxylase plays a role in the conversion of glutamate to GABA (4-aminobutyrate), which presumably functions as a signalling molecule to balance carbon to nitrogen ratio during natural senescence (Buchanan-Wollaston *et al.*, 2005).

Carbohydrates

Carbohydrates, specifically sugars, function as both metabolites and signalling molecules during leaf senescence (Rolland *et al.*, 2006). The differences of transcriptome profiles between natural senescence and senescence of detached dark-held leaves are probably due to the dark-induced carbon-deprivation. To cope with the daily period of darkness, starch and sugars are produced in *Arabidopsis* leaves through photosynthesis during the day, which are then mostly used during the night. For example, it has been reported that only 10% of starch and 50% of sucrose and reducing sugars are left by the end of the night compared with their accumulated amount during the day (Usadel *et al.*, 2008). If the night is extended, the carbohydrate contents fall to extremely low levels while the level of free amino acids such as phenylalanine and asparagine increase.

The dark-induced metabolite changes are executed by altering around 90% of the biochemical pathways (Lin and Wu, 2004). In dark-treated or otherwise sugar-starved leaves, numerous metabolic pathways are induced to provide alternative carbohydrate sources. For instance, β-oxidation genes which function in breaking down the straight chain fatty acids are activated during sugar depletion-induced but not developmentally-induced senescence because a sufficient sugar level must be maintained during natural senescence (Graham and Eastmond, 2002; Lin and Wu, 2004). Similarly, genes encoding enzymes that participate in branched-chain amino acid catabolic pathways are only

induced in dark-induced sugar-depleted cell culture tissue of Arabidopsis to provide an alternative carbon source (Fujiki *et al.*, 2000). Moreover, another signalling molecule trehalose-6-phosphate (T-6-P), also involved in regulation of sugar metabolism, may help the plant to cope with the carbohydrate imbalance that results from carbon-deprivation (Eastmond *et al.*, 2003; Thimm *et al.*, 2004). Genes encoding T-6-P synthase and T-6-P phosphatase are only up-regulated upon sucrose starvation during dark-induced senescence but not during natural senescence (Contento *et al.*, 2004; Buchanan-Wollaston *et al.*, 2005).

1.3. Flower senescence

1.3.1. General introduction of flower senescence

Flowers are essential for the plant life cycle as they are responsible for pollination and seed set for the next generation. Compared with leaves, flowers are more complex and are composed of many distinct components including sepals, petals and androecium/gynoecium. These organs interact with each other which makes the study of flower senescence more difficult (Ashman and Schoen, 1994; Oneill, 1997). Petal senescence commences after pollination whereas other floral organs (e.g. carpel) are still developing to produce siliques (Stead, 1992). This requires strict regulation and involves an ordered set of events including structural, biochemical and molecular changes (Hunter *et al.*, 2004b; Tripathi and Tuteja, 2007; Ahmad and Tahir, 2016). Such well-organised senescence program enables nutrients to be transported from petals to other sink tissues such as young leaves and developing ovary (Rogers, 2013).

In general, flower senescence is similar to leaf senescence. Previous study of sepal senescence in broccoli suggests that the sepal senescence is very similar to leaf senescence as it also requires degradation of Chl (Page *et al.*, 2001). In Arabidopsis, microarray analysis revealed numerous common regulators between developmental leaf senescence and dark-induced inflorescence senescence suggesting similarity of the molecular mechanism (Trivellini *et al.*, 2012).

However, petal senescence is more complex, and it shows both similarities and differences compared to leaf senescence. Evolutionarily, a petal is a leaf-derived floral organ (Bowman *et al.*, 1991; Friedman *et al.*, 2004) and petal senescence shares some common regulatory/degradation pathways with leaf senescence (Xu and Hanson, 2000; Price *et al.*, 2008). For example, both petal and leaf senescence require degradation of macromolecules (e.g. membrane proteins and nucleic acids) for nutrient recycling (Shahri and Tahir, 2011; Akhtar *et al.*, 2019) and the senescence processes are regulated by phytohormones such as ET and CK (Jibran *et al.*, 2013; Ma *et al.*, 2018). However, petal senescence is also distinct from leaf senescence in several aspects (Price *et al.*, 2008; Wagstaff *et al.*, 2009). For example, petal senescence is irreversibly and tightly controlled by developmental (e.g. activated by pollination) rather than environment signals, which is different from leaf senescence (Xu and Hanson, 2000; Chen *et al.*, 2002; Rogers, 2013; Woo *et al.*, 2019). In addition, ET-insensitive systems exist during petal senescence in some floral plant species (Woltering and Vandoorn, 1988); whereas ET has critical role in regulating leaf senescence (Jibran *et al.*, 2013). Since petal senescence is extensively investigated compared with other floral organs, some details of petal senescence are described below (Rogers, 2013; Ahmad and Tahir, 2016).

1.3.2. Regulation of petal senescence

Petals play important roles during flower development and they function primarily to promote pollination by attracting pollinators (Glover and Martin, 1998). The longevity of petals is also a key factor affecting vase life and quality of cut flowers in many ornamentals. Visible signs of petal senescence include colour change, wilting and abscission (Hunter *et al.*, 2004b). These are associated with a series of physiological changes including degradation of proteins (e.g. membrane proteins and regulatory proteins), nucleic acids, lipids and carbohydrates (Hunter *et al.*, 2004b; Tripathi and Tuteja, 2007; Ahmad and Tahir, 2016). Petal senescence is a genetically controlled and strictly regulated programme and is mediated by various phytohormones (Shahri and Tahir, 2014; Ma *et al.*, 2018; Shibuya, 2018). Some petal senescence-related hormones and genes are reviewed below.

Hormones

Like leaf senescence, plant hormones ET and ABA promote flower senescence whereas CK and GAs inhibit it [reviewed by Ma *et al.* (2018)]. Auxin can promote or delay senescence in different plant species, and JA has also been reported recently to affect petal senescence [reviewed by Ma *et al.* (2018)]. Here, some details of ET-dependent and ET-independent flower systems are reviewed.

Unlike ET-mediated leaf senescence, both ET-sensitive and -insensitive flower senescence systems exist (Woltering and Vandoorn, 1988). ET plays a central regulatory role during senescence in ET-sensitive flowering plants including Arabidopsis, petunia and carnation (Iqbal *et al.*, 2017; Ma *et al.*, 2018). In those ET-sensitive species, the production of endogenous ET has been suggested to be induced by developmental signals (e.g. pollination) (Woltering and Vandoorn, 1988; Shahri and Tahir, 2011). In carnation, after pollination, ET was produced in petals during senescence, and this is associated with the transcriptional increases of the ET biosynthetic genes such as genes encoding ACC synthase and ACC oxidase (Park *et al.*, 1992; tenHave and Woltering, 1997). Exogenously applied ET or its precursor (e.g. ACC) promoted senescence of the corolla in China rose flowers; whereas treatment with chemicals which inhibited ET biosynthesis or action delayed it (Trivellini *et al.*, 2011a; Trivellini *et al.*, 2011b). Besides biosynthesis, ET signalling is also involved in controlling flower senescence. For example, transgenic carnation and petunia plants expressing the Arabidopsis *etr1-1* gene exhibited delayed flower senescence and extended vase life (Wilkinson *et al.*, 1997; Bovy *et al.*, 1999). In petunia, transgenic plants expressing the *etr1-1* gene of Arabidopsis or with reduced expression of *PhEIN2* showed delays in flower senescence (Shibuya *et al.*, 2004). All these findings again indicate an essential role of ET in the acceleration of flower senescence in diverse ET-sensitive species.

In plant species with ET-insensitive flower systems (e.g. tulip and daylily), ET appears to not affect (or have little effect on) petal senescence though it may be still involved in other plant organ/tissue development such as pedicel elongation and ovary development (Woltering and Vandoorn, 1988; Shahri and

Tahir, 2011; Woltering, 2017). Endogenous ET levels did not show significant increase during petal senescence, and treatment with exogenous ET or chemicals preventing ET action did not show a dramatic effect on petal senescence (Woltering and Vandoorn, 1988). This suggests petal senescence is likely regulated by an ET-independent pathway. In some ET-independent species, ABA is thought to be the primary regulator of petal senescence (Borochov and Woodson, 1989; Panavas *et al.*, 1998; Hunter *et al.*, 2004a). Treatment with exogenous ABA promotes senescence in certain flowers (Borochov and Woodson, 1989). In daffodil (*Narcissus pseudonarcissus*), endogenous ABA content increased in the petals during flower senescence, while exogenous ABA treatment induced transcript abundances of *SAGs* and such ABA-dependent induction was not affected when flowers were pre-treated with an inhibitor of ET action, suggesting this ABA-mediated transcript accumulation is independent of ET (Hunter *et al.*, 2004a). In the petals of ET-insensitive daylily, many senescence-associated changes such as increased ion leakage and proteinase activity were stimulated by exogenous ABA treatment (Panavas *et al.*, 1998). Although some studies have been carried out, the knowledge of the mechanism behind petal senescence in the ET-insensitive flowers is extremely limited thus far (Ma *et al.*, 2018).

ABA also regulates senescence in ET-sensitive flowers and its function is likely to be ET-dependent. For instance, ABA promotes ET production and petal senescence in carnation (Mayak and Dilley, 1976; Ronen and Mayak, 1981), while inhibiting ET signaling suppress ABA production and corolla senescence in petunia (Jones *et al.*, 2009). Other hormones including CK, GA, JA and auxin are also involved in regulation of flower senescence. These hormones do not work alone, but crosstalk with each other to control floral organ senescence (Iqbal *et al.*, 2017; Ma *et al.*, 2018). For example, the transgenic petunia flowers with increased CK production showed delayed corolla senescence and reduced sensitivity to ET (Chang *et al.*, 2003). In some cut roses and carnations, GA acts as antagonist of ET and delays petal senescence (Saks *et al.*, 1992; Saks and Van Staden, 1993; Lü *et al.*, 2014). All in all, phytohormones have essential roles in regulation of flower/petal senescence.

Genes and transcription factors

Petal senescence is thought to be one type of programmed cell death (PCD), and this process is genetically regulated (Rogers, 2006, 2013). Genes that control flower senescence have been identified in various plant species. These genes encode enzymes/proteins involved in phytohormone biosynthesis and signalling, macromolecule degradation (e.g. proteases, lipases and nucleases) and nutrient remobilisation (e.g. transporters) (Shahri and Tahir, 2014; Shibuya, 2018). For example, cysteine proteases are considered to regulate nutrient recycling from senescing floral organs. Genes encoding cysteine proteases have been reported to be induced during senescence in several flower systems [summarised in Shahri and Tahir (2014)]. Some of these genes, such as *SAG12* in Arabidopsis and its orthologues in *Brassica napus* (*BnSAG12-1* and *BnSAG12-2*) and in *Petunia hybrida* (*PhCP10*), have been commonly used as senescence markers (Noh and Amasino, 1999b; Jones *et al.*, 2005).

Genes encoding various TFs, such as NAC and MADS-box TF families, also play key regulatory roles during flower senescence (Shahri and Tahir, 2014; Shibuya, 2018). In the ET-dependent flower systems, including Arabidopsis, petunia and wallflower, multiple NAC genes show up-regulation during petal senescence suggesting their involvement in regulation of ET-mediated flower senescence (Price *et al.*, 2008; Wagstaff *et al.*, 2009; Broderick *et al.*, 2014). For instance, *NAP* and *ANAC092* were up-regulated during developmental-induced petal senescence in Arabidopsis (Wagstaff *et al.*, 2009), while a number of *NAC* genes were down-regulated in ET-insensitive corollas of transgenic petunias with induced expression of *etr1-1* (Wang *et al.*, 2013). In addition to these ET-dependent NACs, some NACs are involved in regulation of petal senescence in the ET-insensitive flower systems. For example, EPHEMERAL1 (EPH1), a TF with sequence similarity to ANAC092 in the NAM sub-family, has been reported to positively regulate petal senescence in the ET-independent Japanese morning glory 'Violet' (Shinozaki *et al.*, 2011; Shibuya *et al.*, 2014). The expression of *EPH1* was not affected by endogenous ET signals or exogenous treatment with an ET signalling inhibitor (Shibuya *et al.*, 2014). Transgenic plants with reduced expression of *EPH1* exhibited delayed petal but not leaf senescence (Shibuya *et al.*, 2014). Interestingly, the

transcript abundances of senescence marker *SAG12* ortholog and several PCD-related gene orthologs such as autophagy-related genes and a vacuolar processing enzyme gene were suppressed in those plants (Shibuya *et al.*, 2014). These findings suggested *EPH1* may be induced by developmental signals and it regulates petal senescence via up-regulation of PCD-related genes in the ET-insensitive flower system.

MADS-box TFs are widely involved in regulating multiple plant developmental processes such as floral organ specification and flower senescence (Smaczniak *et al.*, 2012; Chen *et al.*, 2015). In Arabidopsis, overexpression of MADS-box genes *AGL15* (*AGAMOUS like 15*) or *AGL18* results in delay in perianth senescence and abscission, suggesting they act as negative regulators during flower senescence and abscission (Fernandez *et al.*, 2000; Fang and Fernandez, 2002; Adamczyk *et al.*, 2007). Similarly, *AGL42* (also known as *FOREVER YOUNG FLOWER*; *FYF*) also function as a repressor of floral organ senescence by suppressing ET responses (Chen *et al.*, 2011a; Chen *et al.*, 2015). *AGL42* overexpression lines exhibited significant delay in senescence and abscission of perianth organs (Chen *et al.*, 2011a). This gene also negatively regulates *Ethylene Response DNA-binding Factors 1 to 4* (*EDF1/2/3/4*) in the ET pathway (Chen *et al.*, 2015). Recently, AGAMOUS, another MADS-box gene, has been reported to promote sepal senescence by driving JA production in Arabidopsis (Jibran *et al.*, 2017). These findings reveal essential roles of MADS-box TFs in controlling flower senescence in Arabidopsis.

1.3.3. Regulation of postharvest stress-induced inflorescence senescence

Compared with the extensively investigated leaf and petal senescence (as described above), less is known about postharvest inflorescence senescence. Some studies were carried out on a commercial vegetable broccoli and the model plant Arabidopsis.

Broccoli

Broccoli (*Brassica oleracea* L. *italica*) is considered as one of the healthiest vegetables in the world because it has high content of vitamins and minerals and it also provides many beneficial compounds such as flavonoids, antioxidants and glucosinolates (Chen *et al.*, 2008; Eugenia Gómez-Lobato *et al.*, 2012).

The head of broccoli is composed of a number of immature florets and each consists of a flower enclosed by Chl-containing sepals (Page *et al.*, 2001; Chen *et al.*, 2008). After harvesting, this floret head deteriorates rapidly (within 2-4 days) if stored at room temperature and the most visible phenotype is the yellowing of peripheral sepals which is caused by Chl degradation (Chen *et al.*, 2008) and accompanied by the transcriptional increase of a broccoli SGR gene (Gomez-Lobato *et al.*, 2014). The rapid deterioration of broccoli might be due to a series of postharvest stresses such as loss of water that is normally supplied from roots and reduced phloem import. Sugar-starvation might be one of the major stresses in harvested and dark-stored broccoli heads, which changes the sugar-mediated signalling and metabolism. It has been found that the floret head of broccoli loses almost 50% of their sucrose within 6 h after detachment, while the transport of amino acids such as glutamine and asparagine and ammonia levels increase (Downs *et al.*, 1997). More recently, a study found that the inflorescence type had an effect on the physiological changes of cut broccoli during storage. The primary florets showed lower Chl degradation, less sugar lost and dehydration than lateral florets during storage (Hasperué *et al.*, 2015).

Plant hormone levels are also affected by postharvest stresses. For instance, a burst of ET is produced by broccoli florets after harvest and this probably plays a role in regulating the postharvest sepal degreening (Chen *et al.*, 2008). Interestingly, a high level of ET is produced by the reproductive organs, especially the stamens; whereas relatively low amounts of ET is produced by the sepals and only subsequent to ET produced by the reproductive organs (Tian *et al.*, 1994). The yellowing of sepals is more likely caused by the increased ET that is produced by reproductive organs rather than ET production

by the sepals because removing these reproductive organs reduces the rate of sepal degreening (Tian *et al.*, 1994). Transgenic broccoli with reduced ET production, caused by driving the expression of an antisense ACC oxidase (*BoACO2*), shows delayed Chl loss, declined protease activity and higher content of total protein (Gapper *et al.*, 2005). Similarly, transgenic broccoli with reduced expression of *ACO1*, *ACO2* or *ACS1* exhibit extended shelf life (Higgins *et al.*, 2006).

Consistent with the senescence-inhibiting role of CKs, import of this hormone in broccoli floret heads decreases as a result of detachment. Exogenous application of CK (Tian *et al.*, 1995) or increasing endogenous CK production by over-expressing the CK-biosynthetic gene *IPT* (Chen *et al.*, 2001b) delays floret degreening in broccoli. It has been suggested that CK-mediated retardation of postharvest senescence in transgenic broccoli with *IPT* is caused by the accumulated antioxidant enzyme activity and stress-responsive proteins (Liu *et al.*, 2011).

Arabidopsis

Although some molecular and biochemical mechanisms of postharvest inflorescence senescence are characterised in broccoli (described above), many biological events are not clear so far. Since the transformation of broccoli is time- and space-consuming, a more convenient system is expected to help understand the mechanisms of postharvest senescence in broccoli.

Arabidopsis thaliana, belonging to the *Brassicaceae* family, is a popular model organism that is widely used for studying genetics, cellular and molecular biology, evolution and development in plant science research because of the following advantages: a small and fully sequenced genome, a fast life cycle, small size of adult plants, prolific seed production, efficient transformation, and availability of a large number of mutant lines (TAIR, https://www.arabidopsis.org/). It has been used widely for investigating the biological mechanisms of age- and stress-induced senescence in leaves (see Section 1.2). Recently, it has also been used for studying the postharvest inflorescence senescence (Trivellini *et al.*, 2012; Jibran *et al.*, 2015) and is

considered to be an ideal model for elucidating the gene functions in postharvest broccoli because extensive collinearity between these two genomes for chromosomal segments has been found (Li *et al.*, 2003).

During dark treatment of Arabidopsis inflorescences, the detached immature inflorescences undergo a series of phenotypical and physiological changes, including growth arrest (no flower opening or pedicel elongation), degreening (due to the Chl loss), reduced soluble protein content and increased ion leakage (Trivellini *et al.*, 2012). Phytohormones also had significant effect on the timing of inflorescence degreening. For example, treatment with ABA promoted the yellowing of detached inflorescence; whereas treatment with 6-benzylaminopurine (synthetic CK) delayed this process (Trivellini *et al.*, 2012).

*SAG*s that were differentially regulated during dark-induced inflorescence senescence were also identified (Trivellini *et al.*, 2012). A large number of genes are differentially expressed during both leaf and inflorescence senescence, notably senescence marker gene *SAG12* and senescence-related TF genes such as *ANAC092* and *NAP* (Trivellini *et al.*, 2012). This supports the idea that senescence of some floral organs such as sepals and petals is generally similar to leaf senescence (Page *et al.*, 2001; Price *et al.*, 2008). Genetic analysis also confirmed the roles of some common regulators in controlling dark-induced inflorescence senescence. For example, the defective mutants of *ANAC092* and *NAP* exhibited delayed senescence of cut inflorescences upon dark treatment (Trivellini *et al.*, 2012). In addition, mutants with a defect in *NYC1* also showed delayed senescence of both cut and attached inflorescences when treated in the dark (Jibran *et al.*, 2015). Although some regulators have been identified in Arabidopsis, our knowledge of postharvest stress-induced inflorescence senescence is still limited and further investigation is required.

1.4. Research background

To identify key genes that regulate dark-induced inflorescence senescence in Arabidopsis, a forward genetic approach was applied, and large numbers of ethyl methanesulfonate (EMS) mutants were screened by previous researchers using the Arabidopsis Inflorescence Degreening Assay (AIDA) (Jibran *et al.*, 2015). AIDA allowed the isolation of a number of mutants that show altered timing of inflorescence senescence (Jibran, 2014; Jibran *et al.*, 2015).

Mutants whose immature inflorescences show complete yellowing at day 3 of dark incubation (two days ahead of WT) were named *accelerated inflorescence senescence* (*ais*) while those that exhibit delayed degreening at day 5 compared with WT were named *delayed inflorescences senescence* (*dis*). In total, 10 *ais* and 20 *dis* were identified and their inflorescence degreening phenotypes are shown in Figure 1.3 (Jibran, 2014). Based on this preliminary screen, a total of twenty-one mutants (16 from reported data, see figure 1.3 and 5 from unpublished data) that showed altered time to degreening were used for the further physiological and genetic analysis in this study.

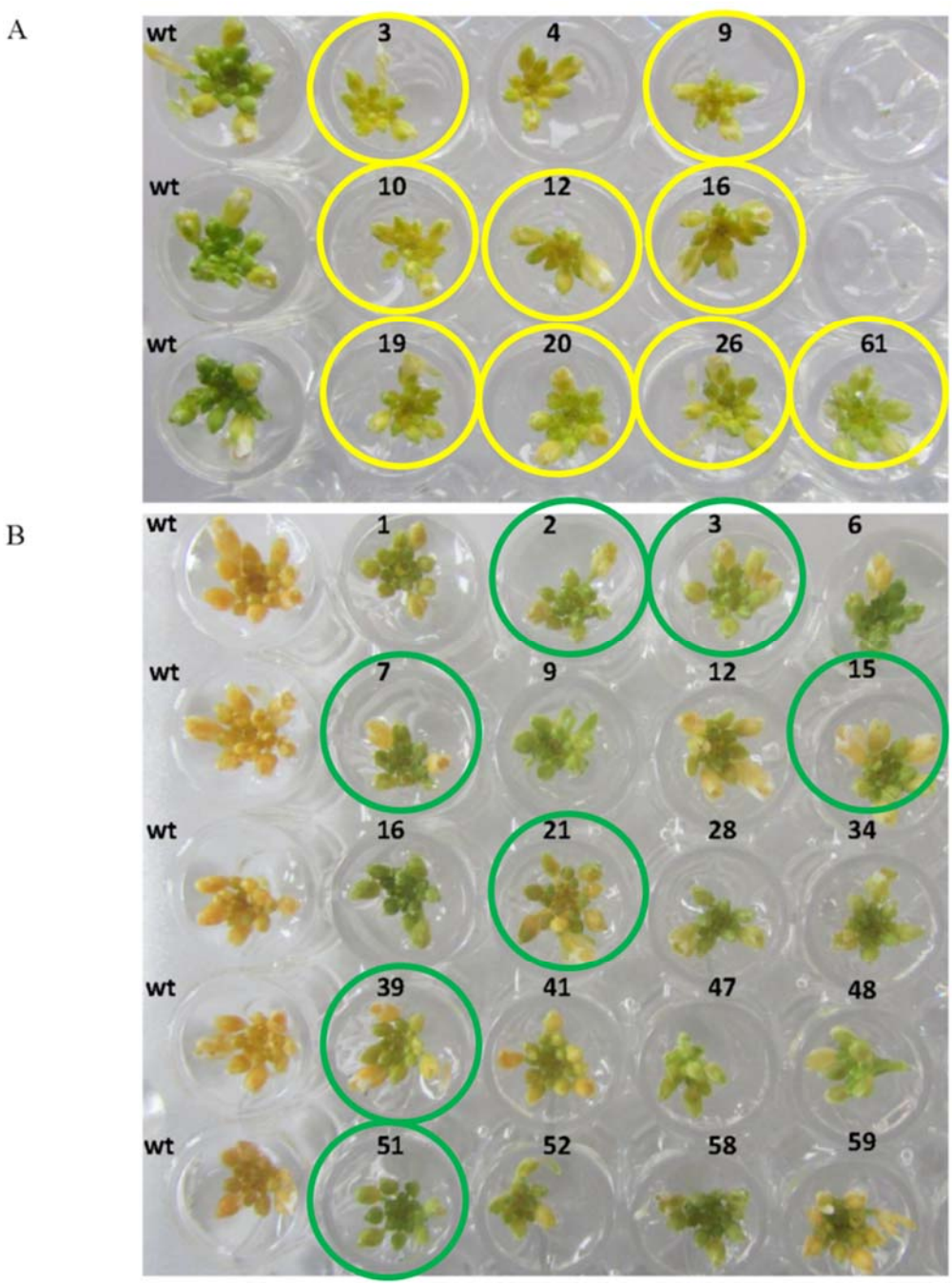

Figure 1.3. Screening of detached-dark-held inflorescences of EMS mutants via AIDA

(A) Degreening of *ais* mutants at day 3. (B) Degreening of *dis* mutants at day 5. Inflorescences were harvested from the M5 plants. Numbers on the top of each well indicate mutant number. wt is an abbreviation of wild type. Mutants with yellow (for *ais*) or green (for *dis*) circles on their inflorescences are investigated further in this research. Figures were edited from Jibran (2014).

1.5. Project aims

This project aims to better understand the key biological processes and regulation of dark-induced inflorescence senescence in *Arabidopsis thaliana*. The specific objectives of this project were as follows:

1) To confirm the altered inflorescence degreening phenotype of selected EMS mutants.
2) To identify the genetic lesions that are responsible for the altered senescence phenotype in a selection of the mutants.
3) To investigate the roles of the identified genes during dark-induced senescence. For instance, in which phytohormone-related pathways or degradation processes they are involved, and how they interact with other genes or signals in those pathways or processes in senescence regulation. Investigating the senescence-related functions of these genes was hypothesised to allow for a better understanding of how postharvest senescence of dark-stored tissue is regulated.

2. Materials and Methods

2.1. Plant materials

Ethyl methanesulfonate (EMS)-mutated seeds (M2) from *Arabidopsis thaliana* ecotype Landsberg *erecta* (L*er*-0) background were purchased from LEHLE Seed Company (Round Rock, TX, USA; www.lehleseeds.com). M2 seeds were screened and the plants that showed altered timing of degreening were self-fertilized to collect M3 seeds. M3 seeds were rescreened and M4 seeds were collected from the self-fertilized positive M3 plants. M4 plants were backcrossed with L*er*-0 and the F1 seeds were sown to produce F2 segregating population. The above work was previously performed by Rubina Jibran (Jibran, 2014). The M4 and F2 (after first backcross to L*er*-0) generation of the identified mutants were provided by Donald Hunter at the New Zealand Institute for Plant & Food Research (PFR; Palmerston North) and the details of these mutants are listed in Table 2.1.

2.2. Chemicals and reagents

Chemicals, reagents, solvents and enzymes were sourced from Duchefa Biochemie (Netherlands), BDH Chemicals (United Kingdom), HydraGene (United States), Sigma (United States), Invitrogen (United States), Merck (Germany) and Roche (Switzerland) and New England Biolabs (United States) unless otherwise stated. Primers were ordered from Macrogen (Korea). Probes for nCounter analysis were ordered from Integrated DNA Technologies (United States). Buffers, solutions and media were prepared with Milli-Q purified water and were sterilised by autoclaving for 20 min at 120°C and 100 kPa or by filter sterilization using 0.2 µm Puradisc™ polyethersulfone filters (Whatman) unless otherwise stated. Lab stock solutions were from Molecular biology and biochemistry lab, PFR, Palmerston North unless otherwise stated.

Table 2.1. Details of 22 previously identified EMS mutants

Mutants	Generation	Seeds status	AIDA phenotype	Other phenotypes (before backcross)
dis2	M4	Homozygous	*dis*	WT-like
dis7	M4	Homozygous	*dis*	WT-like
dis24	M4	Homozygous	*dis*	Unknown
dis29	M4	Homozygous	*dis*	Unknown
dis31	M4	Homozygous	*dis*	Unknown
dis51	M4	Homozygous	*dis*	WT-like
dis54	M4	Homozygous	*dis*	Unknown
dis3	x L*er*-0 F2	Segregating	*dis*	WT-like
dis9	x L*er*-0 F2	Segregating	*dis*	Stunted
dis15	x L*er*-0 F2	Segregating	*dis*	Stunted
dis21	x L*er*-0 F2	Segregating	*dis*	WT-like
dis39	x L*er*-0 F2	Segregating	*dis*	WT-like
ais1	x L*er*-0 F2	Segregating	*ais*	Unknown
ais3	x L*er*-0 F2	Segregating	*ais*	Stunted
ais9	x L*er*-0 F2	Segregating	*ais*	Thin stem and small leaves
ais10	x L*er*-0 F2	Segregating	*ais*	WT-like
ais12	x L*er*-0 F2	Segregating	*ais*	Stunted
ais16	x L*er*-0 F2	Segregating	*ais*	Stunted
ais19	x L*er*-0 F2	Segregating	*ais*	Stunted
ais20	x L*er*-0 F2	Segregating	*ais*	WT-like
ais26	x L*er*-0 F2	Segregating	*ais*	WT-like
ais61	x L*er*-0 F2	Segregating	*ais*	*apetala-1-like*

Mutants and their listed phenotypes were previously identified by Rubina Jibran (Jibran, 2014). M2 seeds were screened and the plants that showed altered timing of degreening were self-fertilized to collect M3 seeds. M3 seeds were rescreened and M4 seeds were collected from the self-fertilized positive M3 plants. M4 plants were backcrossed with L*er*-0 and the F1 seeds were sown to produce F2 segregating population.

2.3. Phenotypic analysis

2.3.1. General plant growth conditions

Seeds of Arabidopsis ecotype Columbia (Col-0), L*er*-0 and EMS mutants were germinated and grown in a temperature-controlled growth chamber set at 21°C with 65% relative humidity and under a 16 h/8 h light (200 µM photons $m^{-2}s^{-1}$; gro-lux and cool-white fluorescent lamps)/dark cycle (long day) unless otherwise stated. For the *in planta* assay, plants were grown in a temperature-controlled growth cabinet (Contherm Model CAT 630, 20-22 °C with 60% relative humidity at a light intensity of ~180 µE with Metal Halide lamps under long day).

2.3.2. Arabidopsis inflorescence degreening assay

Plants were screened by using AIDA as described in (Trivellini *et al.*, 2012; Jibran *et al.*, 2015; Hunter *et al.*, 2018). In brief, immature inflorescences [growth stages 6.00–6.10; (Boyes *et al.*, 2001)] were cut from primary bolts of 4-6 weeks old (after sowing) M2 plants and were placed in Milli-Q purified water in a microtitre plate. The plate was then housed in a black container (to mimic dark conditions) and incubated in the dark at 21°C. Photos were taken at 3 and 5 days of dark treatment. This required a brief illumination period of less than 2 minutes to minimise the light contamination. Mutants with inflorescences that showed altered time to degreening were selected for further genetic analysis. For long day (defined in Section 2.3.1) treatment, similar procedures were used with the exception that inflorescences were placed in a transparent container that was covered with transparent film and incubated under long day conditions.

2.3.3. Calculation of bolting and flowering percentages

Twenty-four plants per phenotype were sown and grown under long day conditions and were used for investigating the time to bolting and flowering between WT and mutants. Bolting was defined as the plant having a 5 mm primary bolt, and flowering as the plant having its first flower open in the primary bolt. The number of the plants that were bolting and flowering were counted on indicated days and expressed as percentages. Percentages were calculated as the number of bolting or flowering plants divided by the total number of plants multiplied by 100.

2.3.4. Synchronisation of flowering time

Time to flowering between WT and mutants was synchronised by sowing mutants ahead of WT. The purpose of synchronisation was to be able to harvest the inflorescences that have their first flower opened at the same time or to collect the first cauline leaves at the same age. *dis2* and *dis51* were sowed 12 and 4 days before their WT controls respectively. Inflorescences were harvested from plants having their first flower opened at the same time but at different plant ages between mutants and WT. For *dis2*, inflorescences from 29 days old L*er*-0 and 41 days old *dis2* plants were collected; whereas inflorescences from 28 days old L*er*-0 and 32 days old *dis51* plants were

detached for *dis51*. AIDA screening was applied in the dark as described in Section 2.2.1. Photos were taken before (day 0) and after 5 and 7 days of dark treatment.

2.3.5. Degreening assay of detached and dark-held leaves

The synchronisation also allowed collecting the first cauline leaves at the similar age between WT and mutants. About 2 weeks after sowing, the leaf numbers were counted and recorded. A leaf with a length longer than 2 mm was considered as emerged. The number and the emergence date of the first cauline leaf was recorded. Leaves at similar ages (time differences less than one to two days) between WT and mutant were detached and placed in a round petri dish (90x15 mm; CITOTEST, CN) with filter paper (90 mm; Whatman, UK) moistened with 3 mL sterilised water. The petri dish was then sealed and incubated at 21˚C in the dark. Photos were taken before (day 0) and after 5 and 7 days of dark treatment.

2.4. Physiological analysis

2.4.1. Chlorophyll analysis

Chl was extracted from single inflorescence. The fresh weights of uncrushed inflorescences were measured and the Chl was extracted by incubating samples in 96% (v/v) ethanol (1 mg of tissue per 30 µL of ethanol) for 4 days in the dark at 4°C. The concentration of Chl was quantified by measuring the absorbance of 2 µL of the supernatant at the wavelengths of 649 (A649) and 665 (A665) nm with a Nanodrop ND-1000 spectrophotometer. The absolute Chl content (µg/mg) was calculated using the following equation (Wintermans and de Mots, 1965):

Chl a = 13.70 * A665 - 5.76 * A649

Chl b = 25.80 * A649 - 5.76 * A665

Total Chl = 6.1 * A665 + 20.04 * A649

The Chl retention at day 3 or day 5 was expressed as percentage, which was calculated as the day 3 or day 5 Chl content divided by day 0 Chl content multiplied by 100.

2.4.2. Phytohormone treatment

2.4.2.1. Ethylene treatment

Preparation of Murashige and Skoog (MS) salts medium

Half MS salts medium was prepared using standard protocols (Murashige and Skoog, 1962). Half MS basal salt mixture (2.165 g/L) was dissolved in Milli-Q purified water and the pH of the medium was adjusted to 6.2 using 1M KOH solution and then 1% agar was added. The medium was autoclaved and then was cooled to 50-55˚C and poured equally to petri dishes under sterilised conditions. Approximately 20 mL or 60 mL of liquid medium was poured to a round petri dish (90x15 mm) or a square one (120x120x17 mm), respectively. The petri dishes were left at room temperature for the media to solidify.

Preparation of 1-Aminocyclopropane-1-carboxylic acid (ACC)

To make 10 mM stock solution, 0.01g ethylene precursor ACC (sigma, USA) was dissolved in 10 mL 10% ethanol and was filter sterilised.

Seeds sterilisation

100 mL of 70% (v/v) ethanol, 50% (v/v) Janola Premium Bleach and 0.1% (v/v) Triton X-100 solutions were prepared for seed sterilization. Arabidopsis WT and *dis51* seeds were first sterilised with 70% ethanol for 1 minute and then washed with 50% bleach for 6-8 minutes. The seeds were then rinsed with 0.1% Triton X-100 solution for 2-3 times around 1 minute each time. Finally, the seeds were rinsed with sterile water twice.

Triple response assay

The triple response assay was carried out according to the protocol described in Jing *et al*. (2002). Sterilized seeds (20 seeds per genotype) were sown on the half MS medium and grown under long day conditions for 2 days for germination. After germination, the seeds were transferred carefully by using forceps to half MS plate with and without 10 µM ACC (20 µL 10mM ACC per 20 mL half MS medium) and were incubated in the dark at 21˚C for 5 days.

2.4.2.2. Strigolactone treatment

To make 10 mM stock solution, 1.49 mg SL analogue racemic-GR24 (rac-GR24; Chiralix, NL) was dissolved in 500 µL pure DMSO and was diluted with 1% DMSO to different concentrations for experiments. Detached inflorescences were treated with diluted rac-GR24 or 1% DMSO (mock) and were incubated in the dark or long day at 21˚C.

2.5. Genetic and high-resolution melt (HRM)-analysis

2.5.1. Determination of genetic nature of selected *ais* or *dis* mutants

Homozygous M4 mutants that showed stable altered degreening phenotype were selected were backcrossed with L*er*-0 and Col-0 following the protocol of Koornneef *et al.* (2006) for the genetic analysis. F1 plants were selfed to generate the F2 populations for mapping. F2 plants were screened by AIDA and followed by segregation analysis. Pearson's chi-squared test was used to determine the genetic nature (e.g. no significant difference between observed ratio and expected ratio 3:1 was considered to be a monogenic recessive trait) of selected mutants and was performed with online P-value calculator (http://graphpad.com/quickcalcs/chisquared1/). The *P*-value was determined at one degree of freedom and $P<0.05$ indicated a statistically significant difference.

2.5.2. Primer design

The primers for HRM-analysis were designed using Primer3web version 4.1.0 (Koressaar and Remm, 2007; Untergasser *et al.*, 2012) according to the settings described in Jibran *et al*. (2015). Primers were designed with default parameters, except for the following changes: set "Max Self Complementarity" to 4, "Max 3' Self Complementarity" to 1, "Primer GC%" Min to 40 and Max to 50 and "Product Size Ranges" to 70 - 150. Primers were designed to single nucleotide polymorphisms (SNPs) between Col-0 (TAIR10) and L*er*-0 sequence (L*er*-0 sequence provided by Korbinian Schneeberger, Max Planck Institute for Plant Breeding Research) and the sequence alignment was performed with Geneious software (version 10.0.3). Primers were listed in Appendix 1.

2.5.3. HRM-based polymerase chain reaction (PCR)

HRM-analysis was performed using the genomic DNA isolated from the leaves of F2 positive plants of the mutants, homozygous WT plants (Col-0 and L*er*-0) and heterozygous F1 progeny of crossed L*er*-0 and Col-0. Genomic DNA was extracted according to the protocol of Dellaporta *et al.* (1983) or by SlipStream Automation (www.slipstream-automation.co.nz). The causal mutations were coarse mapped by Rubina Jibran (Jibran, 2014) to chromosome 3 between markers 3-1 and 3-2 for *dis9* and chromosome 2 between markers 2-4 and 2-5 for *dis15* (Hunter *et al.*, 2018). Markers 3-1 and 3-2 in Hunter *et al.*, 2018 correspond to markers 3-14 and 3-16 in Jibran, 2014; while markers 2-4 and 2-5 corresponding to markers 2-8 and 2-11. For fine-mapping of *dis9* and *dis51*, HRM reaction was prepared using HRM master mix (Roche) and the PCR was carried out with LightCycler 480 instrument (Roche) following the procedures described in Jibran *et al.* (2015) and Hunter *et al.* (2018). The PCR reaction mixtures for 96-well and 384-well plates screen were shown in Table 2.2 and the PCR conditions were shown in Table 2.3. Data analysis was performed with the LightCycler 480 software (version 1.5.0) using the method “Gene scanning”.

Table 2.2. HRM-PCR reaction components

For each reaction	Volume for 96-well plate (µL)	Volume for 384-well plate (µL)
HRM Master Mix	5	3.5
Mg^{2+}	1	0.7
Forward primer (10 µM)	0.2	0.14
Reverse primer (10 µM)	0.2	0.14
H_2O	1.1	0.52
Genomic DNA (5 ng / µL)	2.5	2
Total reaction volume	10	7

Table 2.3. HRM-PCR conditions

	Temperature (°C)	Time
Initial denaturation	95	5 minutes
PCR amplification (40 cycles)	95	10 seconds
	56 (specific to primers)	30 seconds
	72	15 seconds
HRM analysis	95	1 minute
	40	1 minute
	65	0.01 second
Cooling	95	-
	40	30 second

2.5.4. Linkage analysis

Linkage of causal mutations of *dis* mutants to SNP markers was determined as recombination frequency which was calculated by the following formula:
Recombination frequency = (number of heterozygotes + 2 * number of homozygous Col-0) / (2 * total number of plants tested).

2.6. Molecular cloning

2.6.1. Plasmid constructions

For MAX1 constructs for complementation of *max1-5*/*dis15*, the fragment of MAX1-WT (consisting of the 1293 bp region upstream of the start codon, the 2420 bp genomic sequence, and a 185 bp region downstream of the stop codon) or MAX1-G469A (with a G to C mutation at position 1406 relative to the start codon of the MAX1 coding sequence causing a G469A substitution of MAX1 protein) was amplified from genomic DNA and was then cloned into the binary vector *pGreen0229* (Hellens *et al.*, 2000b) via restriction digestion with *Eco*RI and *Not*I (Roche, CH). The details of cloning procedures and the primers used for PCR are described in sections 2.6.2 to 2.6.13. For complementation of *d14-6*/*dis9*, the D14-*pGWB1* construct (comprising 553 bp sequence upstream of the start codon and 804 bp of the coding sequence) was provided by Pilar Cubas (Centro Nacional de Biotecnología/Consejo Superior de Investigaciones Científicas; (Chevalier *et al.*, 2014)). The positions of the mutations and the cloned regions were assigned based on the Col-0 gene and protein reference sequences from TAIR (www.arabidopsis.org).

For transient expression assay, The Arabidopsis Col-0 based SL biosynthetic genes (D27, MAX3, MAX4 and MAX1) were cloned by Yanxia Zhang (University of Amsterdam) and the protocol was described in Zhang *et al.* (2014b). The L*er*-0 based MAX1 genes (MAX1-WT, MAX1-G469R or MAX1-G469A) were cloned using the same protocol. The coding sequence of MAX1 was amplified (and/or point mutated) from the cDNA of WT or *max1-5*/*dis15* inflorescences and was then cloned into impact vector pIV1A_2.1 (containing a CaMV35S promoter) (Ting *et al.*, 2013) via restriction digestion with *Nco*I and *Not*I (Roche, CH). The gene fragments were then transferred to the binary

vector pBin-Plus (Vanengelen *et al.*, 1995) via Gateway LR reaction as described in Section 2.6.13.

The maps of all vectors used for cloning were shown in Appendix 2.

2.6.2. Plant genomic DNA isolation

Plant genomic DNA was isolated by using Plant Genomic DNA Mini Kit (Geneaid Biotech; Taiwan, CN) according to the instruction manual or was extracted according to the protocol of Dellaporta *et al.* (1983). Detailed procedures are as follows: leaf samples were ground to a powder with liquid nitrogen. 20 mg/mL RNase A (Roche, CH; 1 µL per sample) was added to the extraction buffer (100 mL extraction buffer consisted of 20 mL of 1 M Tris·HCl (pH 7.5), 5 mL of 5 M NaCl, 5 mL of 0.5 M EDTA (pH 8.0), 5 mL of 10% SDS and 65 mL of sterilised water) just before use. Then 600 µL of extraction buffer was added to each sample and the solution was mixed by vortex for 5 seconds. After that, 600 µL Chloroform/Octanol (v/v, 24:1) was added and followed by vortex for 5 seconds, and then the sample was incubated at 37˚C for 5 minutes. The mixed solution was spun at 18000 RCF or 14000 r.p.m (Sigma 1-15 centrifuge unless otherwise described in chapter 2) for 10 minutes at room temperature. 400 µL supernatant was transferred to a new Eppendorf tube, an equal volume of isopropanol was added for DNA precipitation, and then the solution was mixed and kept at room temperature for 5 minutes. The solution was spun at 14000 r.p.m for 10 minutes and the supernatant was discarded. The DNA pellet was washed with 70% ethanol twice and vacuum dried at room temperature. The DNA pellet was resuspended in 50 µL sterilised water and stored at 4˚C or -20˚C.

2.6.3. Standard polymerase chain reaction (PCR)

Genomic DNA for cloning or sequencing was amplified using iProof™ High-Fidelity DNA Polymerase (BIO-RAD) or KAPA HiFi HotStart PCR Kit (Roche) with primers listed in Appendix 3. The PCR reaction mixtures (Table 2.4) and the PCR conditions (Table 2.5) were prepared and programmed according to the manufacturer's instructions.

Table 2.4. PCR reaction components

iProof High-Fidelity PCR Kit	Volume	KAPA HiFi HotStart PCR Kit	Volume
Sterile water	- µL	Sterile water	- µL
5 x HF Buffer (contain 7.5 mM $MgCl_2$)	10 µL	5 x HiFi Buffer (contain 2 mM $MgCl_2$)	10 µL
10 mM dNTP mix	1 µL	10 mM dNTP mix	1.5 µL
10 µM Forward primer	0.5 µL	10 µM Forward primer	1.5 µL
10 µM Reverse primer	0.5 µL	10 µM Reverse primer	1.5 µL
DNA template (gDNA)	50-500 ng	DNA template (gDNA)	10-100 ng
iProof™ HiFi DNA Polymerase	0.5 µL	KAPA HiFi HotStart DNA Polymerase	1 µL
Total	50 µL	Total	50 µL

Table 2.5. PCR conditions

	iProof High-Fidelity PCR condition			KAPA HiFi HotStart PCR condition		
Step	**Temp.**	**Time**	**Cycles**	**Temp.**	**Time**	**Cycles**
Initial denaturation	98˚C	30 sec	1	95˚C	3 min	1
Denaturation	98˚C	10 sec		98˚C	20 sec	
Annealing	varies*	30 sec	35	varies*	15 sec	30
Extension	72˚C	20 sec/kb*		72˚C	1 min/kb*	
Final extension	72˚C	5 min	1	72˚C	5 min	1

Abbreviations: Temp., temperature; min, minute; sec, second.
*The annealing temperatures are specific to primers used and was set according to the Tm (subjected to the lower one between forward and reverse primer) recommended by Macrogen (Korea) from where these primers were obtained. The extension time was adjusted to the length of amplicon expected.

2.6.4. Site-directed mutagenesis

PCR-based site-directed mutagenesis was used to make the MAX1-G469A substitutions for both Arabidopsis transformation and transient expression assay in *N.benthamiana*. The MAX1-G469A sequence used for Arabidopsis transformation of *dis15* was generated according to the following procedures: forward and reverse primers (named MAX1_G469A_F1 and MAX1_G469A_R1; Appendix 3.1) were designed over the region to be mutated and the G bp in the WT sequence was replaced with a C in both primers. The mutated base pair region of the primers corresponded to position 1406 downstream of the start codon of the MAX1 CDS and it caused a G469A substitution of MAX1 protein. The forward primer (MAX1_G469A_F1) with G/C mutation on MAX1 genome was then partnered with a reverse gene primer (named

MAX1GA_CompNotI_R1; Appendix 3.1) located on the 3'-UTR of the gene and the reverse primer (MAX1_G469A_R1) partnered with a forward gene primer (MAX1GA_CompEcoRI_F1; Appendix 3.1) located on the promoter region of MAX1. The two PCRs were then run independently to generate two amplicons containing the point mutation. These two amplicons were purified (Section 2.6.6) and then combined via another PCR which was performed using the two amplicons as templates with the forward and reverse gene primers (MAX1GA_CompEcoRI_F1/R1) used in the above PCR to generate the full-length of MAX1-G469A sequence for Arabidopsis transformation experiments. For producing the MAX1-G469A sequence for transient expression assay, the same strategy was used except the forward gene primer was designed to the start of the MAX1 CDS and the reverse gene primer was designed to the end of the MAX1 CDS (Appendix 3.3).

2.6.5. Agarose gel electrophoresis

Agarose gel electrophoresis was used to separate DNA following isolation, PCR or restriction enzyme digestion. 1% (w/v) agarose gels were used for agarose gel electrophoresis. 5 µL of ethidium bromide (10 mg/mL) was added to 250 mL of gel solution (lab stock, stored at 50˚C incubator) for DNA staining just before use. Gel solution was poured into a gel apparatus and the comb was placed on this apparatus. Once solidified, the gel was transferred to the electrophoresis tank and submerged by 1x TBE buffer. 10x loading dye was added to DNA samples to make a 1x final concentration before loading onto the gel. After loading the DNA ladders and samples, electrophoresis was carried out at 10 Volt/cm. DNA fragments in the gel were visualised using the UV transilluminator in the BIO-RAD Gel-Image system (BIO-RAD, USA) and digital photographs were obtained using Quantity One software (v4.6.2; BIO-RAD, USA). The length of the DNA fragments was estimated by comparing the mobility of DNA samples against the High DNA Mass Ladder (Invitrogen, USA) and/or 1 Kb Plus DNA Ladder (Invitrogen, USA).

2.6.6. PCR product purification

PCR products were purified using the High Pure PCR Product Purification Kit (Roche, CH) according to the manufacturer's instructions with the exception that purified PCR products were eluted in 30 µL (per sample) elution buffer.

2.6.7. Restriction enzyme digestions

PCR products and vectors were digested using restriction endonucleases. Two different restriction endonucleases were used for each construct to allow directional cloning. Typically, 1-2 µL of PCR product or 100-300 ng of vector was digested with 5 Units (per enzyme) of restriction enzymes (Roche, CH) in their recommended SuRE/Cut buffers (Roche, CH) in a total volume of 10 µL. The digest reaction mixture was incubated at 37°C for 1-2 hours. The digested DNA fragments were purified using PCR product purification kit (Section 2.6.6) and were checked by agarose gel electrophoresis (Section 2.6.5). The concentrations of the gene fragments and vectors were quantified by using Nanodrop ND-1000 spectrophotometer (Thermo Scientific).

2.6.8. Ligation

Digested gene fragments and vectors were ligated using T4 DNA Ligase (New England Biolabs) according to the manufacturer's instructions. Typically, 1 µL of T4 ligase and 2 µL of T4 ligase buffer (10X) were used in a total volume of 20 µL reaction solution. The amount of insert was calculated using online NEBioCalculator™ (v1.9.0) (https://nebiocalculator.neb.com/#!/ligation) according to the following formula: required mass insert (ng) = desired insert/vector molar ratio (3:1) x mass of vector (~50 ng) x ratio of insert to vector lengths. The reaction mixture was incubated at 16°C overnight and then the reaction was inactivated at 65°C for 10 minutes.

2.6.9. Bacterial transformation

2.6.9.1. Preparation of Luria-Bertani (LB) medium

For LB broth (pH 7.5), 1% (w/v) Tryptone, 0.5% (w/v) Yeast extract and 1% (w/v) NaCl were dissolved in water and the pH was adjusted to 7.5 using 1M KOH solution. The medium was autoclaved and stored at room temperature. For solid medium, 1.5% (w/v) Bacto-agar (Difco) was added before autoclaving.

2.6.9.2. Bacterial strains and general growth conditions

Escherichia coli (*E. coli*) strains XL1-blue (Stratagene California, USA), NovaBlue (Novagen, Merck Biosciences, DE), Top 10 (Invitrogen, USA) and DB3.1 (Invitrogen, USA) were used for cloning. XL1-blue and NovaBlue contain resistance to tetracycline. DB3.1 contains the *gyr*A462 allele that renders this strain resistant to the toxic effects of the *ccdB* gene (Bernard and Couturier, 1992) and was used for propagating plasmids containing the *ccdB* gene in GATEWAY™ system. *Agrobacterium tumefaciens* strains GV3101 (containing the disarmed pMP90 Ti plasmid) and AGL0 were used for plant transformation. Both GV3101 (Koncz and Schell, 1986) and AGL0 (Lazo *et al.*, 1991) contain chromosomal resistance to rifampicin but GV3101 also contains resistance to gentamicin because of presence of the disarmed pMP90 Ti plasmid (Hellens *et al.*, 2000a). *E. coli* and *Agrobacterium* were grown at 37°C overnight and at 28°C for 2 days, respectively, on LB-agar plates or LB-broth with appropriate antibiotics. Liquid cultures were shaken at 250 r.p.m in addition to the described growth conditions.

2.6.9.3. Preparation of competent cells

Chemically competent cells

Chemically competent cells of *E.coli* XL1-blue and NovaBlue were from lab stock and were prepared by the method of Inoue *et al.* (1990) using 10 mg/L of tetracycline for selection. Chemically competent cells of *E.coli* Top10 (Invitrogen, USA) were provided by Caroline Kim (PFR, Palmerston North, NZ).

Electrocompetent cells

Electrocompetent *E.coli* DB3.1 cells were prepared according to the following procedures: 500 mL of LB-broth was inoculated with 5 mL of fresh overnight DB3.1 culture. Cells were grown at 37°C and shaken at 250 r.p.m to an OD_{600} of approximately 0.5-0.7. After that, cells were chilled on ice for ~20 minutes and then were harvested by centrifugation at 4000 x g for 10 minutes at 4°C. Cells were washed three times with ice-cold 10% (v/v) glycerol and finally resuspended in 1 mL of 10% (v/v) glycerol. Cells were dispensed into 50 µL aliquots per tube and were snap frozen in liquid nitrogen and stored at -80°C.

Electrocompetent *Agrobacterium* GV3101 cells were from lab stock and were prepared by the methods of McCormac *et al.* (1998) using 20 mg/L of rifampicin for selecting *Agrobacterium* and 20 mg/L gentamicin for selecting disarmed Ti plasmid MP90. Electrocompetent *Agrobacterium* AGL0 cells were provided by Harro Bouwmeester (University of Amsterdam).

2.6.9.4. Bacterial transformation methods

Heat-shock transformation

Heat-shock transformation was applied for transformation of ligated PCR products using chemically competent *E. coli* cells. 10 µL of ligated PCR product was gently added to 100 µL of freshly thawed competent cells and the mixture was placed on ice for ~30 minutes. After that, cells were heat-shocked at 42°C (water bath) for 90 seconds and then 500 µL of LB-broth was added immediately to the cells. Cells were incubated at 37°C and shaken at 250 r.p.m for 1 hour to allow them to recover. Finally, 50-100 µL of cell culture per construct was spread on LB-agar plates with appropriate antibiotics.

Electroporation

Electrocompetent *E.coli* DB3.1 cells were transformed with Gateway destination vector pBin-Plus containing *ccdB* gene (obtained from Harro Bouwmeester, University of Amsterdam, NL; Appendix 2.3.2) and *Agrobacterium* GV3101 or AGL0 cells were transformed with constructed plasmids by electroporation. 50-100 ng of plasmid was gently added to 50 µL of freshly thawed competent cells and the mixture was then placed between the electrodes of a pre-chilled electroporation cuvette (0.1 cm electrode gap, BioRad, USA). Cells were electroporated at 300 V in a Cell-Porator Electroporation System (Life Technologies) following the manufacturer's instruction. After electroporation, cells were transferred to an Eppendorf tube containing 1 mL LB-broth and were recovered by shaking (250 r.p.m) at 37°C for 1 hour or at 28°C for 2 hours for *E.coli* or *Agrobacterium*, respectively. Finally, the recovered transformed cells (50-100 µL) were spread on LB-agar plates containing appropriate antibiotics. The helper plasmid *pSoup* (100 ng) was co-transformed with *pGreen0229* to GV3101 as it is required for the replication of *pGreen0229* in *Agrobacterium* (Hellens *et al.*, 2000b).

2.6.9.5. Antibiotics selection

Antibiotics used for bacterial or transformants selection were prepared by dissolving antibiotic salts in appropriate solvents to make stock solutions. The details of antibiotics preparation and selection were shown in Table 2.6. All stock solutions were filter sterilised and stored in a tube wrapped with aluminium foil to avoid light. Kanamycin (kanamycin sulphate) and gentamicin (gentamicin sulphate) were stored at 4°C. Tetracycline (tetracycline hydrochloride) and rifampicin were stored at -20°C.

Table 2.6. Antibiotics preparation and selection

Antibiotics	Solvents	Stock (mg/mL)	Working (µg/mL)	Bacterial selection	Vectors selection
Kanamycin	Water	50	50	N/A	pGWB1, pGreen0229, pBIN_PLUS
Tetracycline	70% Ethanol	10	10	XL1-blue, NovaBlue	pSoup
Gentamycin	Water	50	50, 20 (pIV1A)	N/A	pMP90, pIV1A_2.1
Rifampicin	DMSO	50	20	Agrobacterium	N/A

2.6.10. Colony PCR

Colony PCR was used to preliminarily screen putative transformants for the presence of transgenes. Individual *E. coli* colonies (used as DNA templates) were picked using sterile toothpicks and were mixed well with PCR reaction mixtures which were prepared using KAPA2G Robust PCR Kit (Roche). Each reaction mixture (25 µL) contains 5 µL of 5X KAPA2G Buffer A, 0.5 µL 10 mM dNTP Mix, 10 µM forward and reverse primers (1.25 µL per primer), 0.1 µL of 5 U/µL KAPA2G Robust DNA Polymerase and PCR-grade water (up to 25 µL). The PCR was performed using the following conditions: Initial denaturation 95°C/3 minutes, 30 cycles of [95°C/15 seconds, Tm -°C (specific to primers; set as described in Section 2.6.3)/15 seconds, 72°C/- minutes (adjusted to the length of amplicon; 30 seconds/kb)] and final extension 72°C/1 minute.

2.6.11. Plasmid DNA isolation

Plasmid DNA was extracted using DNA-spin™ Plasmid DNA Purification Kit (iNtRON Biotechnology, Korea) according to the instruction manual or was isolated using the modified alkaline lysis method that was optimised based on Sambrook *et al.* (1989). Briefly, bacterial cells were collected from 3 mL of

overnight cultures by centrifugation at 6000 r.p.m for 5 minutes at room temperature. The supernatant was discarded, and the cells were resuspended in 200 µL of solution I (50 mM Glucose, 10 mM EDTA, 25 mM Tris pH 8.0). The resuspended cells were lysed with 200 µL of solution II [0.2 M NaOH, 1% (w/v) SDS; prepared just before use] and the solution was then neutralised with 200 µL of solution III [3 M potassium acetate, 11.5% (v/v) glacial acetic acid]. The protein, carbohydrates and genomic DNA mixtures were pelleted by centrifugation at 12000 r.p.m for 15 minutes and ~500 µL of supernatant was transferred to a new microfuge tube where the plasmid DNA was precipitated by adding an equal volume of isopropanol. After that, the precipitated plasmid DNA was pelleted by centrifugation at 12000 r.p.m for 10 minutes. The supernatant was discarded, and the pellet was washed with 700 µL of 70% (v/v) ethanol by gently pipetting the solution to the pellet. Then ethanol was removed, and the pellet was vacuum-dried for around 10 minutes. Finally, the plasmid DNA was dissolved in 20 µL of sterile water.

2.6.12. Standard DNA sequencing

Purified PCR products or plasmids containing appropriate sequencing primers were sent to Macrogen DNA Sequencing Service (Standard-Seq; Seoul, Korea) or Massey Genome Service (ABI Sequencing Service using BigDye™ Terminator Version 3.1 chemistry; Massey University, Palmerston North, NZ) for sequencing. Samples were prepared following the instructions in their websites https://dna.macrogen.com/eng/support/ces/guide/ces_sample_submission.jsp or http://www.massey.ac.nz/massey/learning/departments/centres-research/genome/abi-sequencing-services/abi-sequencing-service-technical-information.cfm, respectively. Sequence alignments were performed with Geneious desktop software (http://www.geneious.com/) (Kearse *et al.*, 2012) using the method “Map to Reference”.

2.6.13. Gateway cloning

Gateway cloning was used for making MAX1 (WT/mutated) constructs for transient expression assay in *N. benthamiana*. The genes were cloned to the Gateway entry vector pIVA_2.1 (Appendix 2.3.1) via restriction enzyme digestion method as described in above Sections 2.6.1-2.6.12. The cloned

genes were then transferred to the binary vector pBin-Plus (destination vector) via the LR reaction using the Gateway™ LR Clonase™ II Enzyme Mix (Invitrogen, USA), according to the manufacturer's instructions with minor changes. Briefly, a total volume of 10 µL reaction mixture containing entry vector (75 ng), destination vector (150 ng), 1 µL of LR Clonase™ II enzyme mix and TE buffer (pH 8.0, up to 10 µL). The reaction was incubated at 25°C for 3 hours and terminated by incubating samples in 2 µL of the Proteinase K solution at 37°C for 10 minutes. The original pBin-Plus vectors were stored and propagated in *E. coli* DB3.1 due to the lethal *ccdB* gene. The recombined pBin-Plus vectors were transformed into *E. coli* Top10 by heat-shock transformation (Section 2.6.9.4). The transformants were selected on LB-Agar plates containing 50 mg/L kanamycin. The confirmed constructs were transformed into *A. tumefaciens* AGL0 by electroporation (Section 2.6.9.4).

2.7. Transcriptional analysis

2.7.1. RNA isolation

Inflorescences from primary bolts (the buds with opened flowers were removed) of 6-7-week-old plants grown in the growth chamber under long day condition (Section 2.3.1) were harvested and snap frozen in liquid nitrogen. Four to six inflorescences from individual plants were pooled to make one biological replicate, and three biological replicates per genotype/treatment were used. Total RNA was isolated with the Quick-RNA™ MiniPrep kit (Zymo Research, USA) according to the instruction manual. Possible traces of DNA were eliminated by In-column DNase I (provided in the Kit) treatment. Total RNA was eluted with 30 µL of DNase/RNase-Free water (per sample) and the concentration of RNA was measured by using Nanodrop ND-1000 spectrophotometer (Thermo Scientific, USA). Total RNAs were stored at -80°C.

2.7.2. cDNA synthesis

The first-strand cDNA was synthesised from total RNA (500 ng). A total volume of 20 µL of reaction mixture was prepared using iScript™ Reverse Transcription Supermix for RT-qPCR (BIO-RAD) following the instruction manual. The mixture was then incubated in a PCR machine (BIO-RAD) according to the

following protocol: Priming at 25°C for 5 minutes, reverse transcription at 46°C for 20 minutes and inactivation at 95°C for 1 minute.

2.7.3. Quantitative Real-Time PCR (qRT-PCR)

qRT-PCR was used to quantify relative transcript abundance of genes of interest in the inflorescences under different treatments. The reaction mixture was prepared using a LightCycler® 480 SYBR Green I Master kit (Roche). For a 384-well plate reaction, each reaction mixture (5 µL) contains 3.75 µL of 2X SYBR Green Master Mix, 10 µM forward and reverse primers (0.14 µL per primer) and 0.97 µL of PCR-grade water. The cDNA (Section 2.7.2) was 10-times diluted before use and 2 µL of cDNA was added to each reaction mixture as a template. The PCR was performed using LightCycler® 480 Instrument II (384-well; Roche) according to the following conditions: initial denaturation at 95°C for 5 minutes, amplification 45 cycles of [95°C/10 seconds, 58°C (specific to primers)/20 seconds, 72°C/10 seconds], melting curve analysis at 95°C for 5 seconds, 65°C for 1 minute and 97°C continuous and finally cooling at 40°C for 10 seconds. Four technical replicates were done for each biological replicate. Primers were designed using QuantPrime online software (Arvidsson *et al.*, 2008) (http://quantprime.mpimp-golm.mpg.de/) or using "Universal ProbeLibrary Assay Design" in Roche website. Primer pairs are listed in Appendix 4. The Cp value was calculated using the algorithm of "Abs Quant / 2nd Derivative Max" present in LightCycler® 480 Software (version 1.5). Data were normalized to the reference gene *PP2AA3* (*At1g13320*) (Czechowski *et al.*, 2005) and relative transcriptional changes were calculated using the *ΔΔ*Ct method relative to one control sample (Livak and Schmittgen, 2001; Dvinge and Bertone, 2009).

2.7.4. nCounter analysis

Transcriptional analysis was performed using the nCounter Analysis System (NanoString, Seattle, WA, USA). This technique enables to count RNA molecules directly by utilising molecular barcodes on gene sequence-specific probes and single molecule imaging (Geiss *et al.*, 2008). Two sets of gene-specific probes (along with a reporter probe and a capture probe) were designed by NanoString support team and their sequences are listed in

Appendix 5. Total RNA (300 ng per sample) was hybridised with probes (A & B) and CodeSets (A-H) using nCounter PlexSet-24 Reagent Pack according to the "PlexSet™ Reagents User Manual". After hybridisation, samples from each column were pooled and were placed on the automated nCounter Prep Station (NanoString, USA) for purification and were immobilised in the cartridge. This cartridge was then transferred to the nCounter Digital Analyzer for data collection. Data analysis was performed with nSolver™ 4.0 Analysis Software according to user manual. All samples passed the quality control. The background threshold was set to "12" according to the count value of the internal negative control and therefore any count below 12 was not considered. Positive control normalization was carried out by using the geometric mean of the Top 3 positive counts. Reference gene normalization was calculated using the geometric mean of counts for the three reference genes *PP2AA3*/*At1g13320*, *ACT2*/*At3g18780* and *MON1*/*At2g28390* (Czechowski *et al.*, 2005).

2.8. Whole genome sequencing (WGS)

Genomic DNA for WGS was isolated from *dis9* using the Plant Genomic DNA Mini Kit (Geneaid, Taiwan, CN) and from *dis15* using the method of Lutz *et al.* (2011). Genomic DNA at a concentration of 100 ng/µL in 1× TE buffer was sent to Macrogen (http://dna.macrogen.com) for 100 bp paired end sequencing on an Illumina HiSeq2000 sequencer. This work was carried out by Kerry Sullivan (PFR, NZ).

2.9. Plant transformation

2.9.1. Arabidopsis transformation

2.9.1.1. Floral dip methods

Arabidopsis transformation was performed by using the floral dip method described in (Zhang *et al.*, 2006). The *dis* mutants were grown in a growth cabinet under normal growth conditions (Section 2.3.1) for ~4 weeks. When plants started to flower, the first bolts were removed to allow proliferation of many secondary inflorescences. The transformation was performed at ~1 week after clipping of first bolts. *Agrobacterium* GV3101 carrying different genes of

interest were grown at 28°C in 500 mL (250 mL per bottle) of LB-broth with appropriate antibiotics to an OD_{600} of 1-1.2. *Agrobacterium* cells were collected by centrifugation at 4000 × g for 10 minutes. Cells were resuspended in 500 mL of freshly made 5% (w/v) sucrose solution and Silwet L-77 was added just before dipping to a concentration of 0.03% (v/v). Aerial parts of plants were inverted and dipped in the *Agrobacterium* solution for 30 seconds with gentle agitation. The treated plants were laid down on their sides and stored in a sealed plastic container to maintain high humidity in the dark at 21°C for 24 hours. After that, plants were transferred to growth cabinet and grown under normal growth conditions (Section 2.3.1). F1 seeds were harvested from the dipped plants upon maturity and were used for transformant selection.

2.9.1.2. Transgenic plants selection

For *dis9* transgenic plants, T1 and T2 seeds were sterilised and sown on half-MS-Agar plates (see Section 2.4.2.1 for seeds sterilisation and half-MS-Agar plate preparation) containing 25 mg/L hygromycin and grown in a temperature-controlled growth chamber under long day condition (Section 2.3.1) for approximately 1 month. Only transformants harbouring hygromycin resistant gene developed true leaves and proper roots. For *dis15* transgenic plants, T1 seeds were sown on soil and grown in a plant house under natural day/night-length conditions at 21-24°C. After germination, 3-day-old seedlings were sprayed with 100 mg/L of BASTA and thereafter every two days for 2-3 weeks. Only transformants harbouring the BASTA resistance gene survived. Standard PCR (Section 2.6.3) and sequencing (Section 2.6.12) were used to confirm the insertion of the WT gene in the mutant background. Genomic DNA was isolated (Section 2.6.2) from the leaves of the potential transformants. PCR was performed with the primers listed in Appendix 3.2 and the positions of the primers on the genes or the vectors were shown in Chapter 5 Figure 5.8A and Figure 5.11A. PCR products were purified (Section 2.6.6) and sent for sequencing.

2.9.2. Transient expression in leaves of *N. benthamiana*

To characterise the enzymatic activity of MAX1 and the mutated MAX1 variants, transient expression in *N. benthamiana* was carried out according to the protocol described in Zhang *et al.* (2014b), except for the following changes: *A. tumefaciens* was resuspended in 50 mM MES [2-(N-Morpholino) ethanesulfonic acid hydrate] (Sigma) - KOH buffer (pH 5.6) containing 2 mM NaH_2PO_4 (Sigma), 100 µM acetosyringone (Sigma) and 0.5% glucose (Duchefa) to a final OD_{600} of 0.5. For preparation of the infiltration solution, equal volumes of the *A. tumefaciens* carrying different constructs were mixed (called gene combinations), and *A. tumefaciens* harbouring empty vectors were used to compensate for the dosage of each gene in each combination (Table 2.7). Instead of *OsD27*, *OsCCD7* and *OsCCD8* that were shown by Zhang *et al.* (2014b) to result in the production of carlactone (CL) upon transient expression in *N. benthamiana*, I used *AtD27*, *MAX3* and *MAX4* to produce CL. By co-infiltrating *MAX1* and genetic variants with these genes, I can study the conversion of CL to carlactonoic acid (CLA). In all infiltration solutions, the agrobacterium strain carrying *p19* gene of tombusvirus was added to suppress gene silencing (Lakatos *et al.*, 2004). The combined solutions were mixed by rolling the tubes at room temperature for 2-3 hours. Infiltration was performed using 4-week-old *N. benthamiana* plants which were soil-grown in pots in a plant house with artificial light to make a photoperiod of 16 h light at 25 °C and 8 h dark 22 °C. Infiltration solutions were slowly injected into the backside of leaves by using a 1-mL syringe. The injection started at the abaxial side of the leaf which allowed the solution spread from abaxial side to the whole leaf area. Leaves at the same stage were selected to minimise the variability and the whole leaf area was infiltrated. For each gene combination, six individual plants (two leaves per plant were infiltrated) were used as biological replicates. Six days after infiltration, the infiltrated leaves were harvested and snap frozen in liquid nitrogen for further analysis.

Table 2.7. Combinations of different gene constructs for infiltration

Construct/gene combinations	Volume (v) of bacterial suspension of each gene added to each combination									
	D27	MAX3	MAX4	MAX1-Col	MAX1-Ler	MAX1-GR	MAX1-GA	P19	pBIN-plus	Total
Empty vector	-	-	-	-	-	-	-	v	4v	5v
CL pathway	v	v	v	-	-	-	-	v	v	5v
CL+MAX1-Col	v	v	v	v	-	-	-	v	-	5v
CL+MAX1-Ler	v	v	v	-	v	-	-	v	-	5v
CL+MAX1-GR	v	v	v	-	-	v	-	v	-	5v
CL+MAX1-GA	v	v	v	-	-	-	v	v	-	5v

CL pathway includes D27, MAX3 and MAX4. 1v = 8 mL.

2.10. Biochemical analysis

2.10.1. Analysis of carlactone and carlactonoic acid in *N. benthamiana*

Samples were analysed for the presence of CL and CLA using UPLC-LC-MS/MS. For sample preparation, 200 mg fine-ground *N. benthamiana* leaves were extracted in 2 mL of ethyl acetate, using GR24 (5 pmol) as internal standard. Samples were vortexed and centrifuged for 20 mins at 2000 r.p.m. at 4 °C. The supernatant was dried *in vacuo*. Prior to mass analysis, samples were reconstituted in 100 µL of 25% acetonitrile/water (v/v) and filtered using a micro-spin 0.2 µm nylon membrane filter (Thermo Fisher Scientific, Waltham, MA, USA).

Extracted samples were submitted to Kristyna Flokova (University of Amsterdam) for CL and CLA analyses. The targeted analysis of CL and CLA was performed by on an Acquity UPLC system (Waters, Milford, MA, USA) coupled to a Xevo® TQ-XS triple-quadrupole mass spectrometer (Waters MS Technologies, Manchester, UK) with electrospray (ESI) interface. Samples were injected onto a reverse-phase UPLC® column Acquity BEH C18 (2.1x100mm, 1.7 µm, Waters), thermostat held at 45°C. The retention of analytes was controlled by gradient elution of 15 mM formic acid in water (A) and 15 mM formic acid in acetonitrile (ACN, B) at a flow rate 0.4 ml/min. The 10 min linear gradient started by isocratic elution 0-0.5 min with 5% B, increased to 60% B in 1.5 min and to 90% B in the next 5.3 min. The column was washed for 1.5 min with 90% B and equilibrated for to initial conditions for 1.5 min. The eluate was introduced in the ESI ion source of the triple quadrupole

MS analyser, operating in both positive and negative mode at following conditions: capillary voltage (1.2 kV), ion source/desolvation temperature (150/600°C), desolvation/cone gas flow (1000/150 L.h-1), cone voltage (20-25 V) and collision energy (18-25 eV). MS data were recorded in multiple reaction monitoring mode (MRM) of four characteristic transitions for each of the compounds. MassLynxTM software package (version 4.2, Waters, Milford, MA, USA) was used to operate the instrument, and acquire and process MS data.

2.10.2. Volatile analysis by Gas Chromatography–Mass Spectrometry (GC-MS)

Volatiles emitted from *dis51* mutant were examined by using GC-MS. Arabidopsis plants were grown in the growth cabinet under normal growth conditions (Section 2.3.1). ~200 mg fully opened flowers (combined from 6 individual plants per genotype) were harvested from 6-7 weeks old WT and *dis51* plants and were collected into 20-mL headspace vials (Shimadzu). After flower collection, vials were sealed and submitted to Martin Hunt (PFR, Palmerston North, NZ) for GC-MS analysis. Samples were incubated at 40°C for 5 minutes before sampling using divinylbenzene (DVB) fibre. Volatiles were screened by GC-MS using solid-phase microextraction (SPME)/cryo-focusing on the GCMS-TQ8050 (Shimadzu, Japan). The *dis51* mutant was also sent to Harro Bouwmeester and Rob Schuurink (both from University of Amsterdam) for volatile analysis.

2.11. Bioinformatic analysis

2.11.1. *In silico* analysis

The three-dimensional structure of *At*D14 was obtained from the SL-induced AtD14-D3-ASK1-complex (PDB: 5HZG) (Yao *et al.*, 2016). The MAX1 protein sequence was submitted to I-TASSER On-line Server (Zhang, 2008; Roy *et al.*, 2010; Yang *et al.*, 2015) (https://zhanglab.ccmb.med.umich.edu/I-TASSER/) and the homology model of MAX1 was calculated using default settings. The 3D images were prepared with the CCP4MG (McNicholas *et al.*, 2011) and were provided by Andrew Sutherland-Smith.

2.11.2. WGS data analysis

The trimmed reads from WGS data of *dis9* and *dis15* were obtained from Donald Hunter (PFR, Palmerston North, NZ). The trimmed reads of *dis9* were aligned to the L*er*-0 reference obtained from Korbinian Schneeberger (Max Planck Institute for Plant Breeding Research). The alignment was carried out using Bowtie 2 software (Langmead and Salzberg, 2012) with the help of Dave Wheeler (Massey University, School of Fundamental Sciences, currently at NSW Department of Primary Industries). Commands used in Bowtie 2 were:

```
# command 1 (Indexing Ler-0 reference genome)
bowtie2-build ler.fa ler_ref
# command 2 (Aligning dis9 reads)
bowtie2 --very-sensitive-local -x ler-ref -1 reads_R1.fq -2 reads_R2.fq -S ler_ref.sam
# command 3 (.bam file was created by Dave Wheeler for saving the space in the disk)
bowtie2 --very-sensitive -p 2 -x ler_ref -1 Dis9_ec.paired.mcf20.A.fastq.gz -2 Dis9_ec.paired.mcf20.B.fastq.gz | samtools view -bS - > output.bam
```

The .bam file was opened with the Integrative Genomics Viewer (IGV) (Robinson *et al.*, 2011; Thorvaldsdottir *et al.*, 2013) for SNP identification in the mapped region.

The trimmed reads of *dis15* were aligned to the MAX1 CDS using the 'Map to Reference' function in Geneious desktop software (Kearse *et al.*, 2012).

2.11.3. Standard sequence alignments

Standard sequence alignments were generally performed using the 'Map to Reference' function in Geneious desktop software (Kearse *et al.*, 2012). Sequences of all cytochrome P450 proteins with cysteine haem-iron ligand signature were aligned using 'Multiple Align' function in Geneious.

2.11.4. Accession numbers

The accession numbers for the Arabidopsis genes (TAIR IDs) are: *NYC1* (*AT4G13250*), *EIN2* (*AT5G03280*), *MAX3* (*AT2G44990*), *MAX4* (*AT4G32810*), *MAX1* (*AT2G26170*), *D14* (*AT3G03990*), *MAX2* (*AT2G42620*), *SMXL6*

(*AT1G07200*), *SMXL7* (*AT2G29970*), *SMXL8* (*AT2G40130*), *NAP* (*AT1G69490*), *ANAC092* (*AT5G39610*), *SAG12* (*AT5G45890*), *SGR1* (*AT4G22920*), *AKINβ1* (*AT5G21170*), *ACS2* (*AT1G01480*), *bZIP63* (*AT5G28770*), *PP2AA3* (*AT1G13320*), *ACT2* (*AT3G18780*) and *MON1* (*AT2G28390*).

The accession numbers for the protein sequences (UniProt IDs) used in this study are as follows: Arabidopsis AtD14 (Q9SQR3), AtKAI2 (Q9SZU7); rice OsD14 (Q10QA5); petunia PhDAD2 (J9U5U9); poplar PtD14a (B9GNP9); pea PsRMS3 (A0A109QYD3); Arabidopsis AtMAX1 (B9DFU2); rice Os900 (M9R6D3), Os1400 (W5QV10), Os1900 (Q0E2P9) and Os5100 (Q5Z6A5); petunia PhMAX1 (I1SSI4); maize ZmMAX1a (C0PKK5), ZmMAX1b (C4PJN6) and ZmMAX1c (B7ZXI8); tomato SlMAX1 (K4CL78); poplar PtMAX1a (U5FFK5) and PtMAX1b (U5G8D7); and Selaginella SmMAX1a (M9R4W4) and SmMAX1b (D8RNA4).

2.12. Statistical analysis

Statistical analysis was performed with GenStat 17th Edition (a VSNI product: https://www.vsni.co.uk/software/genstat/). One-way ANOVA (Fisher's protected LSD test $P<0.05$) was used to determine the statistical significances for the Chl data, qRT-PCR data and nCounter data for a period of 72-h of dark treatment in WT L*er*-0. A linear mixed model was used to determine the differences for the data of a period of 6-h and 18-h treatments in both WT and *max1-5*/*dis15* (with rac-GR24 or 1% DMSO treatment). Comparisons among means were made using least significant differences at $P=0.05$ (5% LSD).

3. Mutant defective in NYC1 exhibits a “stay-green” phenotype of excised Arabidopsis inflorescence upon dark treatment

3.1. Introduction

Forward and reverse genetics are effective approaches for the functional study of specific genes (Alonso and Ecker, 2006). Forward genetics is the classical method in genetics, which starts with a large-scale mutant screen for a particular phenotype and subsequently identifies the causal mutation(s) that is/are responsible for this phenotype (Peters *et al.*, 2003). The mutants used for the phenotypical analysis are usually created by chemical (e.g. ethyl methanesulfonate; EMS) or radiation (e.g. X-rays) treatment or insertional mutagenesis (e.g. T-DNA/transposon) (Koornneef *et al.*, 1982; Alonso and Stepanova, 2003; Kim *et al.*, 2006b). In Arabidopsis, EMS mutagenesis primarily (>99%) induces C/G to T/A transitions in the genome (Greene *et al.*, 2003). Of these EMS-induced mutations, ~5% lead to premature stop codons of the encoded proteins, while 50-65% are missense mutations which cause single amino acid substitutions in the coding region (McCallum *et al.*, 2000; Greene *et al.*, 2003). These missense mutations are very valuable for analysing gene function and protein structures. Apart from creating gain/loss-of-function mutants, EMS mutagenesis also generates leaky mutations that result in partially reduced function of the targeted genes (Maple and Møller, 2007). Thus, it is very useful for studying a gene that is lethal when mutated in plants (Chen *et al.*, 2001a; Katoh *et al.*, 2006; Schippers *et al.*, 2008; Robert *et al.*, 2010; Xu *et al.*, 2010; Effendi *et al.*, 2015). By contrast, T-DNA/transposon insertion usually causes completely knock-out of the targeted genes (Alonso and Stepanova, 2003; Radhamony *et al.*, 2005). Thus, EMS mutagenesis is considered as a powerful tool for identifying novel genes involved in the regulation of various biological processes. The advantages of a forward genetic approach are that they are effective and guaranteed to provide the result. However, it is not an ideal method for systematic genome-wide functional analysis because of the enormous effort required to characterise the genetic lesions (Peters *et al.*, 2003).

By contrast, reverse genetic analysis begins with selecting the gene(s) of interest, and then characterising the gene function by phenotypic analysis of mutants defective in selected genes or transgenic lines that contain gain-of-function (e.g. overexpression) constructs (Peters *et al.*, 2003). In addition to the EMS and T-DNA insertional mutagenesis, other methods that are commonly used for generating mutation(s) of specific gene(s) include RNA interference, overexpressing the gene(s) via 35S CaMV promoter and the recently developed CRISPR/Cas9 system (Agrawal *et al.*, 2003; Lloyd, 2003; Zhang *et al.*, 2016; Hahn *et al.*, 2017). A reverse genetics approach is considered to be the faster and easier approach for functional studies of specific genes in the post-genome era (Alonso and Ecker, 2006). This strategy is especially suitable for studying model plants, e.g. Arabidopsis, owing to the availability of the genome sequence, a large number of mutants for specific genes, and well-developed reverse-genetics technologies (Page and Grossniklaus, 2002; Alonso and Ecker, 2006). Although reverse genetics is widely used in functional genomics nowadays, this strategy is biased due to the dependence of the researcher's judgment for selection of gene candidates. It is also risky because the altered phenotype(s) might not be exhibited in single mutants, owing to gene redundancy (Thomas, 1993; Eshed *et al.*, 2001).

In plant research, both forward and reverse genetics have successfully been applied to identify the genetic regulators of leaf and flower senescence (Oh *et al.*, 1997; Jing *et al.*, 2002; Higgins *et al.*, 2006; Raziuddin *et al.*, 2007; Li *et al.*, 2012; Jibran *et al.*, 2015). These not only include functional regulators of senescence but also genes regulating Chl degradation. For example, mutants defective in functional regulators such as *ANAC092* and *EIN2* affect senescence progression (John *et al.*, 1995; Oh *et al.*, 1997; kim, 2009; Trivellini *et al.*, 2012), whereas those defective in Chl catabolic genes such as *NYC1* and *PPH*, only affect Chl degradation and lead to a cosmetic stay-green phenotype (Kusaba *et al.*, 2007; Horie *et al.*, 2009; Schelbert *et al.*, 2009; Jibran *et al.*, 2015).

In order to study the novel regulators for floral organ senescence, a forward genetic approach was applied in my project, and 21 previously identified EMS

mutants (Jibran, 2014) were rescreened using AIDA (Chapter 2.3.2, Jibran *et al.*, 2015) to confirm their altered inflorescence degreening phenotypes. In this chapter, I describe the phenotypic, physiological and genetic analyses of selected mutants, and the characterisation of the genetic lesion in the *dis2* mutant.

3.2. Results

3.2.1. Phenotypic analysis of Arabidopsis EMS mutants

Screening of M4 plants of Arabidopsis EMS mutants

To identify the key genetic regulators in controlling inflorescence senescence, a large number of EMS mutants of Arabidopsis were screened previously by using AIDA to search for the ones that exhibited altered time to senescence as described in Chapter 1 (Section 1.4). In total, thirty mutants, including 10 *ais* and 20 *dis*, were found (Jibran, 2014). In this study, twenty-one of these mutants were retested to confirm their altered timing of degreening phenotypes.

For the M4 putative homozygous mutants, the delayed inflorescence yellowing phenotype of *dis2*, *dis7*, *dis31* and *dis51* was confirmed at day 5 of dark incubation though there was variation within biological replicates (Figure 3.1A). However, no visible colour difference was observed between *dis29* and WT during dark treatment. Unexpectedly, the *dis24* and *dis54* exhibited accelerated time to degreening of detached dark-held inflorescences as compared to the WT, although their inflorescences were also less green than WT at day 0 (before dark treatment).

Screening of segregating population of Arabidopsis EMS mutants

To characterise the genetic nature of the *ais* or *dis* trait, M4 plants were backcrossed with WT L*er*-0 by previous researchers as described in Chapter 2.1 to generate the F2 population for segregation analysis. Plants were grown from F2 seeds and the segregation of the *ais* and *dis* phenotypes in inflorescences was examined at day 5 of dark incubation (Figure 3.1B). The number of inflorescences that displayed clearly *ais* or *dis* phenotypes (samples circled with orange or green colours in the figure) was counted and the observed WT to mutant ratios were calculated for genetic analysis. The Chi-squared test was used to determine whether the observed ratio was significantly different from the expected ratio (3 to 1 for a monogenic recessive mutation) and the result was presented in Table 3.1. Although the colour difference between WT and mutants was not very clear in all F2 populations, the degreening phenotype was readily distinguishable in *ais3*, *ais10* and *dis3*

compared with WT. The statistical analysis indicated their segregation ratios were not significantly different (P<0.05) from 3 to 1, which suggested their *ais* and *dis* phenotypes were monogenic recessive traits.

In planta phenotypes of the *ais* and *dis* mutants

Besides the *ais* and *dis* phenotypes, some mutants also exhibited other phenotypes *in planta* (Table 3.2). Representative examples are shown in Figure 3.2. For instance, one out of the sixteen F2 plants of *ais3* and all of the M4 plants of *dis7* exhibited round and layered rosette leaves (Figure 3.2A, B), though the leaf phenotype for *dis7* varied (Figure 3.2B1-3). Two out of 24 F2 plants of *ais20* displayed smaller inflorescences and shorter siliques compared with WT (Figure 3.2C), whereas all M4 plants of *dis51* exhibited bigger petal and longer siliques (Figure 3.2D). Interestingly, the flowers of two out of 24 F2 plants of *ais61* showed a leaf-like structure (Figure 3.2C) and such phenotype is similar to the one that was reported on *apetala 1-1* (*ap1-1*) mutant (Irish and Sussex, 1990).

Based on the results above, four *dis* mutants, which are *dis2*, *dis3*, *dis7* and *dis51*, were selected for the further analysis because of their clearer *dis* phenotype and interesting *in planta* phenotypes.

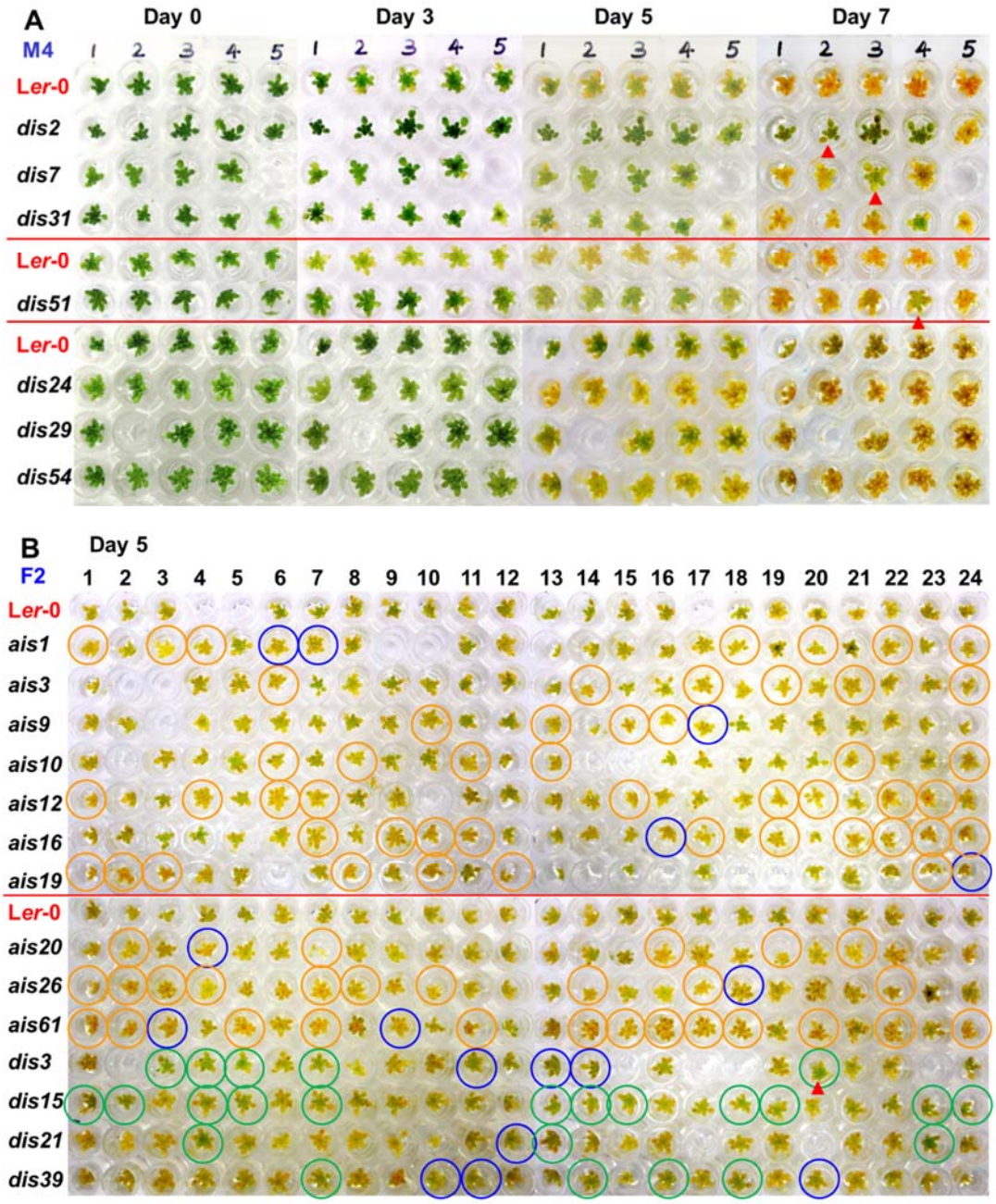

Figure 3.1. Degreening of detached and dark treated inflorescences

(A) AIDA screening of M4 plants. Immature inflorescences were harvested from primary bolts of the *dis* mutants and L*er*-0 WT, respectively. Five biological replicates are shown. Photos were taken at day 0 (before dark incubation), 3, 5 and 7 of dark treatment. (B) AIDA screening of backcrossed (x L*er*-0) F2 segregating population. Immature inflorescences were harvested from primary bolts of the *ais* and *dis* mutants and L*er*-0, respectively. The number of F2 plants investigated per mutant is indicated at the top of the figure. Photos were taken at day 5 of dark incubation. Inflorescences exhibiting *ais* or *dis* phenotypes are circled with orange and green colours respectively. Phenotypes that were not clear are circled in blue. In both (A) and (B), the red lines separate the experiments that were conducted at different times. The degreening phenotype of the mutants is compared to L*er*-0. Red triangles indicate inflorescences from plants for which their progenies in the subsequent generation were retested for *ais* or *dis* phenotypes (Figure 3.3 and 3.6).

Table 3.1. Pearson's chi-squared test for F2 population of *ais*/*dis* x L*er*-0

Mutants	Total plants	WT-like plants	*ais* or *dis* – like plants	Observed ratio (WT : mutant)	χ^2	*P*-values
ais1	22	15	7	~2.1:1	0.545	0.4602
ais3	22	16	6	~2.7:1	0.061	0.8055
ais9	23	19	4	~4.8:1	0.710	0.3994
ais10	21	15	6	~2.5:1	0.143	0.7055
ais12	23	14	9	~1.6:1	2.449	0.1176
ais16	24	14	10	1.4:1	3.556	0.0593
ais19	19	12	7	~1.7:1	1.421	0.2332
ais20	24	19	5	~3.8:1	0.222	0.6374
ais26	24	14	10	1.4:1	3.556	0.0593
ais61	24	11	13	~0.8:1	Not clear	Not clear
dis3	19	14	5	2.8:1	0.018	0.8946
dis15	24	12	12	1:1	Not clear	Not clear
dis21	22	19	3	~6.3:1	1.515	0.2184
dis39	24	20	4	5:1	0.889	0.3458

Chi-squared test was used to test the statistical difference between observed ratio and expected ratio (3:1) of the WT to mutant degreening inflorescence phenotypes. "~" means approximately. $P<0.05$ implies a statistical significance. "Not clear" means the segregation ratios in the F2 population of *ais61* and *dis15* mutants are abnormal, not following the recessive segregation ratio (e.g. 3:1 for monogenic recessive trait). This is against with the previous findings that suggested the *ais* or *dis* trait was a recessive trait (Jibran, 2014). Thus, further analyses are required to determine the genetic nature of these two mutants.

Table 3.2. Summarised phenotypes of 21 EMS mutants

Mutants	*ais* or *dis*	Observed *in planta* phenotypes
dis2	*dis*	Bushy, delayed bolting, flowering and attached sepal degreening, dark green colour of whole plant
dis7	*dis*	Bushy, round and layered rosette leaves, light green colour of whole plant
dis24	*ais*	Accelerated bolting and flowering, light green colour of whole plants
dis29	WT-like	WT-like
dis31	*dis*	Bushy, more branching, light green colour of whole plant
dis51	*dis*	Bushy, delayed bolting, flowering, bigger petal and leaf, with aroma
dis54	*ais*	WT-like
dis3	*dis*	WT-like
dis15	Not clear	WT-like
dis21	*dis*	WT-like
dis39	*dis*	WT-like
ais1	*ais*	WT-like
ais3	*ais*	Only one plant showed round rosette leaf, stunted, short silique and light green colour of whole plant
ais9	*ais*	Five plants showed small leaves and thin stems
ais10	*ais*	WT-like
ais12	*ais*	Three plants showed less rosette leaves
ais16	*ais*	WT-like
ais19	*ais*	Three plants have more rosette leaves and shorter stems
ais20	*ais*	Two plants showed stunted, small inflorescence and short siliques
ais26	*ais*	WT-like
ais61	Not clear	Flowers of two plants showed leaf-like structure

The listed phenotypes were based on the preliminary screening described above. First column specifies original designation of mutant. Second column specifies the *ais* or *dis* phenotype observed in this screening. "Not clear" has the same meaning as explained in Table 3.1.

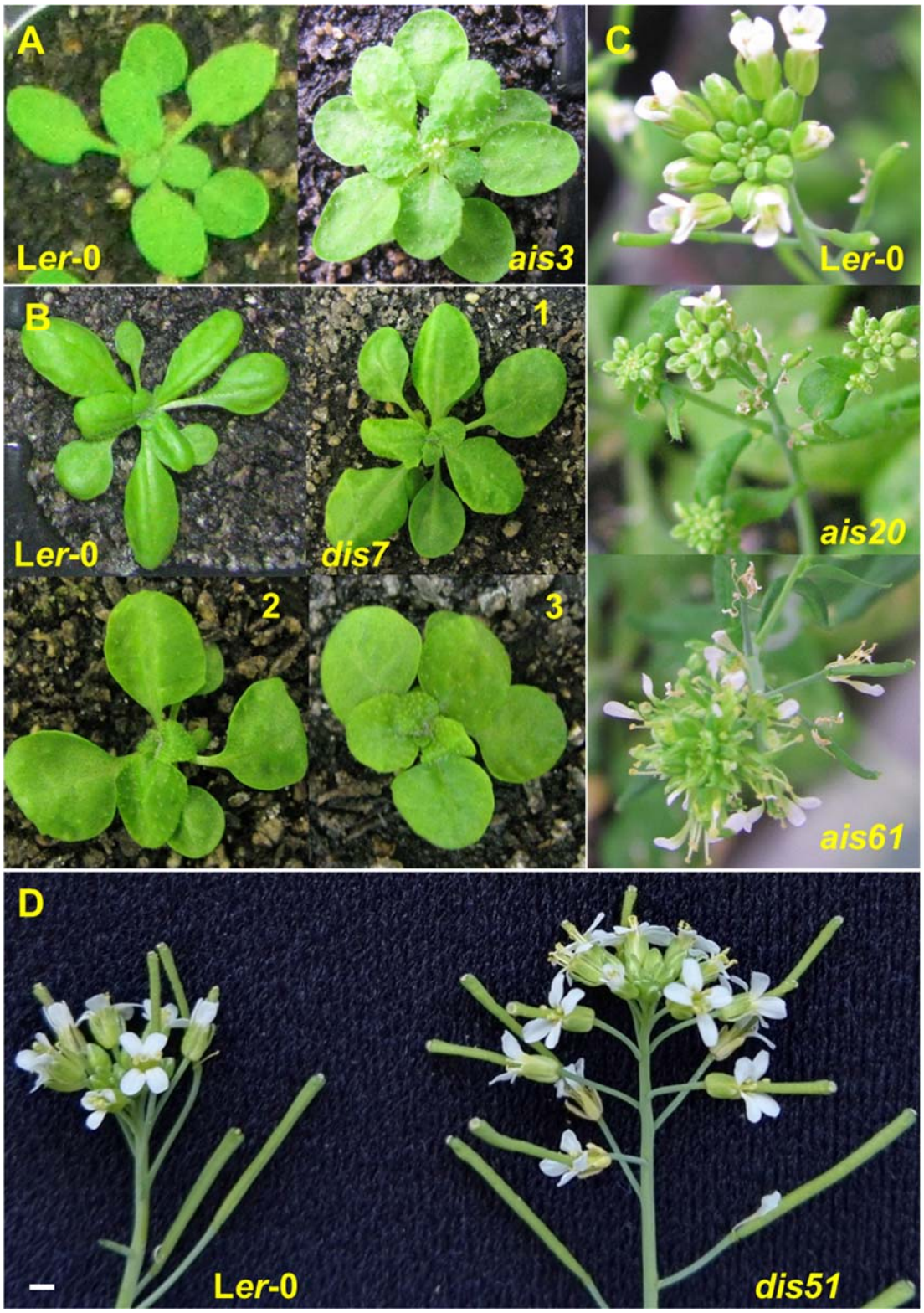

Figure 3.2. *In planta* phenotypes of *ais3*, *ais20*, *ais61*, *dis7* and *dis51*
Rosette leaf phenotypes for (A) 3-week-old *ais3* plant and (B) 4-week-old *dis7* plants. (B 1-3) Variations of rosette leaf phenotypes in different plants. Floral organs and silique phenotypes for (C) 8-week-old *ais20* and *ais61* plants and (D) 7-week-old *dis51* plant. Plants were grown in long day conditions (18-h-light/6-h-dark) and were grown in growth chamber for *ais3*, *ais20*, *ais61* and *dis7* but in growth cabinet for *dis51* (Section 2.3.1).

3.2.2. *dis2*, *dis3*, *dis7* and *dis51* exhibit stable delayed degreening phenotypes in subsequent generation

Since the variation for the *dis* phenotype occurred within biological replicates, the degreening phenotype of *dis3*, *dis7* and *dis51* was rescreened in their subsequent generation for the indicated samples in Figure 3.1. All of them exhibited a stable *dis* phenotype (Figure 3.3). For the *dis2* mutant, the screening was not done in the subsequent M5 plants because the plants were severely damaged by spider mites. However, a separate analysis on M4 plants of *dis2* confirmed its *dis* phenotype (Figure 3.3). Strikingly, the excised inflorescences of these plants were still green at day 11 of dark incubation (Figure 3.3).

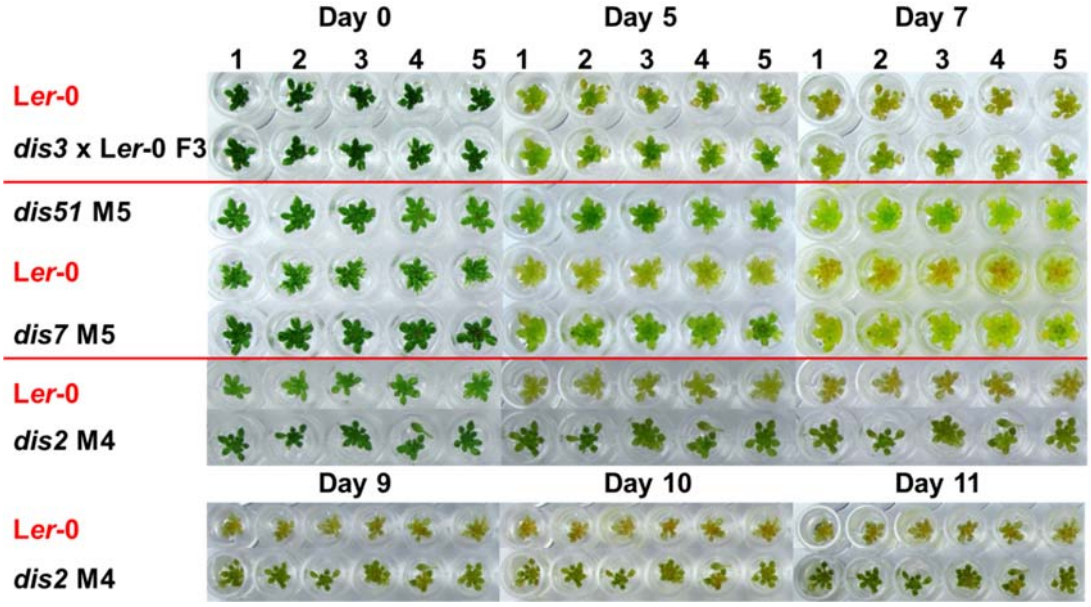

Figure 3.3. The stability of *dis* phenotype in *dis2*, *dis3*, *dis7* and *dis51*
Immature inflorescences were harvested from primary bolts of M4 plants for *dis2*, M5 plants for *dis7* and *dis51*, and backcrossed F3 plants for *dis3* respectively. Red lines separate the independent experiments. The degreening of the mutants is compared with L*er*-0. Five biological replicates are shown. Photos were taken before (day 0) and after 5 and 7 days (and 9, 10 and 11 days for *dis2*) dark treatment.

3.2.3. Chlorophyll analysis of *dis2*, *dis3*, *dis7* and *dis51* during dark incubation

Chl analysis was used to confirm the degreening phenotype of selected *dis* mutants. At day 5 of dark incubation, the *dis2* and *dis51* mutants retained significantly more Chl including total Chl, Chl *a* and Chl *b* than WT in their detached inflorescences (Figure 3.4.A, B). Interestingly, *dis2* exhibited

preferential Chl *b* retention (nearly 1.6 times higher Chl *b* retention than *a*; *P*<0.01), whereas *dis51* retained Chl *a* and Chl *b* at similar levels (*P*>0.05). The Chl analyses for *dis3* and *dis7* were carried out at day 3 of dark incubation because it was difficult to measure the extremely low Chl content of WT inflorescences at day 5. The Chl retention in *dis3* was significantly higher than WT (*P*<0.01), while there was no significant difference in Chl retention between Chl *a* and Chl *b* (Figure 3.4.C). In contrast, *dis7* retained similar amounts of Chl as the WT (Figure 3.4.D).

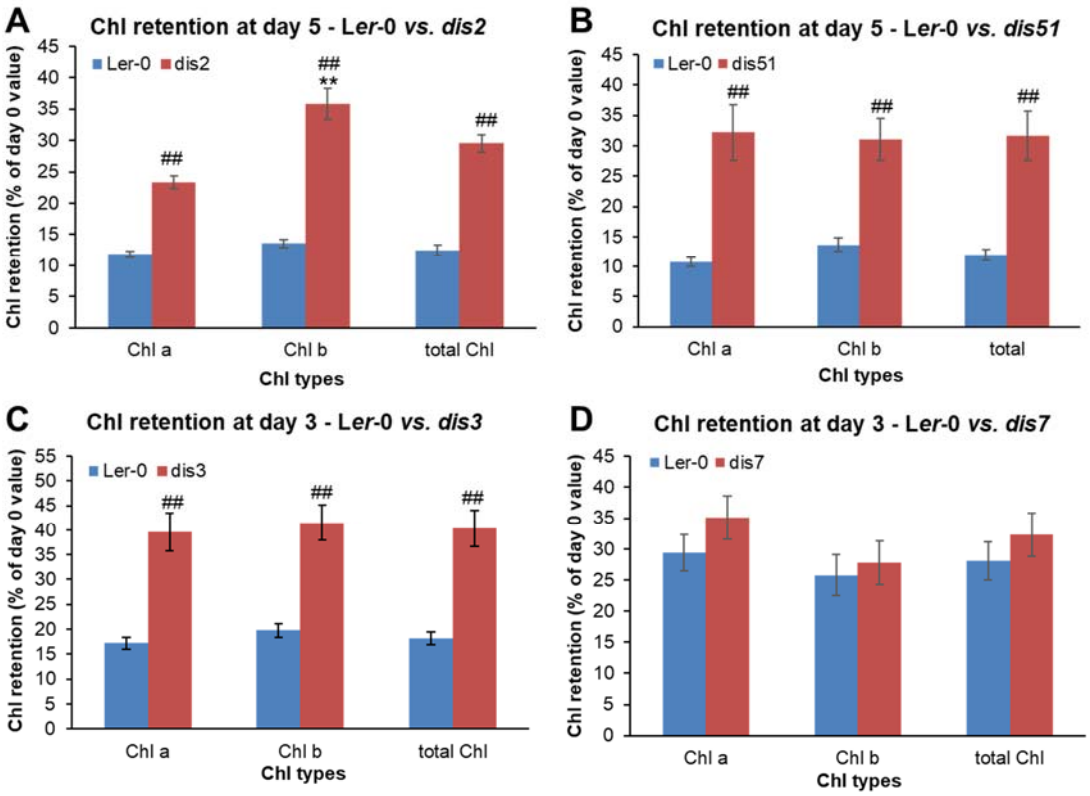

Figure 3.4. Chl retention of *dis* mutants during dark incubation
Chl retention (% of day 0 Chl content) at day 5 for *dis2* (A) and *dis51* (B) or at day 3 for *dis3* (C) and *dis7* (D) of dark incubation. Abbreviations: Chl, chlorophyll. The error bars show the standard error (S.E.). The asterisks represent the significant differences between Chl *a* and Chl *b* in each phenotype. The hash symbols represent the significant differences between L*er*-0 and *dis* mutants in each Chl type. Double asterisks or hash symbols indicate *P*<0.01.

3.2.4. *dis2* exhibits delayed time to bolting and flowering

Apart from *dis* phenotype, M4 plants of *dis2* showed delayed time to bolting and flowering compared with WT (Figure 3.5.A). The time to bolting and flowering of *dis2* was delayed by approximately 14 and 10 days respectively (Figure 3.5.B,

C). Also, such delays for *dis2* plants were also observed in the subsequent M5 generation (Appendix 6.1).

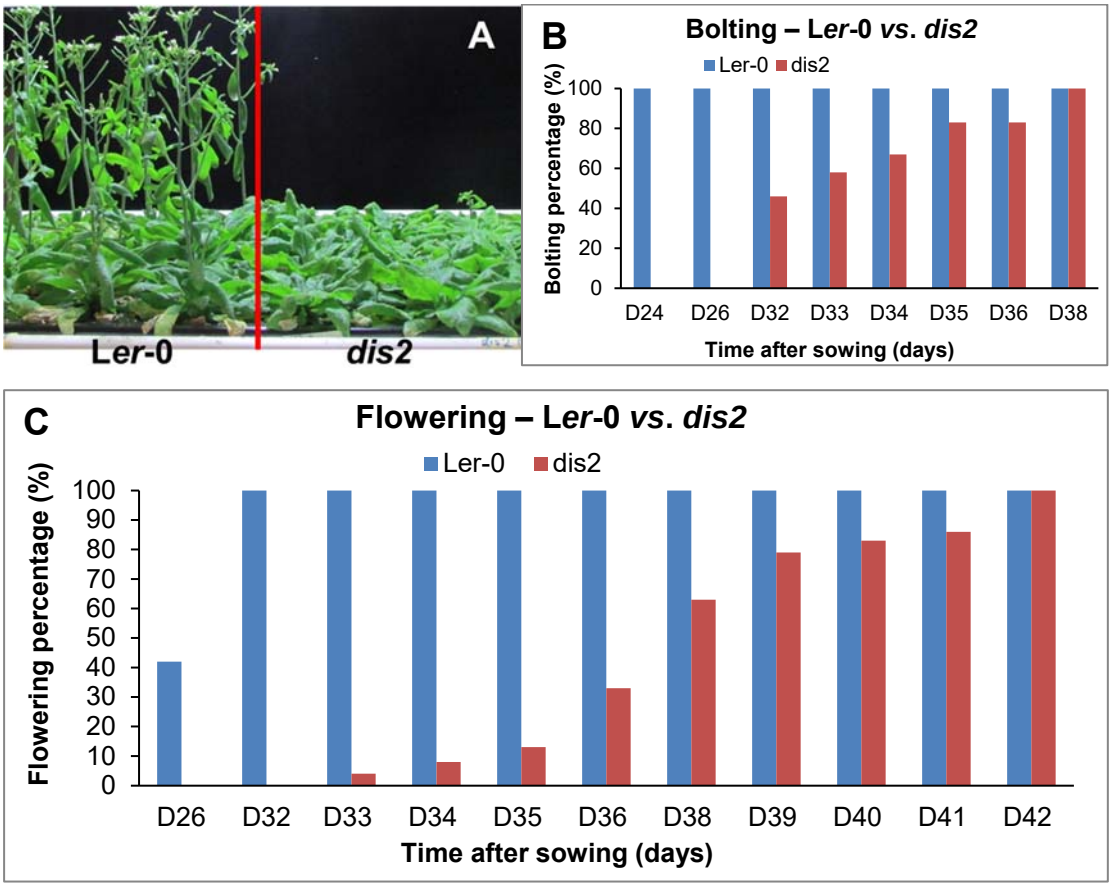

Figure 3.5. Time to bolting and flowering of *dis2*
(A) Delayed bolting and flowering of *dis2* during plant development. M4 plants were grown in growth chamber under long day conditions (18h/6h light/dark). Photo was taken at 32 days after sowing. Red line separates L*er*-0 and *dis2* plants. (B) Percentage of plants that had primary bolts at the specified time after sowing. (C) Percentage of plants that had first flower opened from the primary bolt at the specified time after sowing. D on X axis of (B) and (C) means days after sowing.

3.2.5. The delayed inflorescence degreening of *dis2* is not caused by delayed time to flowering

To test whether the delayed degreening of *dis2* was caused by the delayed transition from juvenile phase (vegetative growth) to reproductive phase (flowering), time to flowering between WT and *dis2* mutant was synchronised by sowing *dis2* seeds ahead of WT (as described in Section 2.3.4). The inflorescences of WT and *dis2* mutant, that were flowering at the same time but were harvested from plants of different ages, exhibited a similar delay in time to yellowing during dark treatment (Figure 3.6) as observed before (Figure 3.3).

Therefore, the delayed degreening of *dis2* was not caused by the delayed time to flowering.

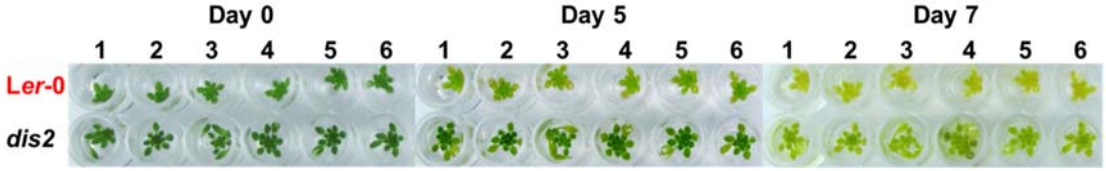

Figure 3.6. Degreening of inflorescences of *dis2* at synchronised flowering time
Samples were collected from the inflorescences that having their first flower opened at the same time but at different plant ages. Inflorescences from 29-day-old L*er*-0 and 41-day-old M5 plants of *dis2* were harvested. Mutants are compared with L*er*-0. Photos were taken before (day 0) and after 5- and 7-days of dark treatment. Six biological replicates are indicated.

3.2.6. Detached cauline leaves of *dis2* exhibit delayed yellowing during dark incubation

To determine whether the delayed degreening of *dis2* was specific to the inflorescences, 12-day-old (after initiation) first cauline leaves of WT and *dis2* were harvested and held in the dark. The leaves of *dis2* exhibited delayed yellowing compared with that of WT at day 7 of dark treatment (Figure 3.7). Thus, the delayed degreening phenotype was not tissue specific in *dis2*.

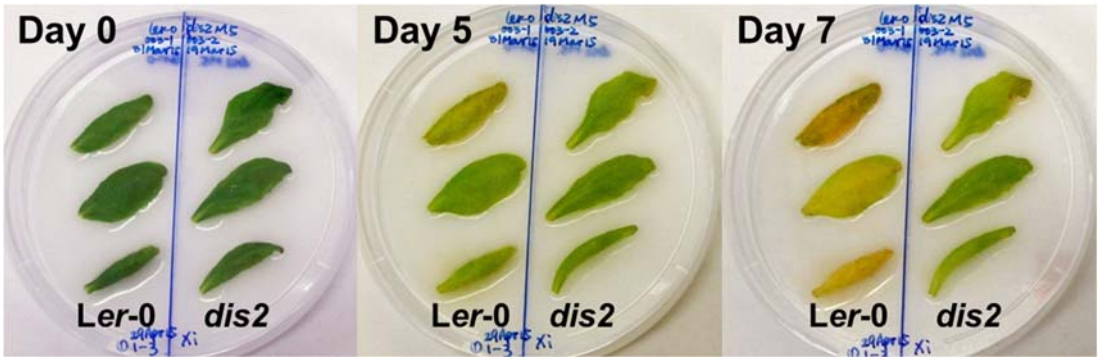

Figure 3.7. Degreening of detached dark-held leaves of *dis2*
Around 12-day-old first cauline leaves were harvested from M5 plants of *dis2* and compared to leaves of L*er*-0 of the same age. Photos were taken at day 0, 5 and 7 of dark treatment. Three representative biological replicates are shown.

3.2.7. The *dis2* phenotype is caused by a monogenic recessive trait

M4 plants of *dis2* were backcrossed to WT L*er*-0 to generate F2 population for segregation analysis. This analysis was used to determine the genetic nature of *dis* trait in *dis2*. In total 143 F2 plants were screened by using AIDA and an example for the segregated degreening phenotypes was shown in Figure 3.8.

The segregation ratio of WT to *dis2* was approximately 4 to 1 which was not significantly different from 3 to 1 by Chi-squared test (P>0.05). This indicated a monogenic recessive trait of *dis* phenotype in *dis2*.

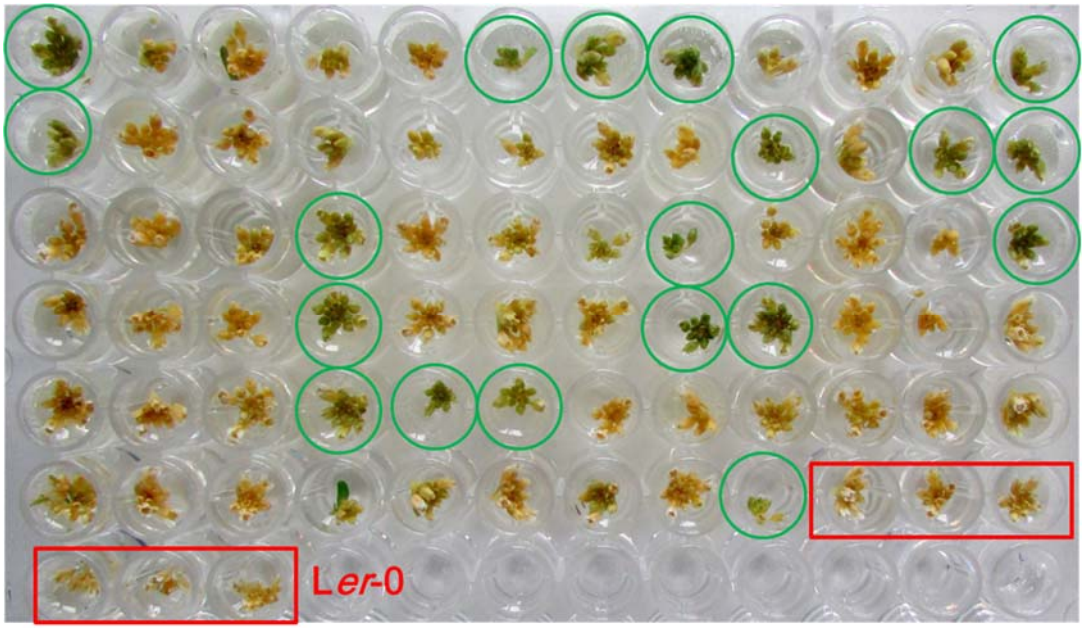

Figure 3.8. Example for segregation of F2 population of *dis2* x L*er*-0
L*er*-0 WT is circled with red rectangle, and the inflorescences showed a *dis* phenotype are marked with green circle. Photos were taken at day 5 of dark incubation.

3.2.8. *dis2* has a missense mutation in the coding sequence of *NYC1*

Amplification of *NYC1* in genomic DNA of *dis2*

The *dis2* phenotype suggested that the causal mutation in this mutant may affect Chl *b* degradation. Previous study has reported that a mutation in *NYC1* caused a phenotype similar to the *dis2* phenotype (Jibran *et al.*, 2015). Therefore, the *NYC1* gene from *dis2* plants was amplified by two independent PCRs with different proof-reading enzymes, and the results are shown in agarose gel images (Figure 3.9). The product size is 4.296 kb for genomic DNA of *NYC1*, which includes promoter, 5'-UTR, exons, introns, and 3'-UTR.

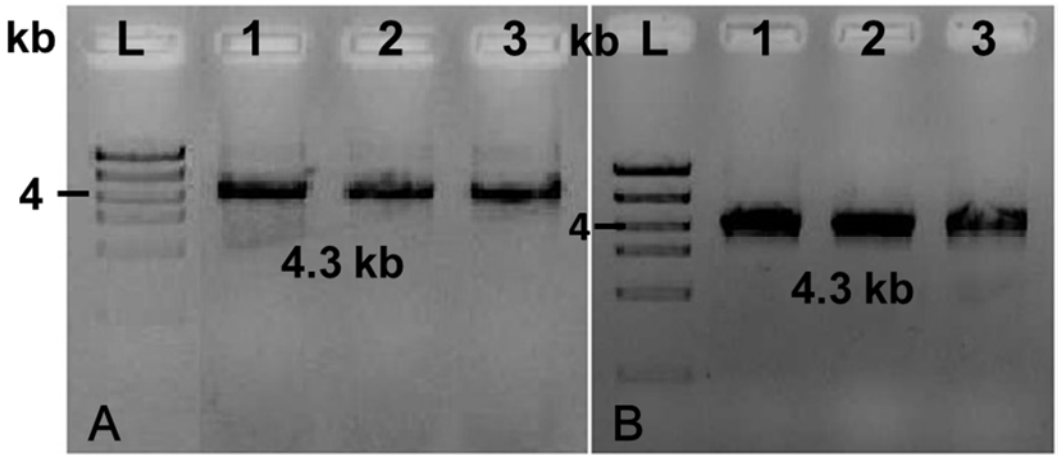

Figure 3.9. Amplification of *NYC1* in genomic DNA of *dis2*
(A) PCR performed with KAPA HiFi HotStart PCR Kit at 55℃ annealing temperature. (B) PCR performed with iProof High-Fidelity PCR Kit at 65℃ annealing temperature. L, high DNA mass ladder; kb, kilobase. The actual size of the amplified band is 4.296kb. Three technical replicates are shown. The number on the left side of the ladder represents the size of the band.

Sequencing of *NYC1* region in *dis2*

By sequencing, a point mutation (C to T) was identified in the area of exon eight of *NYC1* in *dis2* mutant (Figure 3.10). This point mutation causes a proline to serine substitution at amino acid position 360 (P360S) in NYC1 protein which may result in an altered function of this protein. The result suggests that a mutation in *NYC1* is likely to be the cause of the *dis2* phenotype.

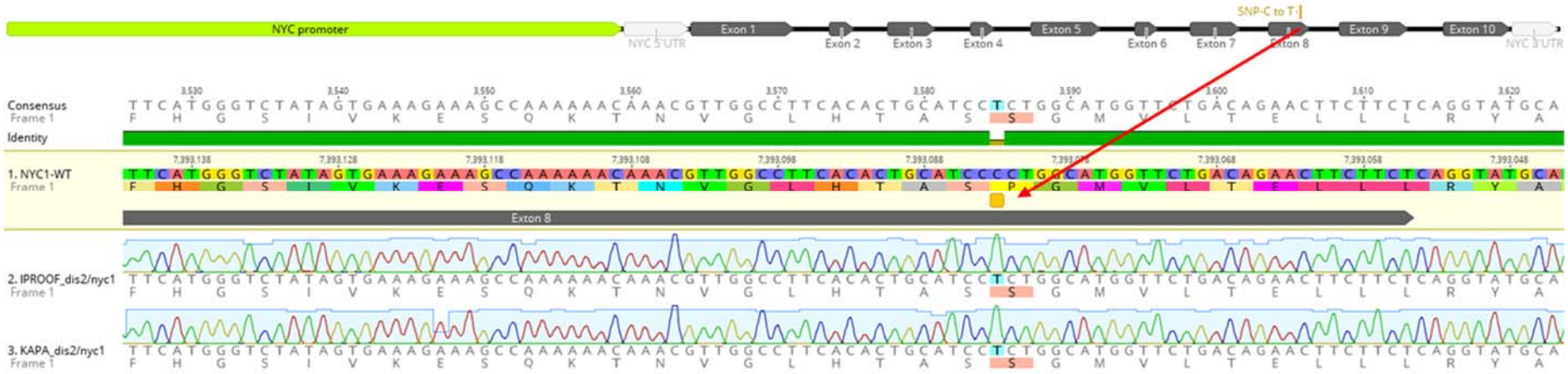

Figure 3.10. Sequencing of *NYC1* region in *dis2*

Sequences from PCR products (amplified with iProof and KAPA HiFi enzymes) were aligned to genomic DNA sequence of the WT *NYC1*. Schematic showing the gene structure of the WT *NYC1*. The mutation is indicated by the red arrow.

3.3. Discussion

3.3.1. Altered degreening phenotypes are confirmed in some EMS mutants

AIDA has been shown to be a useful method for visibly identifying mutants with altered timing of inflorescence degreening (Trivellini *et al.*, 2012; Jibran, 2014; Jibran *et al.*, 2015). Therefore, it was used in my research for multiple purposes, including confirmation of *ais* and *dis* mutants, test for hormone responses, and screening of segregating populations for genetic analysis. In this chapter, the altered degreening phenotypes of seven EMS mutants, with two *ais* and five *dis* mutants, were confirmed by using AIDA.

For the M4 mutants, the delayed degreening phenotype was confirmed for *dis2*, *dis7*, *dis31* and *dis51,* but not for *dis24*, *dis29* and *dis54*. The latter mutants either exhibited similar degreening as WT (e.g. *dis29*) or even displayed an accelerated yellowing (e.g. *dis24* and *dis54*). Differences from Jibran (unpublished data) may have arisen because of different growth environments (e.g. day/night length and temperature), which may change the production of stress-related hormones and thereby affect the timing of senescence (Lim *et al.*, 2007; Jibran *et al.*, 2013).

Of the 14 F2 backcrossed mutants examined, only *ais3*, *ais10* and *dis3* exhibited relatively distinguishable *ais* or *dis* phenotypes compared with WT. Their accelerated or delayed degreening phenotypes segregated in approximately 1:3 (mutant to WT), which suggested monogenic recessive *ais* or *dis* traits in these mutants. As for the rest of the *ais*/*dis* F2 mutants, it was difficult to distinguish whether they were accelerated or delayed in their inflorescence degreening compared with WT in the segregating population. This was reasonable because the altered degreening phenotypes for some of the mutants (e.g. *ais19*, *ais20*, *ais26*, *ais61*, *dis21* and *dis39*) was not very different to that of the WT when examined by Jibran (2014).

Although the altered degreening phenotypes of two *ais* (*ais3* and *ais10*) and five *dis* (*dis2*, *dis3*, *dis7*, *dis31* and *dis51*) mutants were visibly confirmed using

AIDA, Chl analysis was used to provide more precise physiological evidence for altered Chl catabolism in four selected *dis* mutants.

Chl loss is a marker that is typically used as a proxy of senescence progression (Matile *et al.*, 1996; Gan and Amasino, 1997; Trivellini *et al.*, 2012). However, in some instances such as in cosmetic stay-green mutants, measurement of Chl fails to reveal that senescence is occurring because their Chl catabolism is uncoupled from their underlying molecular senescence programme (Hörtensteiner, 2009). Therefore, in these mutants, other physiological markers such as photosynthetic activity and ion leakage are more informative for describing the timing of senescence (Kusaba *et al.*, 2007; Nakano *et al.*, 2014). In WT and functional stay-green mutants, however, Chl loss reliably indicates both initiation and progression of senescence (Woo *et al.*, 2001; Kim *et al.*, 2006a; Trivellini *et al.*, 2012).

In this study, Chl content was quantified to further characterise the *dis* phenotype in *dis2*, *dis3*, *dis7* and *dis51*. The *dis2*, *dis3* and *dis51* mutants retained significantly higher Chl content than WT at day 3 (for *dis3*) or day 5 (for *dis2* and *dis51*) of dark incubation, confirming their *dis* phenotype. Interestingly, *dis2* retained significantly higher Chl *b* than Chl *a* (Chl *a*/*b* ratio was approximately 0.63 for *dis2* but 0.87 for WT) and was still green even at day 11 of dark treatment. These findings raised the possibility that *dis2* was a cosmetic stay-green mutant with a defect in conversion of Chl *b* to Chl *a*, which can be caused by mutations in *NYC1* or *PPH* in *Arabidopsis* (Horie *et al.*, 2009; Schelbert *et al.*, 2009). By contrast, no preferential Chl *a* and Chl *b* retention was observed in *dis51* at day 5 and *dis3* at day 3 respectively, suggesting their mutations may not directly affect Chl catabolism.

Besides the altered inflorescence degreening phenotypes, several mutants also exhibited other phenotypes (list in Table 3.2) such as bushy rosette leaves (e.g. *dis2* and *dis51*) and altered leaf shape and colour (e.g. *ais3* and *dis7*). These multiple phenotypes might be due to the EMS mutagenesis of additional genes as it often causes multiple mutations in plant genomes (Kim *et al.*, 2006b;

Dinh *et al.*, 2014). Confounding background mutations that are unrelated to the *ais* or *dis* phenotypes could be eliminated by additional backcrossing.

I confirmed the *ais* and *dis* phenotypes of 7 mutants previously isolated by Jibran (2014). Chl analysis further confirmed the delayed degreening of 3 selected *dis* mutants. The *dis2* mutant appears to be a cosmetic stay-green mutant, suggesting a defect in a gene affecting Chl catabolism.

3.3.2. *dis2* has a defect in Chl catabolism and the mutation causes a P360S substitution in the NADPH binding pocket of the NYC1 protein

The genetic lesion that led to a stay-green phenotype of *dis2* was identified. Although EMS mutagenesis often induces multiple mutations in each treated plant (Kim *et al.*, 2006b; Dinh *et al.*, 2014), the 3 to 1 (WT to *dis*) segregation ratio suggests a monogenic recessive *dis* trait in the *dis2* mutant. The retained Chl *b*, compared with Chl *a*, in the *dis2* mutant but not WT suggested the mutation likely affects Chl *b* degradation. Chl *b* reductase plays a crucial role in the conversion of Chl *b* to Chl *a* in the initial step of Chl catabolism (Hörtensteiner, 2009; Hörtensteiner, 2013). In *Arabidopsis* and rice, it is encoded by two genes, *NYC1* and *NOL* (Kusaba *et al.*, 2007; Horie *et al.*, 2009). However, only a defect in *NYC1* leads to a stay-green phenotype in *Arabidopsis* (Horie *et al.*, 2009). This made *NYC1* a strong candidate for being the cause of the stay-green phenotype in *dis2*. This hypothesis was confirmed by the identification of a missense mutation (C/T transition) occurring in the exon 8 of the *NYC1* gene in the mutant. Unexpectedly, the same mutation was found in the *nyc1-4* mutant that was published by Jibran *et al.*, (2015). The mutation causes an amino acid change from proline to serine at the position of 360 (P360S) in the amino acid sequence (Jibran *et al.*, 2015).

NYC1 belongs to a short-chain dehydrogenase/reductase (SDR) superfamily, and the Pro360 of NYC1 is highly conserved in this SDR protein family in both plants and animals (Moummou *et al.*, 2012; Jibran *et al.*, 2015). *In silico* analysis indicates that the P360S substitution may change the steric structure of the NADPH binding site, making residue 360 become part of the end of the

β-sheet rather than the beginning of the coil (Jibran *et al.*, 2015). Previous study of the function of an equivalent proline residue (P185) in the recombinant SDR protein (3α-hydroxysteroid dehydrogenase/carbonyl reductase) from a human pathogen found that when P185 was mutated to Ala or Gly, the altered amino acids caused an increased flexibility of the substrate-binding loop (Hwang *et al.*, 2013). This increased flexibility substantially weakens the binding of NAD^+ in the mutant, thereby decreasing the catalytic efficiency of the enzyme (Hwang *et al.*, 2013). NYC1 has been suggested to use NADPH rather than NADH as its cofactor (Kallberg *et al.*, 2002; Kusaba *et al.*, 2007; Yin *et al.*, 2014). The finding in human pathogen raised a possibility that the stay-green phenotype of *dis2*/*nyc1-4* may also be caused by a similar mechanism (i.e. weaker binding of NADPH in the coenzyme pocket of mutated NYC1, which reduced the catalytic activity of this enzyme and thereby prevented the reduction of Chl *b*). The genetic complementation also supported that the delayed degreening of *nyc1-4* (i.e. *dis2*) was caused by the loss-of-function of NYC1 protein resulting from the P360S substitution (Jibran *et al.*, 2015). Thus, I conclude that the C/T transition in *NYC1* gene is responsible for the *dis* phenotype of *dis2* mutant.

Further analysis of *dis2* mutant also found that it exhibited a striking delay in time to bolting and flowering compared to WT. It has been widely suggested that plant organ senescence is under the direct control of age (Clarke *et al.*, 1994; Grbić and Bleecker, 1995; Tian *et al.*, 1995; Jing *et al.*, 2002). For example, the study of detached broccoli heads found that the peripheral older florets showed an earlier degreening than the central younger florets (Clarke *et al.*, 1994; Tian *et al.*, 1995). Similarly, in Arabidopsis it was previously noticed that WT inflorescences with more older buds showed accelerated degreening compared with those with more younger buds (Jibran, 2014). Therefore, this delayed timing of flowering made comparing inflorescence samples between WT and mutant problematic because when harvested at the same time, the WT inflorescences had more older buds than the detached inflorescences from *dis2* mutants. It also raises a possibility that the delayed degreening of *dis2* could have been because its inflorescences were younger than WT. To test this, an experiment was designed (see chapter 2.3.4) to enable inflorescences to be collected from WT and mutants that had the same number of young and old

buds. It was found that the degreening of the *dis2* mutant was still delayed compared with WT, indicating that it was not due to the younger inflorescences of the mutants at harvest time.

So far, it is not clear that the delayed time to bolting and flowering in the *dis2* mutant is also due to the defect in NYC1. Some common regulators have been found to participate in regulating both plant development and senescence (Jibran, 2014). For example, mutant defects in *WRKY53* exhibited both delayed time to flowering and senescence (Miao *et al.*, 2004). For *dis2*, however, the delay in bolting and flowering time is more likely caused by additional mutation(s) rather than the mutation in *NYC1* because these phenotypes have not been reported in other identified *nyc1* mutants (Kusaba *et al.*, 2007; Horie *et al.*, 2009; Sato *et al.*, 2009).

Previous AIDA screening found that the delayed degreening phenotype of many identified *dis* mutants such as *dis13* and *dis47* appeared to be specific to the inflorescence, suggesting that inflorescence senescence may be regulated by inflorescence-specific genes (Jibran, 2014). However, other studies have found that many *SAGs* regulate both leaf and inflorescence senescence. For instance, *Arabidopsis* mutants defective in *EIN2*, *ANAC092*, *MAX2* and *AHK3* showed delayed senescence in both leaf tissue and detached dark-held inflorescences (Kim *et al.*, 2006a; kim, 2009; Trivellini *et al.*, 2012). Here, the delayed degreening phenotype of *dis2* was observed in both inflorescences and leaves. As *dis2* was found to have the mutation in *NYC1*, this result is consistent with the findings that other characterised *nyc1* mutants in both rice and Arabidopsis also showed a stay-green phenotype in leaves (Kusaba *et al.*, 2007; Horie *et al.*, 2009; Sato *et al.*, 2009; Jibran *et al.*, 2015). This suggests *NYC1* regulates Chl catabolism in both tissues.

To sum up, the *dis2* mutant is identified as a non-functional stay-green mutant and it has a defect in *NYC1* gene. This gene regulates Chl degradation in both inflorescences and leaves.

4. Mutation in EIN2 contributes to the delayed degreening phenotypes of the *dis51* mutant

4.1. Introduction

Map-based cloning is a frequently used method for identifying the causal mutations induced by mutagens (Peters *et al.*, 2003; Uchida *et al.*, 2011; Zhu *et al.*, 2016). The first step of this method involves the generation of a segregating population for genetic mapping via linkage analysis. This is usually done by crossing the mutant to another WT accession of the same species between which sufficient genetic variation exists. The mutation can then be mapped to a chromosomal region by determining the linkage of the mutation to DNA polymorphisms (molecular markers) present between the accessions (Peters *et al.*, 2003).

HRM analysis has been shown to be an efficient, cost-effective and labour-saving technology for genotyping genetic variations such as SNPs and mutations in mapping populations (Gundry *et al.*, 2003; Liew *et al.*, 2004; Lochlainn *et al.*, 2011; Chagné, 2015). HRM analysis starts with PCR amplification of the DNA fragments with the variant of interest in the presence of special fluorescent dyes, such as LCGreen or ResoLight. These dyes only show high fluorescence when bound to double-stranded DNA (dsDNA) (Gundry *et al.*, 2003; Wittwer *et al.*, 2003; Liew *et al.*, 2004; Grievink and Stowell, 2008). In a segregating (mapping) population, markers such as SNPs can exist in homozygous or heterozygous state. During amplification, dsDNA fragments are denatured at 95 °C and then quickly reannealed at 40 °C (Chagné, 2015; Hunter *et al.*, 2018). This rapid melting/reannealing step is critical for the subsequent HRM analysis. During this step, homozygous samples reanneal perfectly to form homoduplexes (perfect complementary dsDNA duplexes), whereas heterozygous samples having more than one allele reanneal to form a mixture of homoduplexes and heteroduplexes (Gundry *et al.*, 2003; Chagné, 2015). In the following HRM analysis, PCR products are melted, and the dissociation causes a change in fluorescence, which is represented in a melting curve. Heterozygous samples containing heteroduplexes melt at lower temperature than homozygous samples containing only homoduplexes, and

therefore exhibit different melting profiles from that of homozygous samples. Moreover, since a single nucleotide difference in DNA sequence can cause a slight change in the melting curve, different homozygous alleles can often be distinguished as well (Gundry *et al.*, 2003; Chagné, 2015). Hence, the shape of the melting curve allows the discrimination between each of the homozygous and the heterozygous alleles. Since HRM-based PCR provides results within hours, it has been used extensively for high-throughput screening of segregating populations of EMS mutants in different plant species to map the causal mutations of a phenotype (Gady *et al.*, 2009; Botticella *et al.*, 2011; Lochlainn *et al.*, 2011; Jibran *et al.*, 2015). This technology can be used independently or in combination with whole genome sequencing (WGS) for mutation identification.

WGS has been considered to be an efficient and rapid method for identifying causative EMS-induced mutations by comparing the sequence of the mutant with that of the reference sequence (e.g. sequenced WT genome) (Schneeberger and Weigel, 2011; Thole and Strader, 2015). Such technology is especially suitable for model plants like Arabidopsis due to the availability of WT genome sequences of multiple accessions (Cao *et al.*, 2011) and a database for the genetic markers, e.g. single SNPs (TAIR, Map-based Cloning, https://arabidopsis.org/portals/mutants/mapping.jsp). When HRM analysis only maps the mutation to a chromosomal region, subsequent WGS can quickly identify the causal mutation by screening the SNPs between WT and mutant genomes in the mapped region.

In this chapter, HRM analysis was used to map the *dis* locus of the *dis51* mutant. I furthermore describe the phenotype of the *dis51* mutant and the identification of a mutation that contributes to the *dis51* phenotype.

4.2. Results

4.2.1. *dis51* exhibits delayed time to bolting and flowering

Besides the previous described phenotypes (Section 3.2.1), M4 plants of *dis51* also exhibited delayed time to bolting and flowering compared with WT (Figure 4.1.A). The delay in bolting and flowering times was around five and three days, respectively (Figure 4.1.B, C). Such delay was also observed in the subsequent M5 plants (Appendix 6.2).

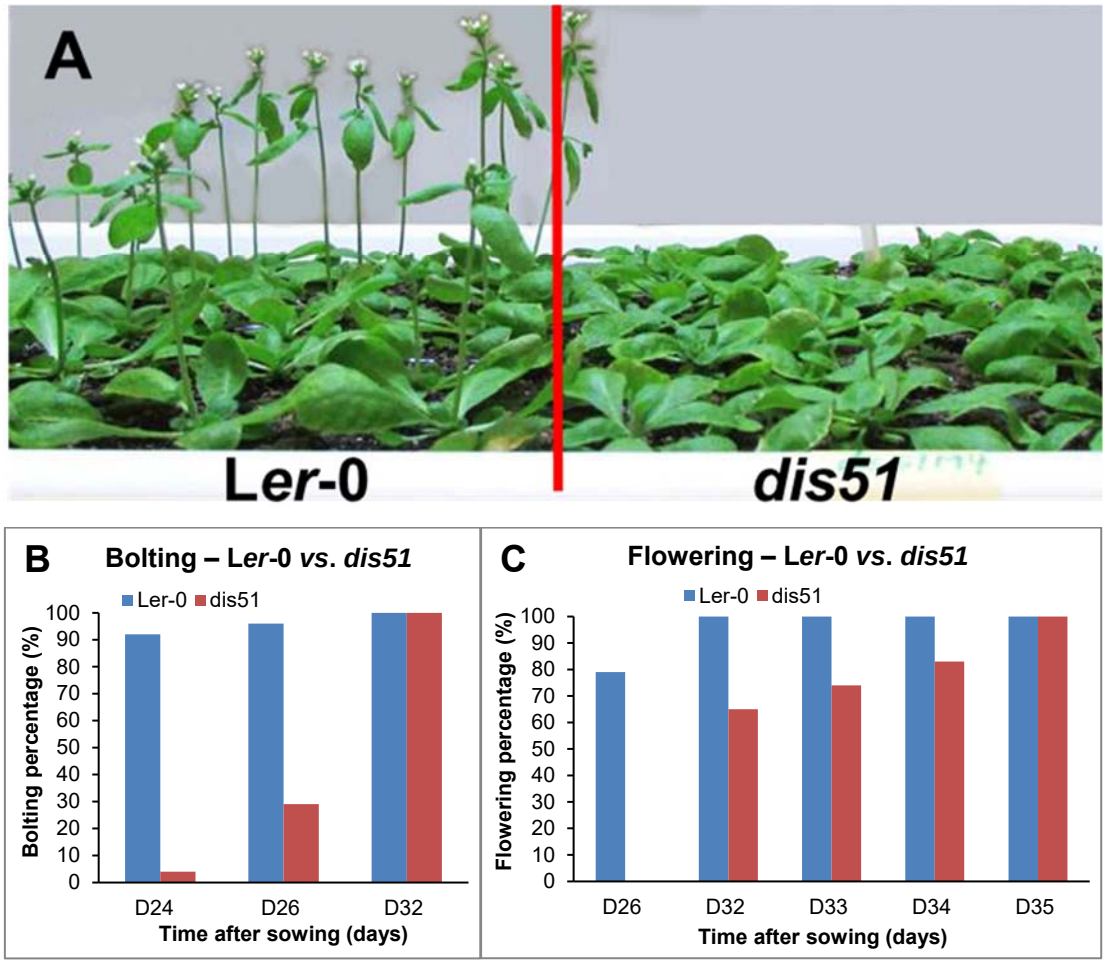

Figure 4.1. Time to bolting and flowering of *dis51*

(A) Delayed bolting and flowering of *dis51* during plant development. M4 plants were grown in growth chamber under long day conditions (18h/6h light/dark). Photo was taken at 26 days after sowing. Red line separates L*er*-0 and *dis51* plants. (B) Percentage of plants that had primary bolts at the specified time after sowing. (C) Percentage of plants that had first flower opened from the primary bolt at the specified time after sowing. D on X axis of (B) and (C) means days after sowing.

4.2.2. The *dis* phenotype of *dis51* is not due to delayed time to flowering

The synchronisation of time to flowering between WT and *dis51* (described in section 2.3.4) allows to examine if the *dis* phenotype of *dis51* was due to the

delayed transition from juvenile phase (vegetative growth) to reproductive phase (flowering). The inflorescences of WT and *dis51* mutant were harvested from the plants of different ages but were flowering at the same time. As observed before (Figure 3.3), inflorescences of *dis51* showed a delay in time to degreening compared with that of WT upon dark incubation (Figure 4.2). Thus, the delayed yellowing of *dis51* was not caused by its delayed time to flower.

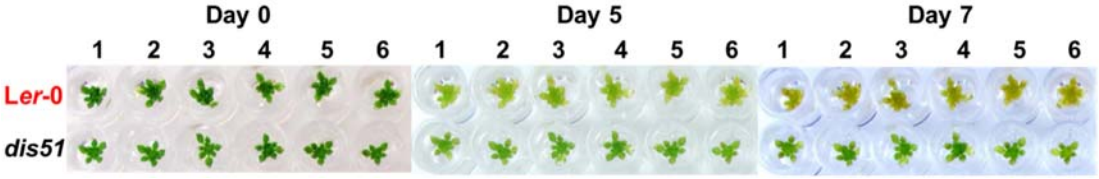

Figure 4.2. Degreening of inflorescences of *dis51* at synchronised flowering time
Samples were collected from the inflorescences that had their first flower opened at the same time but at different plant ages. Inflorescences from 28-day-old L*er*-0 and 32-day-old M5 plants of *dis51* were detached. Mutants are compared with L*er*-0. Photos were taken before (day 0) and after 5 and 7 days of dark incubation. Six biological replicates are shown.

4.2.3. *dis51* shows delayed yellowing of detached dark-held cauline leaves

To test if the delayed yellowing of *dis51* was inflorescence specific, the degreening of leaves were also examined. The first cauline leaves of WT and *dis51* at 14 days after initiation were harvested and incubated in the dark. The delayed leaf yellowing of *dis51* compared with WT was observed at day 5 of dark incubation and the delay was more striking at day 7 (Figure 4.3). Therefore, the delayed yellowing was not a specific trait for the inflorescence in *dis51*.

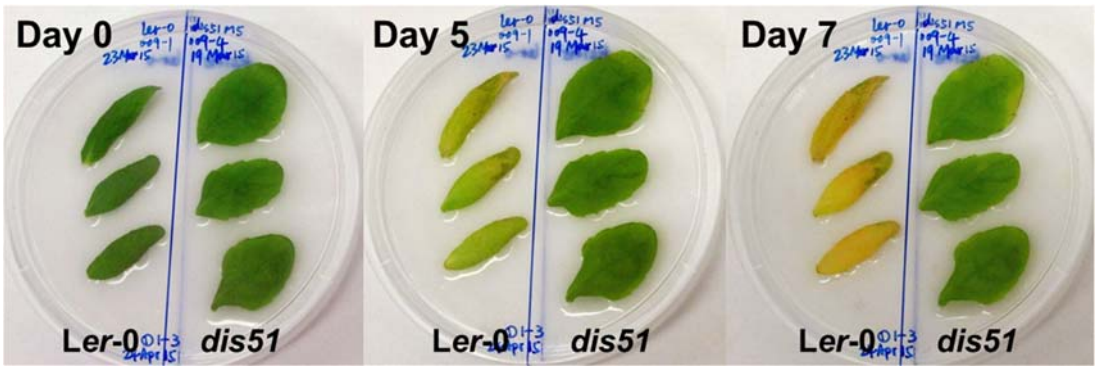

Figure 4.3. Degreening of detached dark-held leaves of *dis51*
Around 14-day-old first cauline leaves were harvested from M5 plants of *dis51* and compared to leaves of L*er*-0 of the same age. Photos were taken at day 0, 5 and 7 of dark treatment. Three representative biological replicates are shown.

4.2.4. The *dis* phenotype of *dis51* is caused by a dual-genic recessive trait

M4 plants of *dis51* were backcrossed to L*er*-0 and Col-0 for segregation analysis and for mapping purpose. The segregation analysis was performed in F2 population after crossing and the plants were screened by using AIDA. Examples of the segregated degreening phenotypes in the F2 inflorescences of *dis51* x L*er*-0/Col-0 are presented in Figure 4.4. The segregation ratio of WT to *dis51* in F2 population of *dis51* x L*er*-0 was around 9.4 to 1. This ratio was compared with both the ratio of 3 to 1 and 15 to 1 by Chi-squared test (Table 4.1). The ratio is significantly different from 3 to 1 ($P<0.01$) but not 15 to 1 ($P>0.05$), suggesting the *dis* trait of *dis51* might be a dual-genic recessive trait rather than monogenic recessive trait. Because the sample size is small (total 125 plants), another analysis was performed with *dis51* x Col-0 mapping population using total number of 1308 plants. The segregation ratio (WT to *dis51*) was approximately 7.8 to 1, which is highly significantly different from both 3 to 1 and 15 to 1 in Chi-squared test ($P<0.01$; Table 4.1). This result is consistent with the result that obtained from F2 population of *dis51* x L*er*-0.

Apart from the two probabilities mentioned above, the observed *dis* phenotype could also be caused by the combination of a recessive and a semi-dominant trait which leads to a segregation ratio of 5.3 to 1. The Chi-squared test indicates that the observed ratios in the F2 population of *dis51* x Col-0 is significantly different from 5.3 to 1 whereas that of *dis51* x L*er*-0 is nearly significant (Table 4.1). Thus, it is less likely that the *dis* trait was resulting from the additive effect of a recessive and a co-dominant mutation.

Therefore, the *dis* phenotype of *dis51* was likely caused by two mutations while it is not clear if these two mutations were linked or not based on the data obtained.

Table 4.1. Pearson's chi-squared test for F2 progenies of *dis51* x L*er*-0/Col-0

Mutants	Total plants	WT-like plants	*dis*-like plants	Observed ratio	Expected ratio	χ^2	*P*-values
dis51 x L*er*-0	125	113	12	~9.4:1	3:1	15.811	<0.0001
dis51 x L*er*-0	125	113	12	~9.4:1	15:1	2.394	0.1218
dis51 x L*er*-0	125	113	12	~9.4:1	5.3:1	3.683	0.0550
dis51 x Col-0	1308	1159	149	~7.8:1	3:1	129.191	<0.0001
dis51 x Col-0	1308	1159	149	~7.8:1	15:1	59.010	<0.0001
dis51 x Col-0	1308	1159	149	~7.8:1	5.3:1	19.674	<0.0001

Chi-squared test was used to test the statistical difference between observed ratio and expected ratio (WT to mutant ratio: 3:1 or 15:1). Chi-squared value was calculated at one degree of freedom. "~" means approximately. *P*<0.05 implies a statistical significance.

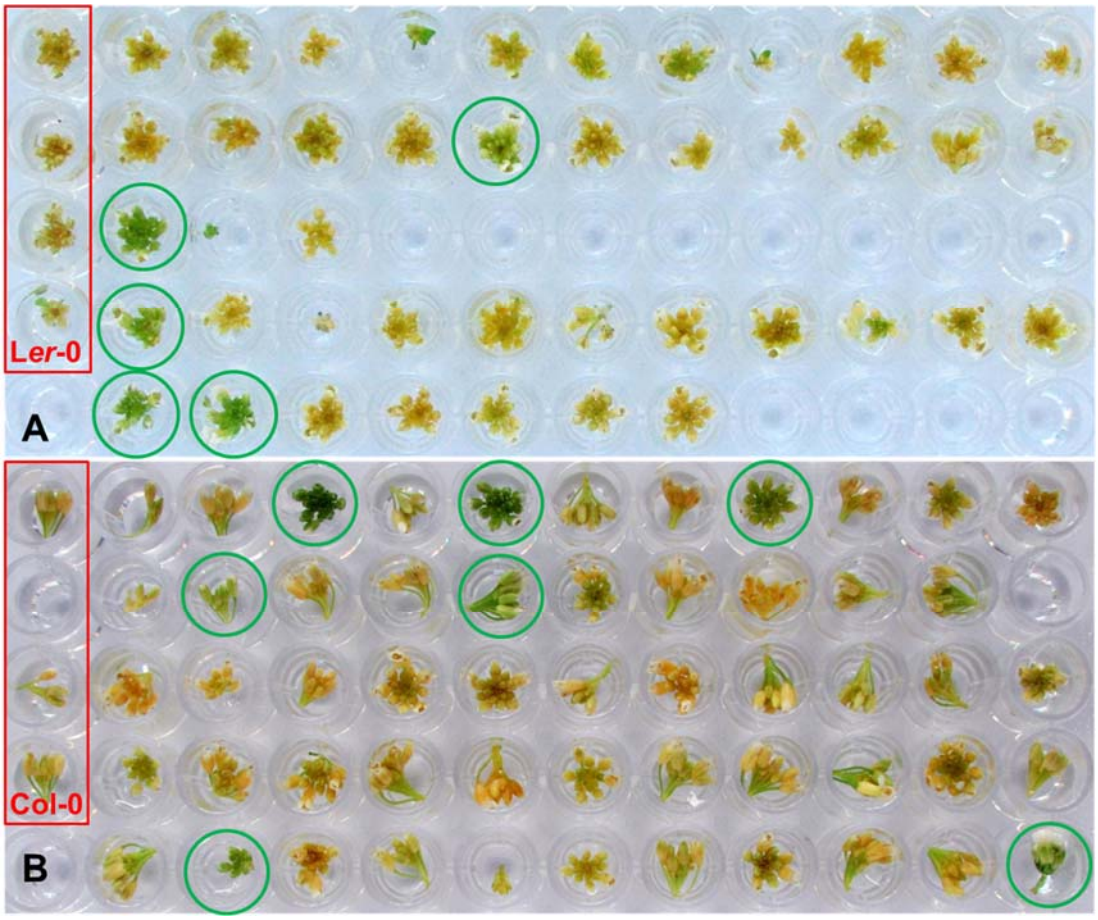

Figure 4.4. Example for segregation of F2 population of *dis51* x L*er*-0/Col-0
Segregation of F2 population of *dis51* x L*er*-0 (A) and x Col-0 (B). L*er*-0 or Col-0 WT is circled with red rectangle, and the inflorescences showed a *dis* phenotype are marked with green circle. Photos were taken at day 5 of dark incubation.

4.2.5. HRM-based mapping of *dis* locus in *dis51*

An iterative HRM analysis was used to map the putative dual-genic recessive mutations that were responsible for the *dis* phenotype of *dis51*. Initially, markers on chromosome 1 to 5 (Figure 4.5B; these markers were published by Hunter

et al., 2018) were used on a population of 13 F2 *dis* plants and the *dis* locus was coarsely mapped to the top arm of chromosome 5 with 8% linkage to the marker 5-2 (Figure 4.5B; Appendix 7.1). Additional markers (5-1 and 5-3; Hunter *et al.*, 2018) on chromosome 5 used on a total of 26 plants, which included the 13 previously used, confirmed that the mutation(s) were within 6 cM of markers 5-1 and 5-2 at the top arm of chromosome 5 (Figure 4.5B; Appendix 7.2). Testing of 65 plants (i.e, a further 39 plants) with markers 5-1 and 5-2 still did not associate the trait preferentially with one of the markers with the genetic distance to both markers 5-1 and 5-2 remaining at ~6 cM (Appendix 7.3).

Based on these results, new markers/primers were designed outside and in between markers 5-1 and 5-2 (Figure 4.5B) and were used for further HRM analysis. It was found from melting profiles that the best markers (i.e., those that best distinguished the different genotypes) were those having two or three SNPs between the forward and reverse primers (Figure 4.5A).

To maximise the efficiency of mapping, initially only the 7 plants that exhibited recombination with markers 5-1 and 5-2 were used with the new markers for further mapping. When there was no crossing over events between the new markers and the mutations in these samples, new plants were tested. Eventually, out of the 92 *dis*-positive F2 plants examined, there was none that separated marker A5-4 from the *dis* locus/loci. This indicated that this marker was very close to the causal mutation(s). A summary of the mapping results is presented in Appendix 7.4, which indicates that the *dis* locus/loci was ultimately mapped to a ~665 kb region between markers 5-1 and A5-5 (Figure 4.5B; Appendix 7.4) at the top arm of chromosome 5.

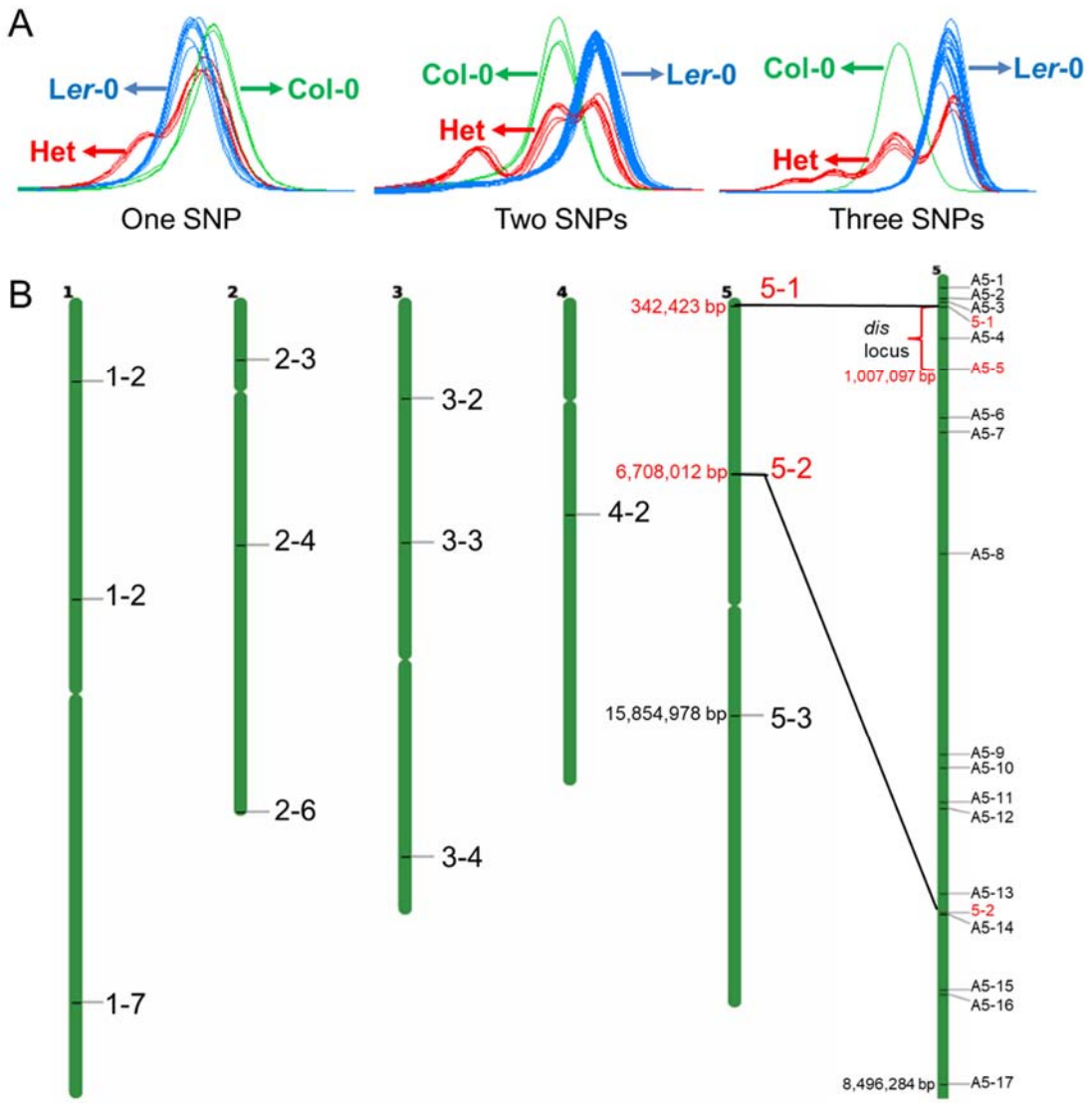

Figure 4.5. HRM-based mapping of *dis* locus in *dis51* mutant

(A) Melting peaks of good markers from HRM analysis. Markers with one, two and three SNPs are shown. Het, heterozygous. (B) Positions of mapping markers indicating mapped region for *dis* locus of *dis51* in Arabidopsis chromosomes. Marker names are indicated on the right side of the chromosomes, and the positions of representative markers are shown on the left. The *dis* mutation was roughly mapped to the chromosome 5 using the markers 5-1 and 5-2 and was eventually mapped to the ~665 kb region in-between markers 5-1 and A5-5. The details of the markers are described in the Appendix 1.2.

4.2.6. Senescence-related genes in the mapped region for *dis* locus of *dis51*

To identify the potential candidate genes in which the mutation(s) may occur, the senescence related genes were searched in the mapped region. Firstly, the gene list in the mapped region was obtained by using SeqViewer (https://seqviewer.arabidopsis.org; Close-up View) in TAIR website. In total 391

genes were found in the mapped region (342423-1007097 bp). Then the senescence related genes were found by searching the key words in the gene description column and the details of these genes were summarised in Table 4.2. From them, *EIN2* was considered as the most promising candidate because the *dis51* mutant also exhibited other phenotypes (e.g. bigger petals and leaves, longer siliques and delayed leaf senescence; Figure 3.2D and Figure 4.3) which were also observed in other *ein2* mutants of *Arabidopsis* (Oh *et al.*, 1997; Feng *et al.*, 2015).

Table 4.2. Senescence-related genes in the mapped region for the *dis* locus/loci in *dis51*

Physical location	AGI (TAIR)	Gene name	Gene description
625254-627124	AT5G02760	APD7/ SSPP	Encodes a phosphatase that functions in sustaining proper leaf longevity and preventing early senescence by suppressing or perturbing SARK-mediated senescence signal transduction.
769438-770563	AT5G03230		senescence regulator (Protein of unknown function, DUF584);(source:Araport11)
787428-793404	AT5G03280	EIN2	Involved in ethylene signal transduction. Acts downstream of CTR1. Positively regulates ORE1 and negatively regulates mir164A,B,C to regulate leaf senescence. A maternally expressed imprinted gene. Mutations in ein2 block ethylene stimulation of flavonol synthesis. The mRNA is cell-to-cell mobile.

4.2.7. *dis51* does not display triple response phenotype upon ACC treatment in the dark

The triple response assay was previously used to characterise ET mutants in Arabidopsis (Guzman and Ecker, 1990). Here, this assay was used to test the hypothesis that the *EIN2* gene was mutated in the *dis51* mutant. The triple response was evaluated in seedlings which were grown on half-MS media containing 10 μM ACC in the dark for 3 days after germination. WT but not *dis51* seedlings displayed triple response phenotypes, i.e., WT exhibited shorter and thicker hypocotyls and roots compared with *dis51* seedlings and WT showed exaggerated curvature of the apical hooks which was not observed in the *dis51* seedlings (Figure 4.6). This confirmed that at least one mutation in *dis51* located in *EIN2* gene.

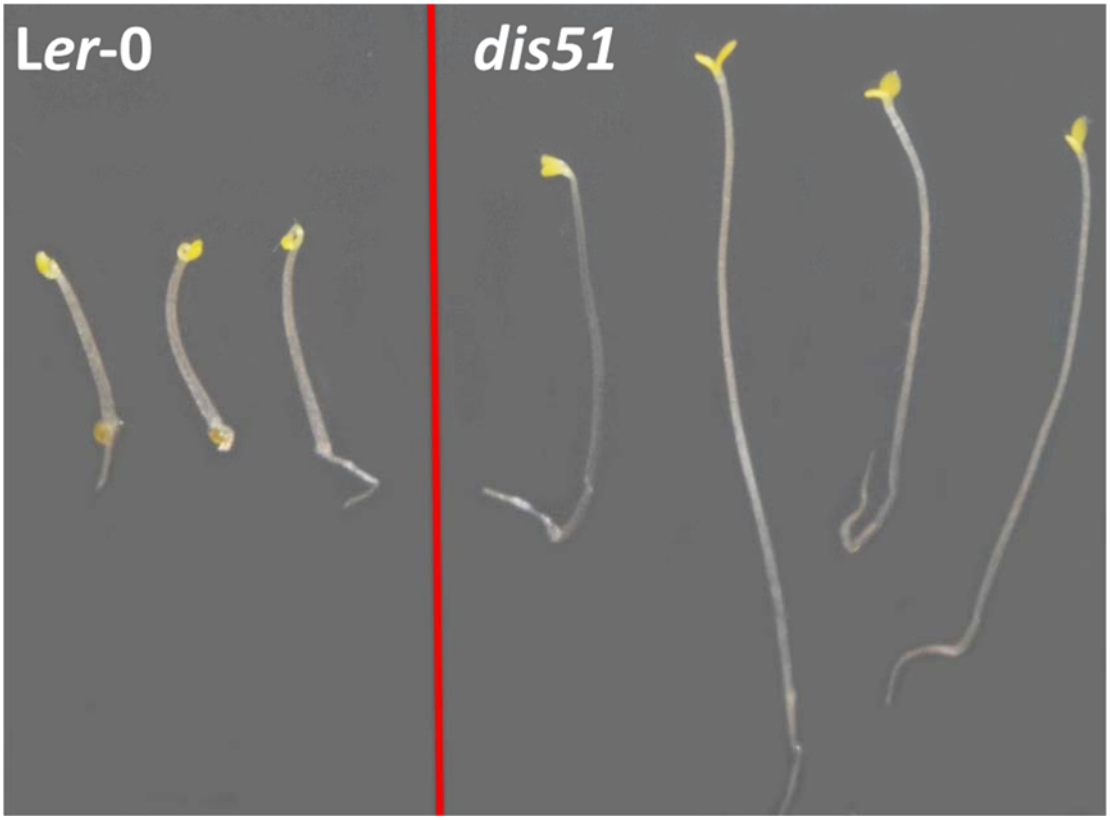

Figure 4.6. The triple response assay for L*er*-0 and *dis51* mutant
Seeds were grown on half MS media under the long day condition for 2 days for germination, and then were transferred to the half-MS plate containing 10 μM ACC and grown in the dark for 3 days.

4.2.8. *dis51* has a nonsense mutation in the coding region of *EIN2*

Amplification of *EIN2* in genomic DNA of *dis51*

Based on the result above, the *EIN2* gene including promoter and 3'-UTR was amplified from the genomic DNA extracted from *dis51* leaves. The full length of amplified fragment is 6.065 kb, and the agarose gel image is shown in Figure 4.7.

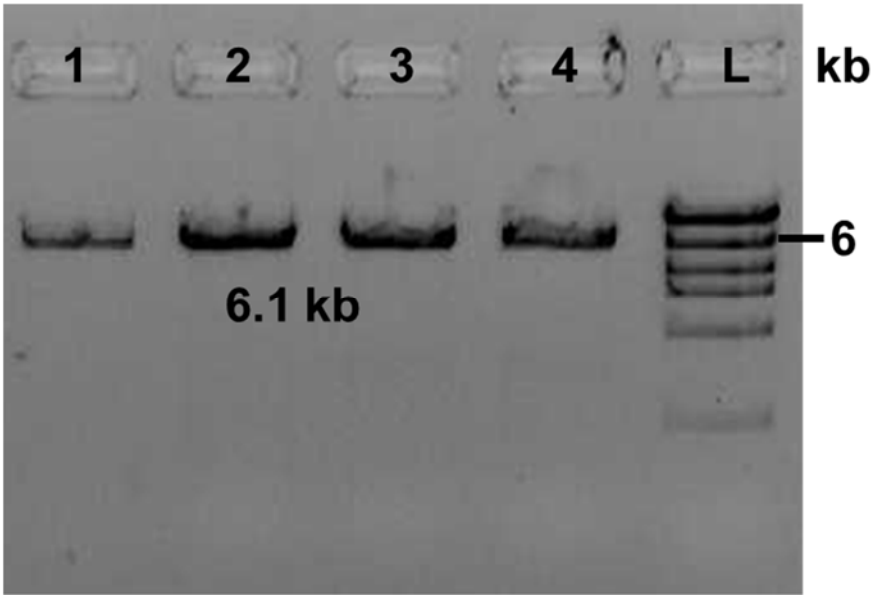

Figure 4.7. Amplification of *EIN2* in genomic DNA of *dis51*
PCR performed using the DNA that isolated from the pooled leaves from 6 individual plants. L, high DNA mass ladder; kb, kilobase. The actual size of the amplified band is 6.065kb. Four technical replicates are shown. The number on the right side of the ladder represents the size of the band.

Sequencing of *EIN2* region in *dis51*

According to sequencing result, a G to A transition was found in the exon 6 of *EIN2* gene in *dis51*, which led to the amino acid tryptophan (W) at position 622 was replaced by a premature stop code in EIN2 protein (Figure 4.8). Such change likely causes loss-of-function of EIN2 protein and thereby contributes to the *dis* phenotype of *dis51*.

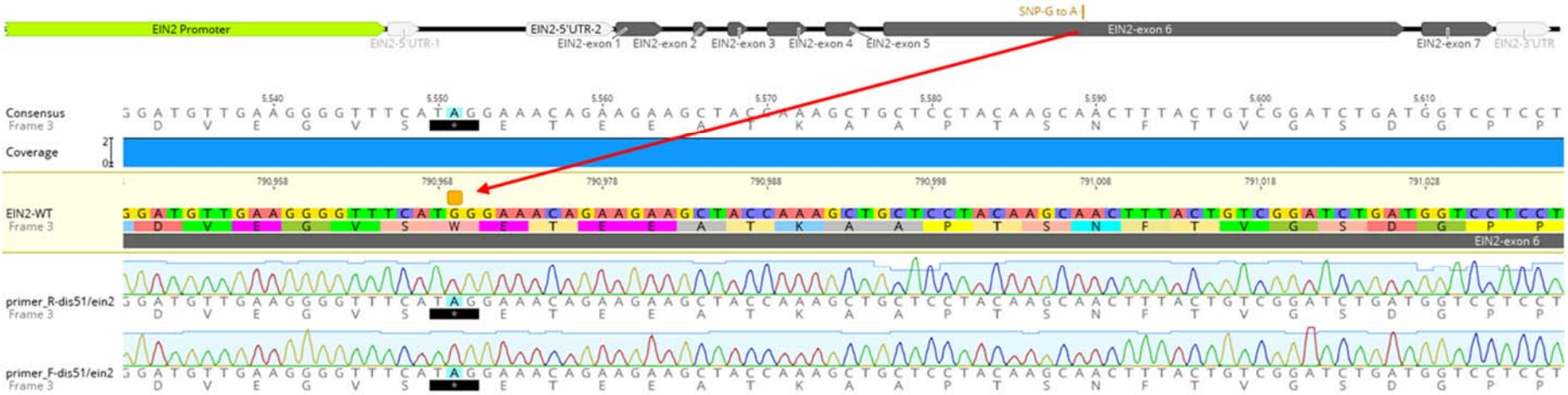

Figure 4.8. Sequencing of *EIN2* region in *dis51*

Sequences from PCR products were aligned to genomic DNA sequence of the WT *EIN2*. Schematic showing the gene structure of the WT *EIN2*. The mutation is indicated by the red arrow. A representative biological replicate that was sequenced using different primers are shown.

4.2.9. *dis51* aroma phenotype is due to the volatile compounds phenylacetaldehyde and phenylethanol

Preliminary screen of volatile compounds in *dis51* and L*er*-0

During the mutant screening, I noticed that whenever flowering *dis51* mutants were grown in the growth chamber, a pleasant fragrance was present in that growth chamber. This led me to hypothesise that the *dis51* phenotype included a change in volatiles. Therefore, ~200 mg fully opened flowers of L*er*-0 and *dis51*, respectively, were prepared for GC-MS analysis to determine if there is any difference in volatile compounds. Examples of the GC-MS profiles for two of the compounds (benzaldehyde and phenylacetaldehyde) that showed striking enhancements in *dis51* compared with in WT are shown in Figure 4.9. In total, four volatile compounds that were emitted from the plants were identified and are listed in Table 4.3.

Rescreen of volatiles in *dis51* and L*er*-0 with a single flower sample for each genotype

The *dis51* mutant and L*er*-0 seeds were sent to the University of Amsterdam for an independent analysis. The GC-MS analysis was carried out with one flower sample from L*er*-0 and *dis51*, respectively. This analysis confirmed the presence of two compounds, phenylacetaldehyde and phenyl ethyl alcohol (Figure 4.10), that were identified from the first experiment. Thus, the aroma of *dis51* is likely caused by the enhanced emission of phenylacetaldehyde and phenylethanol.

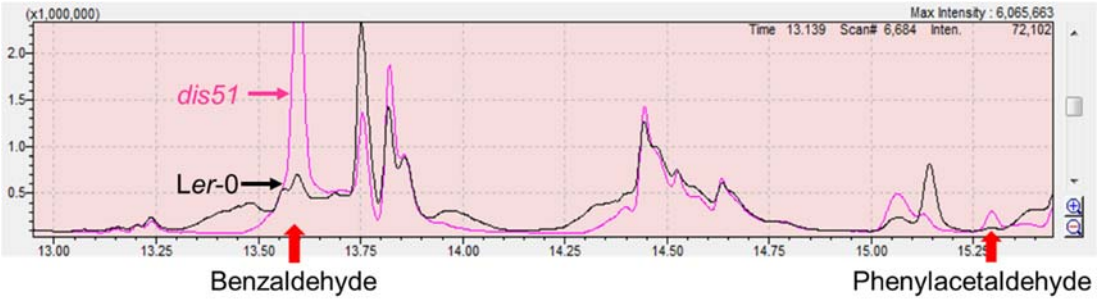

Figure 4.9. GC-MS profiles of volatile compounds in L*er*-0 and *dis51* from preliminary scanning

The analysis was performed using ~200 mg of fully opened flowers that were harvested from 6 individual plants of L*er*-0 or *dis51*. Peak area represents the signal intensity of the compound to the specific mass in L*er*-0 and *dis51*. The pink profile is for *dis51* mutant while the black one is for L*er*-0. The potential volatile compounds responsible for the aroma phenotype in *dis51* mutant are indicated by red arrows. The figure is provided by Martin Hunt (PFR, Palmerston north, NZ).

Table 4.3. Potential volatile compounds that are responsible for the aroma phenotype in *dis51* mutant

		dis51 mutant		L*er*-0 WT		
Compounds	Enhancement	RT (min)	Area	RT (min)	Area	Measured ion (m/z)
benzaldehyde	9.14	13.598	1218305	13.596	133332	106
benzyl alcohol	6.00	18.151	78890	18.152	13141	108
phenylacetaldehyde	6.96	15.253	180616	15.293	25938	91
phenylethanol	3.60	18.563	75973	18.568	21128	91

RT, retention time. The enhancement of potential volatile compounds between *dis51* and L*er*-0 were calculated using area comparisons.

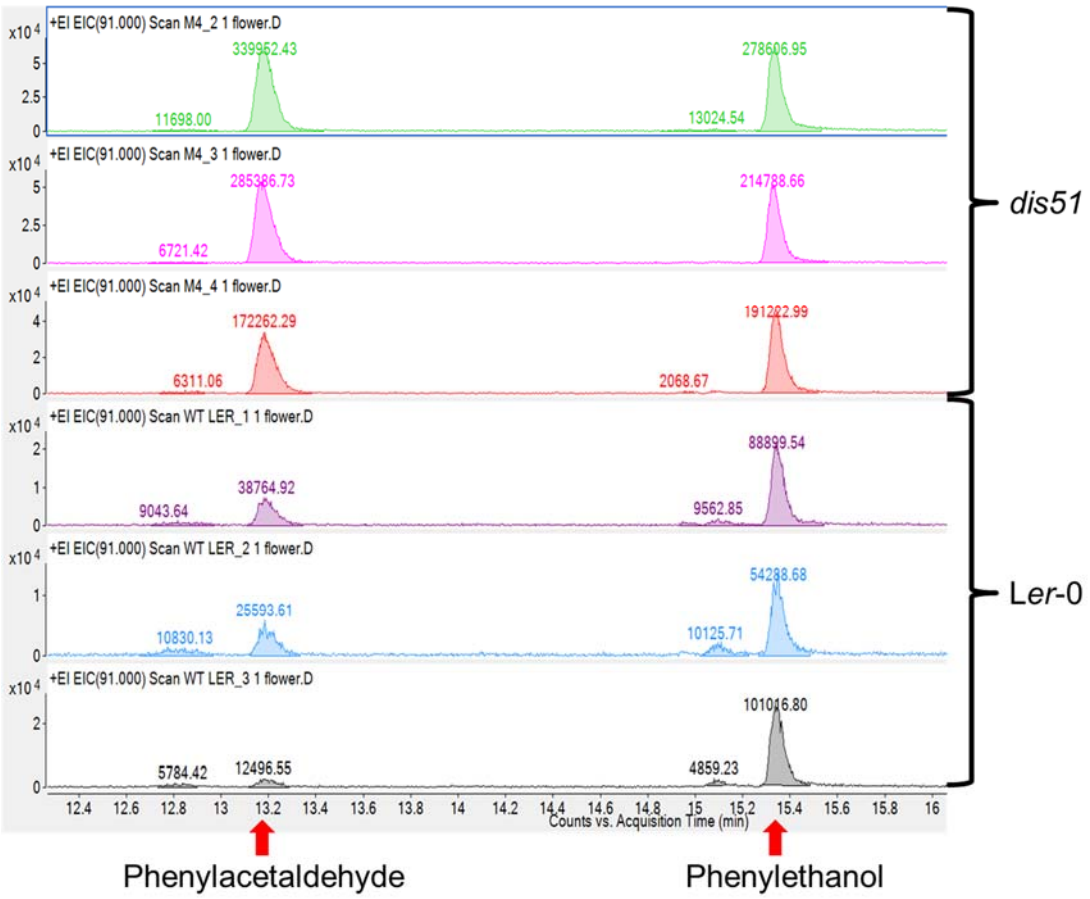

Figure 4.10. GC-MS profiles of volatile compounds in L*er*-0 and *dis51* with one flower for each genotype

The semi-quantitative analysis was performed using one fully opened flower that was harvested from L*er*-0 or *dis51* plant. Three representative biological replicates are shown. Peak area represents the signal intensity of the compound to the specific mass in L*er*-0 and *dis51*. The potential volatile compounds responsible for the aroma phenotype in *dis51* mutant are indicated by red arrows. The figure is provided by Rob Schuurink and Harro Bouwmeester (University of Amsterdam, NL).

4.3. Discussion

4.3.1. A nonsense mutation in the C-terminal region of EIN2 contributes to multiple *dis51* phenotypes

In this chapter, another EMS mutant *dis51* was characterised and one of the causal mutations that was responsible for the *dis* phenotype was identified. The G to A mutation occurs at the exon 6 of *EIN2* gene. It causes a premature stop codon that (likely) removes amino acids from 622 to 1294 at the C-terminal region of the EIN2 protein. This region includes the carboxyl-terminal domain [CEND; 646-1294 at amino acid positions (Qiao *et al.*, 2012)] containing nuclear localization signal [NLS; 1262-1269 at amino acid positions (Bisson and Groth, 2011)] of EIN2 that is necessary for ET signal transduction, more specifically, is required for nuclear translocation of EIN2-CEND to activate downstream ET responses (Wen *et al.*, 2012). Therefore, removal of these amino acids likely results in loss-of-function of EIN2 and defective ET signalling. This is supported by the findings that missing of amino acids from 1262 to 1269 of EIN2-CEND causes failure to interact with ETR1, loss of nuclear localisation and EIN2-CEND functions (Bisson and Groth, 2015; Li *et al.*, 2015). In addition, the C-terminal region (amino acids 1047-1294) is required for targeting by F-box proteins ETP1 and ETP2 for the degradation of EIN2 protein that is essential for triggering ET response. Deletion of this portion in the EIN2-CEND completely lost the ability to interact with ETP1 and ETP2 (Qiao *et al.*, 2009). The mutation in EIN2 is very likely to contribute to the *dis* phenotype of *dis51*. Although the genetic complementation was not carried out for this mutant, the triple response assay confirmed that *dis51* is insensitive to ACC treatment. This is consistent with the finding that loss-of-function *ein2* mutants are completely insensitive to ET (Roman *et al.*, 1995).

ET is a well-known senescence regulatory hormone involved in controlling longevity of both leaves and flowers/petals (Grbić and Bleecker, 1995; Tripathi and Tuteja, 2007; Jibran *et al.*, 2013; Ma *et al.*, 2018). EIN2 plays a critical role in ET signal transduction and acts as a positive regulator downstream of CTR1 (Roman *et al.*, 1995; Alonso *et al.*, 1999). Previous studies reported that the Arabidopsis EIN2 loss-of-function mutants exhibit a delay in both age-

dependent and dark-induced leaf senescence (Oh *et al.*, 1997). Also, mutation in an EIN2 ortholog in petunia showed a significant delay in flower senescence (Shibuya *et al.*, 2004). In this study, *dis51* mutant, which has a nonsense mutation in *EIN2*, exhibited delayed senescence phenotype in both excised inflorescences and first cauline leaves upon dark incubation. This is consistent with the findings in other *ein2* mutants and agrees with the role of ET in regulating both flower and leaf senescence. Unlike the cosmetic stay green mutant *dis2*/*nyc1* (described in Chapter 3), *dis51*/*ein2* mutant is a functional stay green mutant which affects the senescence progression. It is therefore not surprising that the detached dark-incubated inflorescences of *dis51* did not exhibit preferential retention between Chl *a* and Chl *b* and they eventually showed yellowing.

Besides the altered senescence phenotype, *dis51* also displayed other phenotypes including delay in bolting and flowering time and an increase in size of cauline leaf, the delay in bolting time and increase in rosette size were also reported in another *ein2* mutant (Guzman and Ecker, 1990). This is also consistent with the findings that *ein2-1* and *ein2-5* mutants exhibit enlarged organs including leaves, stems, flowers and siliques compared with WT (Feng *et al.*, 2015). The delayed time to bolting, flowering and increased rosette size have also been observed in the ET insensitive mutant *etr1* (Bleecker *et al.*, 1988; Chang *et al.*, 1993). This suggests these phenotypes are likely due to the defect in ET signalling. Although the *dis51* showed a delay in flowering time (delayed ~3 days) compared with WT, its delayed degreening was also observed in the inflorescences that were harvested after synchronisation of the time to flowering (see Chapter 2.3.4) between WT and *dis51*. This suggests that the 3-day delayed flowering time was not the reason that the mutants were delayed in inflorescence degreening.

As discussed in Chapter3, EMS mutagenesis can induce multiple mutations in each treated plant (Ostergaard and Yanofsky, 2004), which could cause complex phenotypes caused by defects in multiple genes. Interestingly, here the segregation ratios in the F2 population of *dis51* x L*er*-0/Col-0 was significantly different from 3 to 1. This suggests the *dis* phenotype is not caused

by a single recessive trait. It also raises the possibility that the *dis* trait results from two or more mutations. Two possibilities were tested, first, the *dis* phenotype might be caused by an unlinked dual-genic recessive trait which leads to a segregation ratio of 15 to 1. With total 125 tested plants in the F2 population of *dis51* x L*er*-0, the observed ratio (9.4:1; WT:*dis*) was not significantly different from 15 to 1, suggesting the phenotype may due to the two unlinked recessive mutations. However, the segregation ratio (7.8:1; WT:*dis*) in the F2 population of *dis51* x Col-0 with total 1308 tested plants showed a significant difference from 15 to 1. Although the phenotypes that segregate between WT L*er*-0 and Col-0 may complicate phenotyping of additional traits, including *dis* trait of *dis51*, the Chi-squared test indicates the two recessive mutations are linked. Another possibility is that *dis* trait is resulted from combined effect of a recessive mutation and a semi-dominant mutation which causes a 5.3 to 1 (WT to dis) segregation ratio. The Chi-squared test appeared to reject this hypothesis though whether the observed ratio was different from 5.3 to 1 in the F2 *dis51* x L*er*-0 was ambiguous (*P*=0.055). These results revealed that the *dis* trait of *dis51* appeared to be caused by two recessive mutations, however it was not clear whether these two mutations were linked or not.

To sum up, the delayed inflorescence/sepal senescence phenotype of *dis51* highlights the role of ET in regulating senescence of sepals/inflorescences of Arabidopsis. One of the lesions that contributes to the *dis* phenotype was identified. The nonsense mutation in *dis51* results in a premature stop codon which likely causes deletion of critical EIN2-CEND region and leads to an ET insensitive phenotype.

4.3.2. Floral fragrance compounds phenylacetaldehyde and phenylethanol are likely the cause for the aroma phenotype of *dis51*

Apart from *dis* or *ein2*-related phenotypes, flowering *dis51* mutants also released a pleasant fragrance. The GC-MS analysis from two independent experiments detected two volatile compounds, phenylacetaldehyde (2-phenylacetaldehyde; 2-PHA or 2-PAld) and phenylethanol (2-phenylethanol; 2-PE), that were likely responsible for the fragrance phenotype. 2-PE and/or 2-

PHA/2-PAld are important volatile compounds that contribute to the flavour of many fruits such as tomato and strawberry (Baldwin *et al.*, 2000; Aubert *et al.*, 2005). It is also the major aromatic component of many flowers (Knudsen *et al.*, 1993) such as rose (Shalit *et al.*, 2004; Rusanov *et al.*, 2005) and petunia (Verdonk *et al.*, 2003; Boatright *et al.*, 2004). These two compounds have essential biological functions in both plant defense and reproduction. For instance, both are potent insect attractants, with each attracting different groups of pollinators and predators (Raguso *et al.*, 2003; Zhu *et al.*, 2005). 2-PE has also been reported to possess antimicrobial properties (Berrah and Konetzka, 1962) and may have protective role for floral organs and fruit as it is synthesised by reproductive organs.

2-PE is synthesised from the aromatic amino acid L-phenylalanine (L-Phe) via phenylacetaldehyde (reviewed by (Dudareva *et al.*, 2013; Muhlemann *et al.*, 2014)). The genes and enzymes involved in the biosynthetic pathway of 2-PE have previously been characterised in several plant species including petunia, rose and tomato (Dudareva *et al.*, 2013; Muhlemann *et al.*, 2014) (Figure 4.11). In petunia petals, conversion of L-Phe to phenylacetaldehyde is catalysed by phenylacetaldehyde synthase (PAAS) which belongs to group II pyridoxal 5'-phosphate-dependent amino acid decarboxylases (AADCs) (Kaminaga *et al.*, 2006). In rose petals, however, an alternative biosynthetic route has been found (Sakai *et al.*, 2007; Farhi *et al.*, 2010; Hirata *et al.*, 2012), while in tomato an additional reaction is required to form 2-PAld/2-PHA (Tieman *et al.*, 2006) (Figure 4.11). Although the biosynthesis of 2-PAld shows different pathways in distinct species, the conversions of 2-PAld to 2-PE in tomato (Tieman *et al.*, 2007) and rose (Sakai *et al.*, 2007; Chen *et al.*, 2011b) are identical and both are catalysed by phenylacetaldehyde reductases (PARs).

In Arabidopsis, the emission and function of 2-PAld varies in different ecotypes (Gutensohn *et al.*, 2011). 2-PAld has been found to be emitted by leaves of Col-0 in response to the MeJA treatment or wounding stress, but by flowers of accessions Sei-0 and Di-G. Two genes (*At2g20340* and *At4g28680*), encoding pyridoxal 5'-phosphate-dependent AADCs and showing high homology to the identified petunia PAAS, have been identified in Arabidopsis. However, only

At2g20340 has been proved to be an aromatic aldehyde synthase (AtAAS) and is responsible for phenylacetaldehyde formation *in planta* (Gutensohn *et al.*, 2011). T-DNA knock-down and transgenic RNA interference (RNAi) lines of *AtAAS* exhibit significant reduction of 2-PAld production. Although it is not clear so far that the ecotype L*er*-0 also produces 2-PAld, the strikingly increased 2-PAld and 2-PE in the mutant compared with L*er*-0 suggests the mutation in *dis51* likely affects the transcription or function of gene(s) involved in this pathway.

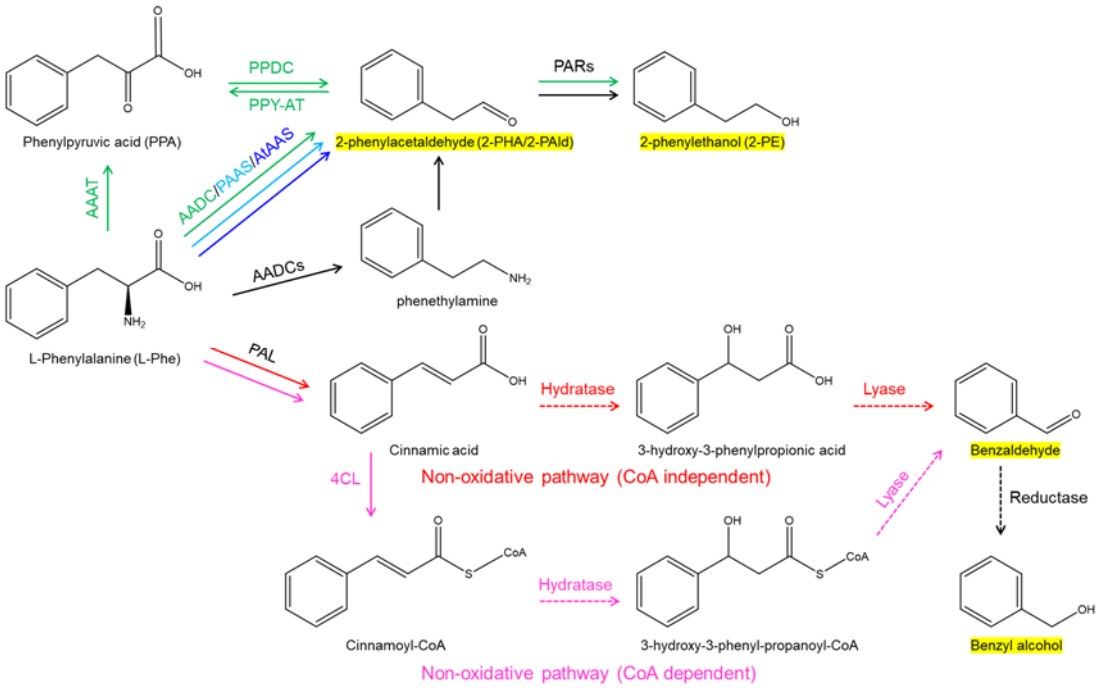

Figure 4.11. Schematic representation of the biosynthetic pathways for phenylacetaldehyde, phenylethanol, benzaldehyde and benzyl alcohol
Figure was made based on the published biosynthetic pathways of phenylpropanoid/benzenoid compounds (Muhlemann *et al.*, 2014; Widhalm and Dudareva, 2015; Hirata *et al.*, 2016). For simplicity, only the formation of the 2-PAld/2-PHA, 2-PE, benzaldehyde and benzyl alcohol are shown, and the names of these four compounds are highlighted with yellow background. Solid and dashed arrows indicate the characterised and speculated pathways/enzymes, respectively. Biosynthesis of 2-PE in petunia (light blue arrow), rose (dark green arrows), Arabidopsis (dark blue arrow) and tomato (black arrows) are presented. Enzymes and routes for CoA independent and dependent non-oxidative pathways are shown in red and pink. AAAT, aromatic amino acid aminotransferase; AtAAAS, Arabidopsis aromatic aldehyde synthase; AADC, aromatic amino acid decarboxylase; 4CL, 4-Coumarate CoA-ligases; PAAS, phenylacetaldehyde synthase; PAL, L-Phenylalanine ammonia lyase; PAR, phenylacetaldehyde reductase; PPDC, phenylpyruvate decarboxylase; PPY-AT, PPA aminotransferase.

Besides the two compounds described above, other two volatile compounds (Benzaldehyde and benzyl alcohol) which showed striking increase in *dis51* compared with WT were also detected in the first experiment. Although they were not detected in the second experiment, I could not ignore the possibility for the presence of these two compounds because it might be caused by the different sample harvest times at these two independent experiments. This is supported by the findings that floral volatile emission exhibits circadian rhythmicity (Kolosova *et al.*, 2001; Picone *et al.*, 2004). Interestingly, benzaldehyde is also derived from L-Phe (Muhlemann *et al.*, 2014; Widhalm and Dudareva, 2015) (Figure 4.11). If the enhancement of benzaldehyde and benzyl alcohol can be confirmed, the mutation in *dis51* is more likely affects the upstream pathway, i.e., biosynthetic pathway of L-Phe (shikimate pathway) (Tzin and Galili, 2010).

So far, whether the aroma phenotype is linked with the *dis* phenotype is not clear. However, a negative correlation has been suggested between floral fragrance and longevity because loss of fragrance has been found when selection for longevity of rose flowers (Vainstein *et al.*, 2001; Guterman *et al.*, 2002). This is also supported by the fact that the common floral aromatic compounds JA and MeJA accelerate flower senescence (Porat *et al.*, 1993; Porat *et al.*, 1995). To my best knowledge, it has not been shown that *ein2* mutants emit increased amounts of aromatic volatiles. Although the aroma phenotype does not appear to dependent on the *ein2* mutation *per se*, a correlation between ET production and floral volatile emission has previously been reported. For example, it has been found that increased ET production (36 h after pollination) or after 10 h of exposure to external ET suppresses the biosynthesis and emission of major volatiles including 2-PHA/2-PAld, 2-PE, benzaldehyde and benzyl alcohol in petunia (Underwood *et al.*, 2005). This is also consistent with the findings that the transcript accumulation of benzenoid/phenylpropanoid biosynthetic genes, including petunia PAAS, were reduced when treated with ET for 2-4 hours (Colquhoun *et al.*, 2010). A similar effect of ET on fragrance production and emission has been also observed in cut sweet pea flowers (Sexton *et al.*, 2005). In rose flowers, however, endogenous ET production or exogenous ET exposure does not affect volatile

emission (Borda *et al.*, 2011). These findings suggest that floral volatile production/emission is differentially regulated among plant species. If ET also involved in regulation of volatile emission in Arabidopsis, the mutation in EIN2 may enhance the aroma emission in *dis51* mutant. Therefore, further investigation is needed to find out if the aroma-related causal mutation is genetically linked with the *dis51*/*ein2* locus. In addition, it will be interesting to determine the relationship between fragrance emission, ET production and senescence in this Arabidopsis mutant.

5. Strigolactone defective mutants of Arabidopsis exhibit delayed sepal senescence

5.1. Introduction

Strigolactones (SLs) are carotenoid-derived phytohormones (Al-Babili and Bouwmeester, 2015). In *Arabidopsis*, SL biosynthesis involves stepwise conversion of all-*trans*-β-carotene into carlactone (CL). This relies on the sequential activities of carotenoid isomerase, encoded by *DWARF27* (*D27*), carotenoid cleavage dioxygenases, encoded by *CCD7*/*MORE AXIALLY GROWTH3* (*MAX3*) and *CCD8/MAX4* (Alder *et al.*, 2012). CL, a common precursor to SLs, is then oxidised into carlactonoic acid (CLA) by the cytochrome P450 enzyme MAX1 (Abe *et al.*, 2014). CLA is further converted into methyl carlactonoate (MeCLA) (also known as SL-LIKE1), a bioactive compound that interacts with SL receptor D14, by an unknown methyltransferase (Abe *et al.*, 2014). Subsequently, MeCLA is converted by LATERAL BRANCHING OXIDOREDUCTASE (LBO) to an unidentified SL-like compound (MeCLA+16 Da, which refers to a MeCLA-like compound with an additional mass of 16 Da) (Brewer *et al.*, 2016). SL signalling requires the receptor AtD14 that binds to SL and hydrolases it to form a covalently linked intermediate molecule (CLIM), which acts as active form of SL (Yao *et al.*, 2016). This allows AtD14 to interact via a conformational change with the F-box protein D3, a rice ortholog of Arabidopsis MAX2, to recruit repressors (e.g. Arabidopsis SMXL6/7/8) for degradation through the 26S proteasome system (Jiang *et al.*, 2013; Zhou *et al.*, 2013; Wang *et al.*, 2015). The biosynthesis and signalling pathways of SL is shown in Figure 5.1.

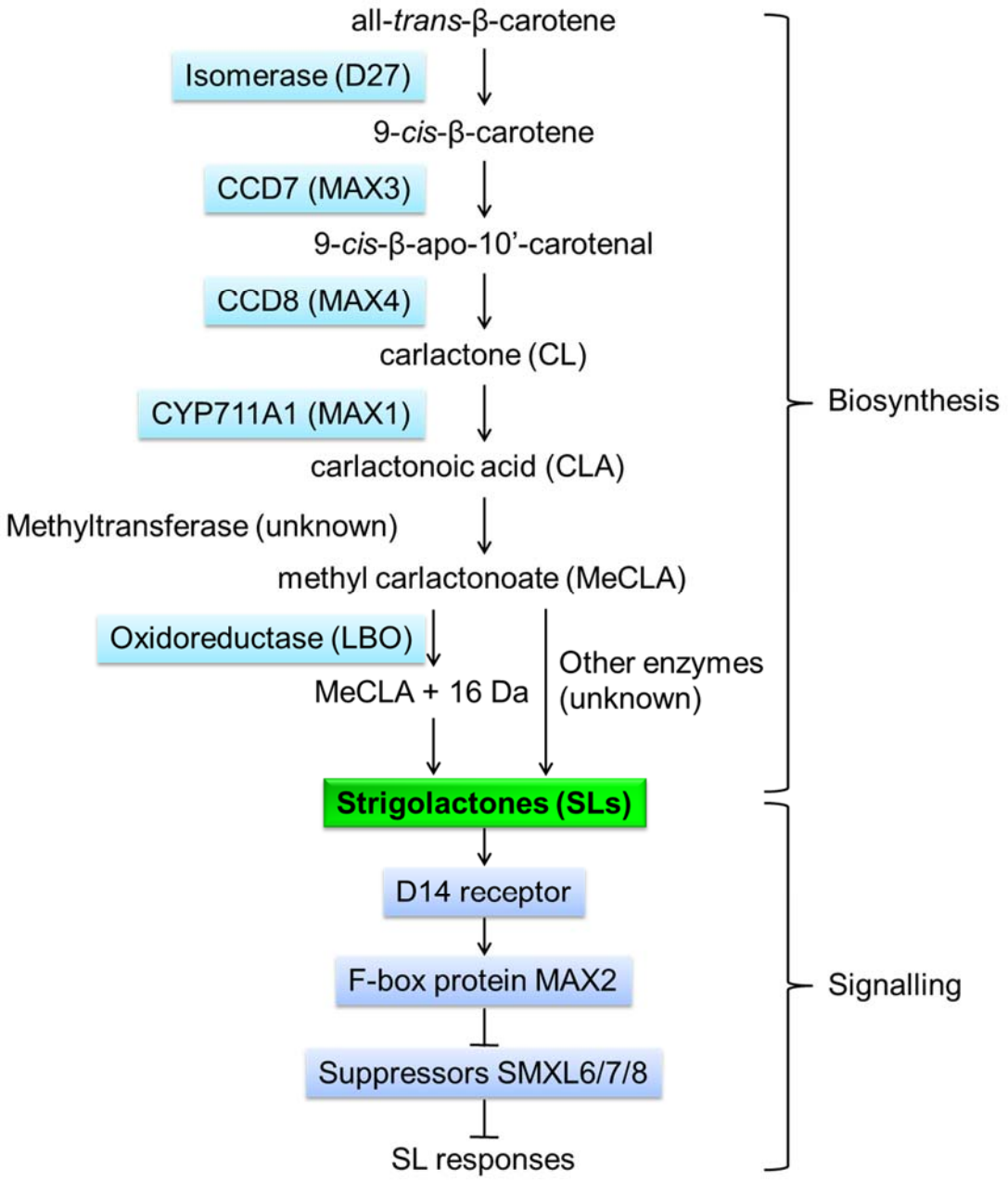

Figure 5.1. The strigolactone biosynthetic and signalling pathways in *Arabidopsis thaliana*
Characterised enzymes and proteins of SL biosynthesis and signalling are highlighted with light and dark blue background, respectively. Intermediate products are indicated, and SLs are highlighted with a green background.

SLs play diverse roles in plant development, including the regulation of leaf senescence (Snowden *et al.*, 2005; Brewer *et al.*, 2013; Yamada and Umehara, 2015; Saeed *et al.*, 2017). However, whether they regulate floral organ senescence has not been reported. Floral organ senescence is tightly regulated and can be initiated precociously by various stresses including prolonged

darkness, which causes starvation and transcriptional changes of sugar-responsive genes and senescence-associated genes (*SAGs*). Such genes include senescence marker gene *SAG12* and transcription factors (TFs) *ANAC092* and *NAP* (Tripathi and Tuteja, 2007; Trivellini *et al.*, 2012; Ahmad and Tahir, 2016).

In this chapter, I describe the identification of two SL defective mutants and suggest a role of SL in regulating flower senescence. Also, I performed the nCounter-based transcriptional analysis to investigate the relationship between SL biosynthesis/signaling and dark/starvation-induced inflorescence senescence in Arabidopsis.

5.2. Results

5.2.1. Phenotypic analysis of *dis9* and *dis15* mutants

The *delayed inflorescence senescence* (*dis*) mutants *dis9* and *dis15* mutants were identified by Rubina Jibran from a preliminary screen using AIDA (Jibran, 2014; Jibran *et al.*, 2015). These two mutants were also found to exhibit increased branch number and decreased plant height *in planta* (Jibran, 2014). The delayed sepal degreening and the observed *in planta* phenotypes were confirmed in this study and were shown in Figure 5.2.

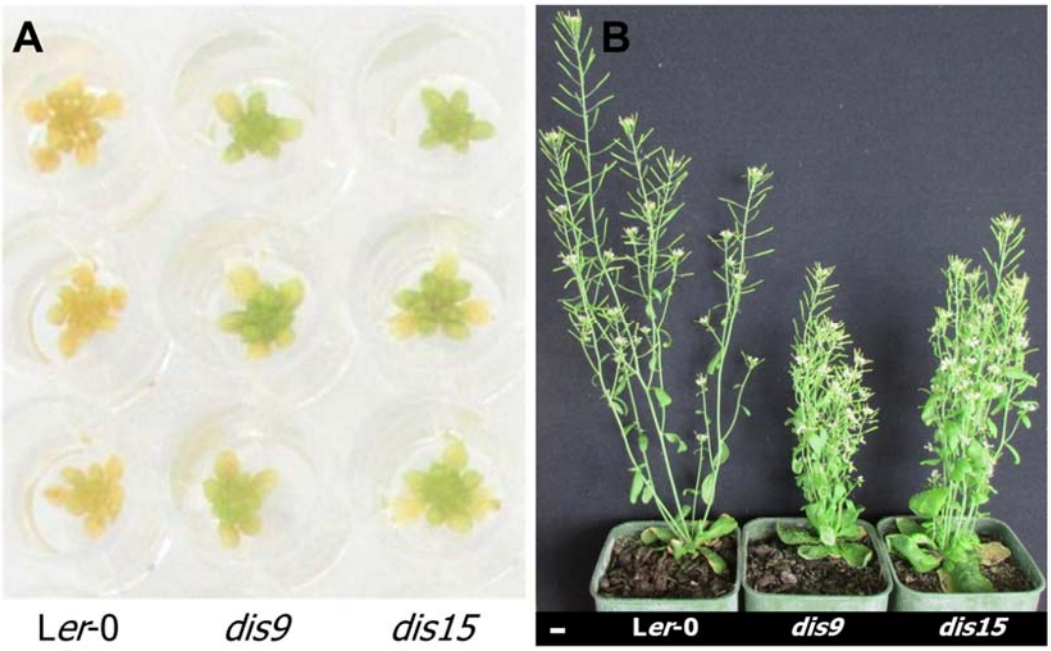

Figure 5.2. Delayed inflorescence degreening and bushy phenotypes of *dis9* and *dis15*

(A). Degreening of detached dark-held inflorescences. Inflorescences were placed in water and were photographed at day 5 of dark incubation. Three biological replicates are shown. (B). Branching phenotype *in planta*. 6-week-old plants grown under long day conditions (16 h/8 h light/dark cycle) were photographed. Bar = 1 cm.

In addition to the two phenotypes described above, *dis9* and *dis15* also exhibited delayed sepal degreening *in planta* (Figure 5.3 A, B; Appendix 8 A) and in detached inflorescences that were subjected to long day conditions (Figure 5.3 C; Appendix 8 B).

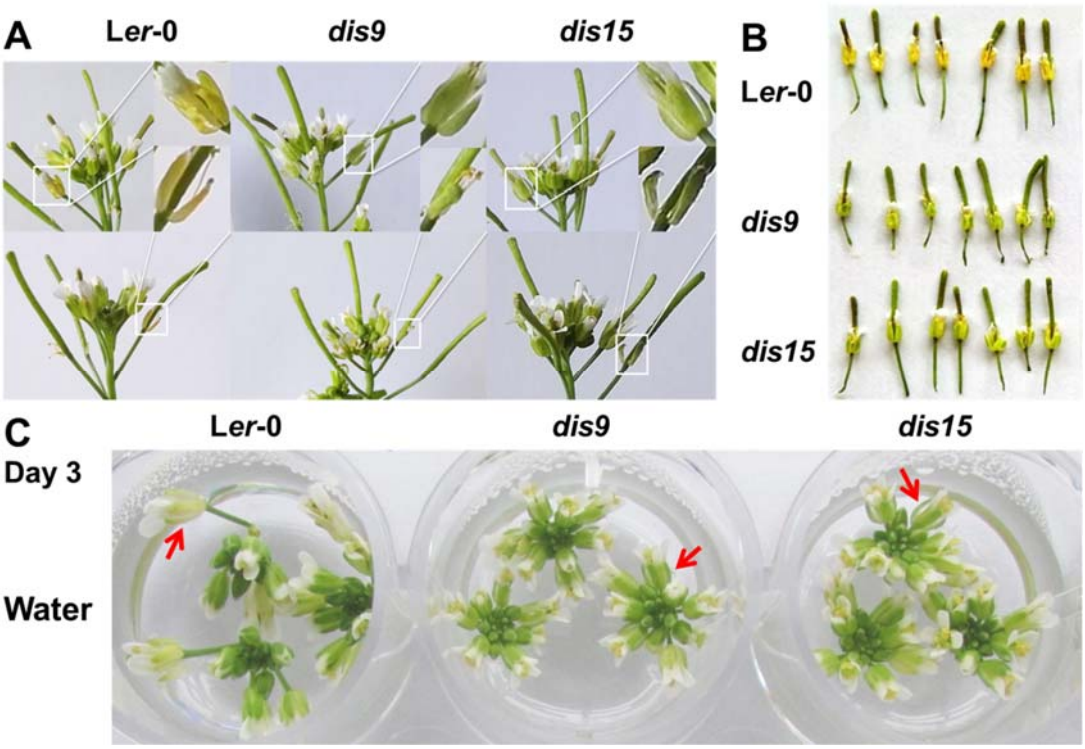

Figure 5.3. Delayed sepal degreening of *dis9* and *dis15 in planta* and in detached inflorescences held in long day conditions

(A) Inflorescences attached to plants. Inflorescences from the primary bolts of 4.5-week-old WT and *dis* plants were photographed. Two biological replicates with representative abscising sepals (circled in white and magnified) are shown. (B) Degreening of sepals *in planta*. Flowers of 5-week-old plants were harvested when their sepals were just starting to abscise. Each flower of the seven biological replicates is from an independent plant. (C) Sepal degreening of excised inflorescences. Inflorescences were harvested from the primary bolts of 4.5-week-old plants that had their first flower opened on the same day. The inflorescences with removed opened buds were placed in water and incubated in long day conditions (16 h/8 h light/dark cycle) for 3 days. Three biological replicates are shown. Representative sepals are indicated by red arrows.

5.2.2. Chlorophyll quantification of *dis9* and *dis15*

The *dis* phenotypes of *dis9* and *dis15* were confirmed by Chl analysis. Both mutants retained significantly higher Chl in excised inflorescences than WT control at day 3 of dark incubation (Figure 5.4).

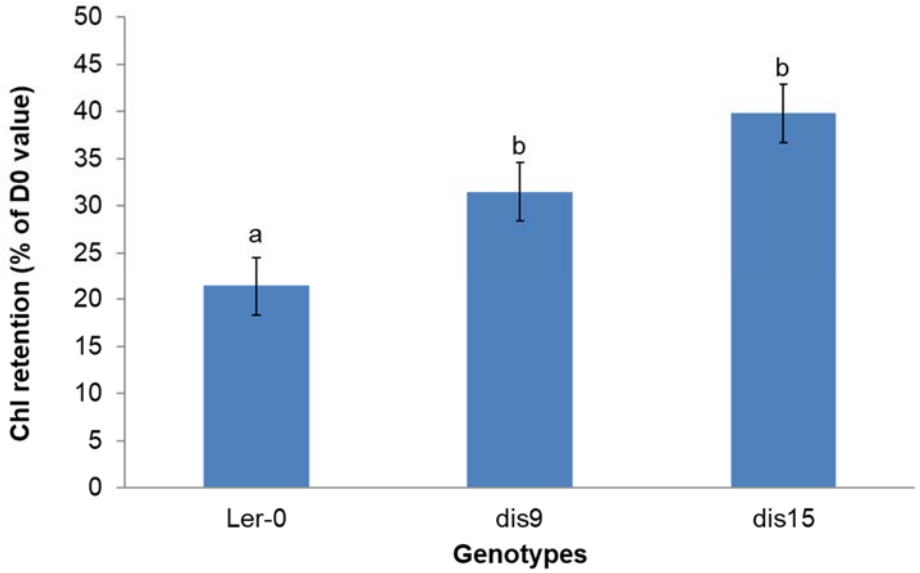

Figure 5.4. Chlorophyll quantification of detached dark-held inflorescences in *dis9* and *dis15* mutants

Total chlorophyll retention (% of day 0 value) at day 3 of dark incubation. Data are mean ± standard error (S.E.) (n=6). Letters represent significant differences between L*er*-0 and *dis* mutants in one-way ANOVA test (Fisher's protected LSD test $P<0.05$).

5.2.3. Transcript abundance of senescence marker genes are suppressed in *dis9* and *dis15* upon dark incubation

To determine whether the stay green phenotype of *dis9* and *dis15* was caused by inability to degrade Chl or by another defect in the senescence programme, the transcript abundances of senescence marker genes *ANAC092* (Kim *et al.*, 2009; Balazadeh *et al.*, 2010; Trivellini *et al.*, 2012) and *SAG12* (Grbic, 2003) in WT and the two mutants during dark treatment were examined. The transcript abundance of the genes increased substantially upon dark treatment in both L*er*-0 WT and mutants, but the increase in the mutants was significantly less than that of WT at 72 h (Figure 5.5). This suggests that senescence progression in the mutants was supressed compared with WT.

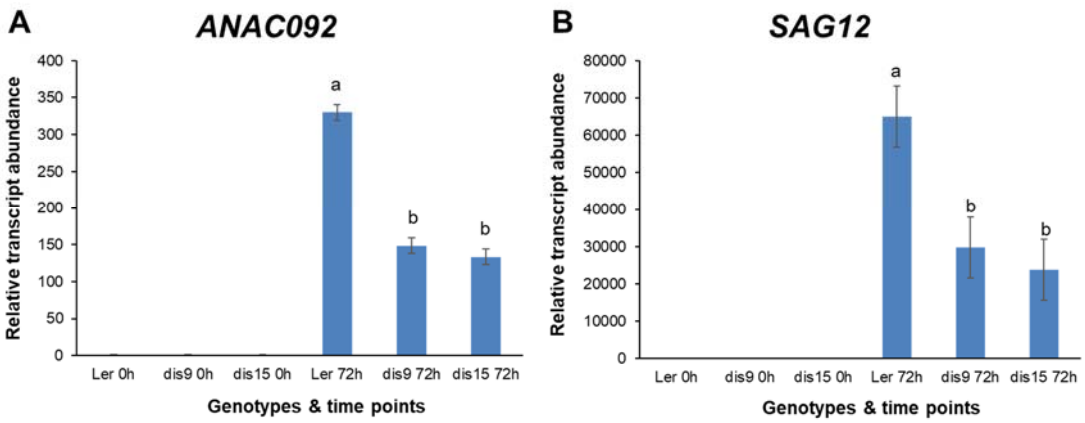

Figure 5.5. Transcript abundance based on qPCR analysis of *ANAC092* and *SAG12* in L*er*-0 and *dis* mutants at 0 h and 72 h

(A) for *ANAC092*. (B) for *SAG12*. In both (A) and (B), transcript abundance was normalised to *PP2AA3* and expressed relative to L*er*-0 0 h. Data are mean ± standard error (n=3). Letters represent significant differences between L*er*-0 and *dis* mutants at 72h dark incubation for each gene comparison in one-way ANOVA (Fisher's protected LSD test $P<0.05$). Means with same letter denote not significantly different between *dis9* and *dis15*.

5.2.4. Segregation analysis of *dis9* and *dis15* mutants

To identify genetic lesions in *dis9* and *dis15*, these two mutants were crossed to WT L*er*-0 and Col-0, respectively. Segregation analysis was used to determine the genetic nature of *dis* trait in both mutants and was performed in the F2 population of crosses between the mutants *dis9* and *dis15* with the WT Col-0 (*dis9* x Col-0 and *dis15* x Col-0). The analysis was previously performed by Rubina Jibran and a 3:1 WT:mutant segregation ratio was confirmed for both mutants by using Chi-squared test (Jibran, 2014; results summarised in Table 5.1). In this study, a total of 1126 F2 plants of a *dis9* x Col-0 cross were screened using AIDA for fine mapping purpose and an example of AIDA screening is shown in Figure 5.6. A 3:1 (WT:mutant) ratio was also confirmed for a *dis9* x Col-0 F2 segregating population using the Chi-square test (Table 5.1). The results described above indicate that a single locus is responsible for the *dis* phenotype in both mutants.

Table 5.1. Pearson's chi-squared test for F2 progenies of *dis9* x L*er*-0/Col-0 and *dis15* x L*er*-0/Col-0

Mutants	Total plants	WT-like plants	*dis*-like plants	Observed ratio	Expected ratio	χ^2	*P*-values
dis9 x L*er*-0*	37	31	6	~5.2:1	3:1	1.523	0.2172
dis15 x L*er*-0*	40	29	11	~2.6:1	3:1	0.133	0.715
dis9 x Col-0*	72	54	18	3:1	3:1	0	1
dis9 x Col-0	1126	850	276	~3.1:1	3:1	0.143	0.705
dis15 x Col-0*	96	76	20	3.8:1	3:1	0.889	0.3458

Chi-squared test was used to test the statistical difference between the expected ratio (3 to 1; WT to mutants) and observed ratios for both *dis9* and *dis15*. Chi-squared value was calculated at one degree of freedom. *P*<0.05 implies a statistical significance. * Results were taken from Jibran (2014).

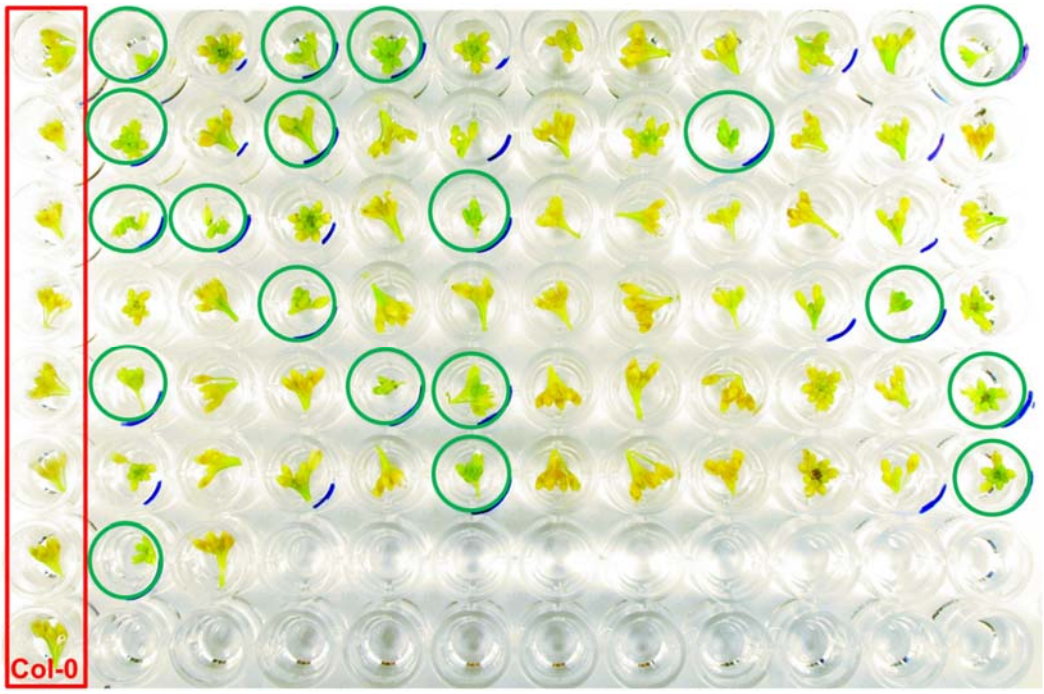

Figure 5.6. An example for screening of *dis9* x Col-0 F2 population
Col-0 WT is marked by red rectangle, and the inflorescences showed a *dis* phenotype are marked by green circles. Photo was taken at day 5 of dark incubation.

5.2.5. HRM-based mapping of *dis9* locus

To identify the genetic lesion that was responsible for the *dis* phenotype in *dis9*, HRM analysis was carried out. The causal mutation was previously mapped by Rubina Jibran to the top arm of chromosome 3 between 0.58-3.89 Mbp using markers 3-1 and 3-2 (Jibran, 2014; Figure 5.7A). In this study, additional HRM primers were designed for further mapping of *dis9* on chromosome 3. Initially,

markers A3-1 and A3-5 (Figure 5.7A) were used on a population of 50 plants (from a segregating population) that exhibited the *dis* phenotype to confirm the linkage and to identify F2 plants in which a recombination event occurred between the marker and the causal mutation in *dis9*. At the same time, markers outside the previously mapped region of chromosome 3 were also used to identify additional F2 plants with crossing over events between the markers used and the *dis9* locus. This allowed me to better estimate the genetic distance between the two loci and the plants were subsequently used for fine-mapping purposes. The *dis9* locus was mapped to an 8 cM distance using the marker A3-1, whereas the linkage for A3-5 was not clear because the genotypes of some samples were not clear based on the melting profiles in HRM analysis (Appendix 9.1). The strategy for the further mapping was to use new markers in the mapped region (between markers A3-1 and 3-2) on the samples that showed recombination events between the markers A3-1 and A3-5 and the *dis9* locus to narrow down the mapped region. This was considered the most efficient and cost-effective strategy. Out of all F2 plants with the *dis9* phenotype used, ultimately no plants were found that indicated a crossing over event between marker A3-3 and the *dis* trait. This suggested that this marker was very close to the causal mutation. The positions of additional markers are shown in Figure 5.7A and a summary of the mapping results is presented in Appendix 9.2. By using the strategy above, the *dis9* locus was eventually mapped to a 0.98 Mbp region on the top arm of chromosome 3 between markers A3-2 and A3-4 (Figure 5.7A; Appendix 9.2).

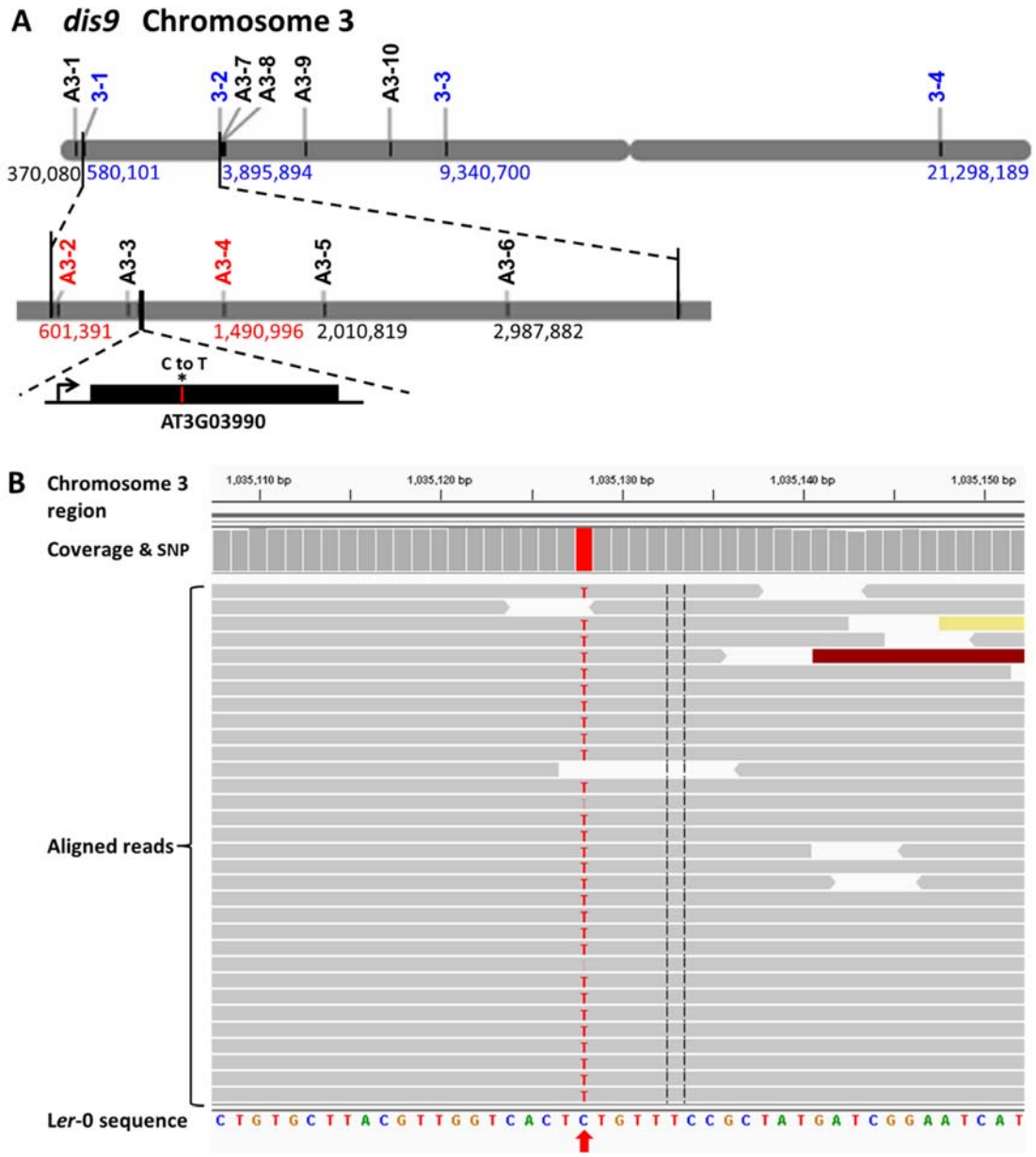

Figure 5.7. HRM and WGS analysis of *dis9*

(A) HRM-based mapping of *dis9* locus. Representation of *Arabidopsis* chromosome 3 showing the position of markers A3-2 and A3-4 which delimited the 889 kb region in which *dis9* was mapped. The mutation in the gene *AT3G03990* (*D14*) responsible for the *dis9* phenotype was identified by WGS analysis (Fig. B) and is indicated. Marker names are indicated above the chromosome, and the positions of representative markers (indicated in bp) shown below. Markers 3-1 to 3-4, corresponding to markers 3-14, 3-16, 3-17 and 3-19 in Jibran, 2014, are listed in Hunter *et al.*, 2018. (B) Identification of C to T mutation in *dis9* according to WGS data. Reads were mapped to L*er*-0 WT sequence and the aligned reads were viewed by IGV. Screenshot from IGV shows the C to T transition (red arrow) in the mapped region of chromosome 3.

5.2.6. WGS analysis of *dis9*

WGS analysis was also performed to identify the potential SNP responsible for the *dis* phenotype of *dis9* in the mapped region. Genomic DNA was isolated and used for WGS as described in Section 2.8. The trimmed reads were aligned to L*er*-0 WT using Bowtie2 (Section 2.11.2). Using IGV (Robinson *et al.*, 2011; Thorvaldsdottir *et al.*, 2013), the aligned reads present within the mapped region were scanned for SNPs between the WT and the *dis9* mutant. Thirty-two SNPs were found and of these, 19 arose from a G/A or C/T transition characteristic of an EMS-based change. Of these, 4 occurred in genes, but only two resulted in nonsynonymous changes in the genes *AT3G03990* and *AT3G04000*, respectively. A transition (C to T) occurred at position 290 relative to the translation start site of the *D14* gene (*AT3G03990*) (Figure 5.7B), encoding a SL receptor (Yao *et al.*, 2016). This mutation was considered to be a promising candidate for causing the increased branch number, decreased plant height and delayed senescence phenotypes in *dis9*, because these phenotypes had previously been reported in other Arabidopsis *d14* mutants (Waters *et al.*, 2012; Chevalier *et al.*, 2014; Ueda and Kusaba, 2015; Yao *et al.*, 2016).

5.2.7. Genetic complementation of *dis9*

Complementation test was used to confirm the delayed sepal yellowing of *dis9* was caused by the lesions in *D14*. The *dis9* plants were transformed via Agrobacterium GV3101 with the D14-*pGWB1* construct (Section 2.6.1), which harbours the WT *D14* sequence, using the floral dip method as described in Section 2.9.1.1. The D14-*pGWB1* construct was obtained from Pilar Cubas and was previously used to rescue the increased branching phenotype of the Arabidopsis *d14-2*/*seto5* mutant (Chevalier *et al.*, 2014). The T1 and T2 transformed seedlings were selected with 25 mg/L hygromycin on half MS-agar plates as described in Section 2.9.1.2. Only true transformants developed true leaves and proper roots. The *dis* phenotype of *dis9* was complemented in those true transformants (Figure 5.8B). Sequencing of the complemented *dis9* plants revealed the presence of both the mutated *D14* and transformed WT sequences in the *dis9* background (Figure 5.8A, C).

The results above confirmed the delayed sepal degreening of *dis9* was caused by the genetic lesion in the coding sequence of *D14*. This mutant was therefore renamed as *d14-6*/*dis9*.

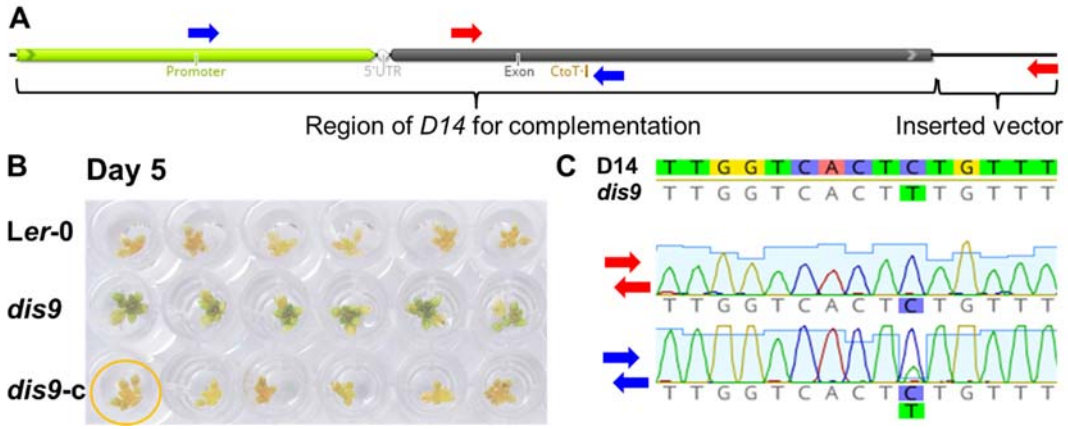

Figure 5.8. Genetic complementation of *dis9*
(A) Schematic showing the WT *D14* fragment used for complementation. The location of the C to T mutation in *D14* gene is indicated. Two sets of primers (indicated by red and blue arrows) were used to confirm the complementation in the T2 plants of transformed *dis9*. Red arrow primers were used to amplify only the WT *D14* sequence present in the inserted construct of the *dis9* background. The blue arrow primers were used to amplify both the mutated *D14* fragment present in the *dis9* background and the WT *D14* fragment transformed into the mutant. (B) Degreening of L*er*-0, *dis9* and complemented *dis9* (*dis9*-c) inflorescences at day 5 of dark incubation. Inflorescences were harvested from T2 *dis9*-c plants. Each T2 plant was the progeny of an independent T1 plant. L*er*-0 and *dis9* inflorescences were used as controls. Six biological replicates are shown. (C) A representative sequencing result for the sample that is circled in figure (B) is shown.

5.2.8. Identification of genetic lesion in *dis15*

Since *dis15* and *dis9* had similar branching and *dis* phenotypes, it was plausible that the causal mutation in *dis15* also caused a defect in the SL pathway. The genetic lesion in *dis15* was previously mapped by Rubina Jibran to the bottom arm of chromosome 2 between 9.6-12.4 Mbp using markers 2-4 and 2-5 (Jibran, 2014). Therefore, this region was interrogated for genes related to SL biosynthesis and signalling. The locations of SL-pathway genes (Table 5.2) on the Arabidopsis chromosome map showed that only the *MAX1* gene (*AT2G26170*) was located in the mapped region between markers 2-4 and 2-5 (Figure 5.9). The trimmed reads from WGS data of *dis15* were obtained and were aligned to the MAX1 coding sequence (CDS) as described in Section 2.8

and 2.11.2 and a G to A transition was identified at position 1405 relative to the translation start site of the MAX1 CDS (Figure 5.10).

Table 5.2. Name and AGI number of strigolactone-pathway genes

SL biosynthesis	AGI (from TAIR)	SL signalling	AGI (from TAIR)
D27	*AT1G03055*	*D14*	*AT3G03990*
MAX3	*AT2G44990*	*MAX2*	*AT2G42620*
MAX4	*AT4G32810*	*SMXL6*	*AT1G07200*
MAX1	*AT2G26170*	*SMXL7*	*AT2G29970*
LBO1	*AT3G21420*	*SMXL8*	*AT2G40130*

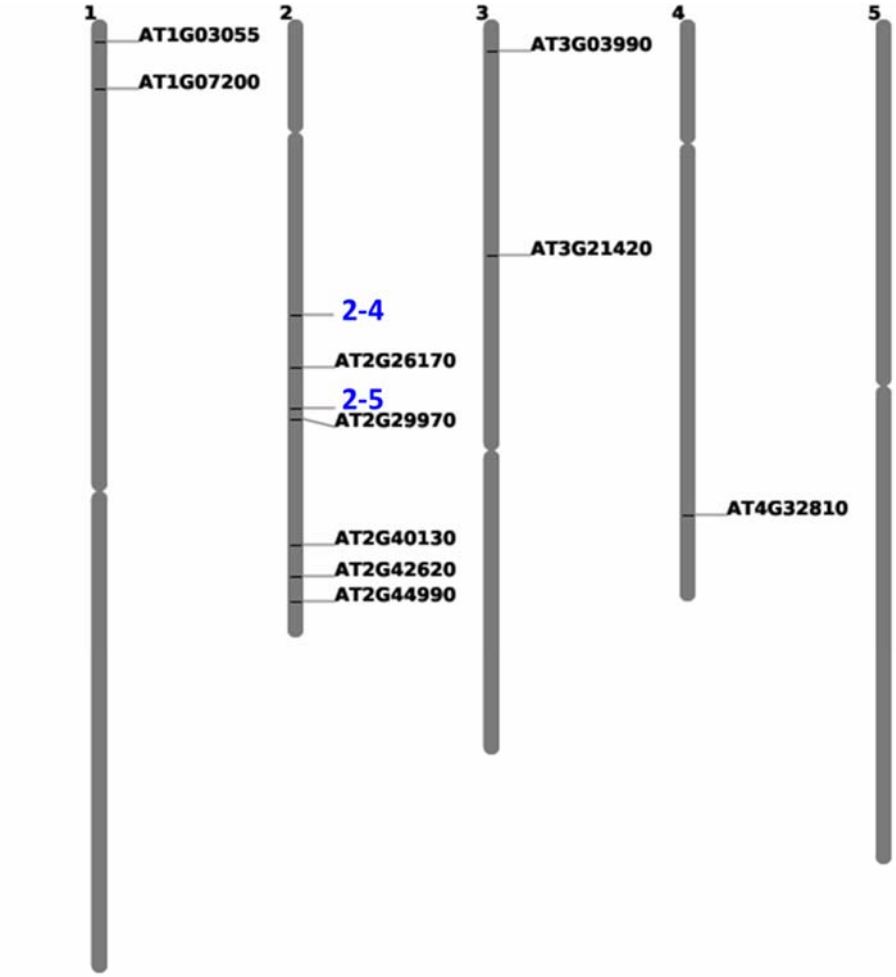

Figure 5.9 Positions of strigolactone-pathway genes and markers indicating mapped region for *dis15* locus in Arabidopsis chromosomes
Representation of chromosome 1 to 5 showing the locations of SL biosynthetic and signalling genes and the positions of markers 2-4 and 2-5 which delimited the 3 mega base region to which *dis15* was mapped (Jibran, 2014; Hunter *et al.*, 2018). Markers 2-4 and 2-5, corresponding to markers 2-8 and 2-11 in Jibran, 2014, were listed in Hunter *et al.*, 2018. The locations of SL-pathway genes on the Arabidopsis chromosome map are shown. The image was created using the Chromosome Map Tool from TAIR website (https://www.arabidopsis.org/jsp/ChromosomeMap/tool.jsp).

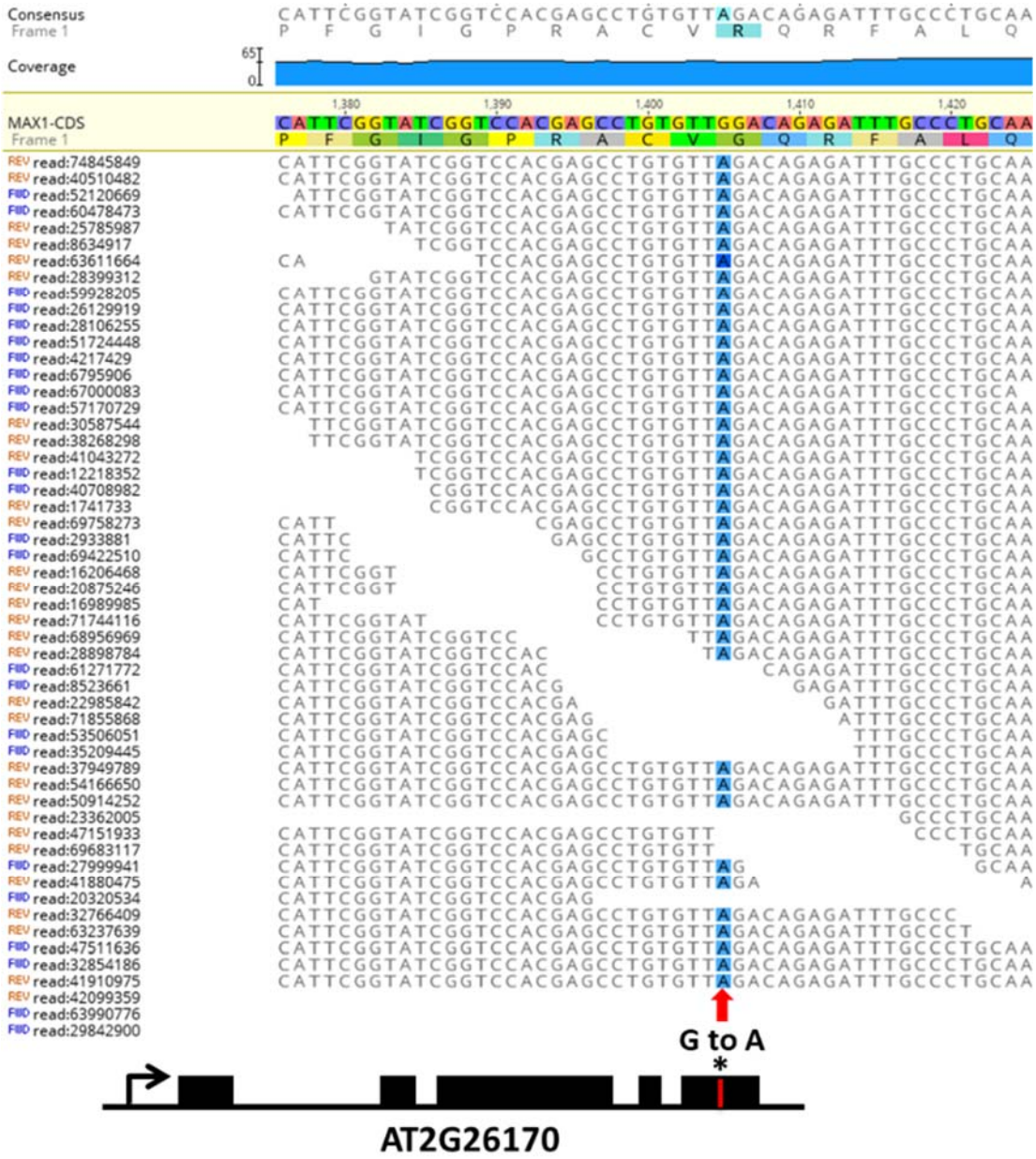

Figure 5.10 Identification of G to A mutation in WGS data of *dis15*
Screenshot from Geneious shows the G to A transition (indicated by red arrow) in the gene *AT2G26170* (*MAX1*). Reads were aligned to MAX1 CDS using the method “map to reference” in Geneious.

5.2.9. Genetic complementation of *dis15*

Genetic complementation was performed to confirm the *dis* phenotype of *dis15* resulted from the mutation in *MAX1*. The WT-MAX1 construct (Section 2.6.1) was cloned and transformed into Agrobacterium GV3101 (see Section 2.6 for details). Arabidopsis transformation of the *dis15* mutant was carried out using the floral dip method (Section 2.9.1.1). The T1 seedlings were grown on soil and were selected by spraying with 100 mg/L of BASTA as described in Section 2.9.1.2 and potential transformants survived. The delayed sepal degreening phenotype of *dis15* was rescued in these potential transformants (Figure 5.11B). Sequencing of the complemented *dis15* plants showed the presence of both the mutated *MAX1* and transformed WT sequences in the *dis15* background (Figure 5.11A, C).

These results confirmed the *dis* phenotype of *dis15* was due to the mutation in the coding sequence of *MAX1*. Thus, this mutant was renamed as *max1-5*/*dis15*.

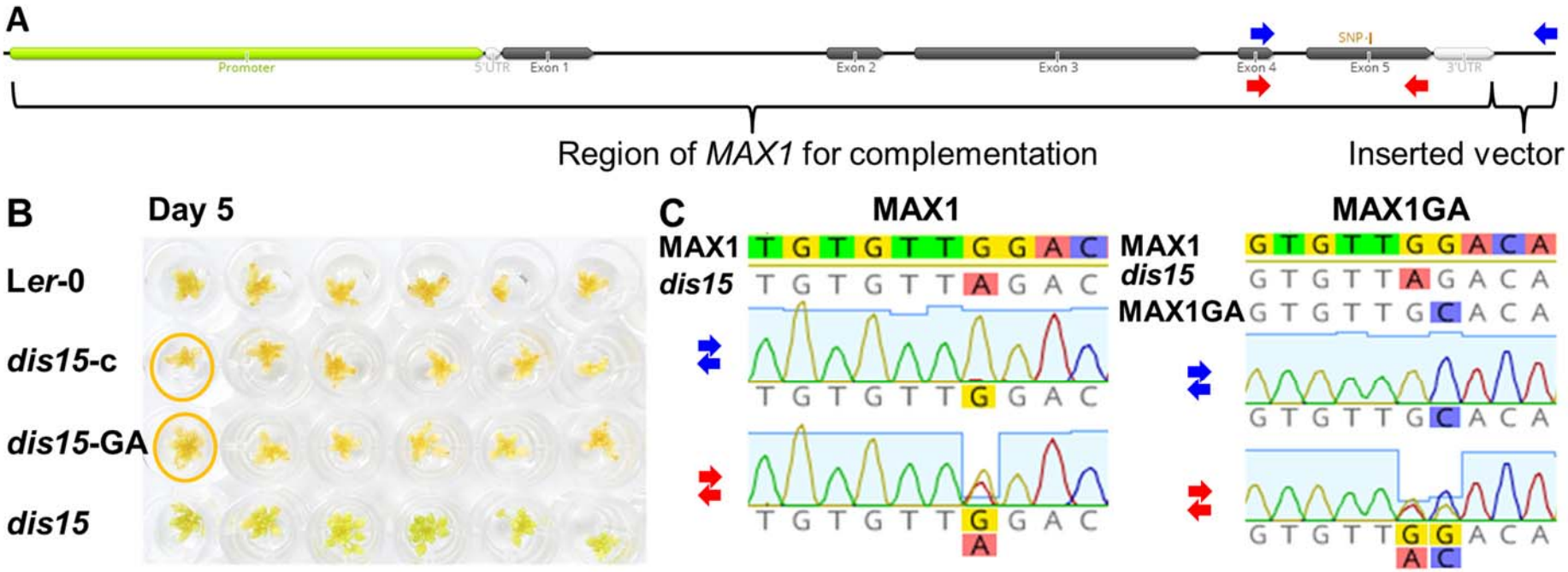

Figure 5.11. Genetic complementation of *dis15*

(A) Schematic showing the WT *MAX1* fragment used for complementation. The location of the SNP (G to A) in *MAX1* gene is indicated. Two sets of primers (indicated by blue and red arrows) were used to confirm the complementation in the T1 plants of transformed *dis15*. Blue arrow primers were used to amplify only the WT *MAX1* fragment (or MAX1 with G469A substitution, Section 5.2.11) present in the construct and then transformed into the *dis15* mutant. The red arrow primers were used to amplify both the mutated *MAX1* fragment present in the *dis15* background and the WT *MAX1* fragment (or MAX1-G469A) transformed into the mutant. (B) Degreening of inflorescences for L*er*-0, *dis15* and complemented *dis15* with both MAX1 WT (*dis15*-c) and MAX1-G469A (*dis15*-GA; Section 5.2.11) at day 5 of dark incubation. Inflorescences were harvested from T1 *dis15*-c (or *dis15*-GA) plants. L*er*-0 and *dis15* inflorescences were used as controls. Six biological replicates are shown. (C) Representative sequencing results for the samples that are circled in figure (B) is shown.

5.2.10. Highly conserved amino acid is substituted in *d14-6*/*dis9* (S97F)

D14 encodes an α/β-fold hydrolase protein that functions as a SL receptor (Arite *et al.*, 2009; Hamiaux *et al.*, 2012; Waters *et al.*, 2012). The mutation in *d14-6/dis9* caused a Ser to be substituted with Phe at position 97 (S97F) of the encoded protein of D14. The D14 S97F substitution occurred at the Ser-His-Asp catalytic triad that is located at the hydrophobic substrate-binding pocket of the D14 hydrolase. S97 in D14 of Arabidopsis is highly conserved in the orthologs from other species (Challis *et al.*, 2013) including the characterised functional orthologues in petunia *Ph*DAD2 (Hamiaux *et al.*, 2012), rice *Os*D14 (Arite *et al.*, 2009; Gao *et al.*, 2009; Liu *et al.*, 2009), poplar *Pt*D14a (Zheng *et al.*, 2016), pea RMS3 (de Saint Germain *et al.*, 2016) and the paralog *At*KAI2 (Waters *et al.*, 2012) (Figure 5.12A). Changing the Ser-97 residue to alanine (a non-nucleophilic residue) was previously reported to cause loss of D14 hydrolase activity (Abe *et al.*, 2014) and prevent formation of a covalently linked intermediate molecule (CLIM) in the active site of the protein (Yao *et al.*, 2016) (Figure 5.12B). The SL-defective phenotype observed in my study strongly suggests that substitution of Ser-97 to Phe (also a non-nucleophilic amino acid) caused loss of receptor activity *in planta*.

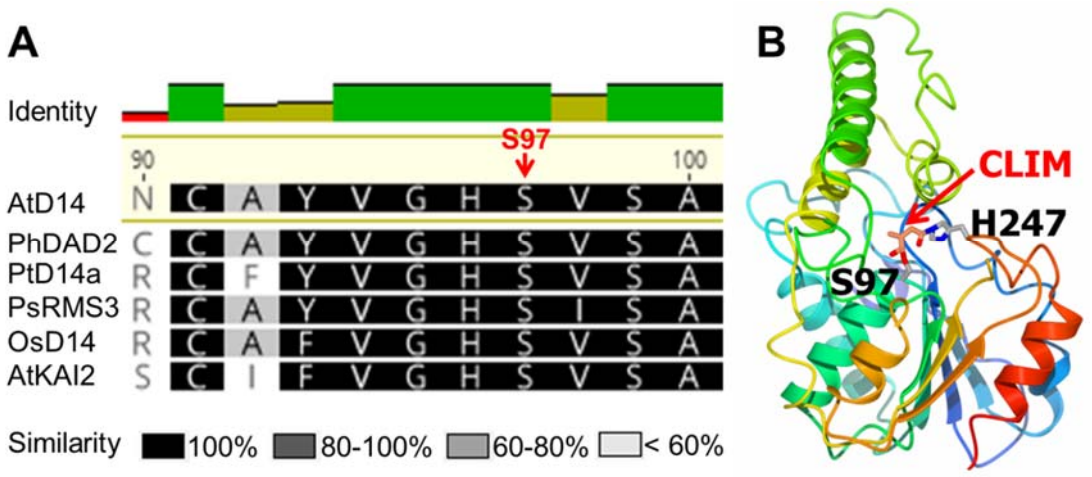

Figure 5.12. The serine to phenylalanine substitution in the D14 protein
(A) Sequence alignment of Arabidopsis D14 with characterised homologs. Position of the mutation at Ser-97 (S97) in AtD14 is indicated in red. Amino acid positions are based on Col-0 sequence from TAIR. Aligned sequences were sorted by the differences to AtD14 reference sequence. Intensity of shading represents the percentage similarity of each residue among D14 homologs. At, Arabidopsis; Os, rice; Ph, petunia; Pt, poplar; Ps, pea. (B) Structure of AtD14 from the SL-induced AtD14-D3-ASK1-complex (PDB: 5HZG). The CLIM is shown as orange and red sticks. The catalytic triad residues Ser-97 and His-247 are shown in atomic colouring as grey/blue/red sticks. AtD14 is shown in cartoon representation coloured in a rainbow scheme (N to C terminus from blue to red).

5.2.11. Highly conserved amino acid is substituted in *max1-5/dis15* (G469R)

MAX1 encodes a cytochrome P450 monooxygenase that is involved in SL biosynthesis (Booker *et al.*, 2005; Abe *et al.*, 2014). The mutation in *max1-5/dis15* led to replacement of Gly to Arg at position 469 (G469R) of the MAX1 protein. The MAX1 G469R substitution occurs in the last residue of the cysteine haem-iron ligand signature [FW]-[SGNH]-x-[GD]-{F}-[RKHPT]-{P}-C-[LIVMFAP]-[GAD], which is highly conserved in the cytochrome P450 superfamily (Prosite: https://prosite.expasy.org/PDOC00081). This G469 residue is invariant in all MAX1 functional orthologues studied thus far (Figure 5.13A) (Yoneyama *et al.*, 2018). However, as the ligand signature [GAD] indicates, glycine (G) can be replaced by alanine (A) or aspartate (D). This occurs at very low frequency in the wider cytochrome P450 protein family with G replaced by A in 3.4% or by D in 0.18% of the 1087 predicted cytochrome P450 proteins that have the cysteine haem-iron ligand pattern (according to the Prosite database) (Appendix 10). The 3D structure of AtMAX1 was modelled

on the most closely related cytochrome P450 (human cytochrome P450 CYP3A4) with a protein crystal structure available (sequence identity of 28% and E value of 7e-51). The model showed that G469 is in the haem pocket packed against the haem group and is close to the haem-iron ligand cysteine (C467) (Figure 5.13B). The G469R substitution may cause loss-of-function of *max1-5*/*dis15* by disrupting the steric structure of this pocket because there is not enough space in this pocket to accommodate Arg, which has one the largest side-chains as compared to Gly that has the smallest one.

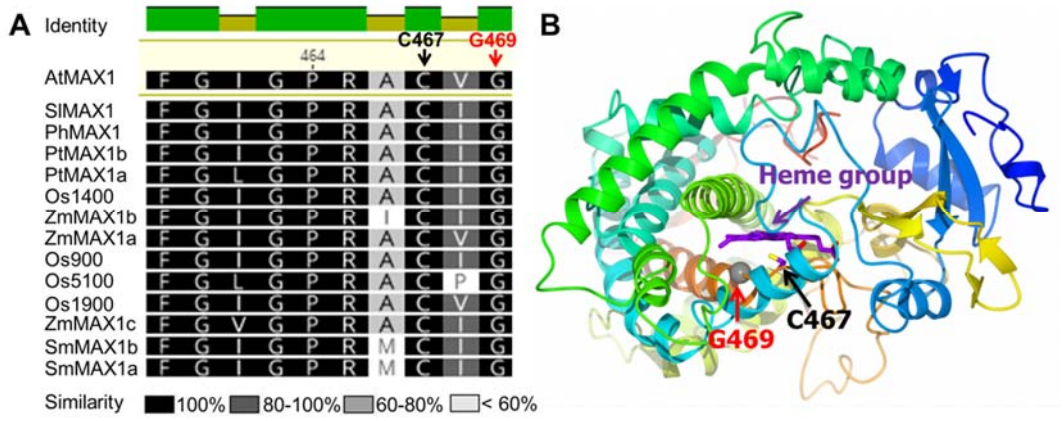

Figure 5.13. The glycine to arginine substitution in the MAX1 protein
(A) Sequence alignment of Arabidopsis MAX1 with its functional orthologs (Yoneyama *et al.*, 2018). Position of mutation at Gly-469 (G469) and of the haem-iron ligand at Cys-467 (C467) in Arabidopsis MAX1 is indicated in red and black, respectively. Amino acid positions are based on Col-0 sequence from TAIR. The sequences of the cysteine haem-iron ligand signature are shown. Aligned sequences were sorted by the differences to AtMAX1 reference sequence. Intensity of shading represents the percentage similarity of each residue among MAX1 orthologs. At, Arabidopsis; Sl, tomato; Sm, *Selaginella*; Os, rice; Ph, petunia; Pt, Poplar; Zm, maize. (B) MAX1 modelled on the structure of the closely related human cytochrome P450 CYP3A4 (PDB: 1TQN) (Yano *et al.*, 2004). The haem group is presented as purple sticks (carbons mostly), which is indicated by a purple arrow. The side chain of Cys-467 (in black; haem ligand) is represented by sticks (carbon is purple and sulphur is yellow). The position of Gly-469 is indicated by the grey sphere and is highlighted by a red arrow. The structure is presented in cartoon representation coloured in a rainbow scheme (N to C terminus from blue to red).

5.2.12. G469R substitution in *max1-5*/*dis15* disrupts enzyme activity of MAX1

To confirm the loss of activity of *max1-5*/*dis15* (MAX1-G469R) suggested by *in silico* prediction, I used transient expression in *N. benthamiana* developed to study the function of SL biosynthetic enzymes (Zhang *et al.*, 2014b).

Arabidopsis *MAX1*-WT, *MAX1*-G469R and *MAX1*-G469A were transiently expressed with the upstream enzyme-encoding genes of the CL biosynthetic pathway (*AtD27*, *AtMAX3*, and *AtMAX4*) in *N. benthamiana* and the substrate (CL) and product (CLA) of MAX1 were measured. Transient expression of *AtD27*, *AtMAX3*, and *AtMAX4* indeed resulted in the production of CL and not CLA (Figure 5.14). When co-expressed with *MAX1*-WT (either L*er*-0 or Col-0 version) or with *MAX1*-G469A, CL was significantly reduced and some CLA was detected. However, when co-expressed with *MAX1*-G469R, the amount of CL did not decrease although CLA was produced to a similar level as that produced by *MAX1*-WT (Figure 5.14). The lack of a decrease in CL suggested that MAX1-G469R had reduced enzymatic activity.

To confirm that the G469R mutation was affecting enzyme activity rather than exerting its effect through transcriptional changes, mRNA abundance of *MAX1*-WT, *MAX1*-G469A and *MAX1*-G469R was analysed. There was no difference in expression among *MAX1*-WT, *MAX1*-G469A and *MAX1*-G469R when they were expressed in *N. benthamiana* (Appendix 11). Thus, the lack of CL conversion in *N. benthamiana* upon co-infiltration of the CL pathway with *MAX1*-G469R was caused by loss-of-activity of the MAX1-G469R enzyme.

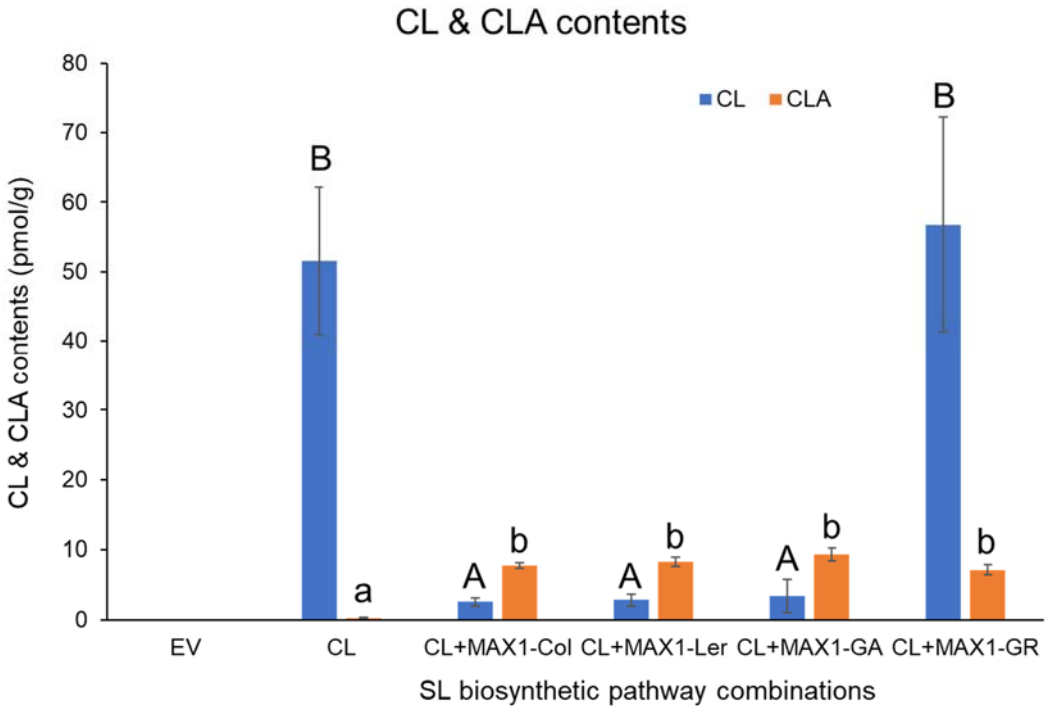

Figure 5.14. Analysis of CL and CLA in *N. benthamiana* leaves infiltrated with strigolactone biosynthetic gene constructs

CL and CLA content in *N. benthamiana* transiently expressing *MAX1* (Col/L*er*-WT or with nucleotide changes resulting in G469R or G469A substitutions) plus CL pathway genes. Data are mean ± standard error (n=6). EV, empty vector (control); CL, carlactone pathway (expressing *AtD27*, *AtMAX3*, and *AtMAX4*); *MAX1*-Col/L*er*, CL pathway plus *MAX1* based on Col-0 or Ler-0 sequence; *MAX1*-GR/GA, CL pathway plus *MAX1* with G469R or G469A substitutions based on L*er*-0 sequence. Letters represent significant differences among different gene combinations for the infiltration for each compound comparison in one-way ANOVA. Upper and lower cases were used to distinguish the difference for each compound. Means for the same compound with the same letter are not significantly different (5% least significant difference comparisons made on log-transformed data).

5.2.13. MAX1 remains functional when Gly-469 is replaced by Ala

As mentioned above, Gly-469 in MAX1 is substituted by Ala in 3.4% of the 1087 predicted cytochrome P450 proteins, but is invariant in MAX1 orthologues. Nevertheless, the above experiments show that Ala can functionally replace Gly-469 (Figure 5.14). The ability of Ala to functionally replace Gly-469 was also supported by *MAX1*-G469A complementing the *dis* phenotype of the *max1-5*/*dis15* mutant. (Figure 5.11). These results indicate that Ala (A), but not Arg (R), is functionally equivalent to Gly-469 at the haem-iron binding pocket of MAX1 protein maintaining enzyme activity.

5.2.14. Treatment with rac-GR24 rescues delayed sepal degreening of *max1-5*/*dis15* but not *d14-6*/*dis9*

To test whether SL could chemically complement the sepal degreening phenotype of the *max1-5/dis15* biosynthetic mutant, the inflorescences of *max1-5/dis15, d14-6/dis9* and L*er*-0 WT were treated with different concentrations (1, 5, 25, 50 µM) of the SL analogue rac-GR24 (Figure 5.15A; Appendix 12 A). rac-GR24 can also induce karrikin (KAR) signalling, but this is likely not relevant for the dark-induced degreening phenotype as defects in KARRIKIN INSENSITIVE 2 (KAI2), a KAR-specific receptor, do not delay dark-induced leaf senescence (Ueda and Kusaba, 2015).

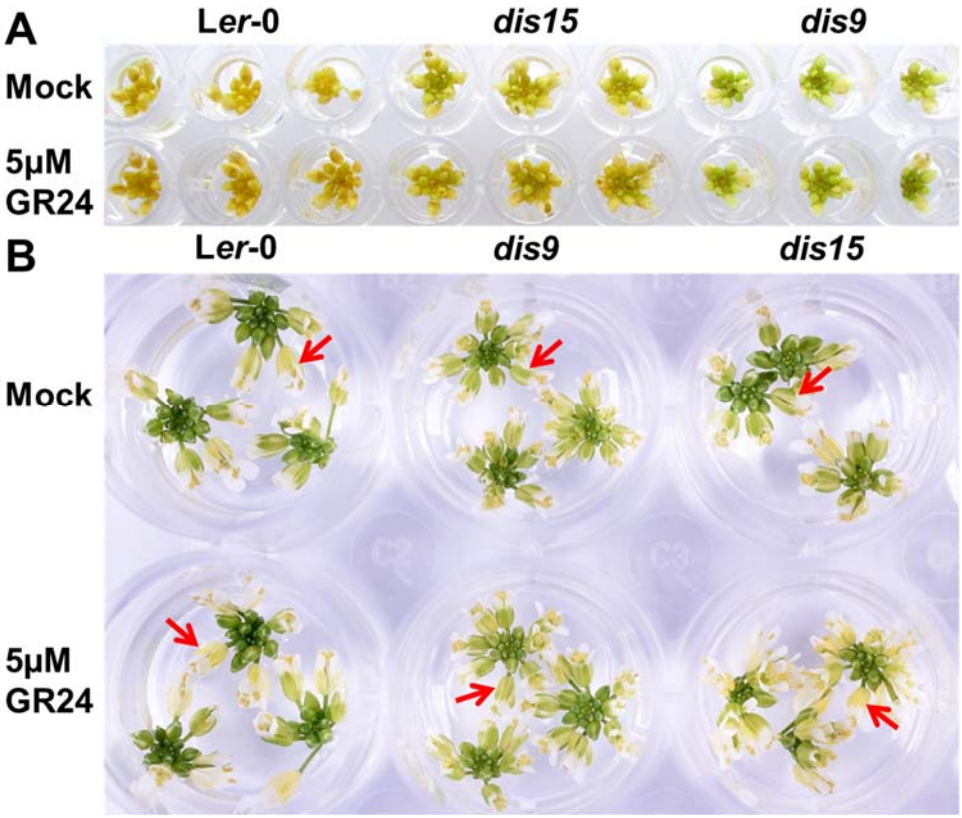

Figure 5.15. Sepal degreening of excised inflorescences treated with rac-GR24
(A) Dark incubated inflorescences. Inflorescences were harvested from the primary bolts of 4.5-week-old plants that had their first flower opened on the same day. The inflorescences with removed opened buds were treated with 1% DMSO (mock) and 5 µM rac-GR24 and incubated in the dark for 5 days. Three biological replicates for each genotype and treatment are shown. (B) Long day (16 h light) treated inflorescences. Inflorescences were harvested from the primary bolts of 4.5-week-old plants that had their first flower opened on the same day. The inflorescences with removed opened buds were treated with 1% DMSO (mock) and 5 µM rac-GR24 and incubated in 16h/8h light/dark cycle for 3 days. Red arrows indicate representative sepals. Three biological replicates are shown.

rac-GR24 at 5 µM was sufficient for rescuing the delayed sepal degreening phenotype in *max1-5*/*dis15* but not *d14-6*/*dis9* at day 5 of dark incubation (Figure 5.15A). Under long day (16-h light) conditions, the hormone analogue also hastened sepal yellowing of *max1-5*/*dis15* but not *d14-6*/*dis9* excised inflorescences (Figure 5.15B; Appendix 12 B).

5.2.15. Strigolactone biosynthetic and response genes are up-regulated by 24 h of dark incubation in inflorescences

The data above showed that SLs participate in controlling inflorescence sepal senescence. I then asked at what stage of senescence SLs were involved. It has been suggested that the SL biosynthetic pathway is induced by senescence signalling (Ueda and Kusaba, 2015). If so, SL pathway genes would be expected to be induced later than senescence marker genes. To test this, I compared the timing of transcriptional changes in selected senescence-marker and SL-pathway genes in excised WT inflorescences every 24 h over a period of 3 days of dark treatment using nCounter Technology (NanoString, Seattle, WA, USA; Figure 5.16). Transcript abundance of early stage senescence markers, i.e. Chl degradation gene *SGR1* (Park *et al.*, 2007) and central regulator of senescence *ANAC092* (Balazadeh *et al.*, 2010) were significantly increased at 24 h (Figure 5.16A), suggesting senescence in the inflorescences had already initiated by this time. Increased transcript abundance of the late stage senescence-specific marker gene *SAG12* (Grbic, 2003) at 48 h indicated that at 2 days of dark incubation senescence was well advanced.

I used the transcript abundance changes of three SL biosynthetic genes *MAX1*, *MAX3* and *MAX4* to determine when SL biosynthesis had initiated in the dark-held inflorescences. *MAX1* transcript abundance did not significantly change during the first 24 h of dark treatment, but then significantly and substantially increased to be highest at 72 h (Figure 5.16B). *MAX3* transcript abundance was slightly increased at 24 h, suggesting that SL production in the tissue was just starting. From 24 h onwards, *MAX3* transcript abundance increased in concert with both early senescence markers *SGR1* and *ANAC092*. qRT-PCR analysis of *MAX4* revealed a pattern of transcript accumulation that was very similar to

that of *MAX3* suggesting co-regulation and beginning of SL synthesis by 24 h (Figure 5.17A).

The timing of SL response was determined by measuring changes in transcript abundance of the SL signalling genes *AtD14*, *SMXL6*, *SMXL7* and *SMXL8*. Transcript abundance of the first three genes increased significantly at 24 h of dark treatment (Figure 5.16C, D), whereas *SMXL8* transcript abundance decreased to be undetectable at 24 h (Figure 5.16D). The nCounter results for *MAX3*, *SMXL6/8*, *ANAC092* and *SAG12* were confirmed by qRT-PCR analysis (Figure 5.17A-C).

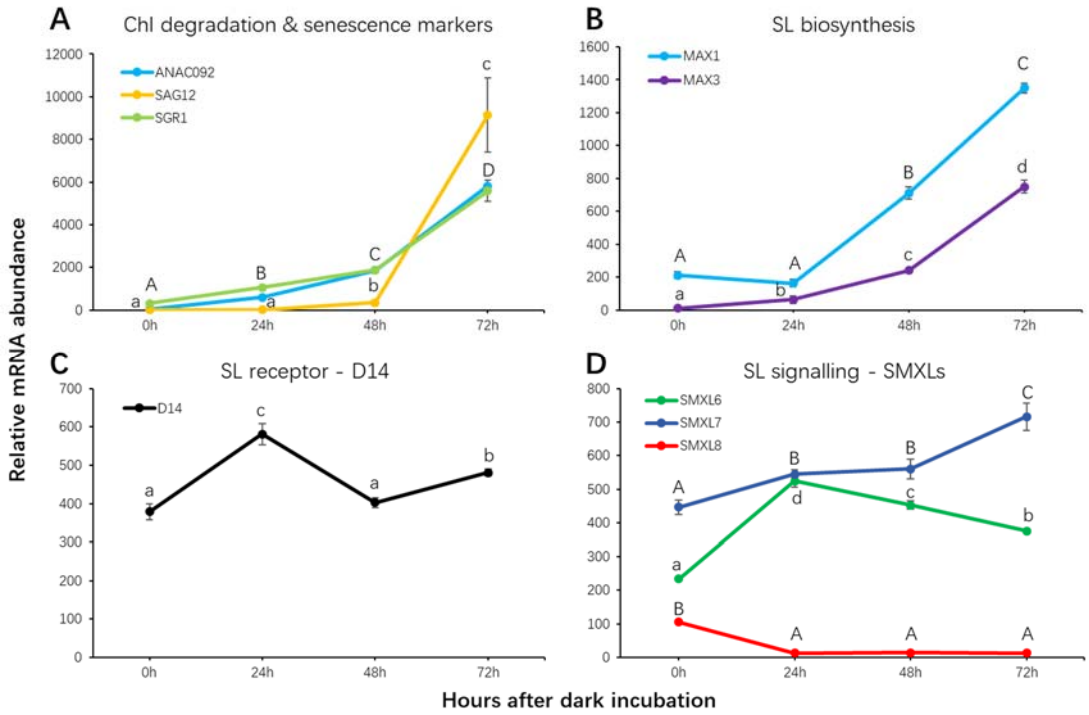

Figure 5.16 Transcript abundance changes of strigolactone pathway and senescence-related genes during a period of 72-h of dark treatment
(A) Chlorophyll (Chl) degradation and senescence marker genes; (B) Strigolactone (SL) biosynthetic genes; (C) SL receptor; (D) SL signalling genes. Transcript abundance was quantified using nCounter technology on RNA isolated from detached WT inflorescences (n = 3 samples, > 4 inflorescences from independent plants per sample) that were incubated in the dark for 0 h, 24 h, 48 h and 72 h. Transcript abundance was normalised to geometric mean of *PP2AA3*, *ACT2* and *MON1*. Data are mean ± standard error. Letters represent significant differences among four time points for each gene comparison in one-way ANOVA (Fisher's protected LSD test $P<0.05$). Upper and lower case letters were used to distinguish the comparisons for each gene. Upper case letters in (A) represented comparisons for both *ANAC092* and *SGR1*.

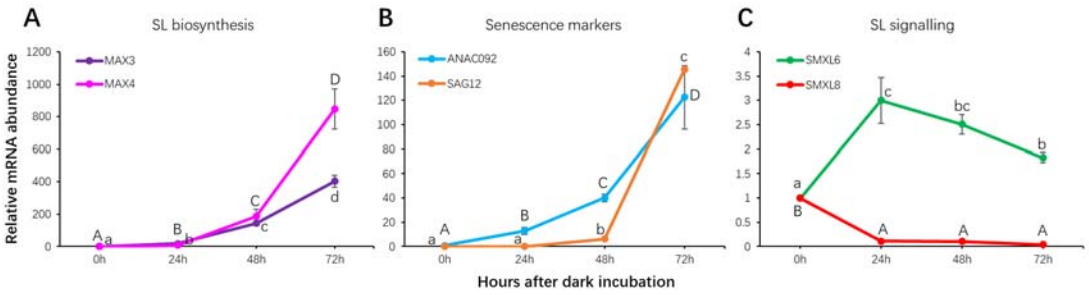

Figure 5.17 Confirmation of transcriptional changes of strigolactone-pathway and senescence-related genes by qRT-PCR analysis

(A) SL biosynthetic genes; (B) senescence marker genes; (C) SL signalling genes. Transcript abundance of each gene was quantified by qRT-PCR using cDNA synthesised from RNA isolated from detached WT inflorescences (n = 3 samples, > 4 inflorescences from independent plants per sample) that had been incubated in the dark for 0 h, 24 h, 48 h and 72 h. Transcript abundance was normalised to *PP2AA3* and expressed relative to the 0 h sample. Data are mean ± standard error. Letters represent significant differences among four time points for each gene comparison in one-way ANOVA (Fisher's protected LSD test P<0.05). Upper and lower cases were used to distinguish the comparisons for each gene. The relative mRNA abundance of *SAG12* is presented as the measured transcript abundance divided by 100.

Overall the results from the transcript profiling of the inflorescence suggest that by 24 h of dark incubation SL biosynthesis has been initiated, SL signalling is occurring, and senescence has started. Thus, earlier time points were investigated to determine the order of pathway activation.

5.2.16. Strigolactone signalling but not biosynthetic genes respond rapidly to the light-dark transition

At 24 h of darkness, the inflorescence tissue had been exposed to 8 h of regular and 16 h of extended night. One of the most notable outcomes of keeping tissue in extended darkness for this length of time is acute carbon starvation caused by exhaustion of starch reserves (Usadel *et al.*, 2008), which causes precocious senescence. This agrees with our previous work that found that carbon-depletion resulting from a 24 h dark treatment is a key senescence stimulus for detached immature inflorescences (Trivellini *et al.*, 2012). I therefore considered the possibility that SL biosynthesis and response early in the extended night are associated with acute carbon deprivation-based signalling. To test this, I compared the timing of expression of transcriptional markers of tissue carbon status (SnRK1-related genes *AKINβ1* and *bZIP63*) (Blasing *et al.*,

2005; Usadel *et al.*, 2008; Li *et al.*, 2009; Mair *et al.*, 2015) with that of SL-associated genes both in the regular and early extended night.

In WT, during the first 6 h into the regular night, transcript abundance of the *AKINβ1* and *bZIP63* increased in the detached inflorescences held in the dark (Figure 5.18A). This was consistent with them being markers of reduced (but not yet acutely limited) carbon availability. Key senescence-regulatory genes *ANAC092* (Kim *et al.*, 2009) and *AtNAP* (Guo and Gan, 2006) that are also sugar responsive were upregulated at 3 h (Figure 5.18B). Since these two genes are also diurnally regulated (Kim *et al.*, 2018; Song *et al.*, 2018), their transcriptional increase was more likely in response to changes in soluble sugar (Blasing *et al.*, 2005; Usadel *et al.*, 2008) and circadian clock rather than senescence. Because of this, we did not expect SL biosynthesis and signalling genes to respond during this early night time frame. As expected, during the first 6 h into the regular night there was no increase in transcript abundance of *MAX1*, while *MAX3* transcripts were not detected (Figure 5.19A). Transcript abundance of *SMXL7* also did not change during the regular night (Figure 5.19B). However, at 3 h into the dark period *SMXL6* and *SMXL8* were up- and down-regulated, respectively (Figure 5.19B).

In the *max1-5*/*dis15* mutant, the two *MAX* and three *SMXL* genes exhibited similar expression patterns to that of WT, although their abundance was lower (Figure 5.19A, B). The reduced expression of the three *SMXL*s was reversed when the mutant was treated with rac-GR24 for 3 h (Figure 5.19B; Appendix 13). Intriguingly, *AtNAP* was significantly upregulated by rac-GR24 at 3 h of treatment (Figure 5.18B), suggesting it is also a SL-inducible gene. Thus, based on transcription, the WT inflorescences experienced a reduction in sugar content during the normal night, but this did not trigger initiation of SL biosynthesis. In the *max1-5*/*dis15* mutant, both SL signalling genes and *AtNAP* respond rapidly to rac-GR24 treatment, indicating these genes were SL-inducible.

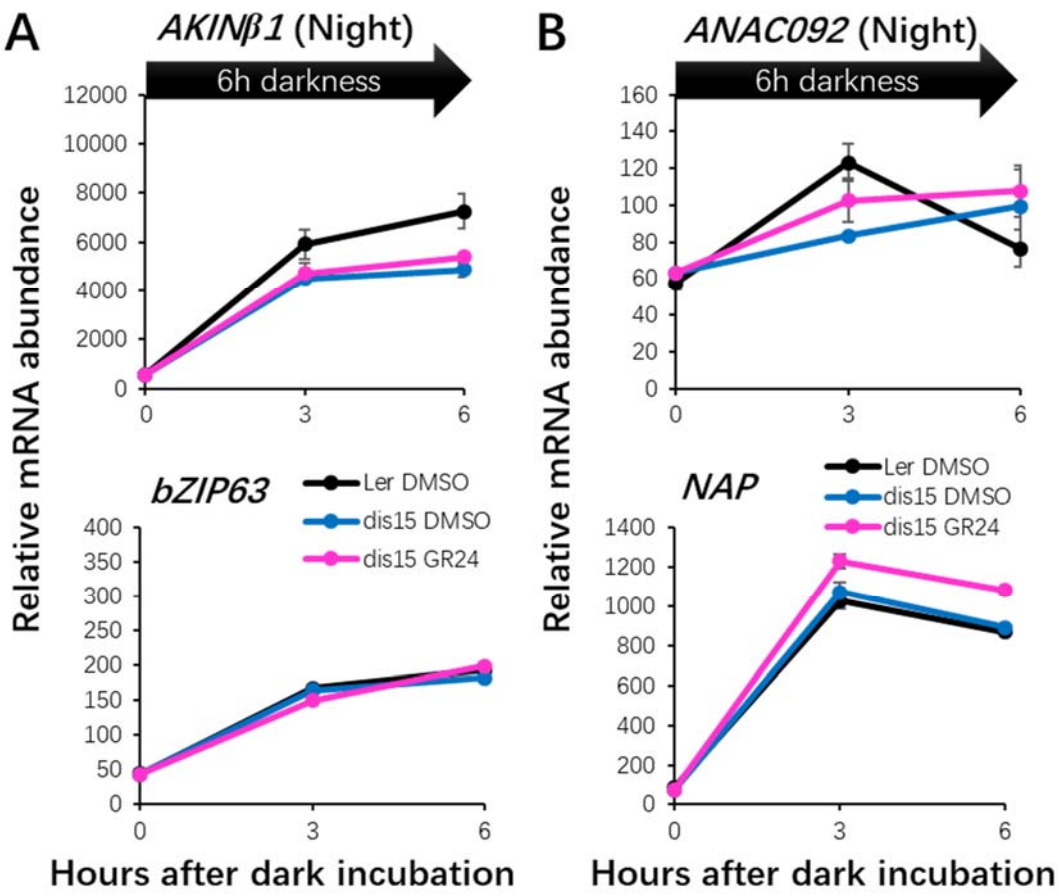

Figure 5.18 Transcriptional changes of sugar- and senescence-related genes during the regular night

(A) SnRK1-related genes; (B) functional senescence regulators. Transcript abundance of each gene was quantified using nCounter technology on RNA isolated from detached WT or *max1-5/dis15* inflorescences (n = 3 samples, > 4 inflorescences from independent plants per sample) that were treated with 1% DMSO for WT and 1% DMSO/rac-GR24 for *max1-5/dis15* and incubated in the dark for 0 h, 3 h and 6 h. Transcript abundance was normalised to geometric mean of *PP2AA3*, *ACT2* and *MON1*. Data are mean ± standard error. Statistical significance of gene expression for all samples is listed in Appendix 13.

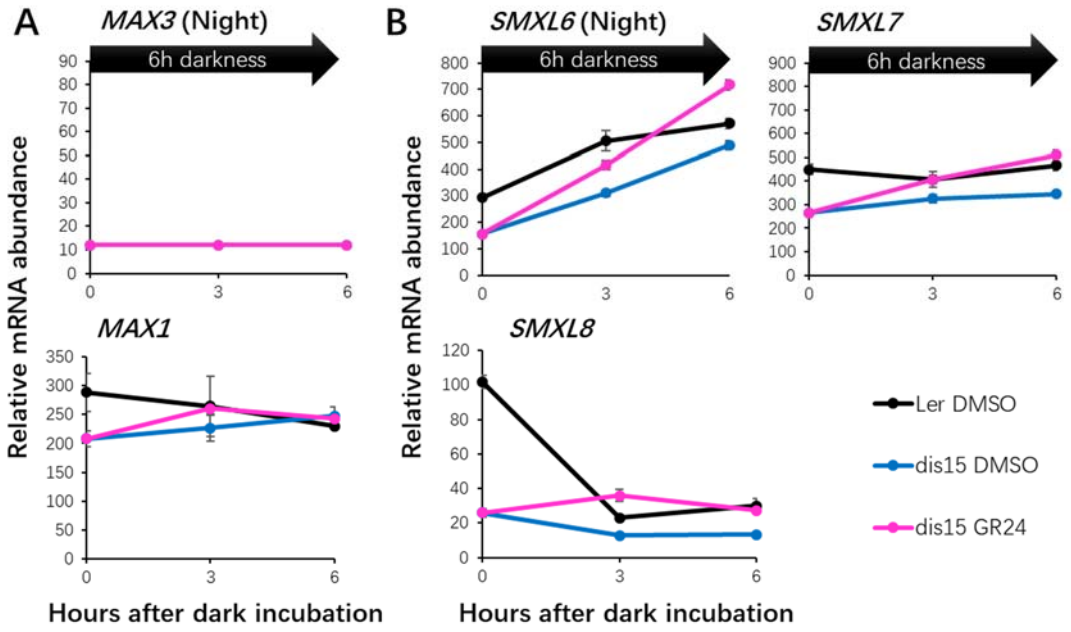

Figure 5.19 Transcriptional changes of strigolactone pathway genes during the regular night

(A) Strigolactone (SL) biosynthetic genes; (B) SL signalling genes. Transcript abundance of each gene was quantified using nCounter analysis on RNA isolated from detached WT or *max1-5*/*dis15* inflorescences (n = 3 samples, > 4 inflorescences from independent plants per sample) that were treated with 1% DMSO for WT and 1% DMSO/rac-GR24 for *max1-5*/*dis15* and incubated in the dark for 0 h, 3 h and 6 h. Transcript abundance was normalised to geometric mean of *PP2AA3*, *ACT2* and *MON1*. Data are mean ± standard error. Statistical significance of gene expression for all samples is listed in Appendix 13. Figure legends apply to all figures.

5.2.17. GR24 supresses the transcript abundance of *SnRK1*-related genes in *max1-5*/*dis15* during an extended night

I next determined the effect of extended darkness (i.e. darkness that surpassed the anticipated night period) on carbon status markers, senescence-markers, and SL biosynthesis and signalling genes. In WT, at 4 h of extended night (i.e. 12 h of dark treatment), transcript abundance of *AKINβ1* and *bZIP63* was substantially increased (Figure 5.20A; Appendix 13). This was consistent with the WT inflorescences experiencing carbon starvation as has been reported for rosette leaves exposed to a 4 h extended night (Usadel *et al.*, 2008). Transcript abundance of *ANAC092* (Kim *et al.*, 2009) and *AtNAP* (Guo and Gan, 2006) were also significantly increased at this time (Figure 5.20B). However, transcript abundance of *MAX1* was not increased by the 4 h night extension and *MAX3* abundance remained undetectable, suggesting SL biosynthesis was not

occurring. By 10 h of extended night (18 h of dark treatment), *MAX1* transcript abundance had still not changed, but that of *MAX3* had increased suggesting SL biosynthesis had started (Figure 5.20C). The three *SMXL* genes were differentially expressed during the extended night (Figure 5.20D). *SMXL8* transcript counts were undetectable at both 4 h and 10 h of extended night; *SMXL6* transcript abundance was increased at 4 h but then declined; and *SMXL7* started to increase at 10 h of extended night in a pattern strikingly similar to *MAX3*.

I then determined how the patterns of expression of the above genes were affected by SL deficiency by examining their transcript accumulation in the *max1-5*/*dis15* mutant. Overall the patterns of accumulation of carbon-status-related, senescence-marker genes and SL biosynthesis and signalling genes in the mutant were very similar to what was seen in WT over the 10 h extended night (Figure 5.20A-D), suggesting that their pattern of regulation was not controlled by SL. Interestingly, when the mutant was treated with rac-GR24, the transcript abundance of sugar-related genes *AKINβ1* and *bZIP63* were suppressed significantly by rac-GR24 at 4 h and not at 10 h of extended night (Figure 5.20A). By contrast, the transcript abundance of the two senescence-related genes *ANAC092* and *AtNAP* was elevated at 12 h by rac-GR24 and so was *MAX1* (Figure 5.20B, C). All three *SMXL* genes were upregulated by rac-GR24 at both time points (Figure 5.20D) as observed during the regular night.

Taken together, the nCounter profiling study has highlighted a temporal sequence of events whereby markers of carbon deprivation and senescence regulation first increase followed within hours by markers for SL production. Secondly, GR24 treatment of the *max1-5*/*dis15* mutant indicated that SL acts to promote transcription of senescence controlling genes and suppress transcription of SnRK1-related genes.

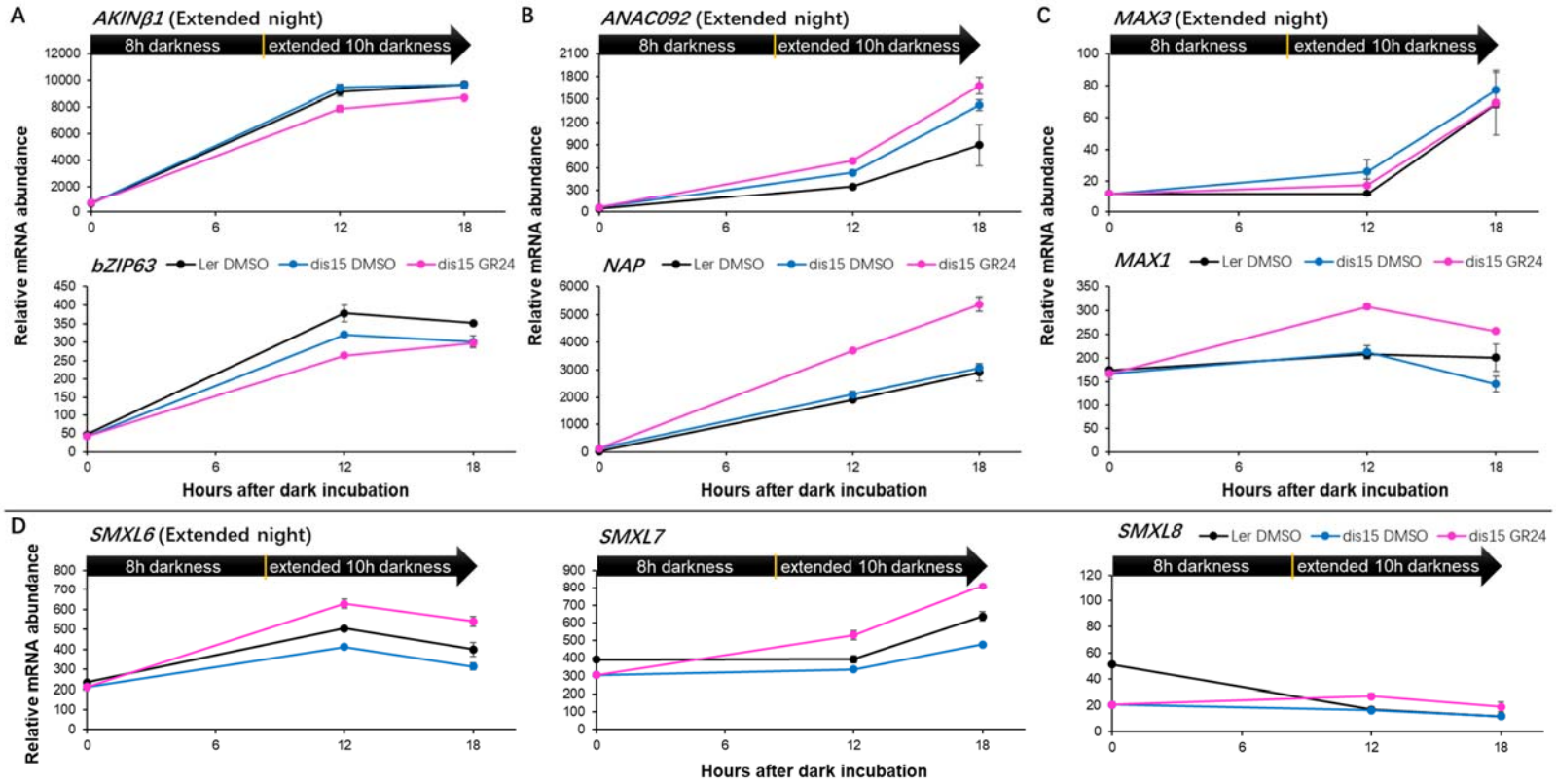

Figure 5.20 Transcriptional changes of sugar, senescence and strigolactone pathway genes during the extended night
(A) *SnRK1*-related genes; (B) functional senescence regulators; (C) strigolactone (SL) biosynthetic genes; (D) SL signalling genes. Transcript abundance of each gene was quantified using nCounter technology on RNA isolated from detached WT or *max1-5*/*dis15* inflorescences (n = 3 samples, > 4 inflorescences from independent plants per sample) that were treated with 1% DMSO for WT and 1% DMSO/rac-GR24 for *max1-5*/*dis15* and incubated in the dark for 0 h, 12 h and 18 h. Transcript abundance was normalised to geometric mean of *PP2AA3*, *ACT2* and *MON1*. Data are mean ± standard error. Statistical significance of gene expression for all samples is listed in Appendix 13.

5.3. Discussion

5.3.1. Strigolactones regulate sepal senescence in Arabidopsis

SLs are plant hormones that affect seed germination (Toh *et al.*, 2012), shoot branching (Gomez-Roldan *et al.*, 2008; Umehara *et al.*, 2008), root architecture (Kapulnik *et al.*, 2011; Ruyter-Spira *et al.*, 2011; Rasmussen *et al.*, 2012). Here I demonstrate that SLs regulate floral organ senescence in addition to their previous demonstrated role in affecting flower development (Snowden *et al.*, 2005; Chevalier *et al.*, 2014). I identified two mutants, *max1-5*/*dis15* (MAX1-G469R) and *d14-6*/*dis9* (D14-S97F), which have novel loss-of-function alleles in the SL biosynthetic gene *MAX1* and receptor *AtD14*, respectively. Both mutants exhibited delayed sepal senescence *in planta* and in detached inflorescences upon dark or long day treatment. Such phenotypes were rescued in the *max1-5*/*dis15* but not *d14-6*/*dis9* mutant by treatment of the detached inflorescences with rac-GR24. Transcript abundance of senescence marker genes was supressed in the two mutants compared with in WT in the dark. These results indicate that SLs regulate both developmental and dark-induced sepal senescence.

5.3.2. Gly-469 of MAX1 is essential for catalysing the conversion of CL into CLA

MAX1 encodes a CYP711A1 protein that belongs to the cytochrome P450 superfamily (Booker *et al.*, 2005). The MAX1 G469R substitution I identified occurs at the last residue in the highly conserved cysteine haem-iron ligand signature of the cytochrome P450 superfamily, which is just two amino acids C-terminal to the absolutely conserved Cys at position 467 of MAX1. To date, no crystal structure of MAX1 has been reported. However, a 3D model based on the closest homologous structure, the human microsomal P450 CYP3A4, revealed that Gly-469 packs against the haem cofactor in the binding pocket and is close to the haem-iron ligand Cys-467 (Figure 5.13B). Since Gly-469 is very close to this Cys, substitution of the smallest amino acid Gly to the larger Arg likely introduces steric clashes within the haem binding pocket and loss of activity of *max1-5*/*dis15* (MAX1-G469R). Interestingly, the G469 residue is invariant in MAX1 orthologues and its closely related proteins in Metazoa,

Bacteria and Archaea [Figure 5.13A; Appendix 10; (Challis *et al.*, 2013)], whereas in the wider cytochrome P450 family in rare instances this residue is replaced by Ala, which suggests that this small nonpolar amino acid may not introduce steric clashes in the wider family of cytochrome P450 proteins. This is consistent with the equivalent Gly to Ala substitution not affecting activity of the Arabidopsis cytochrome P450 CYP83B1, a modulator of auxin homeostasis (Barlier *et al.*, 2000; Bak *et al.*, 2001). The transient expression assay in *N. benthamiana*, and successful genetic complementation of the *max1-5*/*dis15* mutant with MAX1-G469A demonstrated that the Ala substitution did not inactivate MAX1 function, whereas substitution with arginine did. The high content of CL (the substrate of MAX1) and strongly reduced production of CLA hexose conjugates in the leaves infiltrated with the *MAX1*-G469R construct are consistent with accumulation of CL previously observed for the Arabidopsis T-DNA insertion mutant *max1-4* (Seto *et al.*, 2014) and indicates that conversion of the MAX1 substrate is prevented. Thus, I conclude that G469 is an important amino acid for MAX1 function, though it can be replaced by Ala.

5.3.3. Substitution of catalytic Ser-97 affects activity of D14

The *d14-6*/*dis9* mutant displayed delayed dark-induced senescence, increased branch numbers and decreased plant height phenotypes. SL perception and signalling require the D14 receptor. D14 belongs to the protein superfamily of α/β-fold hydrolases (Arite *et al.*, 2009). The crystal structures of *At*D14 and its orthologs in petunia (*Ph*DAD2) and rice (*Os*D14) reveal that they have a hydrophobic substrate-binding pocket containing a Ser-His-Asp catalytic triad essential for hydrolase activity (Hamiaux *et al.*, 2012; Kagiyama *et al.*, 2013; Zhao *et al.*, 2013). Unlike the classical hormone receptors that non-covalently and reversibly bind to hormone molecules, the crystal structure of the SL-induced AtD14–D3–ASK1 complex reveals that AtD14 binds to SL and hydrolyses it into a CLIM (Yao *et al.*, 2016). It is under debate whether this hydrolysis is required for signalling to occur (Seto *et al.*, 2019). Experiments with the F-box protein D3, a rice ortholog of Arabidopsis MAX2 showed that SL triggers SL signalling by enabling AtD14 to bind to MAX2 to recruit repressors (e.g. Arabidopsis SMXL6/7/8) for degradation through the 26S proteasome (Jiang *et al.*, 2013; Zhou *et al.*, 2013; Wang *et al.*, 2015). In the *d14-6*/*dis9*

mutant, Ser-97 in the catalytic triad was replaced by Phe. This produced phenotypes similar to the null mutant *d14-1* suggesting loss of activity of D14 (Waters *et al.*, 2012; Ueda and Kusaba, 2015). This is consistent with mutation of this residue (atd14:S97A) affecting binding of the receptor to the SL analogue GR24 and abolishing hydrolase activity (Abe *et al.*, 2014). Thus, it is probable that the S97F mutation I identified causes complete loss of D14 activity.

5.3.4. Strigolactones regulate dark-induced inflorescence senescence in association with a change of carbon status during the extended night

SLs affect various stress responses including drought, high salinity, nutrient deficiency and light-deprivation/darkness (Bu *et al.*, 2014; Ha *et al.*, 2014; Yamada *et al.*, 2014; Ueda and Kusaba, 2015; Yamada and Umehara, 2015). The findings in this study suggest that SLs also regulate senescence of Arabidopsis sepals under energy-deprivation conditions. Previous studies from our group demonstrated that the energy-deprivation resulting from prolonged darkness causes a reduction in soluble sugars and transcriptional changes of sugar-responsive genes in detached inflorescences (Trivellini *et al.*, 2012). This suggests an interaction between SLs and sugar signalling in controlling dark-induced inflorescence senescence. Crosstalk between SLs and sugar signalling has been reported for regulation of shoot branching and seedling establishment in Arabidopsis (Li *et al.*, 2016; Otori *et al.*, 2017). To investigate the interaction between SLs and sugar signalling in controlling inflorescence senescence, I harvested WT and SL deficient *max1-5*/*dis15* inflorescences at the start of the dark cycle and examined the transcriptional changes of selected genes in SL, sugar, and senescence pathways after different times of dark incubation.

During the night, SnRK1s have a crucial role in the sugar-dependent regulation of transcriptional response (Blasing *et al.*, 2005; Baena-Gonzalez *et al.*, 2007; Usadel *et al.*, 2008). It is therefore not surprising that in WT inflorescences SnRK1-related genes *AKINβ1* (a subunit of SnRK1) (Li *et al.*, 2009) and *bZIP63* (one of the direct targets of SnRK1) (Mair *et al.*, 2015) were both up-regulated at 3 h of dark incubation. Such early upregulation was also observed in

Arabidopsis rosettes and attributed to starch decline during the normal night (Blasing *et al.*, 2005). Interestingly, in WT inflorescences key senescence regulators *ANAC092* (Kim *et al.*, 2009) and *NAP* (Guo and Gan, 2006) were also up-regulated at 3 h. However, in rosette leaves the decline in sugar content during the night does not cause starvation (Blasing *et al.*, 2005; Usadel *et al.*, 2008) and therefore it is unlikely that up-regulation of these marker genes in the inflorescences was indicative of senescence initiation. Moreover, since expression of both genes also depends on sugar content and circadian clock (Blasing *et al.*, 2005; Usadel *et al.*, 2008; Kim *et al.*, 2018; Song *et al.*, 2018), their transcriptional changes more likely result from one or both of these cues. Because of technological limitations, precise quantification of SL content in Arabidopsis is extremely difficult (Seto *et al.*, 2014; Lv *et al.*, 2018). Thus, I used the transcriptional changes of selected SL biosynthetic genes to indirectly estimate SL content (Li *et al.*, 2018). I found in WT during the normal night that *MAX1* abundance was unchanged and *MAX3* counts were below the set threshold for detection. This suggests that SLs are not synthesised during the regular night. I also examined transcriptional changes of SL signalling genes *SMXL6*, *SMXL7* and *SMXL8* to help determine timing of SL response. These three *SMXL*s are functionally redundant in controlling Arabidopsis shoot branching (Soundappan *et al.*, 2015; Wang *et al.*, 2015). I considered their involvement in senescence regulation because senescence and branching phenotypes were tightly linked in *max1-5*/*dis15* and *d14-6*/*dis9* mutants. *SMXL7* transcript abundance was unchanged in WT during the normal night, consistent with expression patterns of the biosynthetic genes. However, *SMXL6* transcript increased significantly at 3 h and *SMXL8* transcript declined rapidly to become undetectable at 3 h and onwards. This raises the possibility that different cues affect transcription of these three *SMXL*s. Transcript abundance of the three *SMXLs* was lower in *max1-5*/*dis15* inflorescences but was restored by rac-GR24 treatment. These findings suggest that the regular night causes sugar levels to decline without affecting SL biosynthesis.

The extended night commences when the regular night ends and it was previously shown that in Arabidopsis rosettes, carbon became severely limited 4 h into the extended night (Usadel *et al.*, 2008). *SnRK1*s, have key roles in

regulating transcriptional reprogramming during energy-deprivation (Baena-Gonzalez *et al.*, 2007; Usadel *et al.*, 2008). Consistent with these observations, I found that transcript abundance of *AKINβ1* and *bZIP63* increased more in WT at 12 h (4 h into extended night) than during the regular night. The sugar-responsive and senescence-controlling genes *ANAC092* and *NAP* also showed further increased transcript abundance 12 h. Then at 18 h (10 h into extended night), *AKINβ1* and *bZIP63* did not show further transcriptional changes. This could be because sugar depletion in the inflorescence is alleviated by metabolic readjustment, similar to what has been found in rosette leaves, where sugar (Glc-6-P and Fru-6-P) levels were partially recovered from 4 h onward in the extended night (Usadel *et al.*, 2008). By contrast, *ANAC092* and *NAP* transcript abundance continued to rise. This raises the possibility that at 18 h the *ANAC092* and *NAP* gene products started to initiate senescence to prevent critically low sugar levels. In the *max1-5*/*dis15* mutant, rac-GR24 treatment transiently repressed *AKINβ1* and *bZIP63* at 12 h, while *ANAC092* and *NAP* were up-regulated. Here, the SL/GR24 treatment may induce senescence – and associated sugar recovery - earlier, alleviating the need for metabolic readjustment. Alternatively, the SL/GR24 may transcriptionally repress key energy-deprivation regulators directly, which then prevents recovery of sugar shortage and as a necessity promotes senescence as another nutrient recovery process. Regardless, these findings are consistent with the idea that SL promotes senescence to restore sugar shortage. SLs may not play a major role in metabolic adjustment until 18 h, when the *MAX3* and *SMXL7* transcripts were up-regulated in the WT. *SMXL7* has been found to exhibit higher transcript abundance than *SMXL6* and *SMXL8* in senescent leaves (Stanga *et al.*, 2013). Thus, the up-regulation of *SMXL7* at 18 h may indicate a senescence regulatory role for this gene. However, I could not ignore the possibility that *SMXL6* is also involved in regulating senescence because of its significantly changed transcript abundance at 12 h and 18 h as well as its important role in regulation of shoot branching (Soundappan *et al.*, 2015; Wang *et al.*, 2015).

Previous studies in our group found during 24-h of dark treatment that soluble sugar and Chl contents reduced substantially in the inflorescence (Trivellini *et al.*, 2012). The dark treatment was accompanied with transcriptome changes

of carbon-deprivation and senescence-related genes including *AKINβ1*, *bZIP63*, *ANAC092* and *NAP* (Trivellini *et al.*, 2012). In my study, expression of senescence-specific marker gene *SAG12* started to increase at 48 h in WT suggesting that senescence was well underway at that time. The transcript abundances of *SAG12*, *ANAC092* and *NAP* (Figure 5.21) increased more strikingly at 72 h and similar increases were found for the SL biosynthetic genes *MAX3*, *MAX4* and *MAX1*. In the SL mutants, the senescence process was slowed down and expression of *ANAC092* and *SAG12* lower than in the WT (Figure 5.5). This demonstrates that SLs contribute to the senescence of dark-detached inflorescences and is consistent with what has been observed during leaf senescence (Ueda and Kusaba, 2015). The expression pattern of signalling gene *SMXL7* showed the strongest correlation with that of SL biosynthetic genes and senescence marker genes, which suggests involvement in senescence regulation. However, the decreased transcript abundance of *SMXL6* after 24 h suggests it may play a more important role in early stages of senescence.

Overall, these results suggest an intricate relationship among sugar starvation, senescence and SL biosynthesis and signalling in excised inflorescences. This is supported by a recent study finding that the SL-induced senescence of bamboo leaves was supressed by exogenous sugar treatment (Tian *et al.*, 2018). SLs do not appear to have a major role in the inflorescences during the normal night but are synthesised during the extended night, perhaps in response to sustained low sugar content and consequent senescence initiation. It seems thus that SLs play an important role in the regulation of nutrient redistribution from leaves and leaf-like organs to other organs of the plant by promoting senescence progression.

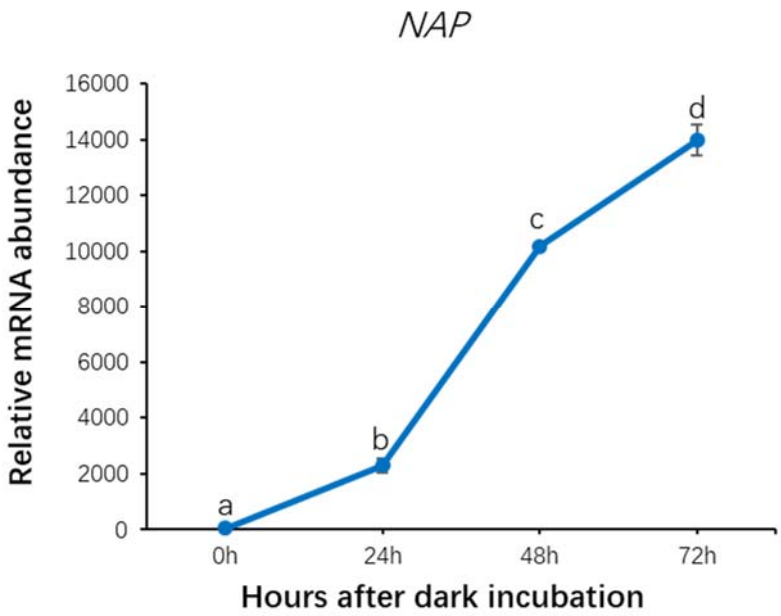

Figure 5.21 Transcriptional change of *NAP* gene during a period of 72 h of dark treatment

Transcript abundance was quantified using nCounter technology on RNA isolated from detached WT inflorescences (n = 3 samples, > 4 inflorescences from independent plants per sample) that were incubated in the dark for 0 h, 24 h, 48 h and 72 h. Transcript abundance was normalised to geometric mean of *PP2AA3, ACT2 and MON1.* Data are mean ± standard error. Letters represent significant differences among four time points in one-way ANOVA (Fisher's protected LSD test $P<0.05$).

6. Conclusion and potential future work

6.1. Summary and conclusion

This project aimed to better understand the regulation of dark-induced senescence of harvested plant tissue or organs via a forward genetic approach. The research was performed on detached dark-incubated immature inflorescences of Arabidopsis, and the overall findings from this work reflect a highly regulated network during energy (light and carbon)-deprivation-induced inflorescence senescence in the model plant Arabidopsis. Here, I summarise the findings of this project and propose a model for part of the regulatory network of dark-induced inflorescence senescence based on these findings (Figure 6.1).

The harvested dark-stored plant tissues or organs experience various stresses, including energy-deprivation resulting from prolonged darkness. Such detachment and dark incubation lead to precocious senescence of immature floral organs (Eason *et al.*, 2005; Gapper *et al.*, 2005; Trivellini *et al.*, 2012). In this project, sugar starvation resulting from prolonged darkness is considered a key stimulus to promote senescence of the detached dark-held inflorescence of Arabidopsis. This hypothesis is supported by two main lines of evidence: first, in Arabidopsis, substantially reduced sugar contents were reported in both leaves and detached inflorescences in response to extended dark treatment (Usadel *et al.*, 2008; Trivellini *et al.*, 2012); second, Trivellini *et al*. (2012) found that glucose treatment delays senescence of detached inflorescence during dark incubation. Consistent with this, the nCounter results (chapter 5) showed that during the extended night SnRK1-related genes *AKINβ1* and *bZIP63* further increased their transcript abundance compared to their diurnal-dependent transcriptional increase during early regular night (3 h of dark treatment), perhaps in response to sugar shortage in WT inflorescences. Since ET and SL are stress-related hormones and are known to regulate dark-induced senescence (Ha *et al.*, 2014; Ueda and Kusaba, 2015; Verma *et al.*, 2016), the starvation stress is likely the cause for the biosynthesis of ET and SL, thereby mediating senescence initiation and progression of the inflorescence. This is supported by my findings that the transcript abundance

of ET and SL biosynthetic genes (*ACS2* and *MAX3*; see Appendix 14 for *ACS2* expression data) gradually increased during the extended night; whereas such increase was not observed during the regular night when starvation did not occur in the tissue. These results are consistent with findings using detached dark-incubated WT leaves of Arabidopsis, where ET was produced and SL biosynthetic genes (*MAX3* and *MAX4*) were upregulated (Ueda and Kusaba, 2015). ET is known to regulate leaf senescence via an EIN2-EIN3-dependent regulatory network which involves key senescence regulators (ANAC092 and NAP) and Chl catabolic enzyme (NYC1) (Li *et al.*, 2013; Kim *et al.*, 2014; Yang *et al.*, 2014; Qiu *et al.*, 2015). This regulatory network is likely also involved in ET-mediated inflorescence senescence. In agreement with this, the *dis* phenotype was observed in *dis51* (*ein2,* chapter 4) and *dis2* (*nyc1*, chapter 3) mutants in this study and in *anac092* and *nap* mutants in Trivellini *et al.* (2012), confirming their involvement in regulation of dark-induced inflorescence senescence. The mechanism behind SL-mediated dark-induced senescence is still not clear. However, the differential expression of SL signalling suppressor genes (*SMXL6, SMXL7* and *SMXL8*) suggested their senescence-related roles, although the role of *SMXL8* remains to be discovered, for example by mutant analysis. The strong association between shoot branching and senescence phenotypes also supported roles of these three *SMXLs* in controlling inflorescence senescence. SMXL6/7/8 (and rice ortholog D53) have been suggested to regulate shoot branching via transcriptional repression of downstream TFs in the absence of SL (Wang *et al.*, 2015; Song *et al.*, 2017). The TF gene *NAP* was found to be SL-inducible gene in this study and in Mashiguchi *et al.* (2009) for *ANAC092*. This makes these two TFs strong candidates that are suppressed by SMXL6/7/8 when SL is absent or SL signalling is blocked during inflorescence senescence in SL defective mutants. If so, these two genes are involved in the overlapping regulatory network between SL- and ET-mediated inflorescence senescence. This agrees with the observation that SL interacts with ET to accelerate leaf senescence (Ueda and Kusaba, 2015). However, the *max1-1*/*ein2-5* double mutants showed an enhanced delay in leaf senescence in the dark, compared with their single mutants (Ueda and Kusaba, 2015), suggesting ET and SL may regulate senescence via ANA092/NAP-independent pathways as well.

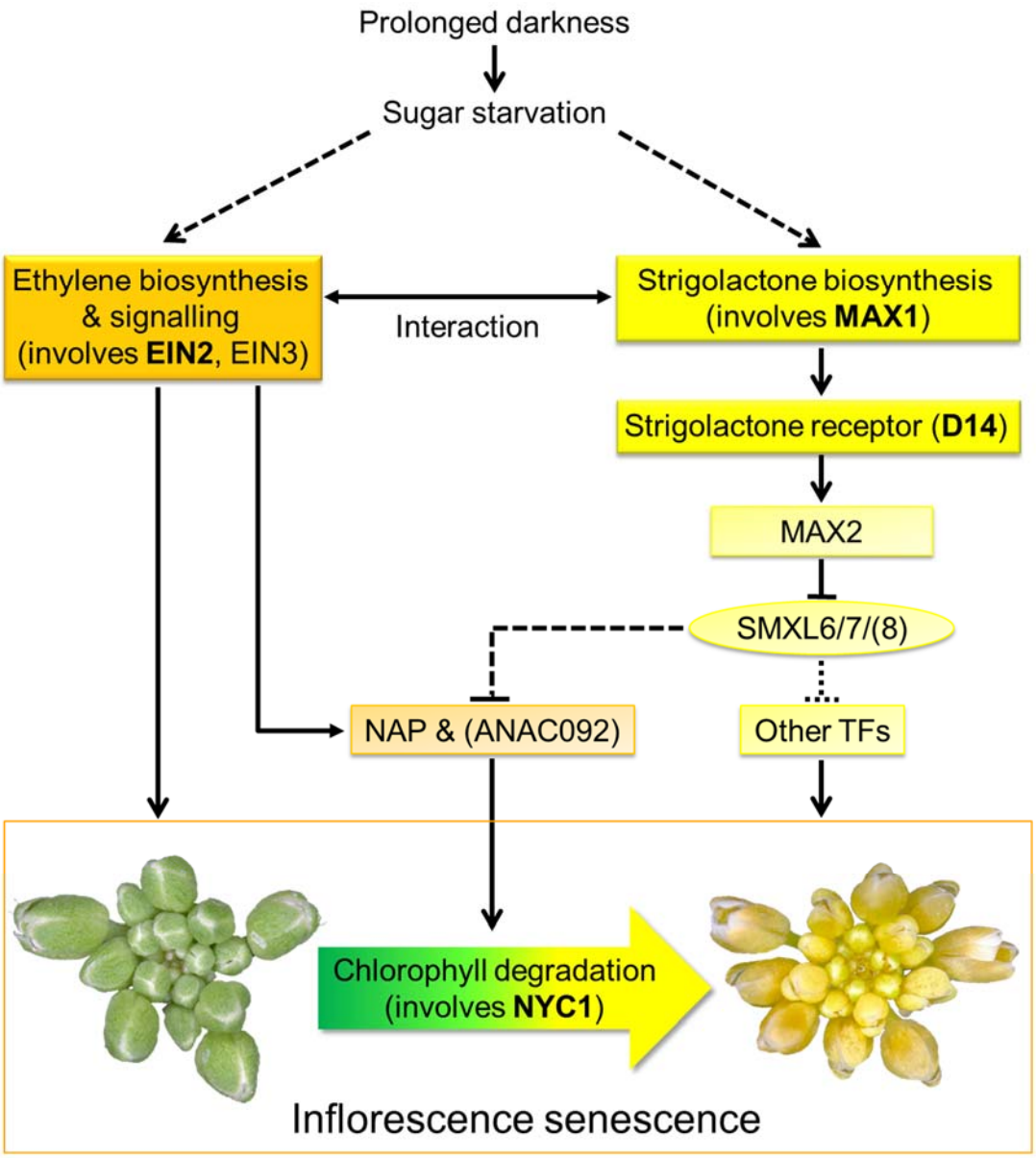

Figure 6.1 A model for dark and starvation-induced, ethylene and strigolactone mediated inflorescence senescence including NYC1-regulated chlorophyll degradation

Solid and dashed arrows/lines indicate the characterised and speculated regulatory pathways, respectively. Proteins in bold (NYC1, chapter 3; EIN2, chapter 4; MAX1 and D14, chapter 5) were studied in this thesis.

In conclusion, this study highlights that sugar-starvation occurs in detached Arabidopsis inflorescences during the extended night, which triggers biosynthesis of stress-related hormones ET and SL. These two hormones then work in concert with each other to accelerate inflorescence senescence including NYC1-mediated Chl degradation. The findings from this work provide a genetic and molecular framework for continued study of postharvest stress-

induced senescence. Moreover, this study will be useful for improving postharvest characteristics of crops that contain floral parts such as broccoli.

6.2. Potential future work

Based on the findings in this thesis, the following future work could either support or reject the model proposed above. First, sugar measurement in the excised inflorescences that were harvested at selected time points (e.g. 0 h, 8 h, 12 h, 18 h and 24 h) during dark treatment. This provides direct evidence for the carbon/sugar status in the tissue throughout the dark treatment and supports the transcriptional analysis for the sugar-responsive genes. Second, investigation of the senescence regulatory roles of SMXL6, SMXL7 and SMXL8 by phenotypic analysis of plants with mutations in their encoding genes. For this, single, double and triple mutants and the *max2*/*smxl6*/*7*/*8* quadruple mutant and gain-of-function mutant of SMXL7 (due to its expression pattern showing the best correlation with the senescence marker genes during dark incubation) should be used. Thirdly, if SMXL6/7/8 were confirmed to regulate senescence, then it should be tested if ANAC092 and NAP were repressed by these three SMXLs in SL signalling. This can be tested by using three different assays: a) transcriptional analysis of ANAC092 and NAP expression in single, double, triple and quadruple mutants of MAX2 and SMXL6/7/8 upon dark treatment; b) *in vitro* assay: yeast two-hybrid assay or bimolecular fluorescence complementation to test physical interaction between these two genes and SMXL6/7/8; c) *in vivo* Chromatin Immunoprecipitation (ChIP) assay and NAP/ANAC092 ChIP-seq analysis of floral tissue in response to dark- and detachment-induced starvation to find out the targets of these TFs. Fourthly, test if these two genes were involved in overlapping or distinct pathways between ET and SL during dark-induced senescence by examination of the *ANAC092* and *NAP* expression in the *dis15* (*max1-5*), *dis51* (*ein2*), and *max1-5*/*ein2* double mutants or by phenotypic analysis of the *dis15*, *dis51*, *anac092* and *nap* single, double, triple and quadruple mutants.

Besides the senescence related work, the fragrance phenotype of the *dis51* mutant is also worth investigating further. To confirm which compounds from identified four ones (PHA, PE, benzaldehyde and benzyl alcohol) are the actual

candidates that contribute to the aroma phenotype of the *dis51* mutant, targeted GC-MS analysis could be carried out on the flower samples that are harvested at different time points during a 24 h day/night cycle. Then genetic analysis, HRM-based mapping and WGS analysis could use to identify the causal mutation(s). Alternatively, the causal mutation(s) could possibly be identified by PCR-based sequencing of the genes involved in the putative biosynthetic pathway(s) of confirmed compounds. Finally, it is also important to investigate if the mutation(s) leading to the aroma phenotype also contribute to senescence phenotype in the *dis51* mutant.

References

Abe S, Sado A, Tanaka K, Kisugi T, Asami K, Ota S, Il Kim H, Yoneyama K, Xie X, Ohnishi T, Seto Y, Yamaguchi S, Akiyama K, Yoneyama K, Nomura T. 2014. Carlactone is converted to carlactonoic acid by MAX1 in Arabidopsis and its methyl ester can directly interact with AtD14 in vitro. Proceedings of the National Academy of Sciences of the United States of America **111**, 18084-18089.

Abeles FB, Dunn LJ, Morgens P, Callahan A, Dinterman RE, Schmidt J. 1988. Induction of 33-kD and 60-kD peroxidases during ethylene-induced senescence of cucumber cotyledons. Plant Physiology **87**, 609-615.

Adamczyk BJ, Lehti-Shiu MD, Fernandez DE. 2007. The MADS domain factors AGL15 and AGL18 act redundantly as repressors of the floral transition in Arabidopsis. Plant Journal **50**, 1007-1019.

Agrawal N, Dasaradhi PVN, Mohmmed A, Malhotra P, Bhatnagar RK, Mukherjee SK. 2003. RNA interference: Biology, mechanism, and applications. Microbiology and Molecular Biology Reviews **67**, 657-685.

Ahmad SS, Tahir I. 2016. How and why of flower senescence: understanding from models to ornamentals. Indian Journal of Plant Physiology **21**, 446-456.

Akhtar S, Ahmad A, Jha SR, Ahmad J. 2019. Chapter 5 - Regulation of Leaf Senescence by Macromolecule Degradation and Hormones. In: Sarwat M, Tuteja N, eds. *Senescence Signalling and Control in Plants*: Academic Press, 61-97.

Al-Babili S, Bouwmeester HJ. 2015. Strigolactones, a novel carotenoid-derived plant hormone. Annual Review of Plant Biology **66**, 161-186.

Alder A, Jamil M, Marzorati M, Bruno M, Vermathen M, Bigler P, Ghisla S, Bouwmeester H, Beyer P, Al-Babili S. 2012. The Path from beta-Carotene to Carlactone, a Strigolactone-Like Plant Hormone. Science **335**, 1348-1351.

Alonso JM, Ecker JR. 2006. Moving forward in reverse: genetic technologies to enable genome-wide phenomic screens in Arabidopsis. Nature Reviews Genetics **7**, 524–536.

Alonso JM, Hirayama T, Roman G, Nourizadeh S, Ecker JR. 1999. EIN2, a bifunctional transducer of ethylene and stress responses in Arabidopsis. Science **284**, 2148-2152.

Alonso JM, Stepanova AN. 2003. T-DNA mutagenesis in Arabidopsis. Plant Functional Genomics **236**, 177-187.

An FY, Zhao QO, Ji YS, Li WY, Jiang ZQ, Yu XC, Zhang C, Han Y, He WR, Liu YD, Zhang SQ, Ecker JR, Guo HW. 2010. Ethylene-Induced Stabilization of ETHYLENE INSENSITIVE3 and EIN3-LIKE1 Is Mediated by Proteasomal Degradation of EIN3 Binding F-Box 1 and 2 That Requires EIN2 in Arabidopsis. Plant Cell **22**, 2384-2401.

Arite T, Umehara M, Ishikawa S, Hanada A, Maekawa M, Yamaguchi S, Kyozuka J. 2009. d14, a strigolactone-insensitive mutant of rice, shows an accelerated outgrowth of tillers. Plant and Cell Physiology **50**, 1416-1424.

Arvidsson S, Kwasniewski M, Riano-Pachon DM, Mueller-Roeber B. 2008. QuantPrime - a flexible tool for reliable high-throughput primer design for quantitative PCR. Bmc Bioinformatics **9**, 465.

Ashman TL, Schoen DJ. 1994. How long should flowers live. Nature **371**, 788-791.

Aubert C, Baumann S, Arguel H. 2005. Optimization of the analysis of flavor volatile compounds by liquid-liquid microextraction (LLME). Application to the aroma analysis of melons, peaches, grapes, strawberries, and tomatoes. Journal of Agricultural and Food Chemistry **53**, 8881-8895.

Baena-Gonzalez E, Rolland F, Thevelein JM, Sheen J. 2007. A central integrator of transcription networks in plant stress and energy signalling. Nature **448**, 938-942.

Bak S, Tax FE, Feldmann KA, Galbraith DW, Feyereisen R. 2001. CYP83B1, a cytochrome P450 at the metabolic branch paint in auxin and indole glucosinolate biosynthesis in Arabidopsis. Plant Cell **13**, 101-111.

Balazadeh S, Kwasniewski M, Caldana C, Mehrnia M, Zanor MI, Xue GP, Mueller-Roeber B. 2011. ORS1, an H2O2-Responsive NAC Transcription Factor, Controls Senescence in Arabidopsis thaliana. Molecular Plant **4**, 346-360.

Balazadeh S, Riano-Pachon DM, Mueller-Roeber B. 2008. Transcription factors regulating leaf senescence in Arabidopsis thaliana. Plant Biol (Stuttg) **10 Suppl 1**, 63-75.

Balazadeh S, Siddiqui H, Allu AD, Matallana-Ramirez LP, Caldana C, Mehrnia M, Zanor MI, Kohler B, Mueller-Roeber B. 2010. A gene regulatory network controlled by the NAC transcription factor ANAC092/AtNAC2/ORE1 during salt-promoted senescence. Plant Journal **62**, 250-264.

Baldwin EA, Scott JW, Shewmaker CK, Schuch W. 2000. Flavor trivia and tomato aroma: Biochemistry and possible mechanisms for control of important aroma components. Hortscience **35**, 1013-1022.

Barlier I, Kowalczyk M, Marchant A, Ljung K, Bhalerao R, Bennett M, Sandberg G, Bellini C. 2000. The SUR2 gene of Arabidopsis thaliana encodes the cytochrome P450 CYP83B1, a modulator of auxin homeostasis. Proceedings of the National Academy of Sciences of the United States of America **97**, 14819-14824.

Bate NJ, Rothstein SJ, Thompson JE. 1991. Expression of Nuclear and Chloroplast Photosynthesis-Specific Genes during Leaf Senescence. Journal of Experimental Botany **42**, 801-811.

Becker W, Apel K. 1993. Differences in gene-expression between natural and artificially induced leaf senescence. Planta **189**, 74-79.

Bennett EJ, Roberts JA, Wagstaff C. 2014. Use of Mutants to Dissect the Role of Ethylene Signalling in Organ Senescence and the Regulation of Yield in Arabidopsis thaliana. Journal of Plant Growth Regulation **33**, 56-65.

Bernard P, Couturier M. 1992. Cell killing by the F-plasmid CCDB protein involves poisoning of DNA-topoisomerase-II complexes. Journal of Molecular Biology **226**, 735-745.

Berrah G, Konetzka WA. 1962. Selective and reversible inhibition of synthesis of bacterial deoxyribonucleic acid by phenethyl alcohol. Journal of Bacteriology **83**, 738-744.

Besseau S, Li J, Palva ET. 2012. WRKY54 and WRKY70 co-operate as negative regulators of leaf senescence in Arabidopsis thaliana. Journal of Experimental Botany **63**, 2667-2679.

Bisson MMA, Bleckmann A, Allekotte S, Groth G. 2009. EIN2, the central regulator of ethylene signalling, is localized at the ER membrane where it interacts with the ethylene receptor ETR1. Biochemical Journal **424**, 1-6.

Bisson MMA, Groth G. 2011. New paradigm in ethylene signaling: EIN2, the central regulator of the signaling pathway, interacts directly with the upstream receptors. Plant signaling & behavior **6**, 164-166.

Bisson MMA, Groth G. 2015. Targeting Plant Ethylene Responses by Controlling Essential Protein-Protein Interactions in the Ethylene Pathway. Molecular Plant **8**, 1165-1174.

Blasing OE, Gibon Y, Gunther M, Hohne M, Morcuende R, Osuna D, Thimm O, Usadel B, Scheible WR, Stitt M. 2005. Sugars and circadian regulation make major contributions to the global regulation of diurnal gene expression in Arabidopsis. Plant Cell **17**, 3257-3281.

Bleecker AB, Estelle MA, Somerville C, Kende H. 1988. Insensitivity to ethylene conferred by a dominant mutation in Arabidopsis-thaliana. Science **241**, 1086-1089.

Bleecker AB, Patterson SE. 1997. Last exit: Senescence, abscission, and meristem arrest in Arabidopsis. Plant Cell **9**, 1169-1179.

Boatright J, Negre F, Chen XL, Kish CM, Wood B, Peel G, Orlova I, Gang D, Rhodes D, Dudareva N. 2004. Understanding in vivo benzenoid metabolism in petunia petal tissue. Plant Physiology **135**, 1993-2011.

Booker J, Sieberer T, Wright W, Williamson L, Willett B, Stirnberg P, Turnbull C, Srinivasan M, Goddard P, Leyser O. 2005. MAX1 encodes a cytochrome P450 family member that acts downstream of MAX3/4 to produce a carotenoid-derived branch-inhibiting hormone. Developmental Cell **8**, 443-449.

Borda AM, Clark DG, Huber DJ, Welt BA, Nell TA. 2011. Effects of ethylene on volatile emission and fragrance in cut roses: The relationship between fragrance and vase life. Postharvest Biology and Technology **59**, 245-252.

Borochov A, Woodson WR. 1989. Physiology and biochemistry of flower petal senescence. Horticultural Reviews **11**, 15-43.

Botticella E, Sestili F, Hernandez-Lopez A, Phillips A, Lafiandra D. 2011. High resolution melting analysis for the detection of EMS induced mutations in wheat SbeIIa genes. Bmc Plant Biology **11**, 156.

Bovy AG, Angenent GC, Dons HJM, van Altvorst AC. 1999. Heterologous expression of the Arabidopsis etr1-1 allele inhibits the senescence of carnation flowers. Molecular Breeding **5**, 301-308.

Bowman JL, Smyth DR, Meyerowitz EM. 1991. Genetic interactions among floral homeotic genes of Arabidopsis. Development **112**, 1-20.

Boyes DC, Zayed AM, Ascenzi R, McCaskill AJ, Hoffman NE, Davis KR, Gorlach J. 2001. Growth stage-based phenotypic analysis of arabidopsis: A model for high throughput functional genomics in plants. Plant Cell **13**, 1499-1510.

Breeze E, Harrison E, McHattie S, Hughes L, Hickman R, Hill C, Kiddle S, Kim YS, Penfold CA, Jenkins D, Zhang C, Morris K, Jenner C, Jackson S, Thomas B, Tabrett A, Legaie R, Moore JD, Wild DL, Ott S, Rand D, Beynon J, Denby K, Mead A, Buchanan-Wollaston V. 2011. High-Resolution Temporal Profiling of Transcripts during Arabidopsis Leaf Senescence supp table. Plant Cell **23**, 873-894.

Brewer PB, Koltai H, Beveridge CA. 2013. Diverse roles of strigolactones in plant development. Molecular Plant **6**, 18-28.

Brewer PB, Yoneyama K, Filardo F, Meyers E, Scaffidi A, Frickey T, Akiyama K, Seto Y, Dun EA, Cremer JE, Kerr SC, Waters MT, Flematti GR, Mason MG, Weiller G, Yamaguchi S, Nomura T, Smith SM, Yoneyama K, Beveridge CA. 2016. LATERAL BRANCHING OXIDOREDUCTASE acts in the final stages of strigolactone biosynthesis in Arabidopsis. Proceedings of the National Academy of Sciences of the United States of America **113**, 6301-6306.

Broderick SR, Wijeratne S, Wijeratn AJ, Chapin LJ, Meulia T, Jones ML. 2014. RNA-sequencing reveals early, dynamic transcriptome changes in the corollas of pollinated petunias. Bmc Plant Biology **14**, 307.

Bu Q, Lv T, Shen H, Luong P, Wang J, Wang Z, Huang Z, Xiao L, Engineer C, Kim TH, Schroeder JI, Huq E. 2014. Regulation of drought tolerance by the F-box protein MAX2 in Arabidopsis. Plant Physiology **164**, 424-439.

Buchanan-Wollaston V, Page T, Harrison E, Breeze E, Lim PO, Nam HG, Lin JF, Wu SH, Swidzinski J, Ishizaki K, Leaver CJ. 2005. Comparative transcriptome analysis reveals significant differences in gene expression and signalling pathways between developmental and dark/starvation-induced senescence in Arabidopsis. Plant Journal **42**, 567-585.

Cao J, Schneeberger K, Ossowski S, Gunther T, Bender S, Fitz J, Koenig D, Lanz C, Stegle O, Lippert C, Wang X, Ott F, Muller J, Alonso-Blanco C, Borgwardt K, Schmid KJ, Weigel D. 2011. Whole-genome sequencing of multiple Arabidopsis thaliana populations. Nature Genetics **43**, 956-U960.

Carrión CA, Costa ML, Martinez DE, Mohr C, Humbeck K, Guiamet JJ. 2013. In vivo inhibition of cysteine proteases provides evidence for the involvement of 'senescence-associated vacuoles' in chloroplast protein degradation during dark-induced senescence of tobacco leaves. Journal of Experimental Botany **64**, 4967-4980.

Carrion CA, Martinez DE, Costa ML, Guiamet JJ. 2014. Senescence-associated vacuoles, a specific lytic compartment for degradation of chloroplast proteins? Plants **3**, 498-512.

Chagné D. 2015. Application of the High-Resolution Melting Technique for Gene Mapping and SNP Detection in Plants. In: Batley J, ed. *Plant Genotyping: Methods and Protocols*. New York, NY: Springer New York, 151-159.

Challis RJ, Hepworth J, Mouchel C, Waites R, Leyser O. 2013. A role for more axillary growth1 (MAX1) in evolutionary diversity in strigolactone signaling upstream of MAX2. Plant Physiology **161**, 1885-1902.

Chang C, Kwok SF, Bleecker AB, Meyerowitz EM. 1993. Arabidopsis ethylene-response gene ETR1 - similarity of product to 2-component regulators. Science **262**, 539-544.

Chang H, Jones ML, Banowetz GM, Clark DG. 2003. Overproduction of Cytokinins in Petunia Flowers Transformed with PSAG12-IPT Delays Corolla Senescence and Decreases Sensitivity to Ethylene. Plant Physiology **132**, 2174-2183.

Chang KN, Zhong S, Weirauch MT, Hon G, Pelizzola M, Li H, Huang S-sC, Schmitz RJ, Urich MA, Kuo D, Nery JR, Qiao H, Yang A, Jamali A, Chen H, Ideker T, Ren B, Bar-Joseph Z, Hughes TR, Ecker JR. 2013. Temporal transcriptional response to ethylene gas drives growth hormone cross-regulation in Arabidopsis. Elife **2**, e00675.

Chao QM, Rothenberg M, Solano R, Roman G, Terzaghi W, Ecker JR. 1997. Activation of the ethylene gas response pathway in Arabidopsis by the nuclear protein ETHYLENE-INSENSITIVE3 and related proteins. Cell **89**, 1133-1144.

Chen JG, Ullah H, Young JC, Sussman MR, Jones AM. 2001a. ABP1 is required for organized cell elongation and division in Arabidopsis embryogenesis. Genes & Development **15**, 902-911.

Chen L, Song Y, Li S, Zhang L, Zou C, Yu D. 2012. The role of WRKY transcription factors in plant abiotic stresses. Biochimica Et Biophysica Acta-Gene Regulatory Mechanisms **1819**, 120-128.

Chen LFO, Hwang JY, Charng YY, Sun CW, Yang SF. 2001b. Transformation of broccoli (Brassica oleracea var. italica) with isopentenyltransferase gene via Agrobacterium tumefaciens for post-harvest yellowing retardation. Molecular Breeding **7**, 243-257.

Chen MK, Hsu WH, Lee PF, Thiruvengadam M, Chen HI, Yang CH. 2011a. The MADS box gene, FOREVER YOUNG FLOWER, acts as a repressor controlling floral organ senescence and abscission in Arabidopsis. Plant Journal **68**, 168-185.

Chen WH, Li PF, Chen MK, Lee YI, Yang CH. 2015. FOREVER YOUNG FLOWER Negatively Regulates Ethylene Response DNA-Binding Factors by Activating an Ethylene-Responsive Factor to Control Arabidopsis Floral Organ Senescence and Abscission. Plant Physiology **168**, 1666-U1974.

Chen WQ, Provart NJ, Glazebrook J, Katagiri F, Chang HS, Eulgem T, Mauch F, Luan S, Zou GZ, Whitham SA, Budworth PR, Tao Y, Xie ZY, Chen X, Lam S, Kreps JA, Harper JF, Si-Ammour A, Mauch-Mani B, Heinlein M, Kobayashi K, Hohn T, Dangl JL, Wang X, Zhu T. 2002. Expression profile matrix of Arabidopsis transcription factor genes suggests their putative functions in response to environmental stresses. Plant Cell **14**, 559-574.

Chen X-M, Kobayashi H, Sakai M, Hirata H, Asai T, Ohnishi T, Baldermann S, Watanabe N. 2011b. Functional characterization of rose phenylacetaldehyde reductase (PAR), an enzyme involved in the biosynthesis of the scent compound 2-phenylethanol. Journal of Plant Physiology **168**, 88-95.

Chen YT, Chen LFO, Shaw JF. 2008. Senescence-associated genes in harvested broccoli florets. Plant Science **175**, 137-144.

Chevalier F, Nieminen K, Sanchez-Ferrero JC, Rodriguez ML, Chagoyen M, Hardtke CS, Cubas P. 2014. Strigolactone promotes degradation of DWARF14, an alpha/beta hydrolase essential for strigolactone signaling in Arabidopsis. Plant Cell **26**, 1134-1150.

Christ B, Hörtensteiner S. 2013. Mechanism and Significance of Chlorophyll Breakdown. Journal of Plant Growth Regulation, 1-17.

Clarke SF, Jameson PE, Downs C. 1994. The Influence of 6-Benzylaminopurine on Postharvest Senescence of Floral Tissues of Broccoli (Brassica-Oleracea Var Italica). Plant Growth Regulation **14**, 21-27.

Colquhoun TA, Verdonk JC, Schimmel BCJ, Tieman DM, Underwood BA, Clark DG. 2010. Petunia floral volatile benzenoid/phenylpropanoid genes are regulated in a similar manner. Phytochemistry **71**, 158-167.

Contento AL, Kim SJ, Bassham DC. 2004. Transcriptome profiling of the response of Arabidopsis suspension culture cells to Suc starvation. Plant Physiology **135**, 2330-2347.

Crooks GE, Hon G, Chandonia JM, Brenner SE. 2004. WebLogo: a sequence logo generator. Genome Research **14**, 1188-1190.

Czechowski T, Stitt M, Altmann T, Udvardi MK, Scheible WR. 2005. Genome-wide identification and testing of superior reference genes for transcript normalization in Arabidopsis. Plant Physiology **139**, 5-17.

de Saint Germain A, Clave G, Badet-Denisot MA, Pillot JP, Cornu D, Le Caer JP, Burger M, Pelissier F, Retailleau P, Turnbull C, Bonhomme S, Chory J, Rameau C, Boyer FD. 2016. An histidine covalent receptor and butenolide complex mediates strigolactone perception. Nature Chemical Biology **12**, 787-794.

Dellaporta SL, Wood J, Hicks JB. 1983. A plant DNA minipreparation: Version II. Plant Molecular Biology Reporter **1**, 19-21.

Dinh TT, Luscher E, Li S, Liu X, Won SY, Chen X. 2014. Genetic screens for floral mutants in Arabidopsis thaliana: enhancers and suppressors. Methods in molecular biology (Clifton, N.J.) **1110**, 127-156.

Downs CG, Somerfield SD, Davey MC. 1997. Cytokinin treatment delays senescence but not sucrose loss in harvested broccoli. Postharvest Biology and Technology **11**, 93-100.

Dubois M, Van den Broeck L, Inze D. 2018. The Pivotal Role of Ethylene in Plant Growth. Trends in Plant Science **23**, 311-323.

Dudareva N, Klempien A, Muhlemann JK, Kaplan I. 2013. Biosynthesis, function and metabolic engineering of plant volatile organic compounds. New Phytologist **198**, 16-32.

Dvinge H, Bertone P. 2009. HTqPCR: high-throughput analysis and visualization of quantitative real-time PCR data in R. Bioinformatics **25**, 3325–3326.

Eason JR, Ryan DJ, Watson LM, Hedderley D, Christey MC, Braun RH, Coupe SA. 2005. Suppression of the cysteine protease, aleurain, delays floret senescence in Brassica oleracea. Plant Molecular Biology **57**, 645-657.

Eastmond PJ, Li Y, Graham IA. 2003. Is trehalose-6-phosphate a regulator of sugar metabolism in plants? Journal of Experimental Botany **54**, 533-537.

Effendi Y, Ferro N, Labusch C, Geisler M, Scherer GFE. 2015. Complementation of the embryo-lethal T-DNA insertion mutant of AUXIN-BINDING-PROTEIN 1 (ABP1) with abp1 point mutated versions reveals crosstalk of ABP1 and phytochromes. Journal of Experimental Botany **66**, 403-418.

Eshed Y, Baum SF, Perea JV, Bowman JL. 2001. Establishment of polarity in lateral organs of plants. Current Biology **11**, 1251-1260.

Eugenia Gómez-Lobato M, Hector Hasperue J, Marcos Civello P, Raquel Chaves A, Adolfo Martinez G. 2012. Effect of 1-MCP on the expression of chlorophyll degrading genes during senescence of broccoli (Brassica oleracea L.). Scientia Horticulturae **144**, 208-211.

Eulgem T, Rushton PJ, Robatzek S, Somssich IE. 2000. The WRKY superfamily of plant transcription factors. Trends in Plant Science **5**, 199-206.

Fang SC, Fernandez DE. 2002. Effect of regulated overexpression of the MADS domain factor AGL15 on flower senescence and fruit maturation. Plant Physiology **130**, 78-89.

Farhi M, Lavie O, Masci T, Hendel-Rahmanim K, Weiss D, Abeliovich H, Vainstein A. 2010. Identification of rose phenylacetaldehyde synthase by functional complementation in yeast. Plant Molecular Biology **72**, 235-245.

Feng G, Liu G, Xiao J. 2015. The Arabidopsis EIN2 restricts organ growth by retarding cell expansion. Plant signaling & behavior **10**, e1017169.

Fernandez DE, Heck GR, Perry SE, Patterson SE, Bleecker AB, Fang SC. 2000. The embryo MADS domain factor AGL15 acts postembryonically: Inhibition of perianth senescence and abscission via constitutive expression. Plant Cell **12**, 183-197.

Fracheboud Y, Luquez V, Bjorken L, Sjodin A, Tuominen H, Jansson S. 2009. The Control of Autumn Senescence in European Aspen. Plant Physiology **149**, 1982-1991.

Friedman WE, Moore RC, Purugganan MD. 2004. The evolution of plant development. American Journal of Botany **91**, 1726-1741.

Fujiki Y, Ito M, Nishida I, Watanabe A. 2000. Multiple signaling pathways in gene expression during sugar starvation. Pharmacological analysis of din gene expression in suspension-cultured cells of Arabidopsis. Plant Physiology **124**, 1139-1147.

Gady AL, Hermans FW, Van de Wal MH, van Loo EN, Visser RG, Bachem CW. 2009. Implementation of two high through-put techniques in a novel application: detecting point mutations in large EMS mutated plant populations. Plant Methods **5**, 13.

Gan SS, Amasino RM. 1995. INHIBITION OF LEAF SENESCENCE BY AUTOREGULATED PRODUCTION OF CYTOKININ. Science **270**, 1986-1988.

Gan SS, Amasino RM. 1997. Making sense of senescence - Molecular genetic regulation and manipulation of leaf senescence. Plant Physiology **113**, 313-319.

Gao ZY, Qian Q, Liu XH, Yan MX, Feng Q, Dong GJ, Liu J, Han B. 2009. Dwarf 88, a novel putative esterase gene affecting architecture of rice plant. Plant Molecular Biology **71**, 265-276.

Gapper NE, Coupe SA, McKenzie MJ, Scott RW, Christey MC, Lill RE, McManus MT, Jameson PE. 2005. Senescence-associated down-regulation of 1-aminocyclopropane-1-carboxylate (ACC) oxidase delays harvest-induced senescence in broccoli. Functional Plant Biology **32**, 891-901.

Geiss GK, Bumgarner RE, Birditt B, Dahl T, Dowidar N, Dunaway DL, Fell HP, Ferree S, George RD, Grogan T, James JJ, Maysuria M, Mitton JD, Oliveri P, Osborn JL, Peng T, Ratcliffe AL, Webster PJ, Davidson EH, Hood L. 2008. Direct multiplexed measurement of gene expression with color-coded probe pairs. Nature Biotechnology **26**, 317-325.

Glover BJ, Martin C. 1998. The role of petal cell shape and pigmentation in pollination success in Antirrhinum majus. Heredity **80**, 778-784.

Goeschl JD, Rappaport L, Pratt HK. 1966. Ethylene as a Factor Regulating the Growth of Pea Epicotyls Subjected to Physical Stress. Plant Physiology **41**, 877-884.

Gomez-Lobato ME, Mansilla SA, Civello PM, Martinez GA. 2014. Expression of Stay-Green encoding gene (BoSGR) during postharvest senescence of broccoli. Postharvest Biology and Technology **95**, 88-94.

Gomez-Roldan V, Fermas S, Brewer PB, Puech-Pages V, Dun EA, Pillot JP, Letisse F, Matusova R, Danoun S, Portais JC, Bouwmeester H, Becard G, Beveridge CA, Rameau C, Rochange SF. 2008. Strigolactone inhibition of shoot branching. Nature **455**, 189-U122.

Graham IA, Eastmond PJ. 2002. Pathways of straight and branched chain fatty acid catabolism in higher plants. Progress in Lipid Research **41**, 156-181.

Graham LE, Schippers JHM, Dijkwel PP, Wagstaff C. 2012. Ethylene and Senescence Processes. *Annual Plant Reviews Volume 44*, Vol. 44: Wiley, Oxford, 305-341.

Gray WM. 2004. Hormonal regulation of plant growth and development. Plos Biology **2**, 1270-1273.

Grbic V. 2003. SAG2 and SAG12 protein expression in senescing Arabidopsis plants. Physiologia Plantarum **119**, 263-269.

Grbić V, Bleecker AB. 1995. Ethylene regulates the timing of leaf senescence in Arabidopsis. Plant Journal **8**, 595-602.

Greene EA, Codomo CA, Taylor NE, Henikoff JG, Till BJ, Reynolds SH, Enns LC, Burtner C, Johnson JE, Odden AR, Comai L, Henikoff S. 2003. Spectrum of chemically induced mutations from a large-scale reverse-genetic screen in arabidopsis. Genetics **164**, 731-740.

Grievink H, Stowell KM. 2008. Identification of ryanodine receptor 1 single-nucleotide polymorphisms by high-resolution melting using the LightCycler 480 System. Analytical Biochemistry **374**, 396-404.

Gundry CN, Vandersteen JG, Reed GH, Pryor RJ, Chen J, Wittwer CT. 2003. Amplicon melting analysis with labeled primers: A closed-tube method for differentiating homozygotes and heterozygotes. Clinical Chemistry **49**, 396-406.

Guo HW, Ecker JR. 2003. Plant responses to ethylene gas are mediated by SCF (EBF1/EBF2)-dependent proteolysis of EIN3 transcription factor. Cell **115**, 667-677.

Guo HW, Ecker JR. 2004. The ethylene signaling pathway: new insights. Current Opinion in Plant Biology **7**, 40-49.

Guo Y, Cai Z, Gan S. 2004. Transcriptome of Arabidopsis leaf senescence. Plant, Cell & Environment **27**, 521-549.

Guo YF, Gan SS. 2006. AtNAP, a NAC family transcription factor, has an important role in leaf senescence. Plant Journal **46**, 601-612.

Guo YF, Gan SS. 2012. Convergence and divergence in gene expression profiles induced by leaf senescence and 27 senescence-promoting hormonal, pathological and environmental stress treatments. Plant Cell and Environment **35**, 644-655.

Gutensohn M, Klempien A, Kaminaga Y, Nagegowda DA, Negre-Zakharov F, Huh J-H, Luo H, Weizbauer R, Mengiste T, Tholl D, Dudareva N. 2011. Role of aromatic aldehyde synthase in wounding/herbivory response and flower scent production in different Arabidopsis ecotypes. Plant Journal **66**, 591-602.

Guterman I, Shalit M, Menda N, Piestun D, Dafny-Yelin M, Shalev G, Bar E, Davydov O, Ovadis M, Emanuel M, Wang J, Adam Z, Pichersky E, Lewinsohn E, Zamir D, Vainstein A, Weiss D. 2002. Rose scent: Genomics approach to discovering novel floral fragrance-related genes. Plant Cell **14**, 2325-2338.

Guzman P, Ecker JR. 1990. Exploiting the triple response of Arabidopsis to identify ethylene-related mutants. The Plant Cell Online **2**, 513-523.

Ha CV, Leyva-Gonzalez MA, Osakabe Y, Tran UT, Nishiyama R, Watanabe Y, Tanaka M, Seki M, Yamaguchi S, Dong NV, Yamaguchi-Shinozaki K, Shinozaki K, Herrera-Estrella L, Tran LS. 2014. Positive regulatory role of strigolactone in plant responses to drought and salt stress. Proceedings of the National Academy of Sciences of the United States of America **111**, 851-856.

Hahn F, Eisenhut M, Mantegazza O, Weber APM. 2017. Generation of Targeted Knockout Mutants in Arabidopsis thaliana Using CRISPR/Cas9. Bio-Protocol **7**, e2384.

Hamiaux C, Drummond RS, Janssen BJ, Ledger SE, Cooney JM, Newcomb RD, Snowden KC. 2012. DAD2 is an alpha/beta hydrolase likely to be involved in the perception of the plant branching hormone, strigolactone. Current Biology **22**, 2032-2036.

Hao D, Sun X, Ma B, Zhang J-S, Guo H. 2017. 6 - Ethylene A2 - Li, Jiayang. In: Li C, Smith SM, eds. *Hormone Metabolism and Signaling in Plants*: Academic Press, 203-241.

Hasperué JH, Lemoine L, Vicente AR, Chaves AR, Martinez GA. 2015. Postharvest senescence of florets from primary and secondary broccoli inflorescences. Postharvest Biology and Technology **104**, 42-47.

Hellens R, Mullineaux P, Klee H. 2000a. A guide to Agrobacterium binary Ti vectors. Trends in Plant Science **5**, 446-451.

Hellens RP, Edwards EA, Leyland NR, Bean S, Mullineaux PM. 2000b. pGreen: a versatile and flexible binary Ti vector for Agrobacterium-mediated plant transformation. Plant Molecular Biology **42**, 819-832.

Higgins JD, Newbury HJ, Barbara DJ, Muthumeenakshi S, Puddephat IJ. 2006. The production of marker-free genetically engineered broccoli with sense and antisense ACC synthase 1 and ACC oxidases 1 and 2 to extend shelf-life. Molecular Breeding **17**, 7-20.

Hirata H, Ohnishi T, Ishida H, Tomida K, Sakai M, Hara M, Watanabe N. 2012. Functional characterization of aromatic amino acid aminotransferase involved in 2-phenylethanol biosynthesis in isolated rose petal protoplasts. Journal of Plant Physiology **169**, 444-451.

Hirata H, Ohnishi T, Watanabe N. 2016. Biosynthesis of floral scent 2-phenylethanol in rose flowers. Bioscience Biotechnology and Biochemistry **80**, 1865-1873.

Horie Y, Ito H, Kusaba M, Tanaka R, Tanaka A. 2009. Participation of Chlorophyll b Reductase in the Initial Step of the Degradation of Light-harvesting Chlorophyll a/b-Protein Complexes in Arabidopsis. Journal of Biological Chemistry **284**, 17449-17456.

Hörtensteiner S. 2004. The loss of green color during chlorophyll degradation—a prerequisite to prevent cell death? Planta **219**, 191-194.

Hörtensteiner S. 2006. Chlorophyll degradation during senescence. Annual Review of Plant Biology **57**, 55-77.

Hörtensteiner S. 2009. Stay-green regulates chlorophyll and chlorophyll-binding protein degradation during senescence. Trends in Plant Science **14**, 155-162.

Hörtensteiner S. 2013. Update on the biochemistry of chlorophyll breakdown. Plant Molecular Biology **82**, 505-517.

Hörtensteiner S, Feller U. 2002. Nitrogen metabolism and remobilization during senescence. Journal of Experimental Botany **53**, 927-937.

Hörtensteiner S, Kräutler B. 2011. Chlorophyll breakdown in higher plants. Biochimica et Biophysica Acta (BBA)-Bioenergetics **1807**, 977-988.

Hörtensteiner S, Vicentini F, Matile P. 1995. Chlorophyll breakdown in senescent cotyledons of rape, Brassica napus L.: Enzymatic cleavage of phaeophorbide a in vitro. New Phytologist **129**, 237-246.

Hua J, Chang C, Sun Q, Meyerowitz EM. 1995. Ethylene insensitivity conferred by Arabidopsis ERS gene. Science **269**, 1712-1714.

Hua J, Meyerowitz EM. 1998. Ethylene responses are negatively regulated by a receptor gene family in Arabidopsis thaliana. Cell **94**, 261-271.

Huang YF, Li H, Hutchison CE, Laskey J, Kieber JJ. 2003. Biochemical and functional analysis of CTR1, a protein kinase that negatively regulates ethylene signaling in Arabidopsis. Plant Journal **33**, 221-233.

Hunter DA, Ferrante A, Vernieri P, Reid MS. 2004a. Role of abscisic acid in perianth senescence of daffodil (Narcissus pseudonarcissus 'Dutch Master'). Physiologia Plantarum **121**, 313-321.

Hunter DA, Jibran R, Dijkwel P, Chagné D, Sullivan K, Kanojia A, Crowhurst R. 2018. Identification of Postharvest Senescence Regulators Through Map-Based Cloning Using Detached Arabidopsis Inflorescences as a Model Tissue. In: Guo Y, ed. *Plant Senescence: Methods and Protocols*. New York, NY: Springer New York, 195-220.

Hunter DA, Lange NE, Reid MS. 2004b. Physiology of Flower Senescence. In: Noodén LD, ed. *Plant Cell Death Processes*. San Diego: Academic Press, 307-318.

Hunter DA, Pinkney TT, Watson LM, Trivellini A, Janssen BJ, Brummell DA, Heyes JA. 2011. Effect of postharvest water deficit stress on gene expression in heads of broccoli (Brassica oleracea var. italica). Postharvest Biology and Technology **59**, 113-123.

Hwang C-C, Chang Y-H, Lee H-J, Wang T-P, Su Y-M, Chen H-W, Liang P-H. 2013. The Catalytic Roles of P185 and T188 and Substrate-Binding Loop Flexibility in 3 alpha-Hydroxysteroid Dehydrogenase/Carbonyl Reductase from Comamonas testosteroni. PLoS One **8**, e63594.

Inoue H, Nojima H, Okayama H. 1990. High efficiency transformation of Escherichia coli with plasmids. Gene **96**, 23-28.

Iqbal N, Khan NA, Ferrante A, Trivellini A, Francini A, Khan MIR. 2017. Ethylene Role in Plant Growth, Development and Senescence: Interaction with Other Phytohormones. Frontiers in Plant Science **8**, 475.

Irish VF, Sussex IM. 1990. Function of the apetala-1 gene during Arabidopsis floral development. Plant Cell **2**, 741-753.

Ishida H, Nishimori Y, Sugisawa M, Makino A, Mae T. 1997. The large subunit of ribulose-1,5-bisphosphate carboxylase/oxygenase is fragmented into 37-kDa and 16-kDa polypeptides by active oxygen in the lysates of chloroplasts from primary leaves of wheat. Plant Physiology **114**, 1054-1054.

James M, Poret M, Masclaux-Daubresse C, Marmagne A, Coquet L, Jouenne T, Chan P, Trouverie J, Etienne P. 2018. SAG12, a Major Cysteine Protease Involved in Nitrogen Allocation during Senescence for Seed Production in Arabidopsis thaliana. Plant and Cell Physiology **59**, 2052-2063.

Jiang L, Liu X, Xiong G, Liu H, Chen F, Wang L, Meng X, Liu G, Yu H, Yuan Y, Yi W, Zhao L, Ma H, He Y, Wu Z, Melcher K, Qian Q, Xu HE, Wang Y, Li J. 2013. DWARF 53 acts as a repressor of strigolactone signalling in rice. Nature **504**, 401-405.

Jibran R. 2014. Identification of genetic regulators of longevity in dark-held detached Arabidopsis inflorescences : a thesis presented in partial fulfilment of the requirements for the degree of Doctor of Philosophy in Plant Biology, Massey University, Palmerston North, New Zealand. Doctoral, Massey University.

Jibran R, Hunter DA, Dijkwel PP. 2013. Hormonal regulation of leaf senescence through integration of developmental and stress signals. Plant Molecular Biology **82**, 547-561.

Jibran R, Sullivan KL, Crowhurst R, Erridge ZA, Chagne D, McLachlan AR, Brummell DA, Dijkwel PP, Hunter DA. 2015. Staying green postharvest: how three mutations in the Arabidopsis chlorophyll b reductase gene NYC1 delay degreening by distinct mechanisms. Journal of Experimental Botany **66**, 6849-6862.

Jibran R, Tahir J, Cooney J, Hunter DA, Dijkwel PP. 2017. Arabidopsis AGAMOUS Regulates Sepal Senescence by Driving Jasmonate Production. Frontiers in Plant Science **8**, 2101.

Jing H-C, Schippers JH, Hille J, Dijkwel PP. 2005. Ethylene-induced leaf senescence depends on age-related changes and OLD genes in Arabidopsis. Journal of Experimental Botany **56**, 2915-2923.

Jing HC, Sturre MJG, Hille J, Dijkwel PP. 2002. Arabidopsis onset of leaf death mutants identify a regulatory pathway controlling leaf senescence. Plant Journal **32**, 51-63.

Jing S, Zhou X, Song Y, Yu D. 2009. Heterologous expression of OsWRKY23 gene enhances pathogen defense and dark-induced leaf senescence in Arabidopsis. Plant Growth Regulation **58**, 181-190.

John I, Drake R, Farrell A, Cooper W, Lee P, Horton P, Grierson D. 1995. Delayed leaf senescence in ethylene‐deficient ACC‐oxidase antisense tomato plants: molecular and physiological analysis. Plant Journal **7**, 483-490.

Jones M, Stead A, G. Clark D. 2009. Petunia flower senescence. *Petunia: evolutionary, developmental and physiological genetics*, 301-324.

Jones ML, Chaffin GS, Eason JR, Clark DG. 2005. Ethylene-sensitivity regulates proteolytic activity and cysteine protease gene expression in petunia corollas. Journal of Experimental Botany **56**, 2733-2744.

Ju CL, Yoon GM, Shemansky JM, Lin DY, Ying ZI, Chang JH, Garrett WM, Kessenbrock M, Groth G, Tucker ML, Cooper B, Kieber JJ, Chang C. 2012. CTR1 phosphorylates the central regulator EIN2 to control ethylene hormone signaling from the ER membrane to the nucleus in Arabidopsis. Proceedings of the National Academy of Sciences of the United States of America **109**, 19486-19491.

Kagiyama M, Hirano Y, Mori T, Kim SY, Kyozuka J, Seto Y, Yamaguchi S, Hakoshima T. 2013. Structures of D14 and D14L in the strigolactone and karrikin signaling pathways. Genes Cells **18**, 147-160.

Kallberg Y, Oppermann U, Jörnvall H, Persson B. 2002. Short‐chain dehydrogenases/reductases (SDRs). European Journal of Biochemistry **269**, 4409-4417.

Kaminaga Y, Schnepp J, Peel G, Kish CM, Ben-Nissan G, Weiss D, Orlova I, Lavie O, Rhodes D, Wood K, Porterfield DM, Cooper AJL, Schloss JV, Pichersky E, Vainstein A, Dudareva N. 2006. Plant phenylacetaldehyde synthase is a bifunctional homotetrameric enzyme that catalyzes phenylalanine decarboxylation and oxidation. Journal of Biological Chemistry **281**, 23357-23366.

Kanojia A, Dijkwel PP. 2018. Abiotic Stress Responses are Governed by Reactive Oxygen Species and Age. *Annual Plant Reviews online*, 1-32.

Kapulnik Y, Delaux PM, Resnick N, Mayzlish-Gati E, Wininger S, Bhattacharya C, Sejalon-Delmas N, Combier JP, Becard G, Belausov E, Beeckman T, Dor E, Hershenhorn J, Koltai H. 2011. Strigolactones affect lateral root formation and root-hair elongation in Arabidopsis. Planta **233**, 209-216.

Katoh A, Uenohara K, Akita M, Hashimoto T. 2006. Early steps in the biosynthesis of NAD in Arabidopsis start with aspartate and occur in the plastid. Plant Physiology **141**, 851-857.

Kearse M, Moir R, Wilson A, Stones-Havas S, Cheung M, Sturrock S, Buxton S, Cooper A, Markowitz S, Duran C. 2012. Geneious Basic: an integrated and extendable desktop software platform for the organization and analysis of sequence data. Bioinformatics **28**, 1647-1649.

Khan M, Rozhon W, Poppenberger B. 2014. The role of hormones in the aging of plants - a mini-review. Gerontology **60**, 49-55.

Kieber JJ, Rothenberg M, Roman G, Feldmann KA, Ecker JR. 1993. CTR1, a negative regulator of the ethylene response pathway in Arabidopsis, encodes a member of the raf family of protein kinases. Cell **72**, 427-441.

Kim H, Kim HJ, Vu QT, Jung S, McClung CR, Hong S, Nam HG. 2018. Circadian control of ORE1 by PRR9 positively regulates leaf senescence in Arabidopsis. Proceedings of the National Academy of Sciences of the United States of America **115**, 8448-8453.

Kim HJ, Hong SH, Kim YW, Lee lH, Jun JH, Phee BK, Rupak T, Jeong H, Lee Y, Hong BS, Nam HG, Woo HR, Lim PO. 2014. Gene regulatory cascade of senescence-associated NAC transcription factors activated by ETHYLENE-INSENSITIVE2-mediated leaf senescence signalling in Arabidopsis. Journal of Experimental Botany **65**, 4023-4036.

Kim HJ, Ryu H, Hong SH, Woo HR, Lim PO, Lee IC, Sheen J, Nam HG, Hwang I. 2006a. Cytokinin-mediated control of leaf longevity by AHK3 through phosphorylation of ARR2 in Arabidopsis. Proceedings of the National Academy of Sciences of the United States of America **103**, 814-819.

kim JH. 2009. Trifurcate Feed-Forward Regulation of Age-Dependent Cell Death Involving miR164 in Arabidopsis. Science **323**, 1053-1057.

Kim JH, Chung KM, Woo HR. 2011. Three positive regulators of leaf senescence in Arabidopsis, ORE1, ORE3 and ORE9, play roles in crosstalk among multiple hormone-mediated senescence pathways. Genes & Genomics **33**, 373-381.

Kim JH, Woo HR, Kim J, Lim PO, Lee IC, Choi SH, Hwang D, Nam HG. 2009. Trifurcate Feed-Forward Regulation of Age-Dependent Cell Death Involving miR164 in Arabidopsis. Science **323**, 1053-1057.

Kim Y, Schumaker KS, Zhu J-K. 2006b. EMS Mutagenesis of Arabidopsis. In: Salinas J, Sanchez-Serrano JJ, eds. *Arabidopsis Protocols*. Totowa, NJ: Humana Press, 101-103.

Knudsen JT, Tollsten L, Bergstrom LG. 1993. Floral scents—a checklist of volatile compounds isolated by head-space techniques. Phytochemistry **33**, 253-280.

Kolosova N, Gorenstein N, Kish CM, Dudareva N. 2001. Regulation of circadian methyl benzoate emission in diurnally and nocturnally emitting plants. Plant Cell **13**, 2333-2347.

Koncz C, Schell J. 1986. The promoter of TL-DNA gene 5 controls the tissue-specific expression of chimaeric genes carried by a novel type of Agrobacterium binary vector. Molecular & General Genetics **204**, 383-396.

Koornneef M, Alonso-Blanco C, Stam P. 2006. Genetic analysis. *Arabidopsis Protocols*: Springer, 65-77.

Koornneef M, Dellaert LWM, Vanderveen JH. 1982. EMS- and relation-induced mutation frequencies at individual loci in Arabidopsis thaliana (L.) Heynh. Mutation Research **93**, 109-123.

Koressaar T, Remm M. 2007. Enhancements and modifications of primer design program Primer3. Bioinformatics **23**, 1289-1291.

Kusaba M, Ito H, Morita R, Iida S, Sato Y, Fujimoto M, Kawasaki S, Tanaka R, Hirochika H, Nishimura M, Tanaka A. 2007. Rice NON-YELLOW COLORING1 is involved in light-harvesting complex II and grana degradation during leaf senescence. Plant Cell **19**, 1362-1375.

Lakatos L, Szittya G, Silhavy D, Burgyan J. 2004. Molecular mechanism of RNA silencing suppression mediated by p19 protein of tombusviruses. Embo Journal **23**, 876-884.

Lam HM, Peng SSY, Coruzzi GM. 1994. Metabolic regulation of the gene encoding glutamine-dependent asparagine synthetase in *Arabidopsis thaliana*. Plant Physiology **106**, 1347-1357.

Langmead B, Salzberg SL. 2012. Fast gapped-read alignment with Bowtie 2. Nature Methods **9**, 357-U354.

Lara MEB, Garcia M-CG, Fatima T, Ehneß R, Lee TK, Proels R, Tanner W, Roitsch T. 2004. Extracellular invertase is an essential component of cytokinin-mediated delay of senescence. The Plant Cell Online **16**, 1276-1287.

Lazo GR, Stein PA, Ludwig RA. 1991. A DNA transformation-competent Arabidopsis genomic library in Agrobacterium. Bio-Technology **9**, 963-967.

Lee TA, Vande Wetering SW, Brusslan JA. 2013. Stromal protein degradation is incomplete in Arabidopsis thaliana autophagy mutants undergoing natural senescence. BMC research notes **6**, 17-17.

Li G, Gao M, Yang B, Quiros CF. 2003. Gene for gene alignment between the Brassica and Arabidopsis genomes by direct transcriptome mapping. Theoretical and Applied Genetics **107**, 168-180.

Li GD, Pan LN, Jiang K, Takahashi I, Nakamura H, Xu YW, Asami T, Shen RF. 2016. Strigolactones are involved in sugar signaling to modulate early seedling development in *Arabidopsis*. Plant Biotechnology **33**, 87-97.

Li W, Nishiyama R, Watanabe Y, Van Ha C, Kojima M, An P, Tian L, Tian C, Sakakibara H, Tran LP. 2018. Effects of overproduced ethylene on the contents of other phytohormones and expression of their key biosynthetic genes. Plant Physiology and Biochemistry **128**, 170-177.

Li WY, Ma MD, Feng Y, Li HJ, Wang YC, Ma YT, Li MZ, An FY, Guo HW. 2015. EIN2-Directed Translational Regulation of Ethylene Signaling in Arabidopsis. Cell **163**, 670-683.

Li XF, Li YJ, An YH, Xiong LJ, Shao XH, Wang Y, Sun Y. 2009. AKINbeta1 is involved in the regulation of nitrogen metabolism and sugar signaling in Arabidopsis. Journal of Integrative Plant Biology **51**, 513-520.

Li ZH, Peng JY, Wen X, Guo HW. 2012. Gene Network Analysis and Functional Studies of Senescence-associated Genes Reveal Novel Regulators of Arabidopsis Leaf Senescence. Journal of Integrative Plant Biology **54**, 526-539.

Li ZH, Peng JY, Wen X, Guo HW. 2013. ETHYLENE-INSENSITIVE3 Is a Senescence-Associated Gene That Accelerates Age-Dependent Leaf Senescence by Directly Repressing miR164 Transcription in Arabidopsis. Plant Cell **25**, 3311-3328.

Liebsch D, Keech O. 2016. Dark-induced leaf senescence: new insights into a complex light-dependent regulatory pathway. New Phytologist **212**, 563-570.

Liew M, Pryor R, Palais R, Meadows C, Erali M, Lyon E, Wittwer C. 2004. Genotyping of single-nucleotide polymorphisms by high-resolution melting of small amplicons. Clinical Chemistry **50**, 1156-1164.

Lim PO, Kim HJ, Nam HG. 2007. Leaf senescence. Annual Review of Plant Biology **58**, 115-136.

Lim PO, Lee IC, Kim J, Kim HJ, Ryu JS, Woo HR, Nam HG. 2010. Auxin response factor 2 (ARF2) plays a major role in regulating auxin-mediated leaf longevity. Journal of Experimental Botany **61**, 1419-1430.

Lim PO, Woo HR, Nam HG. 2003. Molecular genetics of leaf senescence in Arabidopsis. Trends in Plant Science **8**, 272-278.

Lin JF, Wu SH. 2004. Molecular events in senescing Arabidopsis leaves. Plant Journal **39**, 612-628.

Liu M-S, Li H-C, Chang Y-M, Wu M-T, Chen L-FO. 2011. Proteomic analysis of stress-related proteins in transgenic broccoli harboring a gene for cytokinin production during postharvest senescence. Plant Science **181**, 288-299.

Liu WZ, Wu C, Fu YP, Hu GC, Si HM, Zhu L, Luan WJ, He ZQ, Sun ZX. 2009. Identification and characterization of HTD2: a novel gene negatively regulating tiller bud outgrowth in rice. Planta **230**, 649-658.

Livak KJ, Schmittgen TD. 2001. Analysis of relative gene expression data using real-time quantitative PCR and the 2(T)(-Delta Delta C) method. Methods **25**, 402-408.

Lloyd A. 2003. Vector Construction for Gene Overexpression as a Tool to Elucidate Gene Function. In: Grotewold E, ed. *Plant Functional Genomics*. Totowa, NJ: Humana Press, 329-344.

Lochlainn SO, Amoah S, Graham NS, Alamer K, Rios JJ, Kurup S, Stoute A, Hammond JP, Ostergaard L, King GJ, White PJ, Broadley MR. 2011. High Resolution Melt (HRM) analysis is an efficient tool to genotype EMS mutants in complex crop genomes. Plant Methods **7**, 43.

Lohman KN, Gan SS, John MC, Amasino RM. 1994. Molecular analysis of natural leaf senescence in *Arabidopsis thaliana*. Physiologia Plantarum **92**, 322-328.

Lü P, Zhang C, Liu J, Liu X, Jiang G, Jiang X, Khan MA, Wang L, Hong B, Gao J. 2014. RhHB1 mediates the antagonism of gibberellins to ABA and ethylene during rose (Rosa hybrida) petal senescence. The Plant Journal **78**, 578-590.

Lutz KA, Wang W, Zdepski A, Michael TP. 2011. Isolation and analysis of high quality nuclear DNA with reduced organellar DNA for plant genome sequencing and resequencing. BMC Biotechnology **11**, 54.

Lv S, Zhang Y, Li C, Liu Z, Yang N, Pan L, Wu J, Wang J, Yang J, Lv Y, Zhang Y, Jiang W, She X, Wang G. 2018. Strigolactone-triggered stomatal closure requires hydrogen peroxide synthesis and nitric oxide production in an abscisic acid-independent manner. New Phytologist **217**, 290-304.

Ma N, Ma C, Liu Y, Shahid MO, Wang CP, Gao JP. 2018. Petal senescence: a hormone view. Journal of Experimental Botany **69**, 719-732.

Mair A, Pedrotti L, Wurzinger B, Anrather D, Simeunovic A, Weiste C, Valerio C, Dietrich K, Kirchler T, Nagele T, Vicente Carbajosa J, Hanson J, Baena-Gonzalez E, Chaban C, Weckwerth W, Droge-Laser W, Teige M. 2015. SnRK1-triggered switch of bZIP63 dimerization mediates the low-energy response in plants. Elife **4**, e05828.

Maple J, Møller SG. 2007. Mutagenesis in Arabidopsis. In: Rosato E, ed. *Circadian Rhythms: Methods and Protocols*. Totowa, NJ: Humana Press, 197-206.

Martínez DE, Costa ML, Gomez FM, Otegui MS, Guiamet JJ. 2008. 'Senescence-associated vacuoles' are involved in the degradation of chloroplast proteins in tobacco leaves. Plant Journal **56**, 196-206.

Marzec M. 2016. Strigolactones as Part of the Plant Defence System. Trends in Plant Science **21**, 900-903.

Mashiguchi K, Sasaki E, Shimada Y, Nagae M, Ueno K, Nakano T, Yoneyama K, Suzuki Y, Asami T. 2009. Feedback-regulation of strigolactone biosynthetic genes and strigolactone-regulated genes in Arabidopsis. Bioscience, Biotechnology, and Biochemistry **73**, 2460-2465.

Matile P, Hortensteiner S, Thomas H, Krautler B. 1996. Chlorophyll breakdown in senescent leaves. Plant Physiology **112**, 1403-1409.

Mayak S, Dilley DR. 1976. Regulation of Senescence in Carnation (Dianthus caryophyllus) - Effect of Abscisic Acid and Carbon Dioxide on Ethylene Production Plant Physiology **58**, 663-665.

McCallum CM, Comai L, Greene EA, Henikoff S. 2000. Targeted screening for induced mutations. Nature Biotechnology **18**, 455-457.

McCormac AC, Elliott MC, Chen DF. 1998. A simple method for the production of highly competent cells of Agrobacterium for transformation via electroporation. Molecular Biotechnology **9**, 155-159.

McNicholas S, Potterton E, Wilson KS, Noble MEM. 2011. Presenting your structures: the CCP4mg molecular-graphics software. Acta Crystallographica Section D-Biological Crystallography **67**, 386-394.

Meguro M, Ito H, Takabayashi A, Tanaka R, Tanaka A. 2011. Identification of the 7-hydroxymethyl chlorophyll a reductase of the chlorophyll cycle in Arabidopsis. The Plant Cell Online **23**, 3442-3453.

Merchante C, Brumos J, Yun J, Hu QW, Spencer KR, Enriquez P, Binder BM, Heber S, Stepanova AN, Alonso JM. 2015. Gene-Specific Translation Regulation Mediated by the Hormone-Signaling Molecule EIN2. Cell **163**, 684-697.

Merchante C, Stepanova AN. 2017. The Triple Response Assay and Its Use to Characterize Ethylene Mutants in Arabidopsis. In: Binder BM, Eric Schaller G, eds. *Ethylene Signaling: Methods and Protocols*. New York, NY: Springer New York, 163-209.

Miao Y, Laun T, Zimmermann P, Zentgraf U. 2004. Targets of the WRKY53 transcription factor and its role during leaf senescence in Arabidopsis. Plant Molecular Biology **55**, 853-867.

Morris K, Mackerness SAH, Page T, John CF, Murphy AM, Carr JP, Buchanan-Wollaston V. 2000. Salicylic acid has a role in regulating gene expression during leaf senescence. Plant Journal **23**, 677-685.

Moummou H, Kallberg Y, Tonfack LB, Persson B, Van der Rest B. 2012. The Plant Short-Chain Dehydrogenase (SDR) superfamily: genome-wide inventory and diversification patterns. Bmc Plant Biology **12**, 219.

Mueller-Roeber B, Balazadeh S. 2014. Auxin and Its Role in Plant Senescence. Journal of Plant Growth Regulation **33**, 21-33.

Muhlemann JK, Klempien A, Dudareva N. 2014. Floral volatiles: from biosynthesis to function. Plant Cell and Environment **37**, 1936-1949.

Murashige T, Skoog F. 1962. A Revised Medium for Rapid Growth and Bio Assays with Tobacco Tissue Cultures. Physiologia Plantarum **15**.

Nakano M, Yamada T, Masuda Y, Sato Y, Kobayashi H, Ueda H, Morita R, Nishimura M, Kitamura K, Kusaba M. 2014. A Green-Cotyledon/Stay-Green Mutant Exemplifies the Ancient Whole-Genome Duplications in Soybean. Plant and Cell Physiology **55**, 1763-1771.

Nakashima K, Takasaki H, Mizoi J, Shinozaki K, Yamaguchi-Shinozaki K. 2012. NAC transcription factors in plant abiotic stress responses. Biochimica Et Biophysica Acta-Gene Regulatory Mechanisms **1819**, 97-103.

Nelson DC, Scaffidi A, Dun EA, Waters MT, Flematti GR, Dixon KW, Beveridge CA, Ghisalberti EL, Smith SM. 2011. F-box protein MAX2 has dual roles in karrikin and strigolactone signaling in Arabidopsis thaliana. Proceedings of the National Academy of Sciences of the United States of America **108**, 8897-8902.

Noh YS, Amasino RM. 1999a. Identification of a promoter region responsible for the senescence-specific expression of SAG12. Plant Molecular Biology **41**, 181-194.

Noh YS, Amasino RM. 1999b. Regulation of developmental senescence is conserved between Arabidopsis and Brassica napus. Plant Molecular Biology **41**, 195-206.

Oh SA, Park JH, Lee GI, Paek KH, Park SK, Nam HG. 1997. Identification of three genetic loci controlling leaf senescence in Arabidopsis thaliana. Plant Journal **12**, 527-535.

Olsen AN, Ernst HA, Lo Leggio L, Skriver K. 2005a. DNA-binding specificity and molecular functions of NAC transcription factors. Plant Science **169**, 785-797.

Olsen AN, Ernst HA, Lo Leggio L, Skriver K. 2005b. NAC transcription factors: structurally distinct, functionally diverse. Trends in Plant Science **10**, 79-87.

Oneill SD. 1997. Pollination regulation of flower development. Annual Review of Plant Physiology and Plant Molecular Biology **48**, 547-574.

Ostergaard L, Yanofsky MF. 2004. Establishing gene function by mutagenesis in Arabidopsis thaliana. Plant J **39**, 682-696.

Otegui MS, Noh YS, Martinez DE, Vila Petroff MG, Andrew Staehelin L, Amasino RM, Guiamet JJ. 2005. Senescence-associated vacuoles with intense proteolytic activity develop in leaves of Arabidopsis and soybean. Plant Journal **41**, 831-844.

Otori K, Tamoi M, Tanabe N, Shigeoka S. 2017. Enhancements in sucrose biosynthesis capacity affect shoot branching in Arabidopsis. Bioscience, Biotechnology, and Biochemistry **81**, 1470-1477.

Page DR, Grossniklaus L. 2002. The art and design of genetic screens: Arabidopsis thaliana. Nature Reviews Genetics **3**, 124-136.

Page T, Griffiths G, Buchanan-Wollaston V. 2001. Molecular and biochemical characterization of postharvest senescence in broccoli. Plant Physiology **125**, 718-727.

Panavas T, Walker EL, Rubinstein B. 1998. Possible involvement of abscisic acid in senescence of daylily petals. Journal of Experimental Botany **49**, 1987-1997.

Park KY, Drory A, Woodson WR. 1992. Molecular cloning of an 1-aminocyclopropane-1-carboxylate synthase from senescing carnation flower petals. Plant Molecular Biology **18**, 377-386.

Park SY, Yu JW, Park JS, Li J, Yoo SC, Lee NY, Lee SK, Jeong SW, Seo HS, Koh HJ, Jeon JS, Park YI, Paek NC. 2007. The senescence-induced staygreen protein regulates chlorophyll degradation. Plant Cell **19**, 1649-1664.

Peters JL, Cnudde F, Gerats T. 2003. Forward genetics and map-based cloning approaches. Trends in Plant Science **8**, 484-491.

Picone JM, Clery RA, Watanabe N, MacTavish HS, Turnbull CGN. 2004. Rhythmic emission of floral volatiles from Rosa damascena semperflorens cv. 'Quatre Saisons'. Planta **219**, 468-478.

Podzimska-Sroka D, O'Shea C, Gregersen PL, Skriver K. 2015. NAC Transcription Factors in Senescence: From Molecular Structure to Function in Crops. Plants (Basel) **4**, 412-448.

Porat R, Borochov A, Halevy AH. 1993. Enhancement of Petunia and Dendrobium flower senescence by jasmonic acid methyl ester is via the promotion of ethylene production. Plant Growth Regulation **13**, 297-301.

Porat R, Reiss N, Atzorn R, Halevy AH, Borochov A. 1995. Examination of the possible involvement of lipoxygenase and jasmonates in pollination - induced senescence of *Phalaenopsis* and *Dendrobium* orchid flowers. Physiologia Plantarum **94**, 205-210.

Potuschak T, Lechner E, Parmentier Y, Yanagisawa S, Grava S, Koncz C, Genschik P. 2003. EIN3-dependent regulation of plant ethylene hormone signaling by two Arabidopsis F box proteins: EBF1 and EBF2. Cell **115**, 679-689.

Price AM, Orellana DFA, Salleh FM, Stevens R, Acock R, Buchanan-Wollaston V, Stead AD, Rogers HJ. 2008. A comparison of leaf and petal senescence in wallflower reveals common and distinct patterns of gene expression and physiology. Plant Physiology **147**, 1898-1912.

Pružinská A, Shindo T, Niessen S, Kaschani F, Tóth R, Millar AH, van der Hoorn RAL. 2017. Major Cys protease activities are not essential for senescence in individually darkened Arabidopsis leaves. Bmc Plant Biology **17**, 4.

Qiao H, Chang KN, Yazaki J, Ecker JR. 2009. Interplay between ethylene, ETP1/ETP2 F-box proteins, and degradation of EIN2 triggers ethylene responses in Arabidopsis. Genes & Development **23**, 512-521.

Qiao H, Shen ZX, Huang SSC, Schmitz RJ, Urich MA, Briggs SP, Ecker JR. 2012. Processing and Subcellular Trafficking of ER-Tethered EIN2 Control Response to Ethylene Gas. Science **338**, 390-393.

Qiu K, Li Z, Yang Z, Chen J, Wu S, Zhu X, Gao S, Gao J, Ren G, Kuai B, Zhou X. 2015. EIN3 and ORE1 Accelerate Degreening during Ethylene-Mediated Leaf Senescence by Directly Activating Chlorophyll Catabolic Genes in Arabidopsis. PLoS Genet **11**, e1005399.

Radhamony RN, Prasad AM, Srinivasan R. 2005. T-DNA insertional mutagenesis in Arabidopsis: a tool for functional genomics. Electronic Journal of Biotechnology **8**, 82-106.

Raguso RA, Levin RA, Foose SE, Holmberg MW, McDade LA. 2003. Fragrance chemistry, nocturnal rhythms and pollination "syndromes" in Nicotiana. Phytochemistry **63**, 265-284.

Rasmussen A, Mason MG, De Cuyper C, Brewer PB, Herold S, Agusti J, Geelen D, Greb T, Goormachtig S, Beeckman T, Beveridge CA. 2012. Strigolactones Suppress Adventitious Rooting in Arabidopsis and Pea. Plant Physiology **158**, 1976-1987.

Raziuddin, Wollaston VB, Farhatullah, Sardar A. 2007. Characterization of EMS induced leaf senescing mutants in Arabidopsis. Sarhad Journal of Agriculture **23**, 601-609.

Rivero RM, Kojima M, Gepstein A, Sakakibara H, Mittler R, Gepstein S, Blumwald E. 2007. Delayed leaf senescence induces extreme drought tolerance in a flowering plant. Proceedings of the National Academy of Sciences of the United States of America **104**, 19631-19636.

Robatzek S, Somssich IE. 2001. A new member of the Arabidopsis WRKY transcription factor family, AtWRKY6, is associated with both senescence- and defence-related processes. Plant Journal **28**, 123-133.

Robatzek S, Somssich IE. 2002. Targets of AtWRKY6 regulation during plant senescence and pathogen defense. Genes & Development **16**, 1139-1149.

Robert S, Kleine-Vehn J, Barbez E, Sauer M, Paciorek T, Baster P, Vanneste S, Zhang J, Simon S, Covanova M, Hayashi K, Dhonukshe P, Yang Z, Bednarek SY, Jones AM, Luschnig C, Aniento F, Zazimalova E, Friml J. 2010. ABP1 Mediates Auxin Inhibition of Clathrin-Dependent Endocytosis in Arabidopsis. Cell **143**, 111-121.

Robinson JT, Thorvaldsdottir H, Winckler W, Guttman M, Lander ES, Getz G, Mesirov JP. 2011. Integrative genomics viewer. Nature Biotechnology **29**, 24-26.

Rogers HJ. 2006. Programmed cell death in floral organs: How and why do flowers die? Annals of Botany **97**, 309-315.

Rogers HJ. 2013. From models to ornamentals: how is flower senescence regulated? Plant Molecular Biology **82**, 563-574.

Roitsch T, Gonzalez MC. 2004. Function and regulation of plant invertases: sweet sensations. Trends in Plant Science **9**, 606-613.

Roitsch T, Tanner W. 1996. Cell wall invertase: Bridging the gap. Botanica Acta **109**, 90-93.

Rolland F, Baena-Gonzalez E, Sheen J. 2006. Sugar sensing and signaling in plants: Conserved and novel mechanisms. *Annual Review of Plant Biology*, Vol. 57, 675-709.

Rolny N, Costa L, Carrion C, Guiamet JJ. 2011. Is the electrolyte leakage assay an unequivocal test of membrane deterioration during leaf senescence? Plant Physiology and Biochemistry **49**, 1220-1227.

Roman G, Lubarsky B, Kieber JJ, Rothenberg M, Ecker JR. 1995. Genetic Analysis of Ethylene Signal Transduction in Arabidopsis Thaliana: Five Novel Mutant Loci Integrated into a Stress Response Pathway. Genetics **139**, 1393-1409.

Ronen M, Mayak S. 1981. Interrelationship between Abscisic Acid and Ethylene in the Control of Senescence Processes in Carnation Flowers. Journal of Experimental Botany **32**, 759-765.

Roy A, Kucukural A, Zhang Y. 2010. I-TASSER: a unified platform for automated protein structure and function prediction. Nature Protocols **5**, 725-738.

Rusanov K, Kovacheva N, Vosman B, Zhang L, Rajapakse S, Atanassov A, Atanassov I. 2005. Microsatellite analysis of Rosa damascena Mill. accessions reveals genetic similarity between genotypes used for rose oil production and old Damask rose varieties. Theoretical and Applied Genetics **111**, 804-809.

Rushton PJ, Somssich IE, Ringler P, Shen QJ. 2010. WRKY transcription factors. Trends in Plant Science **15**, 247-258.

Ruyter-Spira C, Kohlen W, Charnikhova T, van Zeijl A, van Bezouwen L, de Ruijter N, Cardoso C, Lopez-Raez JA, Matusova R, Bours R, Verstappen F, Bouwmeester H. 2011. Physiological Effects of the Synthetic Strigolactone Analog GR24 on Root System Architecture in Arabidopsis: Another Belowground Role for Strigolactones? Plant Physiology **155**, 721-734.

Saeed W, Naseem S, Ali Z. 2017. Strigolactones Biosynthesis and Their Role in Abiotic Stress Resilience in Plants: A Critical Review. Frontiers in Plant Science **8**, 1487.

Sakai H, Hua J, Chen QHG, Chang CR, Medrano LJ, Bleecker AB, Meyerowitz EM. 1998. ETR2 is an ETR1-like gene involved in ethylene signaling in Arabidopsis. Proceedings of the National Academy of Sciences of the United States of America **95**, 5812-5817.

Sakai M, Hirata H, Sayama H, Sekiguchi K, Itano H, Asai T, Dohra H, Hara M, Watanabe N. 2007. Production of 2-phenylethanol in roses as the dominant floral scent compound from L-phenylalanine by two key enzymes, a PLP-Dependent decarboxylase and a phenylacetaldehyde reductase. Bioscience Biotechnology and Biochemistry **71**, 2408-2419.

Saks Y, Van Staden J. 1993. Effect of gibberellic acid on ACC content, EFE activity and ethylene release by floral parts of the senescing carnation flower. Plant Growth Regulation **12**, 99-104.

Saks Y, Van Staden J, Smith MT. 1992. Effect of gibberellic acid on carnation flower senescence: evidence that the delay of carnation flower senescence by gibberellic acid depends on the stage of flower development. Plant Growth Regulation **11**, 45-51.

Sakuraba Y, Schelbert S, Park SY, Han SH, Lee BD, Andres CB, Kessler F, Hortensteiner S, Paek NC. 2012. STAY-GREEN and Chlorophyll Catabolic Enzymes Interact at Light-Harvesting Complex II for Chlorophyll Detoxification during Leaf Senescence in Arabidopsis. Plant Cell **24**, 507-518.

Sambrook J, Fritsch EF, Maniatis T. 1989. *Molecular cloning: a laboratory manual*. Cold Spring Harbor, N.Y.: Cold Spring Harbor Laboratory.

Sato Y, Morita R, Katsuma S, Nishimura M, Tanaka A, Kusaba M. 2009. Two short-chain dehydrogenase/reductases, NON-YELLOW COLORING 1 and NYC1-LIKE, are required for chlorophyll b and light-harvesting complex II degradation during senescence in rice. Plant Journal **57**, 120-131.

Schaller GE. 2012. Ethylene and the regulation of plant development. Bmc Biology **10**, 9.

Schelbert S, Aubry S, Burla B, Agne B, Kessler F, Krupinska K, Hortensteiner S. 2009. Pheophytin Pheophorbide Hydrolase (Pheophytinase) Is Involved in Chlorophyll Breakdown during Leaf Senescence in Arabidopsis. Plant Cell **21**, 767-785.

Schippers JH, Jing H, Hille J, Dijkwel PP. 2007. Developmental and Hormonal Control of Leaf Senescence. *Annual Plant Reviews Volume 26: Senescence Processes in Plants*.

Schippers JHM, Nunes-Nesi A, Apetrei R, Hille J, Fernie AR, Dijkwel PP. 2008. The Arabidopsis onset of leaf death5 Mutation of Quinolinate Synthase Affects Nicotinamide Adenine Dinucleotide Biosynthesis and Causes Early Ageing. Plant Cell **20**, 2909-2925.

Schippers JHM, Schmidt R, Wagstaff C, Jing HC. 2015. Living to Die and Dying to Live: The Survival Strategy behind Leaf Senescence. Plant Physiology **169**, 914-930.

Schneeberger K, Weigel D. 2011. Fast-forward genetics enabled by new sequencing technologies. Trends in Plant Science **16**, 282-288.

Seto Y, Sado A, Asami K, Hanada A, Umehara M, Akiyama K, Yamaguchi S. 2014. Carlactone is an endogenous biosynthetic precursor for strigolactones. Proceedings of the National Academy of Sciences of the United States of America **111**, 1640-1645.

Seto Y, Yasui R, Kameoka H, Tamiru M, Cao M, Terauchi R, Sakurada A, Hirano R, Kisugi T, Hanada A, Umehara M, Seo E, Akiyama K, Burke J, Takeda-Kamiya N, Li W, Hirano Y, Hakoshima T, Mashiguchi K, Noel JP, Kyozuka J, Yamaguchi S. 2019. Strigolactone perception and deactivation by a hydrolase receptor DWARF14. Nature Communications **10**, 191.

Sexton R, Stopford AP, Moodie WT, Porter AEA. 2005. Aroma production from cut sweet pea flowers (Lathyrus odoratus): the role of ethylene. Physiologia Plantarum **124**, 381-389.

Shahri W, Tahir I. 2011. Flower Senescence-Strategies and Some Associated Events. Botanical Review **77**, 152-184.

Shahri W, Tahir I. 2014. Flower senescence: some molecular aspects. Planta **239**, 277-297.

Shalit M, Shafir S, Larkov O, Bar E, Kaslassi D, Adam Z, Zamir D, Vainstein A, Weiss D, Ravid U, Lewinsohn E. 2004. Volatile compounds emitted by rose cultivars: Fragrance perception by man and honeybees. Israel Journal of Plant Sciences **52**, 245-255.

Shibuya K. 2018. Molecular aspects of flower senescence and strategies to improve flower longevity. Breeding Science **68**, 99-108.

Shibuya K, Barry KG, Ciardi JA, Loucas HM, Underwood BA, Nourizadeh S, Ecker JR, Klee HJ, Clark DG. 2004. The central role of PhEIN2 in ethylene responses throughout plant development in petunia. Plant Physiology **136**, 2900-2912.

Shibuya K, Shimizu K, Niki T, Ichimura K. 2014. Identification of a NAC transcription factor, EPHEMERAL1, that controls petal senescence in Japanese morning glory. Plant Journal **79**, 1044-1051.

Shinozaki Y, Tanabata T, Ogiwara I, Yamada T, Kanekatsu M. 2011. Application of Digital Image Analysis System for Fine Evaluation of Varietal Differences and the Role of Ethylene in Visible Petal Senescence of Morning Glory. Journal of Plant Growth Regulation **30**, 229-234.

Smaczniak C, Immink RG, Angenent GC, Kaufmann K. 2012. Developmental and evolutionary diversity of plant MADS-domain factors: insights from recent studies. Development **139**, 3081-3098.

Smith SM, Li C, Li J. 2017. 1 - Hormone function in plants. *Hormone Metabolism and Signaling in Plants*: Academic Press, 1-38.

Snowden KC, Simkin AJ, Janssen BJ, Templeton KR, Loucas HM, Simons JL, Karunairetnam S, Gleave AP, Clark DG, Klee HJ. 2005. The Decreased apical dominance1/Petunia hybrida CAROTENOID CLEAVAGE DIOXYGENASE8 gene affects branch production and plays a role in leaf senescence, root growth, and flower development. Plant Cell **17**, 746-759.

Song X, Lu Z, Yu H, Shao G, Xiong J, Meng X, Jing Y, Liu G, Xiong G, Duan J, Yao XF, Liu CM, Li H, Wang Y, Li J. 2017. IPA1 functions as a downstream transcription factor repressed by D53 in strigolactone signaling in rice. Cell Research **27**, 1128-1141.

Song Y, Jiang Y, Kuai B, Li L. 2018. CIRCADIAN CLOCK-ASSOCIATED 1 Inhibits Leaf Senescence in Arabidopsis. Frontiers in Plant Science **9**, 280.

Soundappan I, Bennett T, Morffy N, Liang Y, Stanga JP, Abbas A, Leyser O, Nelson DC. 2015. SMAX1-LIKE/D53 Family Members Enable Distinct MAX2-Dependent Responses to Strigolactones and Karrikins in Arabidopsis. Plant Cell **27**, 3143-3159.

Stanga JP, Smith SM, Briggs WR, Nelson DC. 2013. SUPPRESSOR OF MORE AXILLARY GROWTH2 1 controls seed germination and seedling development in Arabidopsis. Plant Physiology **163**, 318-330.

Stead AD. 1992. Pollination-induced flower senescence: a review. Plant Growth Regulation **11**, 13-20.

Stirnberg P, van de Sande K, Leyser HMO. 2002. MAX1 and MAX2 control shoot lateral branching in Arabidopsis. Development **129**, 1131-1141.

Sun GL, Mei YY, Deng DW, Xiong L, Sun LF, Zhang XY, Wen ZW, Liu S, You X, Nasrullah, Wang D, Wang NN. 2017. N-Terminus-Mediated Degradation of ACS7 Is Negatively Regulated by Senescence Signaling to Allow Optimal Ethylene Production during Leaf Development in Arabidopsis. Frontiers in Plant Science **8**, 2066.

tenHave A, Woltering EJ. 1997. Ethylene biosynthetic genes are differentially expressed during carnation (Dianthus caryophyllus L) flower senescence. Plant Molecular Biology **34**, 89-97.

Thimm O, Blasing O, Gibon Y, Nagel A, Meyer S, Kruger P, Selbig J, Muller LA, Rhee SY, Stitt M. 2004. MAPMAN: a user-driven tool to display genomics data sets onto diagrams of metabolic pathways and other biological processes. Plant Journal **37**, 914-939.

Thole JM, Strader LC. 2015. Next-generation sequencing as a tool to quickly identify causative EMS-generated mutations. Plant signaling & behavior **10**, 1-4.

Thomas H. 2013. Senescence, ageing and death of the whole plant. New Phytologist **197**, 696-711.

Thomas H, Howarth CJ. 2000. Five ways to stay green. Journal of Experimental Botany **51**, 329-337.

Thomas H, Ougham H, Canter P, Donnison I. 2002. What stay-green mutants tell us about nitrogen remobilization in leaf senescence. Journal of Experimental Botany **53**, 801-808.

Thomas JH. 1993. Thinking about genetic redundancy. Trends in Genetics **9**, 395-399.

Thompson JE, Froese CD, Madey E, Smith MD, Hong YW. 1998. Lipid metabolism during plant senescence. Progress in Lipid Research **37**, 119-141.

Thorvaldsdottir H, Robinson JT, Mesirov JP. 2013. Integrative Genomics Viewer (IGV): high-performance genomics data visualization and exploration. Briefings in Bioinformatics **14**, 178-192.

Tian M-q, Jiang K, Takahashi I, Li G-d. 2018. Strigolactone-induced senescence of a bamboo leaf in the dark is alleviated by exogenous sugar. Journal of Pesticide Science **43**, 173-179.

Tian MS, Davies L, Downs CG, Liu XF, Lill RE. 1995. Effects of Floret Maturity, Cytokinin and Ethylene on Broccoli Yellowing after Harvest. Postharvest Biology and Technology **6**, 29-40.

Tian MS, Downs CG, Lill RE, King GA. 1994. A Role for Ethylene in the Yellowing of Broccoli after Harvest. Journal of the American Society for Horticultural Science **119**, 276-281.

Tieman D, Taylor M, Schauer N, Fernie AR, Hanson AD, Klee HJ. 2006. Tomato aromatic amino acid decarboxylases participate in synthesis of the flavor volatiles 2-phenylethanol and 2-phenylacetaldehyde. Proceedings of the National Academy of Sciences of the United States of America **103**, 8287-8292.

Tieman DM, Loucas HM, Kim JY, Clark DG, Klee HJ. 2007. Tomato phenylacetaldehyde reductases catalyze the last step in the synthesis of the aroma volatile 2-phenylethanol. Phytochemistry **68**, 2660-2669.

Ting HM, Wang B, Ryden AM, Woittiez L, van Herpen T, Verstappen FWA, Ruyter-Spira C, Beekwilder J, Bouwmeester HJ, van der Krol A. 2013. The metabolite chemotype of Nicotiana benthamiana transiently expressing artemisinin biosynthetic pathway genes is a function of CYP71AV1 type and relative gene dosage. New Phytologist **199**, 352-366.

Toh S, Kamiya Y, Kawakami N, Nambara E, McCourt P, Tsuchiya Y. 2012. Thermoinhibition uncovers a role for strigolactones in Arabidopsis seed germination. Plant and Cell Physiology **53**, 107-117.

Torres-Vera R, García JM, Pozo MJ, López-Ráez JA. 2014. Do strigolactones contribute to plant defence? Molecular Plant Pathology **15**, 211-216.

Tripathi SK, Tuteja N. 2007. Integrated signaling in flower senescence: an overview. Plant signaling & behavior **2**, 437-445.

Trivellini A, Ferrante A, Vernieri P, Mensuali-Sodi A, Serra G. 2011a. Effects of Promoters and Inhibitors of Ethylene and ABA on Flower Senescence of Hibiscus rosa-sinensis L. Journal of Plant Growth Regulation **30**, 175-184.

Trivellini A, Ferrante A, Vernieri P, Serra G. 2011b. Effects of abscisic acid on ethylene biosynthesis and perception in Hibiscus rosa-sinensis L. flower development. Journal of Experimental Botany **62**, 5437-5452.

Trivellini A, Jibran R, Watson LM, O'Donoghue EM, Ferrante A, Sullivan KL, Dijkwel PP, Hunter DA. 2012. Carbon Deprivation-Driven Transcriptome Reprogramming in Detached Developmentally Arresting Arabidopsis Inflorescences. Plant Physiology **160**, 1357-1372.

Tzin V, Galili G. 2010. The Biosynthetic Pathways for Shikimate and Aromatic Amino Acids in Arabidopsis thaliana. The arabidopsis book **8**, e0132-e0132.

Uchida N, Sakamoto T, Kurata T, Tasaka M. 2011. Identification of EMS-Induced Causal Mutations in a Non-Reference Arabidopsis thaliana Accession by Whole Genome Sequencing. Plant and Cell Physiology **52**, 716-722.

Ueda H, Kusaba M. 2015. Strigolactone Regulates Leaf Senescence in Concert with Ethylene in Arabidopsis. Plant Physiology **169**, 138-147.

Ueguchi C, Koizumi H, Suzuki T, Mizuno T. 2001. Novel family of sensor histidine kinase genes in Arabidopsis thaliana. Plant and Cell Physiology **42**, 231-235.

Umehara M, Hanada A, Yoshida S, Akiyama K, Arite T, Takeda-Kamiya N, Magome H, Kamiya Y, Shirasu K, Yoneyama K, Kyozuka J, Yamaguchi S. 2008. Inhibition of shoot branching by new terpenoid plant hormones. Nature **455**, 195-200.

Underwood BA, Tieman DM, Shibuya K, Dexter RJ, Loucas HM, Simkin AJ, Sims CA, Schmelz EA, Klee HJ, Clark DG. 2005. Ethylene-regulated floral volatile synthesis in petunia corollas. Plant Physiology **138**, 255-266.

Untergasser A, Cutcutache I, Koressaar T, Ye J, Faircloth BC, Remm M, Rozen SG. 2012. Primer3--new capabilities and interfaces. Nucleic Acids Research **40**, e115.

Usadel B, Blaesing OE, Gibon Y, Retzlaff K, Hoehne M, Guenther M, Stitt M. 2008. Global transcript levels respond to small changes of the carbon status during progressive exhaustion of carbohydrates in Arabidopsis rosettes. Plant Physiology **146**, 1834-1861.

Vainstein A, Lewinsohn E, Pichersky E, Weiss D. 2001. Floral fragrance. New inroads into an old commodity. Plant Physiology **127**, 1383-1389.

van der Graaff E, Schwacke R, Schneider A, Desimone M, Fluegge U-I, Kunze R. 2006. Transcription analysis of arabidopsis membrane transporters and hormone pathways during developmental and induced leaf senescence. Plant Physiology **141**, 776-792.

Vanengelen FA, Molthoff JW, Conner AJ, Nap JP, Pereira A, Stiekema WJ. 1995. pBINPLUS: an improved plant transformation vector based on pBIN19. Transgenic Research **4**, 288-290.

Verdonk JC, de Vos CHR, Verhoeven HA, Haring MA, van Tunen AJ, Schuurink RC. 2003. Regulation of floral scent production in petunia revealed by targeted metabolomics. Phytochemistry **62**, 997-1008.

Verma V, Ravindran P, Kumar PP. 2016. Plant hormone-mediated regulation of stress responses. Bmc Plant Biology **16**, 86.

von Saint Paul V, Zhang W, Kanawati B, Geist B, Faus-Kessler T, Schmitt-Kopplin P, Schaeffner AR. 2011. The Arabidopsis Glucosyltransferase UGT76B1 Conjugates Isoleucic Acid and Modulates Plant Defense and Senescence. Plant Cell **23**, 4124-4145.

Wagstaff C, Yang TJW, Stead AD, Buchanan-Wollaston V, Roberts JA. 2009. A molecular and structural characterization of senescing Arabidopsis siliques and comparison of transcriptional profiles with senescing petals and leaves. Plant Journal **57**, 690-705.

Wang H, Stier G, Lin J, Liu G, Zhang Z, Chang YH, Reid MS, Jiang CZ. 2013. Transcriptome Changes Associated with Delayed Flower Senescence on Transgenic Petunia by Inducing Expression of etr1-1, a Mutant Ethylene Receptor. PLoS One **8**, e65800.

Wang KLC, Li H, Ecker JR. 2002. Ethylene biosynthesis and signaling networks. Plant Cell **14**, S131-S151.

Wang L, Wang B, Jiang L, Liu X, Li X, Lu Z, Meng X, Wang Y, Smith SM, Li J. 2015. Strigolactone Signaling in Arabidopsis Regulates Shoot Development by Targeting D53-Like SMXL Repressor Proteins for Ubiquitination and Degradation. Plant Cell **27**, 3128-3142.

Wang Y, Bouwmeester HJ. 2018. Structural diversity in the strigolactones. Journal of Experimental Botany **69**, 2219-2230.

Waters MT, Nelson DC, Scaffidi A, Flematti GR, Sun YK, Dixon KW, Smith SM. 2012. Specialisation within the DWARF14 protein family confers distinct responses to karrikins and strigolactones in Arabidopsis. Development **139**, 1285-1295.

Weaver LM, Gan S, Quirino B, Amasino RM. 1998. A comparison of the expression patterns of several senescence-associated genes in response to stress and hormone treatment. Plant Molecular Biology **37**, 455-469.

Wen X, Zhang CL, Ji YS, Zhao Q, He WR, An FY, Jiang LW, Guo HW. 2012. Activation of ethylene signaling is mediated by nuclear translocation of the cleaved EIN2 carboxyl terminus. Cell Research **22**, 1613-1616.

Widhalm JR, Dudareva N. 2015. A familiar ring to it: biosynthesis of plant benzoic acids. Molecular Plant **8**, 83-97.

Wilkinson JQ, Lanahan MB, Clark DG, Bleecker AB, Chang C, Meyerowitz EM, Klee HJ. 1997. A dominant mutant receptor from Arabidopsis confers ethylene insensitivity in heterologous plants. Nature Biotechnology **15**, 444-447.

Wintermans JF, de Mots A. 1965. Spectrophotometric characteristics of chlorophylls a and b and their pheophytins in ethanol. Biochim Biophys Acta **109**, 448-453.

Wittwer CT, Reed GH, Gundry CN, Vandersteen JG, Pryor RJ. 2003. High-resolution genotyping by amplicon melting analysis using LCGreen. Clinical Chemistry **49**, 853-860.

Wojciechowska N, Sobieszczuk-Nowicka E, Bagniewska-Zadworna A. 2018. Plant organ senescence - regulation by manifold pathways. Plant Biology **20**, 167-181.

Woltering EJ. 2017. Flower Senescence. In: Thomas B, Murray BG, Murphy DJ, eds. *Encyclopedia of Applied Plant Sciences (Second Edition)*. Oxford: Academic Press, 292-299.

Woltering EJ, Vandoorn WG. 1988. Role of Ethylene in Senescence of Petals—Morphological and Taxonomical Relationships. Journal of Experimental Botany **39**, 1605-1616.

Woo HR, Chung KM, Park JH, Oh SA, Ahn T, Hong SH, Jang SK, Nam HG. 2001. ORE9, an F-box protein that regulates leaf senescence in Arabidopsis. Plant Cell **13**, 1779-1790.

Woo HR, Kim HJ, Lim PO, Nam HG. 2019. Leaf Senescence: Systems and Dynamics Aspects. Annual Review of Plant Biology **70**, 347-376.

Woo HR, Kim JH, Kim J, Kim J, Lee U, Song IJ, Kim JH, Lee HY, Nam HG, Lim PO. 2010. The RAV1 transcription factor positively regulates leaf senescence in Arabidopsis. Journal of Experimental Botany **61**, 3947-3957.

Xu T, Wen M, Nagawa S, Fu Y, Chen J-G, Wu M-J, Perrot-Rechenmann C, Friml J, Jones AM, Yang Z. 2010. Cell Surface- and Rho GTPase-Based Auxin Signaling Controls Cellular Interdigitation in Arabidopsis. Cell **143**, 99-110.

Xu Y, Hanson MR. 2000. Programmed cell death during pollination-induced petal senescence in petunia. Plant Physiology **122**, 1323-1333.

Yamada Y, Furusawa S, Nagasaka S, Shimomura K, Yamaguchi S, Umehara M. 2014. Strigolactone signaling regulates rice leaf senescence in response to a phosphate deficiency. Planta **240**, 399-408.

Yamada Y, Umehara M. 2015. Possible Roles of Strigolactones during Leaf Senescence. Plants (Basel) **4**, 664-677.

Yan H, Saika H, Maekawa M, Takamure I, Tsutsumi N, Kyozuka J, Nakazono M. 2007. Rice tillering dwarf mutant dwarf3 has increased leaf longevity during darkness-induced senescence or hydrogen peroxide-induced cell death. Genes & Genetic Systems **82**, 361-366.

Yang J, Worley E, Udvardi M. 2014. A NAP-AAO3 regulatory module promotes chlorophyll degradation via ABA biosynthesis in Arabidopsis leaves. Plant Cell **26**, 4862-4874.

Yang J, Yan R, Roy A, Xu D, Poisson J, Zhang Y. 2015. The I-TASSER Suite: protein structure and function prediction. Nature methods **12**, 7-8.

Yang SF, Hoffman NE. 1984. Ethylene Biosynthesis and its Regulation in Higher Plants. Annual Review of Plant Physiology and Plant Molecular Biology **35**, 155-189.

Yano JK, Wester MR, Schoch GA, Griffin KJ, Stout CD, Johnson EF. 2004. The structure of human microsomal cytochrome P450 3A4 determined by X-ray crystallography to 2.05-A resolution. Journal of Biological Chemistry **279**, 38091-38094.

Yao RF, Ming ZH, Yan LM, Li SH, Wang F, Ma S, Yu CT, Yang M, Chen L, Chen LH, Li YW, Yan C, Miao D, Sun ZY, Yan JB, Sun YN, Wang L, Chu JF, Fan SL, He W, Deng HT, Nan FJ, Li JY, Rao ZH, Lou ZY, Xie DX. 2016. DWARF14 is a non-canonical hormone receptor for strigolactone. Nature **536**, 469-473.

Yin B, Cui D, Zhang L, Jiang S, Machida S, Yuan YA, Wei D. 2014. Structural insights into substrate and coenzyme preference by SDR family protein Gox2253 from Gluconobater oxydans. Proteins: Structure, Function, and Bioinformatics.

Yoneyama K, Mori N, Sato T, Yoda A, Xie X, Okamoto M, Iwanaga M, Ohnishi T, Nishiwaki H, Asami T, Yokota T, Akiyama K, Yoneyama K, Nomura T. 2018. Conversion of carlactone to carlactonoic acid is a conserved function of MAX1 homologs in strigolactone biosynthesis. New Phytologist **218**, 1522-1533.

Yoshida S. 2003. Molecular regulation of leaf senescence. Current Opinion in Plant Biology **6**, 79-84.

You S-C, Cho S-H, Zhang H, Paik H-C, Lee C-H, Li J, Yoo J-H, Lee B-W, Koh H-J, Seo HS, Paek N-C. 2007. Quantitative trait loci associated with functional stay-green SNU-SG1 in rice. Molecules and Cells **24**, 83-94.

Zhang DD, Li ZX, Li JF. 2016. Targeted Gene Manipulation in Plants Using the CRISPR/Cas Technology. Journal of Genetics and Genomics **43**, 251-262.

Zhang WY, Xu YC, Li WL, Yang L, Yue X, Zhang XS, Zhao XY. 2014a. Transcriptional Analyses of Natural Leaf Senescence in Maize. PLoS One **9**.

Zhang X, Henriques R, Lin SS, Niu QW, Chua NH. 2006. Agrobacterium-mediated transformation of Arabidopsis thaliana using the floral dip method. Nature Protocols **1**, 641-646.

Zhang Y. 2008. I-TASSER server for protein 3D structure prediction. Bmc Bioinformatics **9**, 40.

Zhang Y, van Dijk AD, Scaffidi A, Flematti GR, Hofmann M, Charnikhova T, Verstappen F, Hepworth J, van der Krol S, Leyser O, Smith SM, Zwanenburg B, Al-Babili S, Ruyter-Spira C, Bouwmeester HJ. 2014b. Rice cytochrome P450 MAX1 homologs catalyze distinct steps in strigolactone biosynthesis. Nature Chemical Biology **10**, 1028-1033.

Zhao LH, Zhou XE, Wu ZS, Yi W, Xu Y, Li S, Xu TH, Liu Y, Chen RZ, Kovach A, Kang Y, Hou L, He Y, Xie C, Song W, Zhong D, Xu Y, Wang Y, Li J, Zhang C, Melcher K, Xu HE. 2013. Crystal structures of two phytohormone signal-transducing alpha/beta hydrolases: karrikin-signaling KAI2 and strigolactone-signaling DWARF14. Cell Research **23**, 436-439.

Zheng KJ, Wang XP, Weighill DA, Guo HB, Xie M, Yang YG, Yang J, Wang SC, Jacobson DA, Guo H, Muchero W, Tuskan GA, Chen JG. 2016. Characterization of DWARF14 Genes in Populus. Scientific Reports **6**, 21593.

Zhou F, Lin Q, Zhu L, Ren Y, Zhou K, Shabek N, Wu F, Mao H, Dong W, Gan L, Ma W, Gao H, Chen J, Yang C, Wang D, Tan J, Zhang X, Guo X, Wang J, Jiang L, Liu X, Chen W, Chu J, Yan C, Ueno K, Ito S, Asami T, Cheng Z, Wang J, Lei C, Zhai H, Wu C, Wang H, Zheng N, Wan J. 2013. D14-SCF(D3)-dependent degradation of D53 regulates strigolactone signalling. Nature **504**, 406-410.

Zhou X, Jiang YJ, Yu DQ. 2011. WRKY22 transcription factor mediates dark-induced leaf senescence in Arabidopsis. Molecules and Cells **31**, 303-313.

Zhu J, Obrycki JJ, Ochieng SA, Baker TC, Pickett JA, Smiley D. 2005. Attraction of two lacewing species to volatiles produced by host plants and aphid prey. Naturwissenschaften **92**, 277-281.

Zhu X, Guo S, Wang Z, Du Q, Xing Y, Zhang T, Shen W, Sang X, Ling Y, He G. 2016. Map-based cloning and functional analysis of YGL8, which controls leaf colour in rice (Oryza sativa). Bmc Plant Biology **16**, 134.

Zwack PJ, De Clercq I, Howton TC, Hallmark HT, Hurny A, Keshishian EA, Parish AM, Benkova E, Mukhtar MS, Van Breusegem F, Rashotte AM. 2016. Cytokinin Response Factor 6 Represses Cytokinin-Associated Genes during Oxidative Stress. Plant Physiology **172**, 1249-1258.

Zwack PJ, Rashotte AM. 2013. Cytokinin inhibition of leaf senescence. Plant Signaling and Behavior **8**, 24737e.

Zwack PJ, Robinson BR, Risley MG, Rashotte AM. 2013. Cytokinin Response Factor 6 Negatively Regulates Leaf Senescence and is Induced in Response to Cytokinin and Numerous Abiotic Stresses. Plant and Cell Physiology **54**, 971-981.

Appendices

1. List of primers and SNP markers for HRM-analysis

1.1. HRM primers for fine-mapping of *dis9*

Chr.	Col-0 Pos. (bp) (TAIR10)	ID	Forward primers	Reverse primers	SNP (C/L)
3	370080 370107	A3-1	CTGATCCCAAACTTAGCTGCA	TCGAGAGGATGATGGCAGAA	A/G T/C
3	601391 601413	A3-2	TCCACCATCCACCACAAGAA	CTTGAATACTAGAGACGAGATAGGT	T/C T/C
3	978506	A3-3	CAACGCAAGTTATTAGACCACA	AGCATTCAACAGCAAATGGA	A/G
3	1490996	A3-4	ATGAACCAACAGCAGCAACA	ATAAGGCCGAGCGTACATCA	T/C
3	2010819	A3-5	ACCCTTCAATTCCCACCATT	CGTGCTTCAGTTTTTCTTGTTG	G/A
3	2987882	A3-6	TCAGAGAGGGGACAGAACTTACA	TGGCTATGAGTCTTTTCTTGG	G/A
3	3920554	A3-7	TTCCTTGCTCTCCTGTGCTT	GGAAGCCATCGACATCTTTATC	C/A
3	3956761	A3-8	GTTTTTGGTGAGTACGGAAACT	AAACCGCTTCTCTTTCTAACACTC	T/C
3	5949493 5949497	A3-9	AGCCCTACCTAACGAGCTGA	GGACTGTGCAAGGCTGGTAA	G/A G/T
3	7976473 7976483	A3-10	TCCTCTACCAAACCAAAACCA	AGTTCAAGTCCACAGCACCA	A/G A/G

1.2. HRM primers for fine-mapping of *dis51*

Chr.	Col-0 Pos. (bp) (TAIR10)	ID	Forward primer	Reverse primer	SNP (C/L)
5	144389	A5-1	CCTTTCCAGAGAGCACGAAC	TCTCCAACCAATCGACGTAA	T/G
5	252210	A5-2	CGTCGAGGTGATTCGTCTTT	GGTCAATAACAAGTAAAGCTCTGTG	T/C
5	298229	A5-3	GCGGTGGATCACATAGTTGG	GCTGCGTTTATTTTGGCTGT	C/T
5	675977	A5-4	CGTCAGATTTTCAGGGTCAA	TGTTGTGTGGGAAAGTGTCAA	A/G
5	1007097/ 1007098	A5-5	AAGCTGCCACTCCATTGTTT	GGCCCATTACAAGTTACACATC	T/C T/C
5	1522285/ 1522325/ 1522339	A5-6	ACCTGGAATGAGCAACAGGA	TGCACCAGAGATTGCGAGA	T/C T/C T/C
5	1665083	A5-7	GGCTGGTGACTTTTGCTTTC	TCTGGTGGTGAGTTCTGTGG	A/G
5	2938561/ 2938597	A5-8	GAAAATTCACCCCAATCCAA	ACTTCTCCGTCGTCTTCCAC	C/T C/A
5	5056405	A5-9	CCTGACTGGATAAACAAAGAAGG	TTGGCTAATCTGTGGAGTAACA	A/G
5	5191744	A5-10	CCGTAAGGTTTCCATTTCCA	GCGATACACGAACACCAAAA	T/C
5	5546722	A5-11	AGCCAACACTCCCATGAACT	GGCATGTAGCATTTCCCTCT	A/G
5	5614941	A5-12	CCAAACCCTTTCTCACAGTTTC	CAGAGCTGGTTAGTCGATTGG	C/T
5	6508875/ 6508877	A5-13	AAACGAAACACAAACCGTGA	TGGATGTATGCTGGTCTGCT	A/G T/G
5	6724721/ 6724722	A5-14	GTCCGTAGTGCTCCTGTCAA	GCTGTCTTCAGCAACCGTCT	A/G A/C
5	7505495	A5-15	TGTCTCATGGAGTTGGCTTATC	GAAACATGCCCTTACAATATCC	C/T
5	7554175/ 7554207	A5-16	ACGAAAACGGTGCCAAATAG	AGAAAAAGCGGTGAGCAAAA	C/T C/T
5	8496284	A5-17	GACAGCACAGCCAGAGTGAA	TTCTCCATCAAAGGCAAACC	G/A

The causal mutation in *dis51* was roughly mapped to Chr 5 by using the primers 1-2, 1-4, 1-7, 2-3, 2-4, 2-6, 3-2, 3-3, 3-4, 4-2, 5-1, 5-2 and 5-3 that listed in Hunter *et al.*, (2018). SNP positions were based on the Col-0 genomic sequence downloaded from TAIR10. L/C indicates L*er*-0/Col-0. Only good primers which clearly distinguished Col-0, Ler-0 and Col-0/Ler-0 heterozygous are listed in the tables.

2. Maps of cloning vectors

2.1. Map of D14pro&D14-CDS-pGWB1 construct

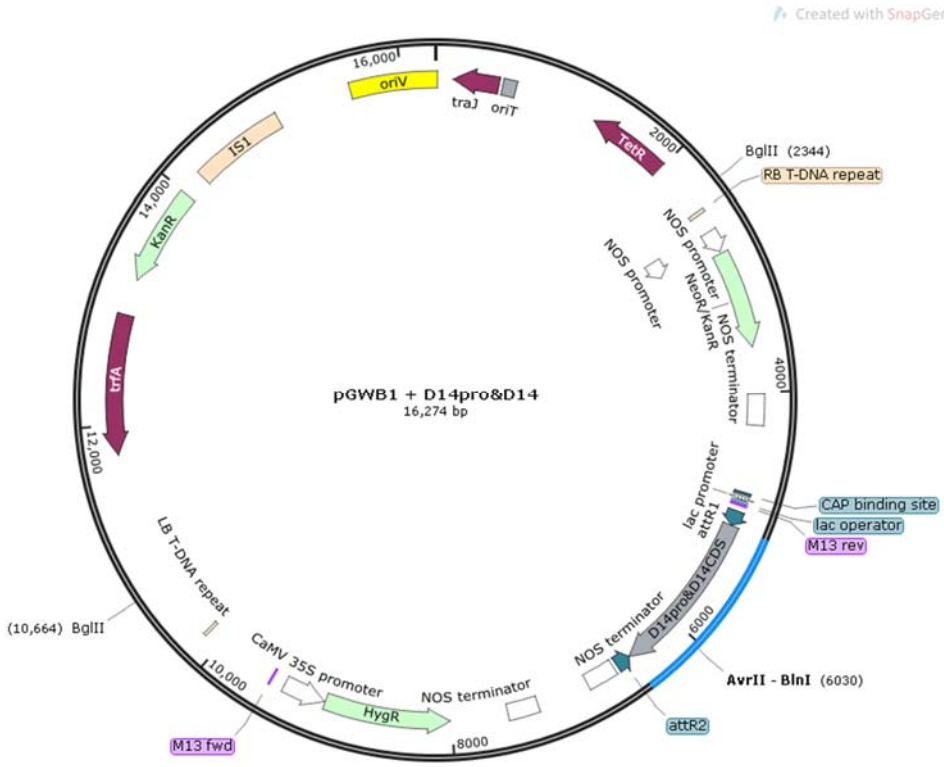

2.2. Map of pGreen0229 & pSoup

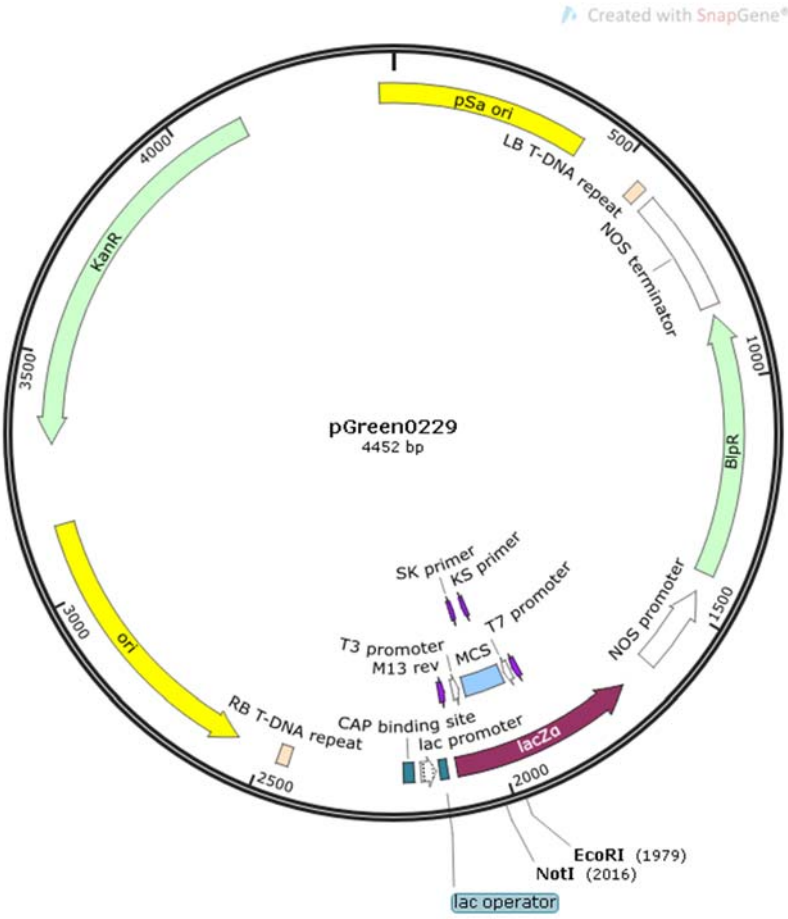

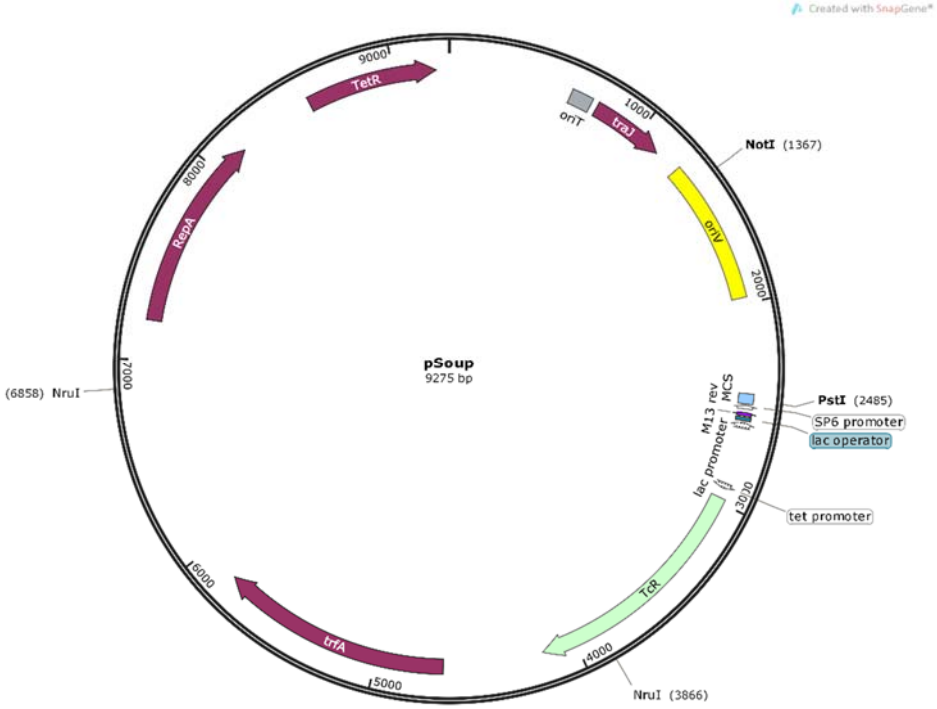

2.3. Vectors for gateway cloning

2.3.1. Map of pIV1A_2.1 (Entry vector)

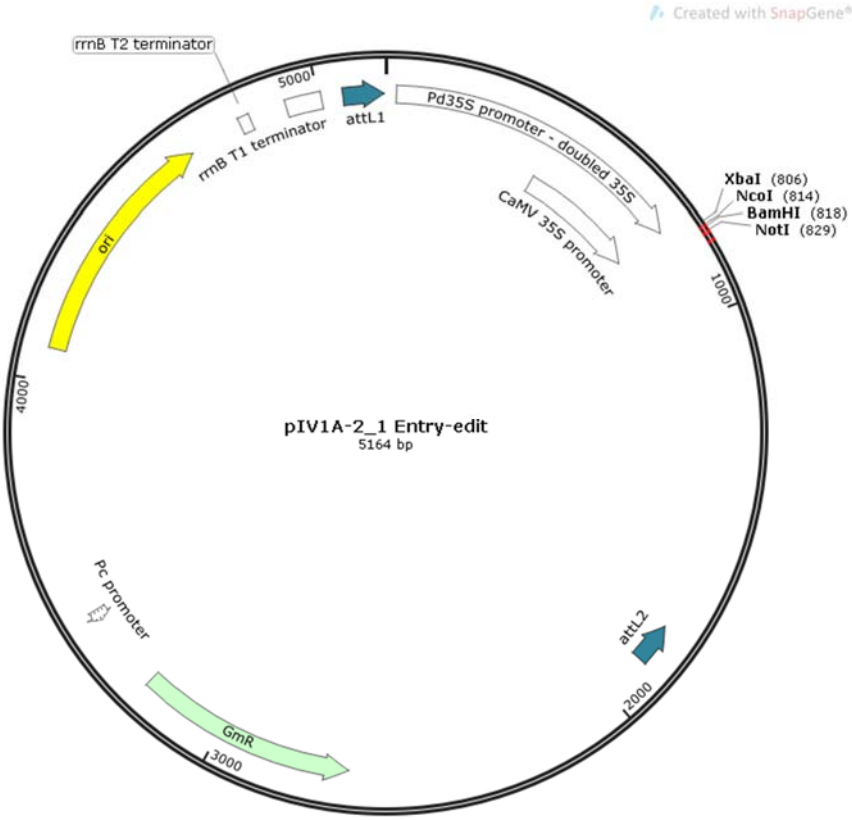

2.3.2. Map of pBin-Plus (Destination vector)

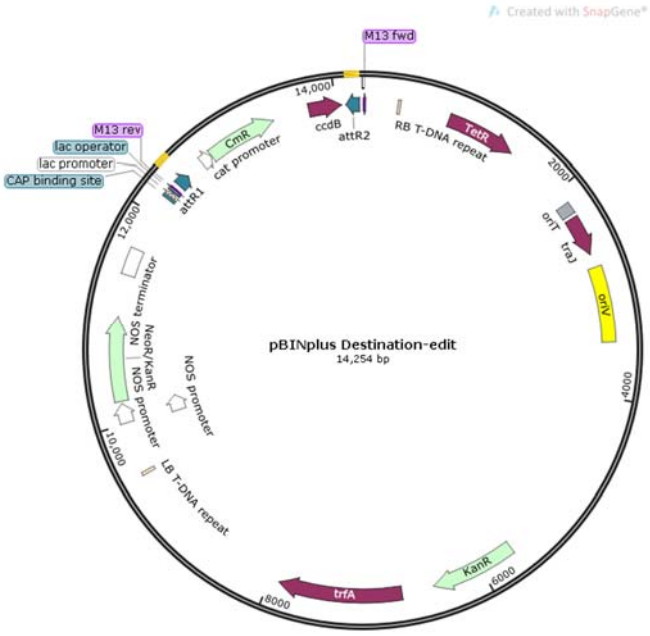

3. List of primers for standard PCR

3.1. Primers for cloning MAX1 and MAX1-G469A for complementation

Primer name	Restriction site	Sequence (5' to 3') *
MAX1_CompEcoRI_F	EcoRI	ccggaattcCTTACGTGGGCTGGACTATAA
MAX1_CompNotI_R	NotI	cgcgcggccgcGATTCGAGAAGCCGAGAGGT
MAX1GA_CompEcoRI_F1	EcoRI	ccggaattcCTTACGTGGGCTGGACTATAATCCATCCAATTCCT
MAX1_G469A_R1	N/A	GATCTCTTGCAGGGCAAATCTCTGTGCAACACAGGCT
MAX1_G469A_F1	N/A	TATCGGTCCACGAGCCTGTGTTGCACAGAGATTTG
MAX1GA_CompNotI_R1	NotI	cgcgcggccgcGATTCGAGAAGCCGAGAGGTTAAATGTGACCTTG

* Restriction sites were included in the primer sequences.

3.2. Primers for confirmation of Arabidopsis transformants

Primer name	Position	Sequence (5' to 3') *
C_D14SNP_F	D14 gene	TTGGCACTTGATCCTTCCTT
C_pGWB1_R	pGWB1 vector	AGCCTCCTCATCTCCCAGTT
G-d14-1_F* (MW221)	D14 promoter	AAGAATATGGCAAGTGCAAC
G-d14-1_R* (MW222)	D14 gene	GATGATTCCGATCATAGCG
MAX1PCR_F	MAX1 gene	GAAGTGGAGATAGGAGG
M13_R	pGreen0229 vector	CAGGAAACAGCTATGAC
MAX1CDS-PCR_F	MAX1 gene	GAAACTGCTAAAGAAGTGGAG
MAX1CDS_R2	MAX1 gene	TCAGAATCTTTTGATGGTTCTGAGC

* Primers are equivalent to the primers MW221 and MW222 in (Waters *et al.*, 2012).

3.3. Primers for MAX1-related constructions for Agro-infiltration in *N.benthamiana*

Primer name	Restriction site	Sequence (5' to 3') *
MAX1_NcoI_XF	NcoI	catgCCATGGCAATGAAGACGCAACATCAATGGTGGGAAGTTCTTGATC
MAX1_G469A_R1	N/A	GATCTCTTGCAGGGCAAATCTCTGTGCAACACAGGCT
MAX1_G469A_F1	N/A	TATCGGTCCACGAGCCTGTGTTGCACAGAGATTTG
MAX1_NotI_XR	NotI	atttGCGGCCGCTCAGAATCTTTTGATGGTTCTGAGCTTAACCCCGTTC

* Restriction sites were included in the primer sequences.

3.4. Primers for amplification of *NYC1* and *EIN2*

Primer name	Genes	Sequence (5' to 3')
at4g13250Scomp_F*	NYC1	AAATTTTGACAACACGACTACTGG
at4g13250SAScomp_R*	NYC1	TTCAACAACGACACATTCTACAAC
EIN2-G_F	EIN2	CACGAGCACCCATAACCTTC
EIN2-G_R	EIN2	ACGTGCAGAGATCCGGTTTA

* Primers were provided by Donald Hunter (PFR, Palmerston North, NZ).

4. Primers for qRT-PCR analysis

Primer name	Sequence (5’ to 3’)
qPP2AA3_F	GACCGGAGCCAACTAGGAC
qPP2AA3_R	AAAACTTGGTAACTTTTCCAGCA
qMAX3_F	GGGCATTCACGGATACTCAC
qMAX3_R	TGGTGACATTCCGCACATAG
qSMXL7_F	TCAGTGGCTGCAAACTGTTC
qSMXL7_R	GCGGGAACACACTTTTGTCT
qSMXL8_F	TGCCTCACAACAAGTCCAGT
qSMXL8_R	ACCGGAGAAGGGTAGTTTCAG
qANAC092_F	TTCTCTGCTACTGCCATTGGT
qANAC092_R	TCTCCCATCTTAGCCTTCCA
qSAG12_F	CTTTGCCGGTTTCTGTTGAC
qSAG12_R	TGAAAACGCCCAACAACAT
qBenPP2A_F	GACCCTGATGTTGATGTTCGCT
qBenPP2A_R	GAGGGATTTGAAGAGAGATTTC
qMAX1_F1	GATCAAACTCACATTACTGCATCTC
qMAX1_R1	CAGTGGTATCTCCATTTCTAGGG

5. Probes for nCounter analysis

Probe Name	Sequence (5' to 3')
MAX3 _A	CAT AGC CGC TAT GGA ACC TAT TGG ATT AAG CTT GAC TCG GTT GGC AAA GAC CTC AAG ACC TAA GCG ACA GCG TGA CCT TGT TTC A
MAX1 _A	TTC TTC CCG GAA AGA CCG AAG TCG ACT CCA AAA GCC GCT TGT CCG ATG ATC ATC CTC TTC TTT TCT TGG TGT TGA GAA GAT GCT C
D14 _A	CAC TAA GCT GCG GCA AAT GTC CTT CAG TTT TAA GAG TCT CCA CAG TAG TAC ACA ATT CTG CGG GTT AGC AGG AAG GTT AGG GAA C
SMXL6 _A	TCA TAC TAA TCA CTC TTC CAT GCA AAT CAC GGA TTT TCC CCG TAC TCA CAC TGT TGA GAT TAT TGA GCT TCA TCA TGA CCA GAA G
SMXL7 _A	TCT GGC TAG AAG AAC CAA GCT GAA GCG GGA ACT GCG GTC TAA CGG GCT GAC AAA GAC GCC TAT CTT CCA GTT TGA TCG GGA AAC T
SMXL8 _A	AGA TCA GTG GTG ACC GAT TTA GCT GAA CAG GTC GAT GCA GAA GCA CTG CTC GAA CCT AAC TCC TCG CTA CAT TCC TAT TGT TTT C
NAP _A	GAA ATC TGA ACC CTG GAG GGA GGG TAG ATT GGG AAG TTA CTT CCA TGA TTC AAC AGC CAC TTT TTT TCC AAA TTT TGC AAG AGC C
SGR1 _A	AAG AGT CTC AGT CTT GTG ACC ATC AGG CGA AAC AGC TTC CCA AAG CGG ACC AGA TAA GGT TGT TAT TGT GGA GGA TGT TAC TAC A
AKINBETA1 _A	CGT CCA CAA TCA CCT TGT AGT GGT ATA TGC CAG ATG GAA GGA CAA AGA GAC TTC CTT CCT GTG TTC CAG CTA CAA ACT TAG AAA C
bZIP63 _A	AAC AAT CTG AGG CAT ATT GTG GAA CAT TGG GTT AAA GCC AGT GAG TCT CTC TGG TCA AGA CTT GCA TGA GGA CCC GCA AAT TCC T
ANAC092 _A	CGG AGA AGC AGG TCA CGT GAG ACG ACG AAC CGG TGA AGG AGT CTC GTT GAC GAT TGC TGC ATT CCG CTC AAC GCT TGA GGA AGT A
SAG12 _A	CTT CAT CAG TGC TTG CTC ATC ATT AAC CGG GAC ATC CTC ATA ACC TGT AAC TGA GGC TGT TAA AGC TGT AGC AAC TCT TCC ACG A
PP2AA3 _A	GGA AAA TCC CAC ATG CTG ATA CTC TGG CTG TGA ACC ATT CAC CAG CTG AAC TAG GAC GCA AAT CAC TTG AAG AAG TGA AAG CGA G
ACT2 _A	TGA GAG CTT AGA AAC ATT TTC TGT GAA CGA TTC CTG GAC CTG CCT CAT CAC CAC GCG ATG ACG TTC GTC AAG AGT CGC ATA ATC T
MON1 _A	TCT TGC AAT ATG GTT CCT GTA GCT TGC CTT AAC GCA TAT GGA AGG GGA AGC ATT TGG AAT GAT GTG TAC TGG GAA TAA GAC GAC G
MAX3 _B	CGA AAG CCA TGA CCT CCG ATC ACT CTC GTT GCT TGG GTT TAA CGA TAA CGC TGA TAC CAT TGG TGA CAT TCC GCA
MAX1 _B	CGA AAG CCA TGA CCT CCG ATC ACT CAG TAG ACA TGC TGG TTT ATG AAA TCA GTC ACC TCC ACA TCT TTG ATT GGT
D14 _B	CGA AAG CCA TGA CCT CCG ATC ACT CAA GTC ACC GAG GAA GAG CTC GCC GGA GAA ACT GAG CAA GCT GCG CCG GAG
SMXL6 _B	CGA AAG CCA TGA CCT CCG ATC ACT CAG TGG CAT TAT CCT TGG CAA TCC CAG ACG TCA CAA CAA CAA TCA CAT TTT
SMXL7 _B	CGA AAG CCA TGA CCT CCG ATC ACT CCG TCC TAG TGC AAA CAA TTT TCT CAG TTG GGC TTC CAA GAC TCA TCT TGG
SMXL8 _B	CGA AAG CCA TGA CCT CCG ATC ACT CAA TGC TTC TTG AGA CCG GAT CCT GTG GTG ACT GAA CTT ACC CTA AGA TTC
NAP _B	CGA AAG CCA TGA CCT CCG ATC ACT CCA TGG TCT GGT TTC GAA GAT AGT AAA CGA TGA GTT CTT CGT CGG TAG GAT
SGR1 _B	CGA AAG CCA TGA CCT CCG ATC ACT CCT AAC GGT TGG AAA ACA ACA ACT ACA CTC GTC CGC ACA CCG AGC CTC GGG
AKINBETA1 _B	CGA AAG CCA TGA CCT CCG ATC ACT CGC CAA CTT CGT CTG CTA CAA AGG GTA AAT CTG GGA TGT ATT TGG ATT CAC
bZIP63 _B	CGA AAG CCA TGA CCT CCG ATC ACT CCT TGT AGT GTC TGG AGA ATT TGA TGT CTC TGA AGG AAG AGA GAC AGT TGA
ANAC092 _B	CGA AAG CCA TGA CCT CCG ATC ACT CAA AAC CGT CTT TGG ACT CGT GGA CAA GTC TTT TGT CTT CGG TTT CTT GGT
SAG12 _B	CGA AAG CCA TGA CCT CCG ATC ACT CTC AAA ACC ACC TCC TTC AAT TCC AAC GCT AAC CGG TTG GTG TGC CAC TGC
PP2AA3 _B	CGA AAG CCA TGA CCT CCG ATC ACT CTG ATC TTA GCT CCG TCT TTA GCA CAT CTG GGG CAC TTG GGT ATG CAA TAT
ACT2 _B	CGA AAG CCA TGA CCT CCG ATC ACT CAG AAA CTT TGA TCC CAT TCA TAA AAC CCC AGC TTT TTA AGC CTT TGA TCT
MON1 _B	CGA AAG CCA TGA CCT CCG ATC ACT CCC TTG TGT CTG CAC ATT AGT AGT GAG AAT AAG ACA CCA GAC GCG CAA ACT

6. Time to bolting and flowering of *dis2* and *dis51* in M5 plants

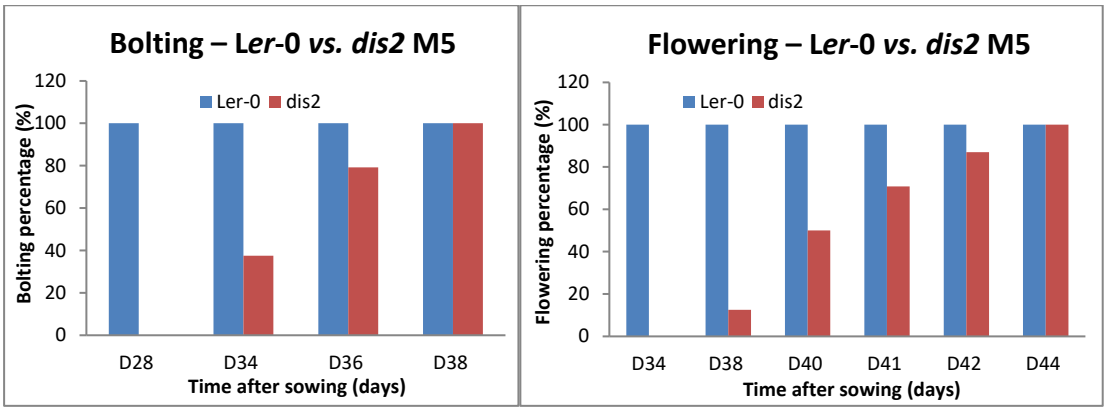

Appendix 6.1. Time to bolting and flowering of *dis2* (M5 plants)

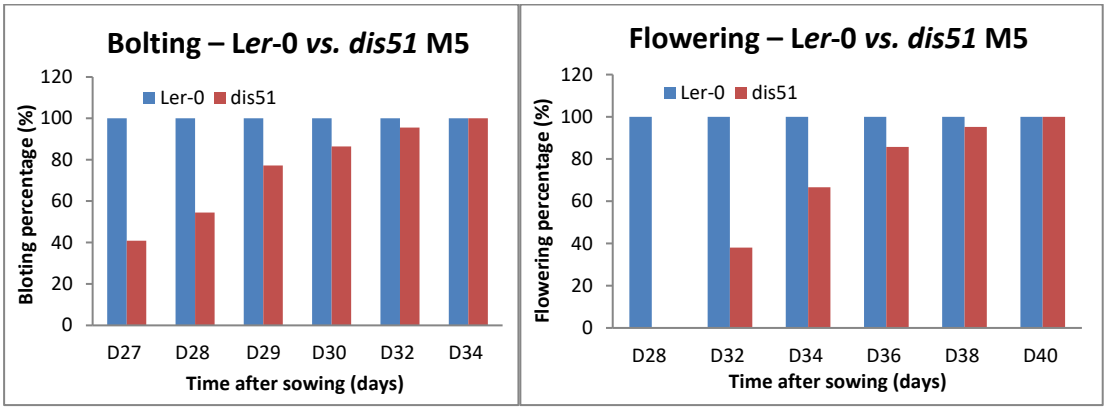

Appendix 6.2. Time to bolting and flowering of *dis51* (M5 plants)

7. HRM-based mapping of *dis* locus in *dis51*

Appendix 7.1. Linkage analysis of *dis51* in chromosome 1 to 5

		DNA samples													Linkage analysis				
Chr	Marker	1	2	3	4	5	6	7	8	9	10	11	12	13	Total	Col-0	Hetero (H)	Linkage (%)	cM
1	1-2	H	H	H	H	H	H	L	H	C	H	L	H	H	13	1	10	46.15	46
	1-4	H	L	H	H	H	H	L	L	C	H	L	H	C	13	2	7	42.31	42
	1-7	H	L	L	L	H	H	C	H	C	H	H	C	L	13	3	6	46.15	46
2	2-3	C	H	C	H	L	C	L	L	H	C	C	H	L	13	5	4	53.85	54
	2-4	C	H	C	H	H	C	L	H	C	C	H	H	C	13	6	6	69.23	69
	2-6	H	H	C	H	H	L	L	L	H	H	L	C	H	13	2	7	42.31	42
3	3-2	C	C	C	C	H	H	C	H	C	H	C	C	L	13	8	4	76.92	77
	3-3	C	C	C	H	H	H	C	L	C	H	C	C	L	13	7	4	69.23	69
	3-4	H	H	H	C	H	H	C	H	C	H	H	C	L	13	4	8	61.54	62
4	4-2	H	H	H	H	C	L	C	H	L	H	H	L	C	13	3	7	50.00	50
5	5-2	L	L	L	L	L	H	L	H	L	L	L	L	L	13	0	2	7.69	8
	5-3	C	C	C	H	C	H	H	C	L	H	C	H	L	13	6	5	65.38	65

Appendix 7.2. Linkage analysis of *dis51* in chromosome 5 using 26 plants

Chr 5	DNA samples																									Linkage analysis				
Marker	1	2	3	4	5	6	7	8	9	10	11	12	13	14	15	16	17	18	19	20	21	22	23	24	25	26	Total	Col-0	Hetero (H)	Linkage (%)	cM
5-1	L	L	L	L	L	H	L	H	L	L	L	L	L	L	L	L	L	L	L	L	H	L	L	L	L	L	26	0	3	5.77	6
5-2	L	L	L	L	L	H	L	H	L	L	L	L	L	L	L	L	L	L	L	L	H	L	L	L	L	L	26	0	3	5.77	6
5-3	C	C	C	H	C	H	H	C	L	H	C	H	L	C	C	C	H	L	C	H	C	L	H	C	H	H	26	12	10	65.38	65

Appendix 7.3. Linkage analysis of *dis51* in chromosome 5 using 65 plants

Chr5	DNA samples																																
Marker	1	2	3	4	5	6	7	8	9	10	11	12	13	14	15	16	17	18	19	20	21	22	23	24	25	26	27	28	29	30	31	32	33
5-1	L	L	L	L	L	H	L	H	L	L	L	L	L	L	L	L	L	L	L	L	H	L	L	L	L	L	L	L	L	L	L	L	L
5-2	L	L	L	L	L	H	L	H	L	L	L	L	L	L	L	L	L	L	L	L	H	L	L	L	L	L	L	L	L	L	L	L	L

Chr5	DNA samples																															Linkage analysis				
Marker	34	35	36	37	38	39	40	41	42	43	44	45	46	47	48	49	50	51	52	53	54	55	56	57	58	59	60	61	62	63	64	65	Total	Col-0	Hetero (H)	Linkage (%)	cM
5-1	L	L	L	L	L	L	L	L	L	L	L	L	H	L	L	L	L	L	L	L	L	L	L	H	L	L	L	L	H	C	L	L	65	1	6	6.15	6
5-2	L	L	L	L	L	L	L	L	L	L	L	L	H	L	L	L	L	L	L	L	L	L	L	H	L	L	L	L	H	C	L	L	65	1	6	6.15	6

In Appendices 7.1-7.3, plant genotypes identified by HRM: L*er*-0 homozygous (L, blue); Col-0 homozygous (C, green); heterozygous (H, red). Chr, chromosome; cM, centimorgan.

Appendix 7.4. Summary of the mapping of *dis51* based on recombination events occurring in chromosome 5

Chr5	Physical location	DNA samples																	
Markers	Mbp	84	85	86	6	79	14	15	16	24	27	28	40	42	45	51	59	65	71
A5-1	0.14						L	H	L	L									
A5-2	0.25	H	H	H	H	L					L	L	L	L	L	L	L	L	L
A5-3	0.29				H														
5-1	0.34				H		L	L	L	L	L	L	L	L	L	L	L	L	
A5-4	0.67			L	L	L	L	L	L	L									
A5-5	1.01			L		H	L	L	L										
A5-6	1.52	H	H	L		H	H	H	H	L	H	H	H	H	H	H	H	H	H
A5-7	1.66				L		H	H	H	L									
A5-8	2.90						H	H	H	H									
A5-9	5.05				L														
A5-10	5.19			L	L	H	C	H	C	H									
A5-11	5.54				L														
A5-12	5.61				L		C	H	C	H									
A5-13	6.51						C	H	C	H									
5-2	6.71				H		L	L	L	L	L	L	L	L	L	L	L	L	
A5-14	6.72						C	H	C	H									
A5-15	7.50				L		C	H	C	H									
A5-16	7.55						C	H	C	H									
A5-17	8.49						C	H	C	C									
Note*		P	P	P	P	P	P	P	P	P	P	P	P	P	P	P	P	P	P

Markers	20	17	18	19	22	23	25	26	1	2	3	4	5	7	9	10	11	12	13
A5-1	L	L	L	L	L	L	L	L											
A5-2																			
A5-3																			
5-1	L	L	L	L	L	L	L	L											
A5-4	L	L	L	L	L	L	L	L											
A5-5																			
A5-6																			
A5-7	L	L	L	L	L	L	L	L											
A5-8	L	L	L	L	L	L	L	L											
A5-9																			
A5-10	L	L	L	L	L	L	L	L											
A5-11																			
A5-12	L	L	L	L	L	L	L	L											
A5-13																			
5-2	L	L	L	L	L	L	L	L	L	L	L	L	L	L	L	L	L	L	L
A5-14																			
A5-15	H	L	L	L	L	L	L	L											
A5-16																			
A5-17	H	L	L	L	L	L	L	L											
Note*	P	P	P	P	P	P	P	P	P	P	P	P	P	P	P	P	P	P	P

Markers	29	30	31	32	33	34	35	36	37	38	39	41	43	44	47	48	49	50	52	53	54	55	56	58	60	61	64
A5-1																											
A5-2	L	L	L	L	L	L	L	L	L	L	L	L	L	L	L	L	L	L	L	L	L	L	L	L	L	L	L
A5-3																											
5-1	L	L	L	L	L	L	L	L	L	L	L	L	L	L	L	L	L	L	L	L	L	L	L	L	L	L	L
A5-4																											
A5-5																											
A5-6	L	L	L	L	L	L	L	L	L	L	L	L	L	L	L	L	L	L	L	L	L	L	L	L	L	L	Failed
A5-7																											
A5-8																											
A5-9																											
A5-10																											
A5-11																											
A5-12																											
A5-13																											
5-2	L	L	L	L	L	L	L	L	L	L	L	L	L	L	L	L	L	L	L	L	L	L	L	L	L	L	L
A5-14																											
A5-15																											
A5-16																											
A5-17																											
Note*	P	P	P	P	P	P	P	P	P	P	P	P	P	P	P	P	P	P	P	P	P	P	P	P	P	P	P

Markers	66	67	68	69	70	72	73	74	75	76	77	78	80	81	83	87	88	89	90	91	92	8	21	46	57	62	63	82
A5-1																							H					
A5-2	L	L	L	L	L	L	L	L	L	L	L	L	L	L	L	L	L	L	L	L	L	H	H					C
A5-3																						H	H					
5-1																						H	H	H	H	H	C	
A5-4																						H	H					
A5-5																						H	H					
A5-6	L	L	L	L	L	L	L	L	L	L	L	L	L	L	L	L	L	L	L	L	L		H					H
A5-7																						H	H					
A5-8																							H					
A5-9																						H	H					
A5-10																						H	H					
A5-11																						H	H					
A5-12																						H	H					
A5-13																							H					
5-2																						H	H	H	H	H	C	
A5-14																							H					
A5-15																						H	H					
A5-16																							H					
A5-17																							H					
Note*	P	P	P	P	P	P	P	P	P	P	P	P	P	P	P	P	P	P	P	P	P	FP	FP	FP	FP	FP	FP	FP

Plant sample 6 and 79 are the two informative samples for identifying the region containing the causal mutation for the *dis* phenotype in *dis51*. They reveal that the mutation is located between 0.34-1.01 Mbp in chromosome 5. Plant genotypes identified by HRM: L*er*-0 homozygous (L, blue); Col-0 homozygous (C, green); heterozygous (H, red). P, positive; FP, false positive (the *dis* phenotype for these samples was unclear, therefore treated with caution and concluded as false positive after HRM analysis).

8. Sepal degreening of *dis9* and *dis15*

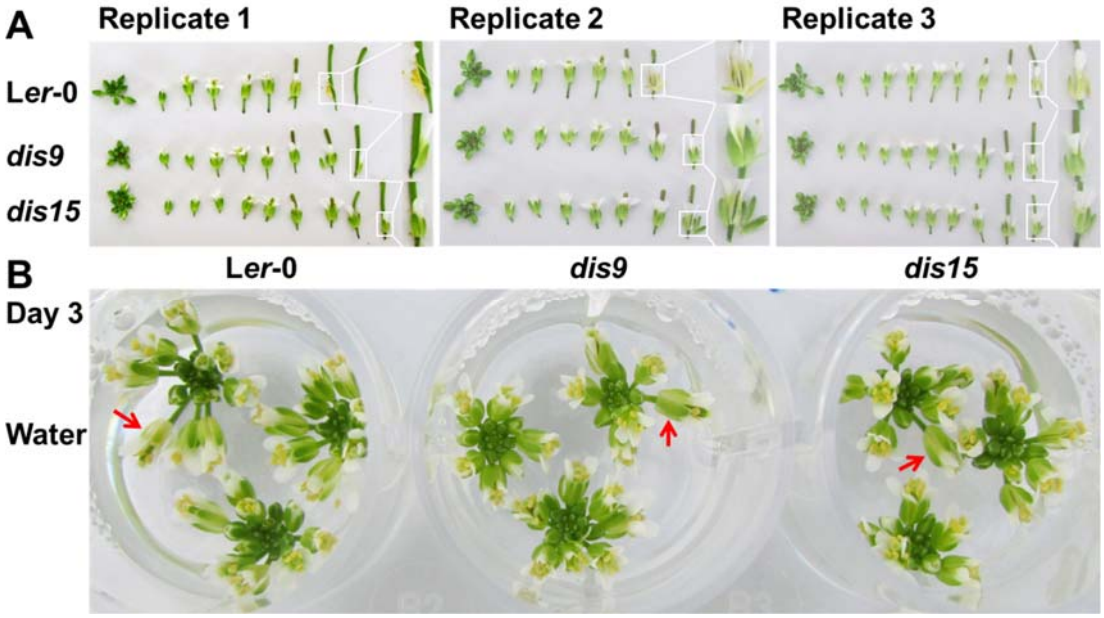

Appendix 8. Delayed sepal degreening of *dis9* and *dis15 in planta* and in detached inflorescences held in the long day conditions (16 h/8 h light/dark cycle) (A) Dissection of attached inflorescences *in planta*. Inflorescences were harvested from the primary bolts of 4-week-old wild-type and *dis* plants that had their first flower opened on the same day. Additional three representative biological replicates from an independent experiment are shown. (B) Excised inflorescences at day 3 of long-day incubation. Inflorescences were harvested from the primary bolts of 4.5-week-old plants that had their first flower opened on the same day. The inflorescences with removed opened buds were placed in water and incubated in the 16 h/8 h light/dark cycle for 3 days. Additional three biological replicates from an independent experiment are shown. The representative sepals are pointed by red arrows.

9. HRM-based mapping of *dis9* locus

Appendix 9.1 Linkage analysis of *dis9*

Chr 3	Physical location	DNA samples																							
Marker	Mbp	1	2	3	4	5	6	7	8	9	10	11	12	13	14	15	16	17	18	19	20	21	22	23	24
A3-1	0.37	L	L	L	L	L	L	L	C	H	L	L	L	L	L	L	L	L	L	L	L	L	L	L	L
A3-5	2.01	L	?	L	L	H	L	L	C	L	?	L	L	L	?	?	L	?	H	?	?	L	L	?	L
Phenotype		BD	BD	BD	BD	BD	BD	BD	NBD	BD	BD	BD	BD	BD	BD	BD	BD	BD	BD	BD	BD	BD	BD	BD	BD
Note*		P	P	P	P	P	P	P	FP	P	P	P	P	P	P	P	P	P	P	P	P	P	P	P	P

Chr 3	Physical location	DNA samples																										
Marker	Mbp	25	26	27	28	29	30	31	32	33	34	35	36	37	38	39	40	41	42	51	52	53	54	55	56	57	58
A3-1	0.37	L	L	L	L	L	L	H	H	L	L	H	L	L	L	L	L	L	H	H	L	L	L	L	L	L	L
A3-5	2.01	?	?	?	L	L	L	H	L	?	?	?	?	H	?	L	?	?	H	H	L	L	H	L	L	L	L
Phenotype		BD	BD	BD	BD	BD	BD	BD	BD	BD	BD	BD	BD	BD	BD	BD	BD	BD	NBD	NBD	BD	BD	BD	BD	BD	BD	BD
Note*		P	P	P	P	P	P	FP	P	P	P	P	P	P	P	P	P	P	FP	FP	P	P	P	P	P	P	P

Chr 3	Linkage analysis				
Marker	Total	Col-0	Hetero (H)	linkage (%)	cM
A3-1	50	1	6	8	8
A3-5	not clear				
Phenotype					
Note*					

Plant genotypes identified by HRM: L*er*-0 homozygous (L, blue); Col-0 homozygous (C, green); heterozygous (H, red); not clear based on HRM profile (?, pink). Plant phenotypes: BD, bushy and delayed sepal degreening; NBD, non-bushy and delayed sepal degreening. P, positive; FP, false positive (the *dis* phenotype for these samples was unclear, therefore treated with caution and concluded as false positive after HRM analysis); cM, centimorgan.

Appendix 9.2 Summary of the mapping of *dis9* based on crossing over events occurring in chromosome 3

Chr 3	Physical location	DNA samples																		
Marker	Mbp	1	3	4	14	16	17	23	26	28	34	36	38	39	52	53	2	119	133	134
A3-1	0.37	L	L	L	L	L	L	L	L	L	L	L	L	L	L	L	L	L	L	L
A3-2	0.6	L	L	L	L	L	L	L	L	L	L	L	L	L	L	L	L			
A3-3	0.98																L			
A3-4	1.49																L	L	L	L
A3-5	2.01	L	L	L	?	L	?	?	?	L	?	?	?	L	L	L	?			
A3-6	2.99																L	L	L	L
A3-7	3.92																L	L	L	L
A3-8	3.96																L	L	L	L
A3-9	5.94																L	L	L	L
A3-10	7.97	H	H	H	H	H	H	H	H	H	H	H	H	H	H	H	H	H	H	H
Phenotype		BD	BD	BD	BD	BD	BD	BD	BD	BD	BD	BD	BD	BD	BD	BD	BD	BD	BD	BD
Note*		P	P	P	P	P	P	P	P	P	P	P	P	P	P	P	P	P	P	P

Chr 3	Physical location	DNA samples																								
Marker	Mbp	162	190	192	54	5	37	18	9	32	35	105	188	6	7	10	11	12	13	15	19	20	21	22	24	25
A3-1	0.37	L	L	L	L	L	L	L	H	H	H	H	H	L	L	L	L	L	L	L	L	L	L	L	L	L
A3-2	0.6				L	L	L	L	H	H	H			L	L	L	L	L	L	L	L	L	L	L	L	L
A3-3	0.98				L	L	L	L	L	L	L															
A3-4	1.49	L	L	L		L	H	H				L	L													
A3-5	2.01				H	H	H	H	L	L	?			L	L	?	L	L	L	?	?	?	L	L	L	?
A3-6	2.99	L				H	H	C		L	L	L														
A3-7	3.92	L				H	H	C		L	L	L														
A3-8	3.96	L				H	H	C		L	L	L														
A3-9	5.94	L	L	H								L	L													
A3-10	7.97	H	H	H		H	H	C	L	L	H	L	L	L	L	L	L	L	L	L	L	L	L	L	L	L
Phenotype		BD	BD	BD	BD	BD	BD	BD	BD	BD	BD	BD	BD	BD	BD	BD	BD	BD	BD	BD	BD	BD	BD	BD	BD	BD
Note*		P	P	P	P	P	P	P	P	P	P	P	P	P	P	P	P	P	P	P	P	P	P	P	P	P

Chr 3	Physical location	DNA samples																				
Marker	Mbp	27	29	30	33	40	41	55	56	57	58	167	170	191	187	31	42	51	71	146	181	189
A3-1	0.37	L	L	L	L	L	L	L	L	L	L	L	L	L	C	H	H	H	H	L	H	H
A3-2	0.6	L	L	L	L	L	L	L	L	L	L					H	H	H				
A3-3	0.98															H	H	H	H			
A3-4	1.49											L	Failed	L	C	H	H		H	H	H	H
A3-5	2.01	?	L	L	?	?	?	L	L	L	L					H	H	H				
A3-6	2.99											L	L			H	L		H	H		
A3-7	3.92											L	L			H	L		L	H		
A3-8	3.96											L	L			H	L		L	H		
A3-9	5.94											L	L	L	H		L	L	L	H	H	H
A3-10	7.97	L	L	L	L	L	L	L	L	L	L	L	L	L	H	H	L	L	L	L	C	C
Phenotype		BD	BD	BD	BD	BD	BD	BD	BD	BD	BD	BD	BD	BD	NBD	BD	NBD	NBD	NBD	NBD	NBD	NBD
Note*		P	P	P	P	P	P	P	P	P	P	P	P	P	FP	FP	FP	FP	FP	FP	FP	FP

Chr 3	Physical location	DNA samples								
Marker	Mbp	98	128	152	182	183	184	185	186	8
A3-1	0.37	H	H	H	H	H	H	H	H	C
A3-2	0.6									C
A3-3	0.98									C
A3-4	1.49	H	H	H	H	H	H	H	H	
A3-5	2.01									C
A3-6	2.99	H	H	H						
A3-7	3.92	H	H	H						
A3-8	3.96	H	H	H						
A3-9	5.94	H	H	H	H	H	H	H	H	
A3-10	7.97	H	H	H	H	H	H	H	H	
Phenotype		NBD	NBD	NBD	NBD	NBD	NBD	NBD	NBD	NBD
Note*		FP	FP	FP	FP	FP	FP	FP	FP	FP

The five most informative plant samples for identifying the region containing the causal mutation are indicated by the red square box. They indicate that the mutation is located between 0.6-1.49 Mbp in chromosome 3. Plant genotypes identified by HRM: L*er*-0 homozygous (L, blue); Col-0 homozygous (C, green); heterozygous (H, red); not clear based on HRM profile (?, pink). Plant phenotypes: BD, bushy and delayed sepal degreening; NBD, non-bushy and delayed sepal degreening. P, positive; FP, false positive (the *dis* phenotype for these samples was unclear, therefore treated with caution and concluded as false positive after HRM analysis).

10. Sequence alignment of AtMAX1, AtMAX1-related proteins and other cytochrome P450 proteins with the haem-iron ligand signature

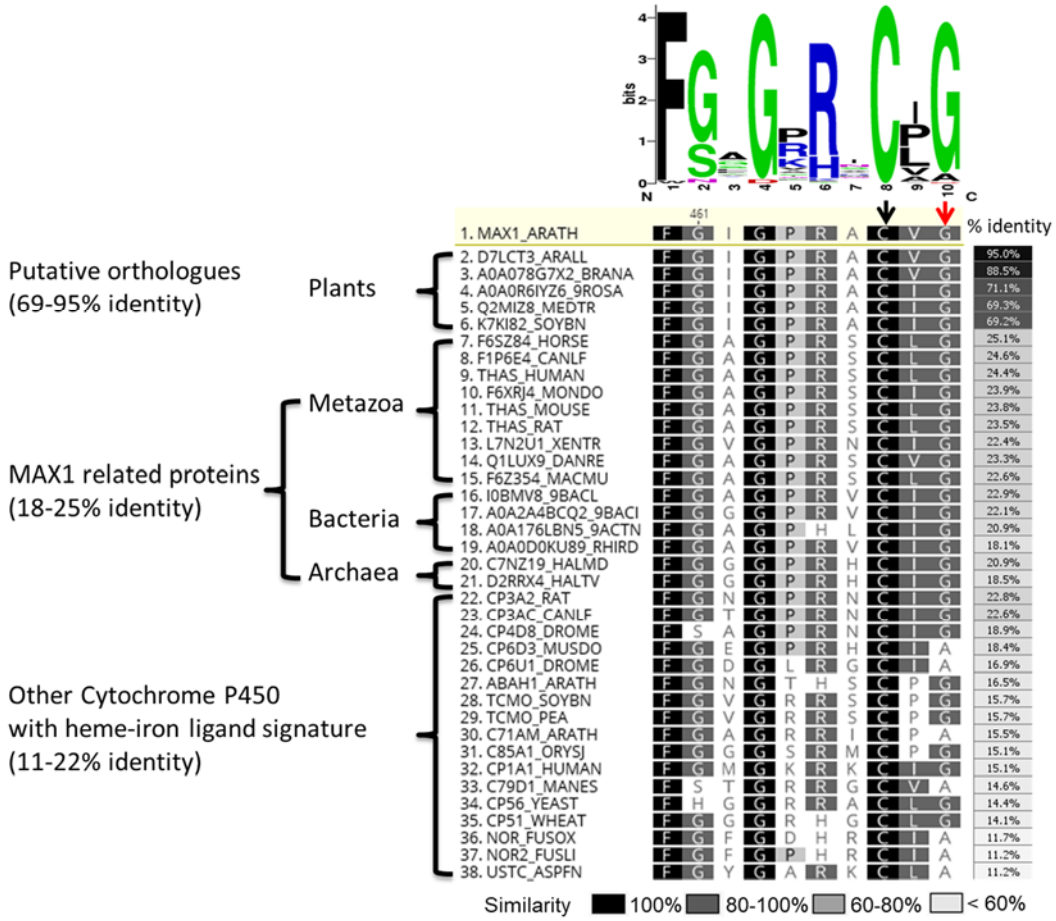

Appendix 10. Sequence alignment of *Arabidopsis* MAX1 with its putative orthologs, related proteins and other cytochrome P450 proteins with the haem-iron ligand signature

Putative orthologs and related proteins were selected based on sequence similarity and the representative examples that were most similar to AtMAX1 are shown. Positions of the mutation at Gly-469 (G469) and of the haem-iron ligand at Cys-467 (C467) in *Arabidopsis* MAX1 are indicated in red and black arrows, respectively. Amino acid positions are based on the Col-0 sequence from TAIR. The sequences of the cysteine haem-iron ligand signature are shown. Aligned sequences were sorted by the % identity to the AtMAX1 reference sequence. % identity is shown using the heatmap and numbers style in Geneious. The intensity of shading of aligned sequences represents the percentage similarity of each residue among all aligned sequences. The sequence names are UniProt IDs (http://www.uniprot.org/) and the logo of the haem-iron ligand signature is from Prosite. Amino acids are coloured according to their chemical properties (Crooks *et al.*, 2004): polar amino acids are indicated in green, basic in blue, acidic in red, and hydrophobic in black. Letter size represents percentage of conservation within cytochrome P450 proteins that shared this signature.

11. *MAX1* expression in the infiltrated leaves of *N. benthamiana*

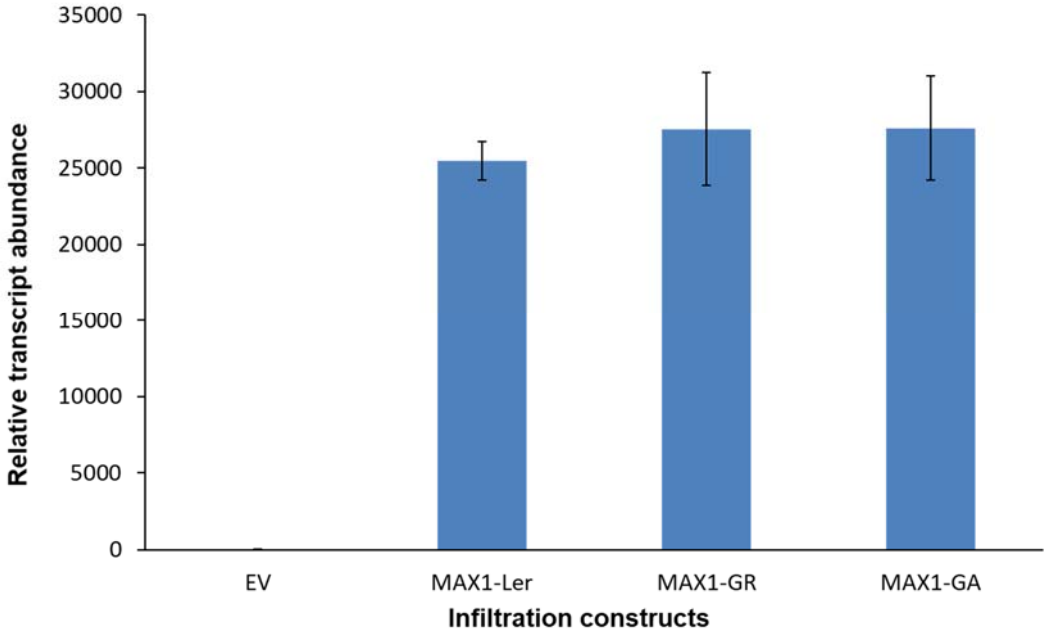

Appendix 11. Transcript abundance of *MAX1* in the leaves of *N.benthamiana* infiltrated with constructs carrying MAX1-WT, -G469R or -G469A

EV, empty vector control; *MAX1*-L*er*, *MAX1* based on L*er*-0 sequence; *MAX1*-GR/GA, *MAX1* with G469R or G469A substitutions based on L*er*-0 sequence. Data are mean ± standard error (n=3)

12. Degreening of inflorescences treated with rac-GR24

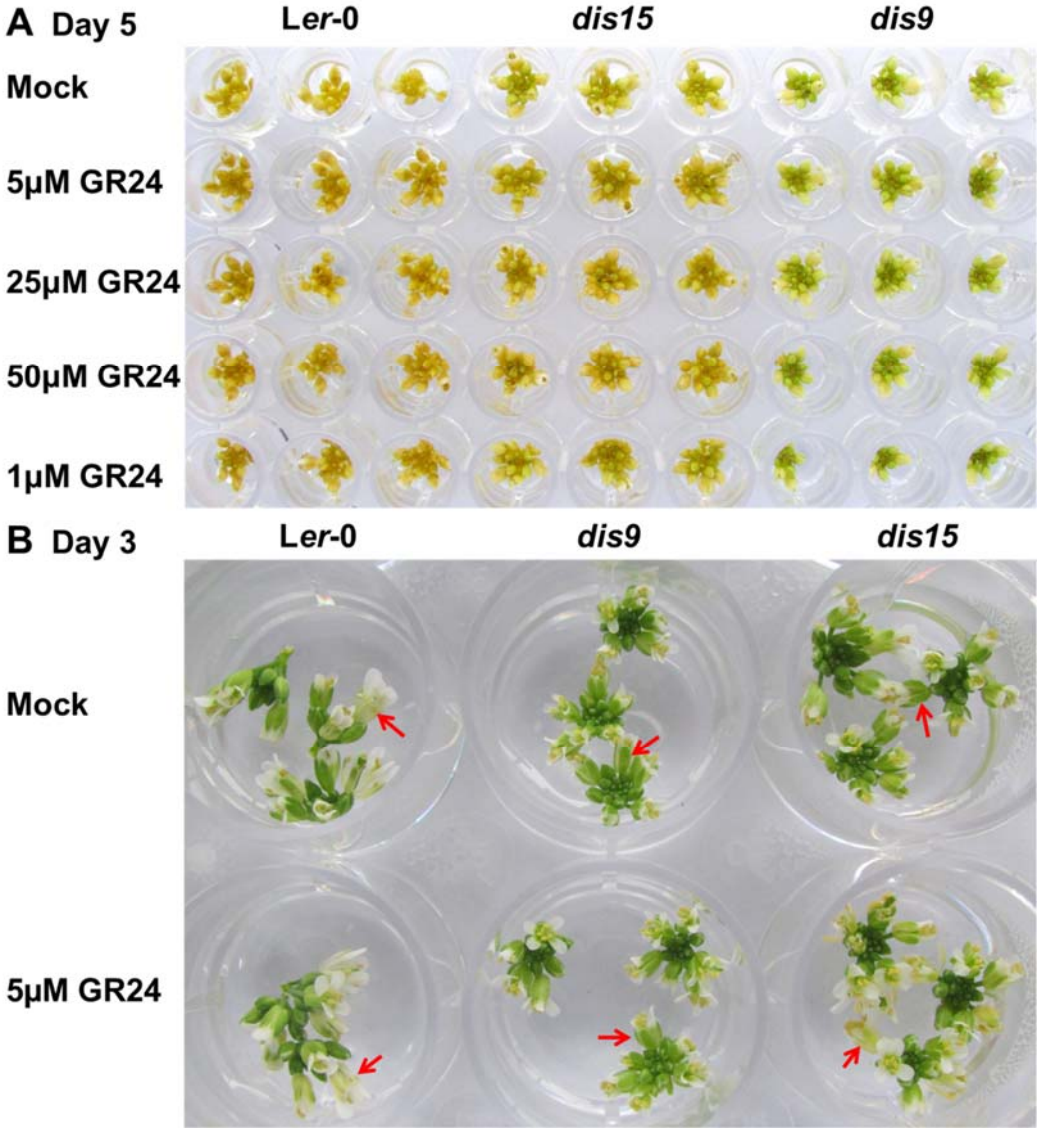

Appendix 12. Degreening of inflorescences treated with rac-GR24
Inflorescences were harvested from the primary bolts of 4.5-week-old plants that had their first flower opened on the same day. Inflorescences with removed opened buds were used for experiment. (A) Inflorescences were treated with 1% DMSO (mock) and rac-GR24 at 1, 5, 25, 50 μM and were incubated in the dark for 5 days. Three biological replicates are shown. (B) Inflorescences were treated with 1% DMSO (mock) and 5 μM of rac-GR24 and were incubated in the long day conditions (16 h/8 h light/dark cycle) for 3 days. The representative sepals were pointed by red arrows. Additional three biological replicates from an independent experiment are shown.

13. Statistical analysis of nCounter data for 0, 3, 6 h and 0, 12, 18 h treatments

Gene	Treatments (0, 3, 6 h)	Difference*	Treatments (0, 12, 18 h)	Difference*
MAX1	0 h - Ler	a	0 h - Ler	ab
	0 h - dis15	a	0 h - dis15	ab
	3 h - Ler DMSO	a	12 h - Ler DMSO	ac
	3 h - dis15 DMSO	a	12 h - dis15 DMSO	ac
	3 h - dis15 GR24	a	12 h - dis15 GR24	d
	6 h - Ler DMSO	a	18 h - Ler DMSO	abcd
	6 h - dis15 DMSO	a	18 h - dis15 DMSO	a
	6 h - dis15 GR24	a	18 h - dis15 GR24	abcd
AKINβ1	0 h - Ler	a	0 h - Ler	a
	0 h - dis15	a	0 h - dis15	a
	3 h - Ler DMSO	bc	12 h - Ler DMSO	c
	3 h - dis15 DMSO	b	12 h - dis15 DMSO	c
	3 h - dis15 GR24	b	12 h - dis15 GR24	b
	6 h - Ler DMSO	c	18 h - Ler DMSO	c
	6 h - dis15 DMSO	b	18 h - dis15 DMSO	c
	6 h - dis15 GR24	b	18 h - dis15 GR24	bc
bZIP63	0 h - Ler	a	0 h - Ler	a
	0 h - dis15	a	0 h - dis15	a
	3 h - Ler DMSO	c	12 h - Ler DMSO	d
	3 h - dis15 DMSO	bc	12 h - dis15 DMSO	c
	3 h - dis15 GR24	b	12 h - dis15 GR24	b
	6 h - Ler DMSO	d	18 h - Ler DMSO	cd
	6 h - dis15 DMSO	cd	18 h - dis15 DMSO	bc
	6 h - dis15 GR24	d	18 h - dis15 GR24	bc
SMXL6	0 h - Ler	b	0 h - Ler	a
	0 h - dis15	a	0 h - dis15	a
	3 h - Ler DMSO	de	12 h - Ler DMSO	d
	3 h - dis15 DMSO	b	12 h - dis15 DMSO	c
	3 h - dis15 GR24	c	12 h - dis15 GR24	e
	6 h - Ler DMSO	e	18 h - Ler DMSO	c
	6 h - dis15 DMSO	d	18 h - dis15 DMSO	b
	6 h - dis15 GR24	f	18 h - dis15 GR24	d
SMXL7	0 h - Ler	d	0 h - Ler	c
	0 h - dis15	a	0 h - dis15	a
	3 h - Ler DMSO	cd	12 h - Ler DMSO	bc
	3 h - dis15 DMSO	ab	12 h - dis15 DMSO	ab
	3 h - dis15 GR24	cd	12 h - dis15 GR24	d
	6 h - Ler DMSO	de	18 h - Ler DMSO	e
	6 h - dis15 DMSO	abc	18 h - dis15 DMSO	d
	6 h - dis15 GR24	e	18 h - dis15 GR24	f
SMXL8	0 h - Ler	c	0 h - Ler	e
	0 h - dis15	b	0 h - dis15	c
	3 h - Ler DMSO	ab	12 h - Ler DMSO	abc
	3 h - dis15 DMSO	a	12 h - dis15 DMSO	abc
	3 h - dis15 GR24	b	12 h - dis15 GR24	d
	6 h - Ler DMSO	b	18 h - Ler DMSO	ab
	6 h - dis15 DMSO	a	18 h - dis15 DMSO	a
	6 h - dis15 GR24	b	18 h - dis15 GR24	bc
ANAC092	0 h - Ler	a	0 h - Ler	a
	0 h - dis15	ab	0 h - dis15	a
	3 h - Ler DMSO	d	12 h - Ler DMSO	b
	3 h - dis15 DMSO	bc	12 h - dis15 DMSO	c
	3 h - dis15 GR24	cd	12 h - dis15 GR24	d
	6 h - Ler DMSO	abc	18 h - Ler DMSO	c
	6 h - dis15 DMSO	cd	18 h - dis15 DMSO	f

	6 h - dis15 GR24	cd	18 h - dis15 GR24	f
NAP	0 h - Ler	a	0 h - Ler	a
	0 h - dis15	a	0 h - dis15	a
	3 h - Ler DMSO	c	12 h - Ler DMSO	b
	3 h - dis15 DMSO	c	12 h - dis15 DMSO	b
	3 h - dis15 GR24	d	12 h - dis15 GR24	d
	6 h - Ler DMSO	b	18 h - Ler DMSO	c
	6 h - dis15 DMSO	b	18 h - dis15 DMSO	c
	6 h - dis15 GR24	c	18 h - dis15 GR24	e

* Differences among treatments for each gene were indicated by lower cases.

14. nCounter analysis of ethylene biosynthetic gene

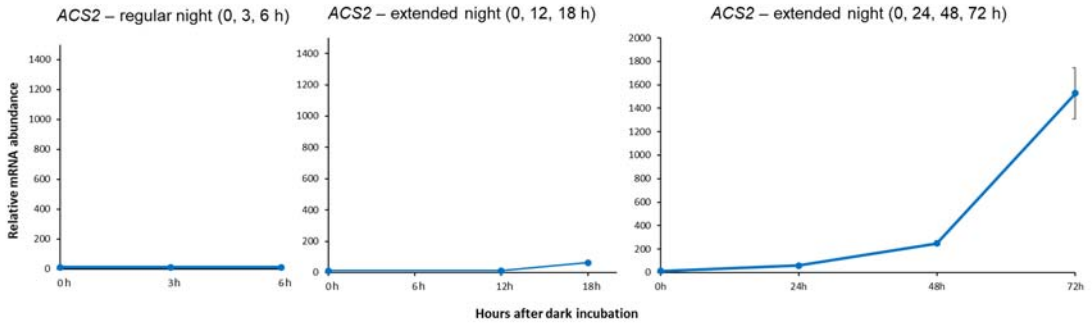

Appendix 14. Transcriptional changes of ethylene biosynthetic gene *ACS2* during the regular and extended night

Transcript abundance was quantified using nCounter technology on RNA isolated from detached WT inflorescences (n = 3 samples, > 4 inflorescences from independent plants per sample) that were incubated in the dark for the indicated time points. Transcript abundance was normalised to the geometric mean of *PP2AA3, ACT2 and MON1.* Data are mean ± standard error.